WARWICK

Polyorthoesters and analogues from a cyclic ketene acetal as surface-erodible materials in additive manufacturing and elastomer fabrication

Gordon Herwig

Submitted for the degree of Doctor of Philosophy

Department of Chemistry

January 2020

THE UNIVERSITY OF WARWICK

Table of Contents

List of Figures

List of Schemes

List of Tables

Acknowledgements

Firstly, I would like to thank my supervisor, Andrew P. Dove, for offering me the opportunity to work on this project following your vision and finding funding for me, both further than you initially envisioned. I appreciate the trust, guidance and leeway you offered, which enabled me to personalise the project and persist until everything finally came together, and simultaneously develop skills to fix basically anything that could possibly malfunction around the lab. Thank you for your continued reminders and advice to keep my academic progress on track though, without it I might have ended up with a giant one-chapter thesis. Finally, I would like to thank you, the University of Warwick (especially the Department of Chemistry) and the University of Birmingham for providing access to such fantastic instruments, facilities and staff, as well as the Leverhulme Trust for the majority of my funding.

My thanks further extend to the members of the Dove and O'Reilly group for sharing their expertise and experiences, as well as for the collegial spirit in the labs and the trust to fix even more problems. Josh and Mar, you deserve a special mention for advising on the really tough academic and intellectual issues, providing short-term proof-reading, and simply being there for everyone – thank you very much. Also on a personal note: Thomas, Christian, Wei, Shu, Sètuhn, Anissa, Connor – I am thankful for all the conversations (academic, political or otherwise), patience with my stereotypically 'German' temper and generally refreshing international perspective – one might just want to call it 'friendship'.

Finally, thanks to my family for keeping everything upright back in Germany, especially my Mom, to try and solve any and all issues wherever in the world I am. The deepest of all my gratitude however is reserved for my wife – you are my love, my passion (just before nature, science, technology and dry humour), my life. Without your love and support this whole adventure of ups (especially mountains) and downs and A LOT of moving in between would have been impossible.

Declaration of Authorship

This thesis is submitted to the University of Warwick in support of my application for the degree of Doctor of Philosophy. It has been composed exclusively by me and has not been submitted in any previous application for any degree. The work presented (including data generated and data analysis) was carried out by the author except in the cases outlined below:

- Elemental analysis, Mass Spectroscopy and GC-MS analysis data (Chapter 2-4) was collected and analysed at the respective departmental facilities at the Universities of Warwick and Birmingham by Heena Makwana/Lianne Hill, Lijiang Song/Chi Tsang and Allen Bowden, respectively
- The handling of the SEM and data collection (Chapter 2) was performed by Paul Stanley of the Centre for Electron Microscopy at the University of Birmingham
- The XPS data (Chapter 3) was obtained and analysed by Marc Walker at the University of Warwick Photoemission Facility
- The cell studies (Chapter 3) were conducted by Maria Mar Perez-Madrigal at the University of Birmingham
- Bis(3-mercaptopropyl) succinate was synthesised by Craig Bell, Ed Cant and Josh Worch (Chapter 3)
- The ASEC 'true' MW data (Chapter 4) was obtained by Jeff Foster of the O'Reilly group at the University of Birmingham

Publications

(1) Herwig, G; Dove, A. P., Synthesis of Rapidly Surface Eroding Polyorthoesters and Polyacetals Using Thiol–ene Click Chemistry. *ACS Macro Lett.* **2019**, *8*, 1268-1274. doi:10.1021/acsmacrolett.9b00463 **(Chapter 2)**

(2) Herwig, G; Perez-Madrigal, M. M.; Dove, A. P., Customized Fading Scaffolds: Strong Polyorthoester Networks via Thiol-Ene Crosslinking for Cytocompatible Surface-Eroding Materials in 3D Printing. *In preparation.* **(Chapter 3)**

(3) Herwig, G; Dove, A. P., Synthesis of Poly(Orthoester-Thioether-Thiourethane-Urethanes) (POETE-Us) from Oligomeric Thiol-Terminated POETEs as Degradable Elastomers. *In preparation.* **(Chapter 4)**

(4) Hua, Z.; Wilks, T.R.; Keogh, R. ; Herwig, G. ; Stavros, V.G.; O'Reilly, R.K., Entrapment and rigidification of adenine by a photo-cross-linked thymine network leads to fluorescent polymer nanoparticles. *Chem. Mater.* **2018**, *30*, 1408-1416. doi:10.1021/acs.chemmater.7b05206 **(Collaboration)**

Abstract of Thesis

Motivated by the advantageous rapid surface-erosion behaviour but problematic manufacturing of pure polyorthoesters (POE), in this thesis, the synthesis and manufacturing of poly(orthoester-thioether) (POETE) materials from stable orthoester (OE) monomers *via* thiol-ene Michael addition are described. Initially, a variety of novel OE compounds was synthesised and comprehensively characterised, followed by UV-initiated thiol-ene coupling with a selection of thiols. The full scope of OE-TE compounds ranged from small molecules over POETE polymer chains and networks, to the use of POETEs as soft segments in polyurethanes (PUs). Subsequently, chromatographic, spectroscopic and microscopic, as well as thermo-mechanical analyses were performed in order to facilitate conclusions on the structure/composition-function relationship, as well as to further investigate the degradation process.

Chapter 1 provides an introduction into the importance, synthesis and degradation properties of polymers like POEs and elastomers such as polyurethanes (PUs), as well as principles of rapid additive manufacturing to process polymers for direct application, as used in the rest of the work.

Chapter 2 details the synthesis of simple OEs, acetals (ATs) and the respective thioethers (TEs) in the form of small molecules and chain polymers, including their comprehensive spectroscopic and chromatographic analysis. The method is then used to produce a strong network material, on which subsequent surface erosion behaviour is documented and degradation products investigated.

Chapter 3 offers an overview of a library of new OE monomers and their spectroscopic properties, as well as comprehensively displays the thermo-mechanical properties of a variety of network materials obtained by crosslinking the OEs with multifunctional thiols. In addition, the results of 3D printing, degradation and cytocompatibility studies are presented.

Chapter 4 introduces a strategy to manufacture poly(thio-urethanes) from POETE oligomers and demonstrates that hydrolytically degradable, strong and elastic, glassy and semi-crystalline materials can be obtained.

Chapter 5 summarises the work reported in Chapters 2 to 4 and advises on future perspectives, optimisations and potential applications.

List of Abbreviations

ABS	Acrylonitrile butadiene styrene rubbers
AFM	Atomic force microscopy
AM	Additive manufacturing
ASEC	Absolute size exclusion chromatography
AT	Acetal
AT-TE	Acetal-thioether
BACA	2-[[(butylamino)carbonyl]oxy]ethyl acrylate
BAPO	Bisacyl phosphine, see Irg819
BBOT	2,5-bis(5-tert-butyl-benzoxazol-2-yl)thiophene)
BHT	Butylated hydroxytoluene
CAD	Computer aided design
CKA	Cyclic ketene acetal
CT	Computer Tomography
δ	Chemical shift
d	Doublet
DBTDL	Dibutyltin dilaurate
DBU	1,8-diazabicyclo[5.4.0]undec-7-ene
DETOSU	3,9-Diethylidene-2,4,8,10-tetraoxaspiro[5.5]undecane
DGEBA	Diglycidyl ether of bisphenol A
DIY	Do-it-yourself
DLS	Dynamic light scattering
$Đ_m$	Polydispersity
DMF	*N*,*N*-Dimethylformamide
DMTA	Dynamic mechanical thermal analysis
DP	Degree of polymerisation
D-PBS	Dulbeco's phosphate-buffered saline solution
DSC	Differential scanning calorimetry
DTPTA	Di(trimethylolpropane) tetraacrylate
E'	Storage Modulus
E''	Loss Modulus
ε	Deborah Number

ECC	3,4-epoxycyclohexylmethyl-3’,4’-epoxycyclohexane carboxylate
eq.	Equivalent
ESBO	Epoxidised soybean oil
ESI-QTOF	Electrospray-ionisation quadrupole time-of-flight
EtOAc	Ethylacetate
FDM	Fused deposition modelling, see FFF
FFF	Fused Deposition Modelling®, see FDM
FT-IR	Fourier-transform infrared spectroscopy
HDI	Hexane-1,6-diisocyanate
HEMA	Hydroxyethyl-methacrylate
H_{12}MDI	4,4'-Methylene dicyclohexyl diisocyanate
%HS	Hard segment content
HSI	Hue-Saturation-Intensity
IR	Infrared
Irg819	Irgacure 819, see BAPO
J	Coupling constant
λ	Wavelength
L_{critical}	Critical Length
m	Multiplet
M_{diiso}	Molecular weight of diisocyanate
M_{diol}	Molecular weight of diol (chain extender)
M_{n}	Number averaged molecular weight
M_{poly}	Molecular weight of macrodi(thi)ol
MRI	Magnetic Resonance Imaging
M_{w}	Weight averaged molecular weight
MW	(Average) molecular weight
m/z	Mass-to-charge ratio
NEt_3	Triethylamine
NMR	Nuclear magnetic resonance
$\tilde{\nu}$	Wavenumber
OE	Orthoester
OEAM	*N*,*N*′-((((oxybis(methylene))bis(1,3-dioxolane-4,2-diyl))bis(oxy))bis(ethane-2,1-diyl))bis(2-methylacrylamide)

OE-TE	Orthoester-thioether
p	Conversion
PA	Polyamide
PAH	Polyanhydride
PAT	Polyacetal
PATTE	Poly(acetal thioether)
PC	Polycarbonates
PCL	Poly(caprolactone)
PE	Polyethylene
PEEK	Poly(ether ether ketones)
PEG	Poly(ethylene glycol)
PEGDA	Poly(ethylene glycol) diacrylate
PEVA	Ethylene-vinylacetate copolymer
PGA	Poly(glycolic acid)
PI	Photoinitiator
PLA	Poly(lactic acid)
POE	Polyorthoester
POEA	Poly(ortohoester amide)
POETE	Poly(orthoester thioether)
POETE-U	Poly(orthoester thioether thiourethane urethane)
POEU	Poly(orthoester urethane)
POM	Poly(oxymethylene)
PP	Polypropylene
ppm	Parts per million
*p*TSA	para-Toluene sulfonic acid
PTUU	Poly(thiourethane urethane)
PU	Polyurethane
PVC	Poly(vinyl chloride)
q	Quartet
qi	Quintet
r/R	Reactant ratio
ROP	Ring opening polymerisation
s	Singlet

SEC	Size exclusion chromatography
SEM	Scanning electron microscopy
SLA	Stereolithography
SMP	Shape memory polymer
STL	Standard tessellation language
t	Triplet
TE	Thioether
T_g	Glass transition temperature
TGA	Thermal gravimetric analysis
THF	Tetrahydrofuran
T_m	Melting temperature
TOE	Thioorthoester
TPET	Trimethylolpropane ethoxylate triacrylate
t-t	*trans-trans*
UV	Ultraviolet
UV-Vis	Ultraviolet-Visible
wt%	Weight percentage
XPS	X-ray photoelectron spectroscopy
3D	Three dimensional
3SH	Trimethylolpropane tris(3-mercaptopropionate)
4SH	Pentaerythritol tetrakis(3-mercaptopropionate)
6SH	Dipentaerythritol hexa(3-mercaptopropionate)

1

Introduction

1.1 Abstract

This chapter introduces general concepts regarding degradable polymer materials and their importance in everyday life, as well as in highly specific applications for biomedicine. Moreover, the underlying degradation mechanisms are explained, and a connection between decomposition rates and the polymer structure and synthetic strategies is established. Furthermore, additive manufacturing is presented as a promising technique of recent interest to promote the application of novel degradable polymers. Hence, special focus is placed on reaction mechanisms with the potential to efficiently combine the presented principles and techniques into one general methodology.

1.2 The Journey of Polymer Materials

1.2.1 Opportunities and Challenges Arising from Polymers

Without polymers, civilisation as we know it today would be unthinkable.[1] Just over a century ago, Bakelite, which is widely praised as the world's first synthetic plastic, completely revolutionised the way appliances and vehicles were fabricated since its development in 1907.[2] The shift from processing natural materials to factory production of synthetic polymers not only meant a significant improvement in output capacity, but also a decrease in manufacturing time and cost. Over the years, countless increasingly complex polymers and polymerisation techniques have been developed for a wide range of applications, *i.e.* from simple components in household and food applications,[3-4] as well as high-performance industrial applications,[5] to highly specialised devices for scientific fields, such as biomedicine,[6] shape-memory materials[7] and electric sensors[8]. Unsurprisingly, the production of plastics has reached unprecedented levels, with the yearly global output rising from already 4 Mt in 1955 up to over 400 Mt in 2015 (Figure 1-1).[1] However, the synthetic nature and enhanced material properties of polymers, such as biological and chemical stability, induce at the same time controversial side effects.

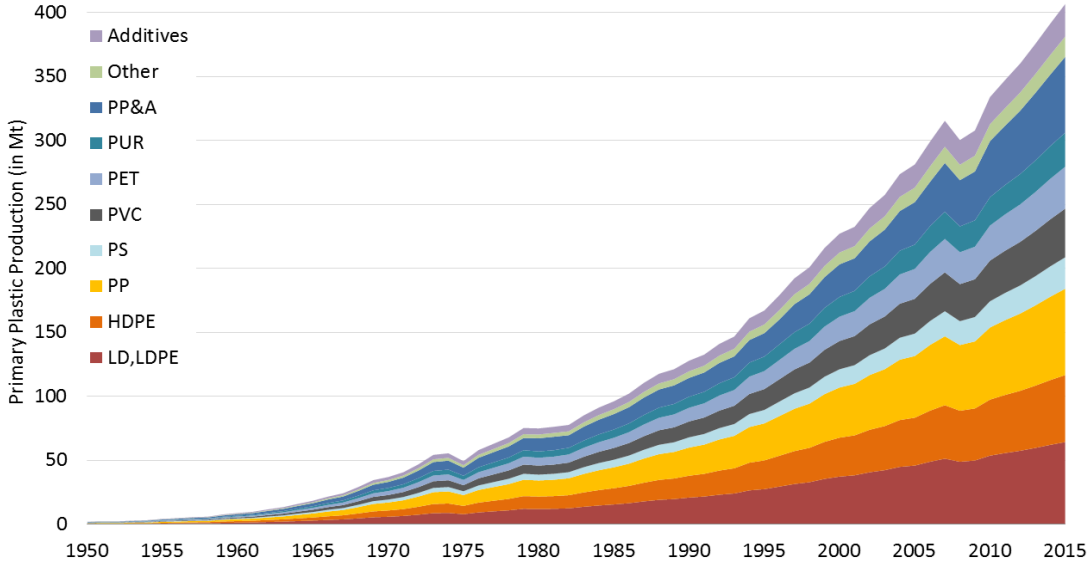

Figure 1-1. Global primary plastics production (in million metric tons) according to polymer type from 1950 to 2015. (from Ref. 1).

Simultaneously with the increase in production, an overwhelming volume of plastic waste has been accumulating, which amounts to more than 5 Gt between the 1950s and today.[1] Even though evidence shows that it is the least environmentally and economically profitable method,[9] over 75% of all plastic waste is still disposed of in landfill or simply discarded into the environment every year (Scheme 1-1). Even from landfill, particles can spread further by the action of wind and fauna or through superficial and ground water.[10]

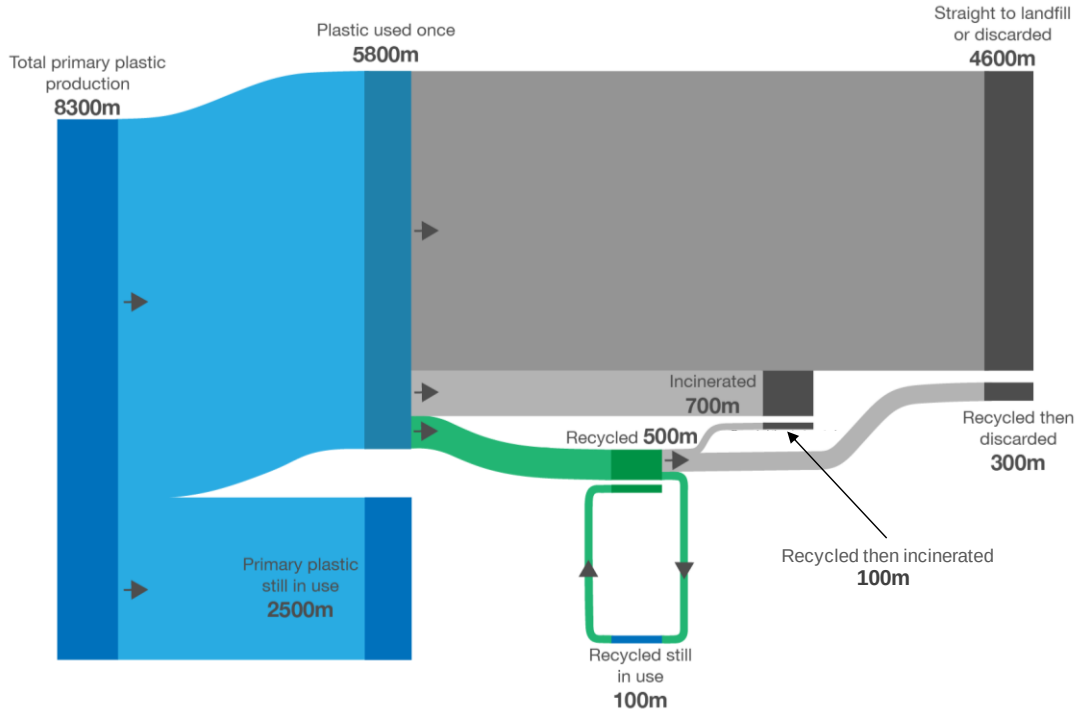

Scheme 1-1. Global plastic production and its fate (1950-2015). (Based on Ref. 1, visualisation by OurWorldInData.org; units m ≙ Mt, modified for clarity).

While the total weight of large plastic pollution in oceans and landscapes is high as a consequence of the stability of polymer materials (Table 1-1),[11] the invisible threat of microplastics, which amounts to roughly 93% of particles by number, has aroused wide concern.[12] Firstly discovered in the 1970s, this category of polymeric materials has been identified as the main source of continued environmental contamination in recent years.[13] Microplastics, which consist of particles in sizes of several millimetres or lower, are either included as such in abrasive or cosmetic formulations (primary) or are formed by polymer disintegration as a consequence of physical causes (secondary).[14] The latter is particularly worrisome as water treatment facilities are yet unable to extract such small particles efficiently,[15] which is the reason why the highest concentrations of microplastics are found in rivers and continue on to reach the oceans.[16] Unfortunately, the effect the resulting microplastics have on the environment is still not entirely understood.[17] Hence, the development of fully chemically degradable materials to limit polymer pollution has become an essential task for a sustainable future.

Table 1-1. Marine decomposition times of various waste products and their likely polymeric components (data from US Environmental Protection Agency, Gulf of Mexico Program and Woods Hole Oceanographic Institution (Ref. 11)).

Waste (Likely material)	Fishing line (PVDF)	Plastic bottle (PET)	Disposable diaper (various)	Six-pack rings (PE)	Aluminimum can	Foamed buoy (PS)	Tin can	Syrofoam cup (PS)	Plastic bag (PE)	Cigarette butt (Cellulose acetate)	Photodeg. six-pack rings (HDPE)	Milk carton (PE)
Marine decomposition time (years)	600	450	450	400	200	80	50	50	20	5	0.5	0.25

1.2.2 Degradation of Synthetic Polymers

Generally, degradable polymer materials are susceptible to environmental attack, and thus become only suitable for non-permanent applications. As such, one strategy for reliable decomposition in a biological environment relies on the use of natural materials or compositions,[18] even in medicine.[19] For synthetic materials, however, polymer degradation as a structural phenomenon is caused either actively by enzymes from microorganisms or passively by hydrolysis.[20]

While the former is likely the dominant mechanism in natural environments,[21] its timeline depends highly on the specific microenvironment and is thus difficult to generalise,[22] which is why models based on hydrolysis can provide a more realistic timeframe.[23]

In order to hydrolytically degrade, polymer structures need to contain weaker linkages than the carbon-carbon bonds present in aliphatic materials, such as polyethylene (PE) and polypropylene (PP). These polymers only degrade by the action of certain species of microorganisms and ultraviolet (UV) photolysis over extended periods of time (Table 1-1), thus remaining indefinitely in lower ocean depths.[24-26] There is additional risk of the release of toxic degradation products or additives as leachate, as it has been proven by studies on poly(vinyl chloride) (PVC) and related halogenated polymers in landfill.[27] In contrast, poly(lactic acid) (PLA) and poly(glycolic acid) (PGA), which are based on ester bonds, degrade hydrolytically within 4 to 12 months.[28] Furthermore, the non-toxic degradation products are immediately utilised by organisms in the environment, whereas the monomers can be synthesised from natural products, which render these polymers renewable and sustainable.[29] As a potential downside, these most common degradable materials exhibit bulk erosion behaviour, *i.e.* the object becomes increasingly brittle and weak over time, until it fragments.[23] However, in a medical context, for instance, implanted scaffolding devices and drug delivery vehicles should preferably degrade in a controlled fashion from the outside in (*i.e.* surface erosion), rather than disintegrate and abruptly release both fragments and loaded drugs (*i.e.* bulk erosion) (Scheme 1-2).

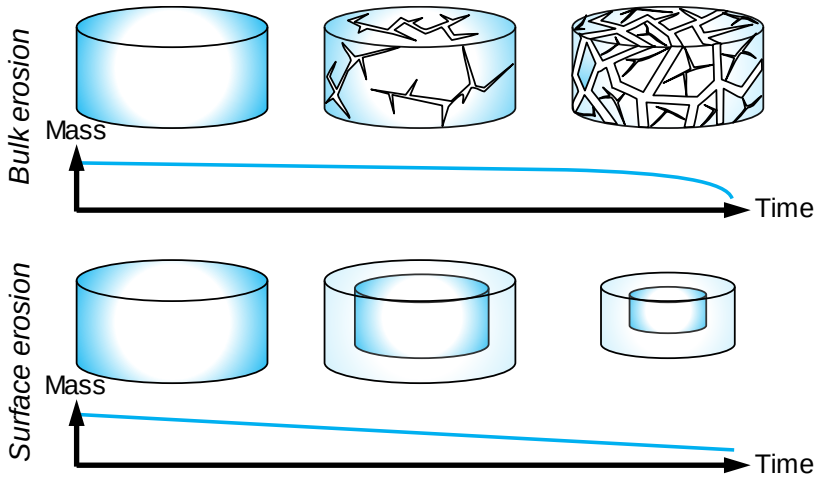

Scheme 1-2. Model of appearance and mass curves of a polymer sample eroding over time in accordance with a bulk (top) and surface (bottom) erosion mechanism (mass loss after Ref. 30).

1.2.3 Erosion Mechanisms of Solid Polymer Materials

Bulk erosion of a material occurs when chemical bonds throughout the whole material start to decompose simultaneously. Hence, during a hydrolytic process, the diffusion rate of water is higher than the rate of hydrolysis through the entire material.[30-31] After an initial diffusion period, the samples become more porous as bonds throughout the material are uniformly broken, which leads to the release of small amounts of degradation products or loaded cargo, such as drugs, early on. In consequence, the object becomes increasingly fragile over time while maintaining the original dimensions, which is ultimately followed by disintegration into fragments and rapid mass loss as the degradation products decompose to lower molecular weights (Scheme 1-2).[30] For applications simply concerned with biodegradability, bulk erosion represents an adequate degradation profile.[32]

In contrast, and prevalent in enzymatic degradation, surface erosion of a material appears as a shedding of small molecule degradation products from the surface only while leaving a solid uncompromised sample of smaller dimensions within.[19] The rate of diffusion throughout the material is lower than the rate of degradation, which only results in superficial decomposition. Consequently, this mechanism, which allows for structural integrity throughout the process while maintaining a steady mass loss, can be applied for supporting scaffolds and the controlled release of embedded drugs.[31]

While it was commonly assumed that there is a clear unconditional distinction between materials exhibiting surface or bulk erosion,[32] further investigations established that all materials can show surface erosion depending on the scale of a homogenous object (see Figure 1-2).[33]

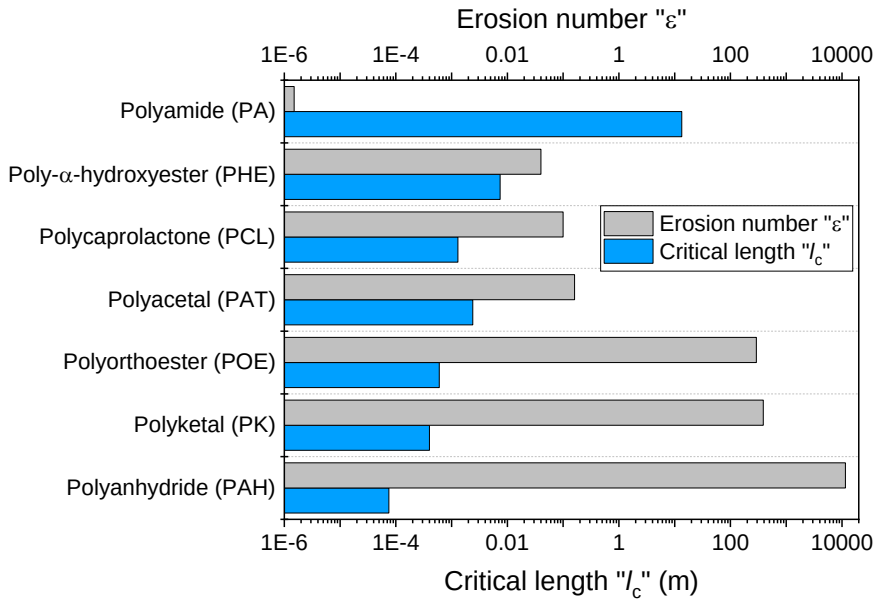

Figure 1-2. Erosion-related critical length ($L_{critical}$) and Erosion (Deborah) number (ε) of a selection of polymer materials (from various sources, processed and summarised in Ref. 33).

Generally, the spectrum of materials can be characterised by the Erosion (Deborah) number (ε), a dimensionless parameter calculated to distinguish between typically surface ($\varepsilon > 1$) and bulk ($\varepsilon < 1$) eroding materials, and their critical length ($L_{critical}$), which indicates the actual thickness of the erosion layer (*i.e.* at what dimension surface erosion can be observed).[33] Consequently, when working at medically relevant dimensions of 1 to 10 mm, materials generally fall into one of those two categories (either surface or bulk eroding) and can be selected for intended applications according to this criterion.

1.3 Synthetic Surface Erodible Polymers for Biomedical Applications

Although a comparative study on tissue regeneration *in vivo* indicated only minor advantages for surface eroding scaffolds compared to bulk eroding devices,[34] the improved structural integrity of the former indisputably provides steadier release profiles and mechanical support while preventing the spreading of particles with thrombotic risk. Consequently, surface erodible materials have already attracted significant scientific interest in the biomedical field.

1.3.1 Polyorthoesters (POEs)

Polyorthoesters (POEs) have become one of the most promising classes of surface erodible materials for biomedical applications, and both their surface erosion behaviour and biocompatibility have been confirmed in extensive studies, mostly conducted by Heller and co-workers on four specific kinds of POEs (Figure 1-3).[35-39]

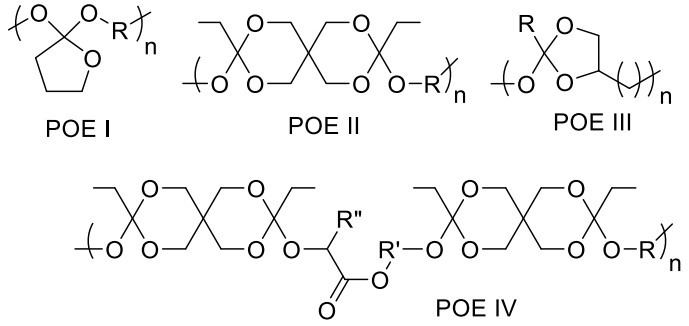

Figure 1-3. Commonly described families of polyorthoesters (POEs).

The incorporated sterically strained triple oxyalkylated OE functionalities offer high susceptibility to hydrolysis, whereas the aliphatic backbone prevents water diffusion into the network. Indeed, POE-based samples (on a millimetre scale) exhibited surface erosion behaviour, degrading completely at pH = 7.4 in approximately one year.[40] An extensive range of degradation times, from just several days to years, was accessible by different strategies: i) selection of different hydrophobic linkers or glycolides as intramolecular latent acids,[41] ii) variation of chain length,[42] and iii) incorporation of basic additives, such as magnesium hydroxide into the matrix.[37] Besides, higher crosslinking density led to increased degradation rates, which was ascribed to either increased strain or higher overall hydrophilicity, which in turn would promote the diffusion of water into the material.[37] Similarly, the incorporation of salt significantly accelerated degradation rates by adding a hygroscopic element into the material.[40] Drug delivery, which was identified as a potential application, was tested *in vivo.* Specifically, various ocular devices were designed as a more efficient alternative for DNA vaccines.[43] Ultimately, such a system would avoid repeat injections,[44] as well as locally managing post-operative pain.[36]

Despite these promising results, a more general application in biomedicine was never realised, the major reason being found in the limitations regarding

material properties. For example, most of the samples were prepared as soft gels or semi-solids, whereas tougher materials were only obtained by increasing the glass transition temperature (T_g) from 20 to 105 °C using stiffer linkers.[35] Although high T_g values greatly limited elasticity and caused brittleness, with yield strains of 3 %, it also resulted in tensile strength values higher than 27 MPa and tensile moduli above 1.2 GPa.[45] Unfortunately, the incorporation of drugs altered the material structure of such POEs by interfering with the polymer chain alignment and hence generally weakened the mechanical properties.[35] Additionally, the complex synthesis reported involved moisture and air sensitive intermediates and precursors, which severely limit the scalability of this procedure. For instance, even though the polycondensation reactions leading to POE I and III were based on relatively stable orthoester compounds (*i.e.* 2,2-diethoxytetrahydrofuran and triethylorthoester, Figure 1-4), their synthesis required multiple steps and the polymerisation yielded hardly reproducible inferior materials, which evidences the reason these materials have been abandoned for decades.[35]

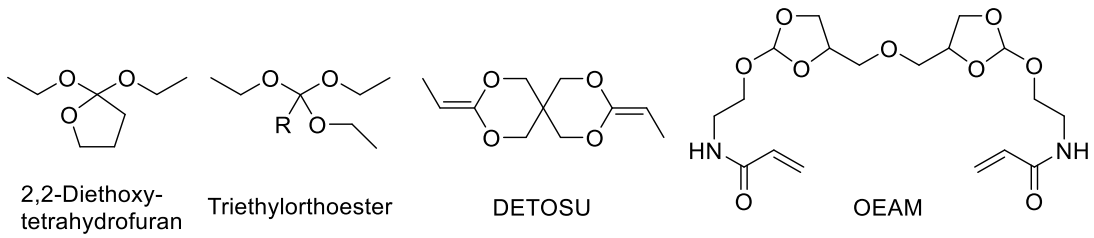

Figure 1-4. Commonly employed precursors in the synthesis of POEs. (DETOSU: 3,9-diethylidene-2,4,8,10-tetraoxaspiro[5.5]undecane; OEAM: N,N′-((((oxybis(methylene))bis(1,3-dioxolane-4,2-diyl))bis(oxy))bis(ethane-2,1-diyl))bis(2-methylacrylamide)).

In contrast, 3,9-diethylidene-2,4,8,10-tetraoxaspiro[5.5]undecane (DETOSU) is used as precursor for a great variety of well-defined POE materials and copolymers; however, it exhibits high sensitivity to moisture and spontaneously isomerises *via* hydrogen transfer, thus requiring extensive purification.[46] Nevertheless, this route was chosen for novel materials, such as poly(amine-*co*-ester-*co*-ortho ester)s[47] and POE-*co*-PEG copolymers, for drug delivery with pH-sensitive properties.[48-49] One of the most recent strategies for the first photo-crosslinkable POE oligomers utilised hydroxyethyl-methacrylate (HEMA) to achieve methacrylate end caps;[50] however, crosslinking was not conducted.

In a similar approach, Tang and co-workers employed as precursors relatively stable and versatile *N*,*N*′-((((oxybis(methylene))bis(1,3-dioxolane-4,2-diyl))bis(oxy))bis(ethane-2,1-diyl))bis(2-methylacrylamide) (OEAM) derivatives, which contained OE functionalities as degradable elements and acrylamide groups for further functionalisation. Starting from methacrylate monomers with OE functionalities in the resulting side chain,[51-52] they developed diamines containing an OE linker to form POE amides (POEAs)[53-54], POE urethanes (POEUs)[55-56] and OE-crosslinked networks from methacrylated PEG[57] and soy proteins.[58] All polymeric materials were found to be biocompatible in cell compatibility and histological studies. Additionally, the suitability of POEAs and POEUs as drug delivery vehicles was demonstrated in several *in vivo* graft tumour studies using doxorubicin and 5-fluorouracil as anti-cancer agents.[54-56, 58] Hence, this route is a significant improvement with respect to previous methodology as it provides control over the polymerisation process, facilitates crosslinking and offers customisability without the need to incorporate additives. Nevertheless, although the polymerisation occurred under mild ambient conditions, the OE monomers still required a multistep synthesis under inert atmosphere involving harsh solvents. Furthermore, because of their low mechanical strength, the resulting manufactured materials were limited predominantly to drug delivery and tissue engineering applications.

Notably, the OE group is well established as an acid sensitive linker for targeted release in lysosomal cell environments in biomedical drug release strategies.[59] Its degradation mechanism was proposed as early as 1921,[60] followed by investigations on the stereochemistry of the degradation products of cyclic orthoesters[61] and their sensitivity to acidity,[59, 62] which revealed that degradation rates correlated directly proportionally to pH values.

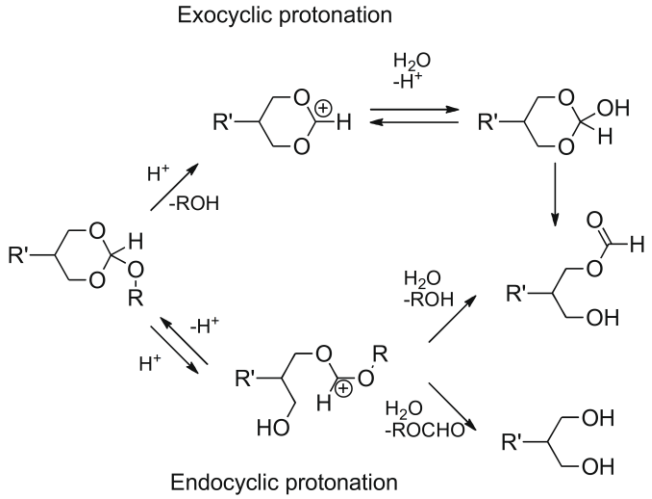

Scheme 1-3. Proposed hydrolytic degradation pathways of a cyclic OE (from Ref. 59).

Furthermore, it has been postulated that during the hydrolysis of cyclic OEs, the protonation occurs either endo- or exocyclic, which results in the release of alcohols, hydroxyesters and carboxylic acids (Scheme 1-3).[59] Generally, organisms tolerate these products very well, which, combined with the tuneable degradation and release rate, explains the sustained interest in POE materials.

1.3.2 Polyanhydrides (PAHs)

Polyanhydrides (PAHs) represent an alternative class of material for robust surface eroding devices, which have been applied already not only as drug carriers, but also medical electronics.[63] For instance, linear polyanhydrides displayed tensile strength values of 4 MPa with yield strains of 14 % and tensile moduli around 45 MPa,[45] whereas samples with a methacrylate-based crosslinked structure reached tensile strength values of 27 MPa and a modulus of 2 GPa.[64] Such performance matches the mechanical properties of strong POE materials while providing less brittle material. Even stronger materials have been developed *via* copolymerisation with amines and urethanes.[63] However, despite these successful results and FDA approval, their application in biomedicine remains hindered by the generally low customisability of the mechanical features and the high acidity of degradation products. While it has already been postulated that the released diacids cause less damage to essential proteins than polyester-derived degradation products,[65] polyanhydrides can also be manufactured to release beneficial substances, such as salicylic acid.[66]

1.3.3 Polyesters Based on Poly(lactic acid) (PLA)

Finally, polyester formulations based on PLA also exhibit surface erosion.[67] However, clinically utilised PLA degrades via bulk erosion and, even though degradation times can be tailored towards the application (for example, from 9% weight loss after 12 months for screws, to 70% weight loss after 42 days for bone implants[68]), fluctuations of the degradation rate under physiological conditions and dynamic load can lead to sudden failure.[69]

Degradation rates of PLA devices depend on the rate of water diffusion, which in turn varies with glass transition temperature and crystallinity.[70] Additionally, the degradation of PLA yields lactic acid, which can diffuse out of the outer layers but not from the core, thus leading to increased acidity within the particle.[71] Not only do high concentrations of lactic acid increase the degradation rate *via* auto-catalysis, but they can also cause tissue irritation, which is worsened by the disintegration of increasingly porous vehicles into fragments.[68] Nevertheless, PLA is generally well tolerated in the human body and, in bioresorbable devices, degrades without the need of applying follow-up surgery.[72] Moreover, because of its sustainable synthesis based on natural renewable resources, PLA-based devices have been exploited in a wide range of applications, such as screws in plastic surgery, tissue engineering scaffolds, and drug release vehicles.[73-74] Interestingly, PLA-based screws have been reported to withstand similar or slightly higher forces than common titanium screws in a tensile test using a grafted porcine knee setup.[75] Furthermore, 3D-printed PLA structures showed ultimate tensile strength values of up to 89.1 MPa at 2% strain with an elastic modulus of 4.2 GPa,[76] which far surpasses commercial polymer materials, such as polycarbonate (with 49.1 MPa at 14% maximum strain[77]), thus further evidencing the versatility and applicability of PLA. Overall, PLA and other aliphatic polyesters represent the most used model compounds for biodegradable medical materials,[68] forming part of the composition of a significant amount of FDA-approved devices to date.[78]

1.3.4 Manufacturing of Polymer Materials for Biomedical Applications

Stainless steel, titanium and ceramics are still materials of choice for a variety of orthopaedic and cardiovascular support structures; however, synthetic

polymeric materials have gained an increasing share of biomedical applications.[79] The contributing factors for such raised interest include a more sustainable sourcing, medical reasons, such as allergies, drug delivery over time[80] and the reduction of follow-up surgery because of their degradability,[81] and also their facile customisability and processing.[82] Potentially even more crucial, even though less intuitive, is the use of polymeric materials for preparing complex surgical operations.[83] Indeed, 3D models of tissue are routinely used as training aids to facilitate detailed spatial planning of operations and to visualise lodged objects or tumours. Using standard CT or MRI techniques, a 3D model of the anatomy of interest is created, which can then be turned into a plastic model using additive manufacturing.

1.4 Additive Manufacturing

Three techniques have been widely established for the production of 3D objects: formative, subtractive, and additive manufacturing.[84-85] While formative techniques are still the predominant industrial standard with high throughput and high consistency, additive and subtractive manufacturing are essential in fields requiring diverse models and sizes. Indeed, these two techniques allow for the rapid creation of customised mould templates to produce complex assemblies in a single process.[86] As the name suggests, subtractive manufacturing requires a solid block of raw material from which excess material is removed and discarded, which makes the process economically inefficient. Furthermore, as 3D models require rather complex setup and production time, the scope of this technique is often limited to simple cutting procedures that involve lasers or water jets. In contrast, additive manufacturing has gained significant attention in recent years as no excess material or complex setup is required.[87] Especially in the biomedicine and engineering fields, where individual 3D prototype models need to be produced in a short amount of time to assess practicality, rapid prototyping has become a widely applied strategy using additive manufacturing or 3D printing.

1.4.1 Rapid Prototyping Techniques

The first recognised 3D printer was patented by Charles Hull in 1984, which encouraged the development of an increasing variety of techniques for rapid prototyping.[88] The list of materials manufactured by this technique consists not only of polymers, but also metals, ceramics and even cells and biomolecules, as well as combinations thereof.[89] Generally, 3D printing methodologies still follow mostly either physical or chemical principles, with Fused Deposition Modelling (FDM) and Stereolithography (SLA) among the most popular polymer processing techniques.

3D printing relies on a three-dimensional computer aided design model (CAD file), which is commonly generated either manually using existing templates and provided software tools or automatically from 3D scans. [88] Then, the software transforms this model into a series of separate slices of usually regular distance or thickness, which represent the average cross section projection of the model between the specified dimensions. The printer subsequently uses these segments as templates for a layered model recreating the computer file (Figure 1-5). Logically, the slice and resulting layer thickness determine the smoothness of surfaces along the z-axis in the resulting model print.

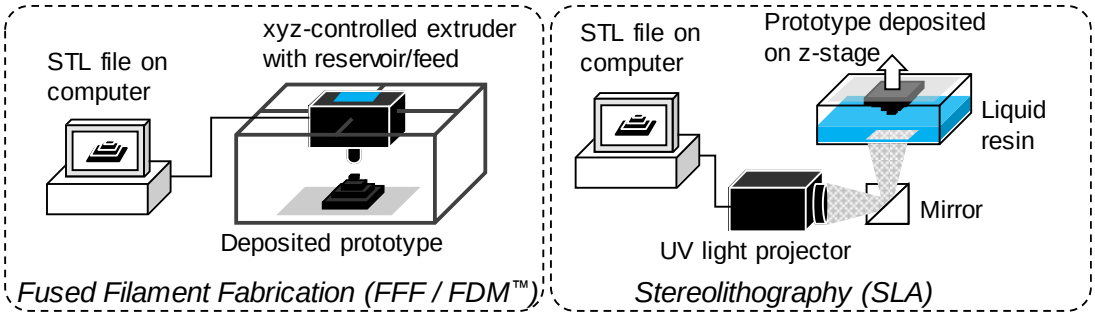

Figure 1-5. Common commercially available rapid prototyping setups. Left: FFF, right: SLA.

FDM is the methodology of choice for most DIY projects at home, as well as for applications in medicine and industry.[90] Briefly, the molten polymer is extruded from a calibrated omnidirectional mobile feed to recreate each layer, with following layers fusing onto the previous one. Hence, this allows for a wide range of thermoplastic materials to be used; however, it also limits the final resolution, which depends on the extruder hole size, while usually yielding opaque specimens with rough material surfaces. [87] The setup and materials are generally

accessible from an economic point of view, as only a simple XYZ stage and a heated nozzle coupled in an automated system is required, which further offers the possibility to easily exchange nozzles and materials.

In contrast, SLA requires a bath of liquid resin and a strong UV source, as well as customised liquid formulations, which leads to higher overall costs.[90] More importantly, however, this technique yields more precise and durable models from a single thermoset polymer network, which often shows exceptional clarity and transparency. Additionally, the printing time is reduced as a complete layer can be cured at once or in a much shorter time. In principle, a laser or a photo mask irradiates specific areas according to the layer template at the respective height, which enables spatial and temporal control of the photo polymerisation. Irradiation times and intensities are customised to achieve sufficient conversion and mechanical integrity, while the unreacted groups that remain ensure crosslinking with the subsequent layer.[91] This accuracy and reliability makes SLA a desirable technique for surface-patterning and jewellery design,[90] as well as for the production of scaffolds for tissue and bone regenerations.[92]

To exploit the increased accessibility and diversity of 3D printers, a wide and continuously extending range of materials has been reported, only limited to suitable physical properties or photochemical reaction mechanisms.

1.4.2 Polymers for Additive Manufacturing

FDM, which is the most economical and prevalent technique for nonprofessionals,[84] is capable of printing a variety of thermoplastic polymers *via* extrusion (Figure 1-6),[93] such as flexible or sturdy acrylonitrile butadiene styrene rubbers (ABS), polyether ether ketones (PEEK) or polycarbonates (PC).[94] While these high performance materials are versatile and used in everyday life applications, sterically demanding aromatic groups isolate the hydrolysable bonds and prevent degradation. On the other hand, poly(lactic acid) (PLA), polycaprolactone (PCL), and even ethylene-vinylacetate copolymer (PEVA), polyamide (Nylon, PA), and polyurethane (PU) all degrade in biological or aqueous environments, albeit at various rates.[95-98]

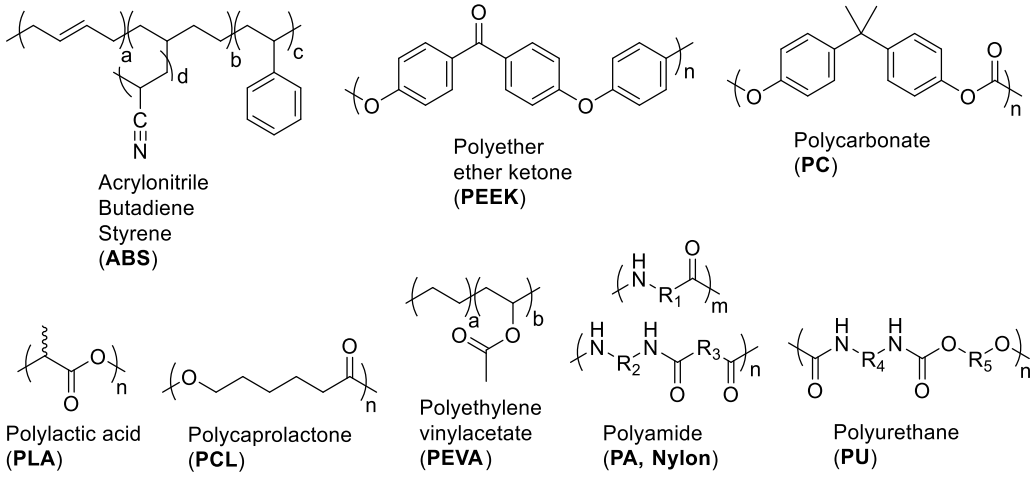

Figure 1-6. Commonly employed polymers in Fused Filament Fabrication (FFF).
Top row: non-degradable materials, bottom row: degradable materials.

In order to further increase their mechanical performance, economic efficiency or degradability, filler materials can be included into the resin composition.[99] As a result, not only do these materials become suitable for biomedicine applications, but also offer opportunities in engineering fields. For instance, the parts for the assembly of a new replication printer were produced by FDM (RepRap project, University of Bath, 2005).[100]

In contrast, SLA produces clear and highly precise printed models with a slightly more expensive setup using resin mixtures based on small molecules or oligomers. In fact, formulations contain predominantly either acrylic or epoxide compounds, and their combination *via* bifunctional monomers or blending yields superior materials as interconnected or interpenetrating networks.[101]

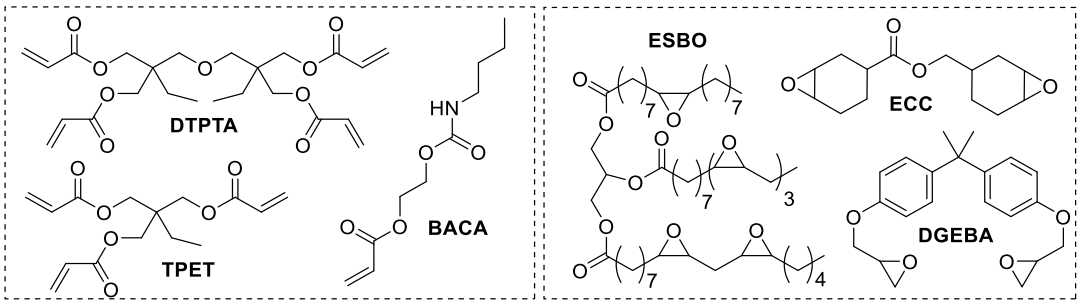

Figure 1-7. Commonly employed monomers in Stereolithography (SLA).
Left: acrylic-based resins; right: epoxide-based resins.

As an example, the acrylic formulation Autodesk PR48 (Figure 1-7) consists of di(trimethylolpropane) tetraacrylate (DTPTA) as structural monomer, as well as 2-[[(butylamino)carbonyl]oxy]ethyl acrylate (BACA) and trimethylolpropane

ethoxylate triacrylate (TPET) to lower the resin viscosity as reactive diluents.[102] Bio-based acrylate alternatives have also been developed.[103] Epoxides, such as epoxidised soybean oil (ESBO), 3,4-epoxycyclohexylmethyl-3',4'-epoxycyclohexane carboxylate (ECC) and bisphenol A diglycidyl ether (DGEBA), are commonly combined with acrylates to provide anchor points for a secondary network, whereby ESBO receives specific interest as a bio-derivative.[104] Despite their toxicity, acrylates and epoxides remain key resin components as a consequence of the resulting superior material strength displayed by the printed devices;[105] however, alternatives based on less toxic methacrylates, oxetanes and non-toxic thiols are available.[84]

Regardless of the resin crosslinking mechanism, SLA requires a customised composition of photo-sensitive initiators and inhibitors to optimise printing conditions, while considering the overall resin cytotoxicity.[106] Commonly used radical initiators, like camphorquinone, require amines as co-initiator in a Norrish type 2 reaction. However, more sophisticated Norrish type 1 systems consist of only one initiator compound, such as an organic phosphine oxide, which undergoes homolytic cleavage of one or more bonds between the carbonyl and adjacent central highly coordinated heteroatom. Other examples of commonly employed initiators (Figure 1-8) include biacylphosphine oxide (BAPO, Irgacure 819) and trimethylbenzoylphosphine oxide (liquid, Irgacure TPO-L),[107] with the latter offering not only a wide absorption range, but also superior solubility. Besides, initiators can be combined to further extend the absorption spectrum.[108] Similarly, cationic initiators, such as sulfonium and iodonium salts, can be tailored and combined with sensitisers to suit the process.[101] Indeed, their low sensitivity to oxygen and continuous self-hardening in a 'dark polymerisation' contributed to the preference of the cationic route for commercial products;[109-110] however, significantly longer curing times were required, thus presenting a potential drawback.

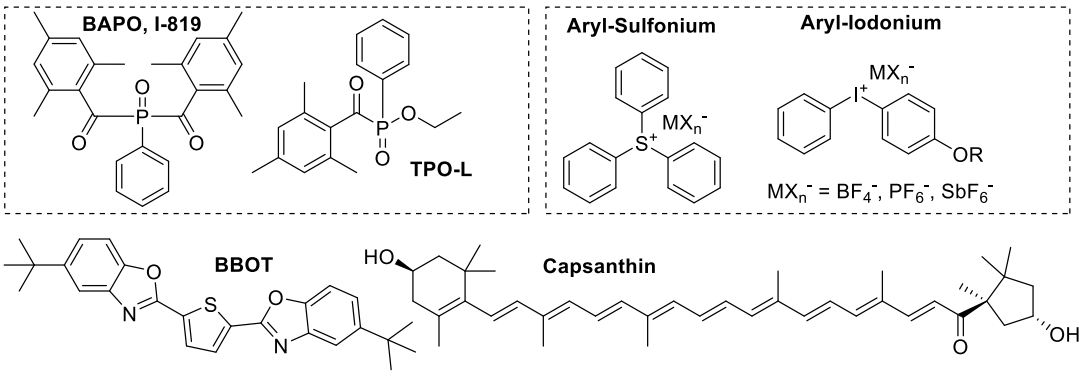

Figure 1-8. Commonly employed radical (top left) and cationic (top right) photo-initiators, as well as photo-inhibitors (bottom) in Stereolithography (SLA).

Additionally, a photo-absorber is usually required to lower the sensitivity of SLA resins against premature exposure and to limit the curing depth for enhanced resolution. Good absorption properties in the UV-vis region usually originate from extended π-electron systems, such as in graphene and natural products. Commonly employed inhibitors include 2,5-bis(5-tert-butyl-benzoxazol-2-yl)thiophene) (BBOT, Figure 1-8) and carotenes, such as capsanthin and capsorubin, which can be added directly in the form of paprika extract as a sustainable natural alternative.[111]

Several biocompatibility studies suggest that many commercially available resins can be employed directly or after simple modifications for medical applications.[112] Alternatively, customised functional materials made of shape memory polymers (SMP) are of particular interest recently.[113-114] However, it is important to bear in mind that for resins to be suitable for SLA and truly rapid manufacturing, crosslinking reactions need to progress as rapidly and efficiently as possible, which are properties usually associated with 'click' reactions.

1.5 Reaction Principles and Mechanisms

1.5.1 General Principles and Mechanisms of 'Click' Reactions

Sharpless and co-workers outlined the criteria for a group of highly efficient reactions to be classified as possessing a 'click' mechanism.[115] These principles include i) short reaction times leading to near full conversion without inert atmosphere; ii) high yield and selectivity towards one product or respective stereoisomers; and iii) simple purification steps, thus avoiding chromatographic techniques. Since then, opinions have differed on whether some recently

discovered specific polymerisations match these criteria,[116] *e.g.* large-scale syntheses often require increased reaction time or heat, which strictly defies the first criterion. Similarly, most common polymerisation methods are highly efficient; however, they often require controlled environments and chromatographic purification. In order to predict the 'click' potential of a reaction, the polymerisation mechanism needs to be considered.

1.5.2 General Principles and Mechanisms of Polymerisations

The synthesis of polyolefins, from alkenes or acrylates, as well as ring opening polymerisations (ROP) have been established as the major examples of chain-growth polymerisations,[117] with the latter offering the benefit of yielding mostly biodegradable polymers.[118] For instance, well-defined high molecular weight (*M*) polymers, such as PLA and PCL, are obtained *via* ROP. Mechanistically, the initiator molecule binds to a monomer and induces ring opening, which in turn leaves an activated end-group to react with further monomer units until none is left (Scheme 1-4).[117] As these reactions occur simultaneously and at the same rate, an extremely narrow polydispersity (*i.e.* $Đ_M \approx 1$, Equation 1) can be achieved.[119] Unfortunately, specific oxygen and moisture sensitive catalysts are often required to efficiently achieve reproducible and high molecular weights.[120]

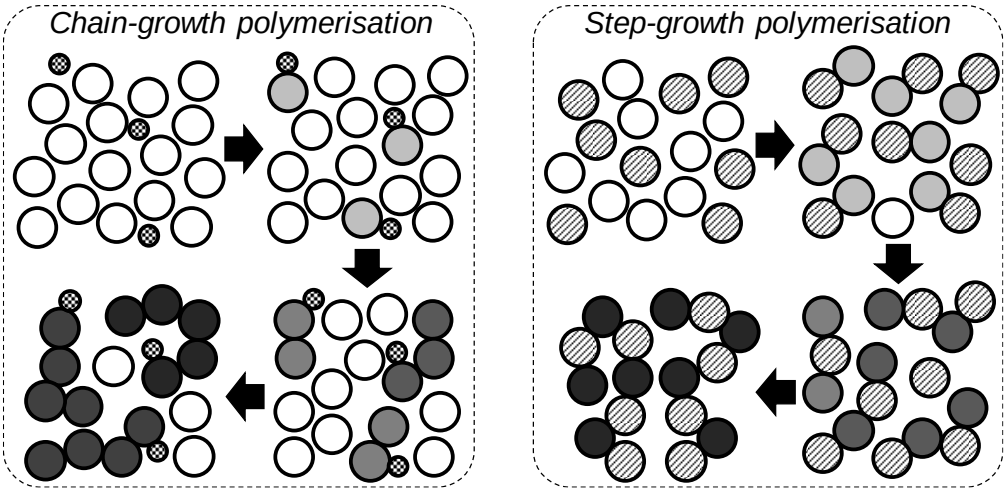

Scheme 1-4. Chain-growth (left) and step-growth (right) polymerisation mechanisms.

Equation 1 $$Đ_{M_1} = \frac{M_w}{M_n} \approx 1$$

$$Đ_{M_2} = \frac{M_w}{M_n} = \frac{M_0 \frac{1+p}{1-p}}{M_0 \frac{1}{1-p}} = 1 + p \leq 2$$ Equation 2

$$Đ_{M_3} = \frac{1+r}{1+r-2rp}$$ Equation 3

Furthermore, polyolefin chain-growth synthesis is commonly used in SLA applications to form crosslinked thermoset network materials from acrylic resins, whereby a well-defined reaction progression is less important.[84] Still, significant issues with such materials remain. For example, the toxicity of the monomers, as well as the high rigidity of the resulting structures, which can only be modified by incorporating additives, severely limit the medical application of the 3D printed specimens.[101] Moreover, the chain-growth proceeds rather inhomogeneously at active centres to reach incomplete conversion as a consequence of the high reaction rate and low mobility of the resulting chains and monomers, which leads to porosity or structural inconsistency.[105]

In contrast, step-growth polymerisation or polyaddition provides a more convenient reaction profile, requiring neither inert atmosphere nor additives to achieve flexible structures. As all monomers are equally likely to react simultaneously, nearly complete dimerization occurs initially, which is followed by further combination to form oligomers and, subsequently, polymers in a homogeneous fashion throughout the material or formulation.[121] High molecular weights are reached at high conversion (p, Equation 2) with a wide distribution of molecular weights, *i.e.* approaching $Đ_M = 2$. This relationship, however, highly depends on whether exact stoichiometry of the reactants is achieved with $r = 1$, as described by Carothers' equation (Equation 2 and 3).[122] In SLA, near complete conversion is generally accomplished by subjecting the crude and fragile printed model to prolonged UV irradiation, potentially followed by thermal post-curing in an oven; thereby, the most widely available epoxide-based resins still struggle with the release of toxic residual monomers. To solve this drawback, completely biocompatible resins and materials are accessible based on thiol-ene additions.

1.5.3 Step-Growth - Thioethers from Thiol-Ene (Thiol-Michael) Addition

Thiol-ene Michael additions are considered some of the most prominent and versatile photo-initiated step-growth reactions. A variety of mechanisms have been established for highly controlled polymerisations[123] and targeted modifications,[124] including various radical, ionic and atom transfer reactions,[125] which can be combined to access complex materials with wide range of properties.[126]

The simple radical-initiated thiol-ene reaction was the first reaction to be used in SLA and remains a central part of new approaches,[127] especially if the presence of ion-sensitive groups, like orthoesters, is desired in the final product.[128] In fact, thiol-ene compositions tend to polymerise following a radical mechanism when subjected to sunlight without any initiator,[129] a consequence of the homolytic cleavage of the rather weak sulfur hydrogen bond, whereas radical photo-initiators are employed to accelerate this process significantly (Scheme 1-5).

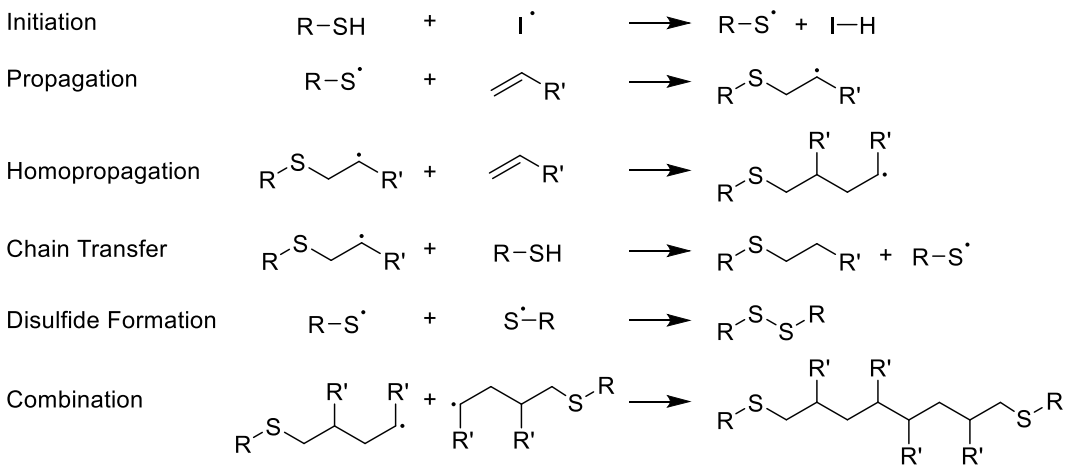

Scheme 1-5. Mechanism for the thiol-ene coupling reaction.

After initiation, the resulting thiyl species propagates by addition to alkene bonds while transferring the radical character, which enables either continued growth or the abstraction of another proton to activate a different monomer or chain in a step-growth manner. The reaction concludes under recombination of radicals, especially in the absence of irradiation to generate new radicals. This principle, which enables the spatial control needed for SLA by targeted irradiation, further offers temporal control by turning the reaction on and off in accordance with the light source.[130] Another significant benefit of thiol-ene systems lies in their low susceptibility to air, as oxygen can be incorporated into the polymer as peroxides or sulfoxides without compromising the polymerisation;[129] even disulfides formed from oxidation are still reactive in the thiol-ene mechanism.[131]

Specifically of interest for medical purposes, the thiol-ene mechanism proceeds in a biorthogonal fashion, *i.e.* the reaction does not interfere with biological systems as reactive alkenes and free thiols occur rarely in organisms, especially in bulky protein environments.[132] Moreover, the monomers and the resulting polymers are usually biocompatible, as demonstrated in a variety of

hydrogels,[133] including pH-sensitive orthoester-based thiol-ene hydrogels[134] and surface erodible anhydride-derived drug delivery vehicles.[135] The latter illustrates that degradable thiol-ene polymers require the presence of hydrolytically labile moieties, such as esters.[136] Interestingly, however, the oxidation of the thioether group to sulfones and sulfoxides increases the glass transition temperature and water-solubility of the materials, which has been reported to be relevant for conductive applications.[137]

Despite its potential, the thiol-ene approach still encounters several issues. Obvious drawbacks, such as the unpleasant smell and weakness of initial materials, have been addressed by employing less odorous and increasingly multifunctional thiols,[129] while methods to increase the shelf life of the resulting materials are based on employing secondary thiols.[138] Mechanistically, however, the slow reaction rates with electron-deficient or internal alkene functionalities, as outlined by Morgan *et al.*[139] and Hoyer, Roper and coworkers,[129] respectively, remains a challenge. Moreover, it was also noted that reversible thiyl radical addition to such bonds leads to isomerisation in cis/trans stereochemistry. Hence, this lack of stereo selectivity illustrates the inherent issue with radical-mediated polymerisations, thus explaining the preference for ionic or chain-transfer mechanisms in the field of synthetic chemistry.

1.5.4 Step-Growth – Polyurethanes from Diisocyanates and Alcohols

Polyurethanes (PUs), which are a class of materials commonly associated with high durability and porosity, are exploited to produce foams for essential items like sponges, cushions, and insulation.[140] While this might falsely suggest a polycondensation mechanism, their production is in fact based on the polyaddition reaction of diols and diisocyanates, which was discovered in 1937.[141] Foaming still occurs as a consequence of the reaction of isocyanates with water to form urea, which releases carbon dioxide;[142] however, to suit the application, desired properties are more reliably achieved by incorporating foaming agents and various nanoparticulate additives.[143]

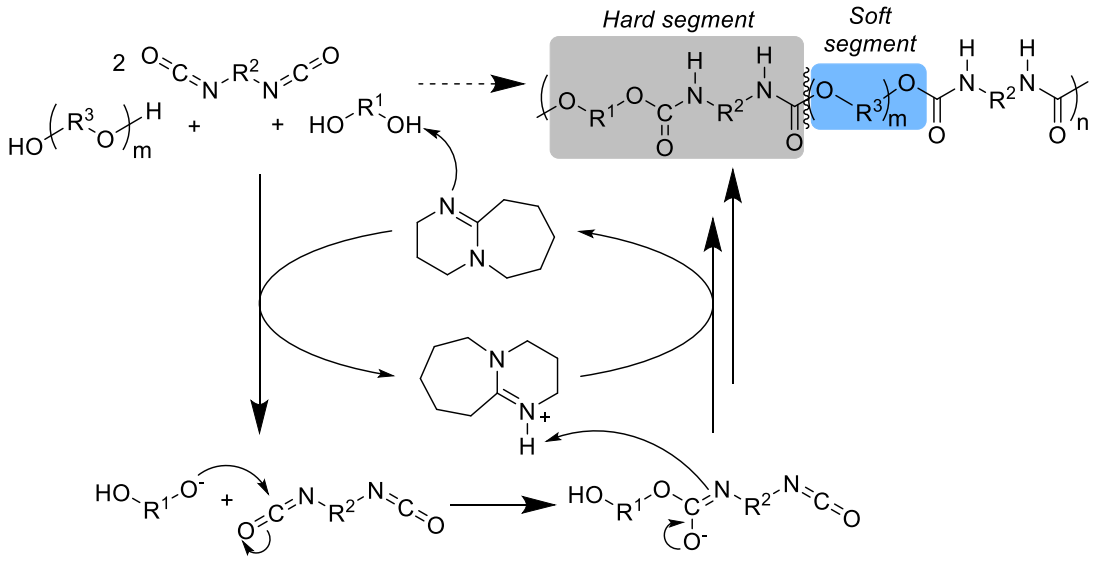

Scheme 1-6. Mechanism for the DBU-catalysed synthesis of polyurethane with hard and soft segments.

In the general step-growth reaction mechanism (Scheme 1-6), a base catalyst, like DBU (1,8-diazabicyclo[5.4.0]undec-7-ene), initiates the reaction by deprotonating an alcohol functionality, which in turn donates electron density in a nucleophilic attack towards the carbonyl within the isocyanate.[144] Subsequently, protonation of the nitrogen atom and restoration of the base catalyst yields the carbamate or urethane functionality. Additionally, experiments with guanidines suggested a supporting nucleophilic effect directly from the electron-rich nitrogen of the catalyst onto the isocyanate carbonyl group.[145] The resulting homopolymers exhibit strong rigidity and crystallinity as a consequence of the abundant intermolecular hydrogen bonds between the proton donating nitrogen-hydrogen and proton accepting carbonyl functionalities in the urethane groups.[146] Flexible materials can be also achieved if a macromolecular diol (R^3) is employed instead, which increases the distance between the re-occurring hydrogen bonds. The most versatile materials, however, are obtained through the combination of both macrodiols (R^3) and short chain extending diols (R^1), which results in a semi-crystalline elastomeric structure. The short extenders enable alignment and maximisation of hydrogen bonding to form harder glassy or crystalline segments, whereas the flexible macromolecular diol creates amorphous regions.[147]

In order to calculate the fraction of hard segments (%HS) from the mol ratio of macrodiol to isocyanate (R), the molecular weight of all compounds has to be known (M_x, Equation 3).[148] Originally developed by Flory,[122, 149] this equation enables the targeted production of PUs within a commonly elastic range between 15 and 80% hard segment content. Logically, an excessive content of hard segments leads to brittle materials, whereas a predominantly soft composition does not provide sufficient anchor points or structural support for elastic properties. Accordingly, for an effective mechanical strength, the molecular weight of the macrodiol usually ranges between 500 and 2000 kDa.

Equation 4 $$\%\mathrm{HS} = \frac{100(R-1)(M_{diol} + M_{diiso})}{(M_{poly} + R(M_{diiso}) + (R-1)(M_{diol}))}$$

The PU composition directly determines the size and distribution of the segments,[147] which can be further modified by the chosen synthetic method, *i.e.* either step-wise or bulk synthesis, or thermal post-treatment of the PU material.[150] This possibility has been exploited to create shape memory polymers (SMPs), which can be deformed and set in the new configuration by heating the material above the glass transition temperature during deformation, for example by aligning crystallites along the deformation axis (Figure 1-9). In order to customise such materials and ensure that the temperature range matches application conditions, understanding the effects of the chemical composition is crucial. While the employed macrodiol is often dictated by the target application, several studies have discussed the effect of both the diisocyanate and the diol linker on the resulting PU material.

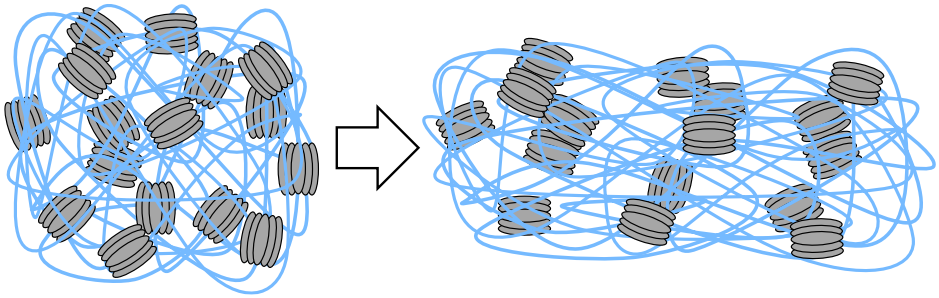

Figure 1-9. Alignment of hard segments in elastomeric polyurethane under strain.

Butane-1,4-diol has been identified as the superior chain extender among both short and long aliphatic extenders, as well as aromatic alcohols, in terms of

tensile strength and elasticity of the resulting PU, which is attributed to its specific crystalline structure and conformation.[146] Furthermore, by manufacturing different PUs based on a consistent macrodiol and chain extender, Pandya[151] and Lee[152] were able to demonstrate the significance of the employed diisocyanate linker. When butane-1,4-diol was used as chain extender at consistent mol fraction, the glass transition temperature of a material with an aliphatic diisocyanate was found to be -50 °C, -18 °C for a cyclic diisocyanate, and -8 °C for an aromatic diisocyanate linker. Similarly, ultimate tensile strength values were determined around 20 MPa for the material with the aliphatic component, 24 MPa when the composition included a cyclic functionality, and 33 MPa when it contained the aromatic linker.[151] Besides, the aliphatic diisocyanate material achieved a maximum elongation of 800% and higher initial elastic modulus, whereas the other materials exceeded 900% at lower modulus. The authors attributed this behaviour to the initially stronger intermolecular interactions and increased organisation between urethane functionalities when the flexible aliphatic linker was used, whereas crystallisation and general stiffness resisted stretching if cyclic and aromatic linkers were involved.[151] Unfortunately, the study was conducted on substituted linkers and reported a significant enhancement of the material properties when dibutyltin dilaurate (DBTDL) was used as a catalyst, which raised concerns regarding incomplete conversion and secondary sterical influences.

In contrast, Lee *et al.* conducted a blind test exclusively based on a macrodiol of M_n = 1-2 kDa without chain extender and, consequently, no hard segments.[152] As a result, glass transition temperatures of around -70 °C and uniform melting points of around 20 °C, were obtained regardless of the diisocyanate structure. At a hard segment content of 40%, glass transition temperatures increased marginally by 5 °C; however, hard segment melting temperatures of 168, 174 and 208 °C were observed for aliphatic, bicyclic and biaromatic isocyanates, respectively, with analogous secondary glass transitions at 85, 96 and 110 °C, according to DMTA.[152] While Young's moduli of all three systems were found within a narrow range of 40 to 50 MPa in the expected order, the variety of ultimate tensile strengths and maximum elongations showed significant variation, with 10.4 MPa at 200%, 24.3 MPa at 710% and 42.9 MPa at 1160%,

respectively, thus proving the significant impact of the linker structure on the material properties. Finally, the authors also concluded that the presence of aromatic diisocyanate linkers led to significant discolouration in the final material through light-induced quinonisation and thermal degradation.

While thermal degradation properties are of interest for industrial purposes, applications in the biomedical field depend on the biodegradation or, at least, biocompatibility of PUs. Hence, this consideration disqualifies PUs made by approaches other than in water, as well as polymers containing aromatic diisocyanates, which tend to form toxic aromatic diamines during degradation and sterilisation.[153-154] Considering that aliphatic diisocyanates and butane diol as chain extender are necessary compounds, the hydrolytic degradation properties of elastic biodegradable PUs depend mostly on the employed macrodiol. The hydrolytic and enzymatic degradation pathways of commonly employed polyesters, such as PLA, PEG and PCL, have been widely investigated and enable temporal control even in PUs. As a notable example, PU-based shape-memory foams degraded following a bulk erosion mechanism, which indicates that water diffusion throughout the material was rather homogeneous and barely affected by the foam structure.[155] Similarly, Ciardelli and co-workers demonstrated that, after a period of enzymatic degradation, cracks appeared within the material. As enzymatic erosion occurs only on the surface because of the size of enzymes, this illustrated that simultaneous water diffusion and hydrolysis rates were sufficient to cause bulk degradation.

Overall, the facile access and impressive versatility of PU materials provides a promising approach to create elastomers by exploiting tailor-made macrodiols for targeted material and degradation properties. While especially strong mechanical properties can easily be achieved, the predetermination of the hydrolytic erosion mechanism behaviour remains difficult.

1.6 Conclusions

Research on degradable polymers currently constitutes an essential branch of development and certainly it will continue to do so for decades to come. As humanity tries to limit its influence on the natural environment, as well as optimise medical care by increasing efficiency and functionality of medical

devices, materials and procedures, specifically biodegradation is an essential concept. On the one hand, some polymeric materials are indeed produced to facilitate recycling and degradation in the environment; however, recycling approaches are not implemented as intended, and the long-term effects of current bulk erosion strategies are still unclear. On the other hand, biomedical research pays special attention to the degradation of biomaterials before their application, as any complication would be severely detrimental to the patient.

Surface erosion has been identified as a promising degradation profile to avoid the unexpected physical failure of the specimen; however, thus far only few materials, like POEs, PAHs and certain PLA compositions, exhibit this degradation behaviour. Unfortunately, these compounds struggle with complex synthesis and undesirable problematic degradation products that commonly create high local acidity with the risk of inflammation and tissue damage. Additionally, the resulting material properties mostly only allow for the formation of gels to drug delivery and soft tissue applications, whereas stronger crystalline compounds pose risks of their own when breakage and sharp fragments are taken into consideration. Furthermore, complex synthesis and limited manufacturing options severely limit the application of most current materials in biomedicine, where production speed and accuracy are key.

From this perspective, additive manufacturing allows for rapid and high precision manufacturing of functional 3D devices. In fact, many hospitals, medical practices and even homes have access to such machines and regularly use this technique for the production of prototype models for training, visualisation and rarely even direct application purposes. The range of materials, however, is still very limited and often contains toxic and hazardous monomers or additives. With SLA as one of the most chemically versatile techniques, research has focused on developing suitable monomers and understanding the underlying reaction principles for further optimisation. For instance, step-growth polymerisations have been of particular interest as syntheses can be conducted without complicated setups or controlled environments, and materials are usually highly homogeneous and reliable. Thiol-ene and urethane reactions, which are among the most promising mechanisms, offer efficient coupling of functional monomers for targeted and tailored materials.

Despite the constant development in the areas outlined above, a lack of perspective towards the 'bigger picture' is apparent, with optimisation often driven within a limited field of research in chemistry, medicine, or engineering, respectively. Hence, this thesis aims to combine all mentioned areas of research to produce strong, customisable and biocompatible materials with surface erosion behaviour to be processed using additive manufacturing.

1.7 Aims and Objectives

As the central objective, this work intended to demonstrate a novel route to access polyorthoesters, which avoids previous issues in POE production and facilitates access to these promising surface-erodible polymer materials. Ultimately, the goal of the project was to develop a formulation for direct utilisation in 3D printers employed by hospitals and hobbyists to yield surface-erodible devices suitable for immediate implantation and implementation. The aims of this thesis therein focused on the development of a range of initial POETE-based materials and an assessment regarding their applicability. In particular, this work was intended to: i) establish an optimised general procedure for the production of CKA, OEs, OETEs, POETEs and analogues, as well as to confirm the identity and purity of several representative compounds, ii) provide a comprehensive overview over physical, chemical and degradation properties of an initial pool of crosslinked POETE materials to draw conclusions on their structure-function relationship, followed by the corroboration of the biocompatibility and 3D printability *via* stereolithography of these POETE materials, and finally iii) document the production and material properties of a range of recyclable, elastomeric, surface-erodible PUs based on POETE precursors.

1.8 References

(1) Geyer, R.; Jambeck, J. R.; Law, K. L., Production, use, and fate of all plastics ever made. *Sci. Adv.* **2017,** *3* (7), e1700782. doi:10.1126/sciadv.1700782

(2) Crespy, D.; Bozonnet, M.; Meier, M., 100 Years of Bakelite, the Material of a 1000 Uses. *Angew. Chem. Int. Ed.* **2008,** *47* (18), 3322-3328. doi:10.1002/anie.200704281

(3) Finkelstein, N. H., *Plastics*. Marshall Cavendish Benchmark: **2008**.

(4) Kirwan, M. J.; Strawbridge, J. W., Chapter 7: Plastics in food packaging. In *Food Packaging Technology*, Coles, R.; McDowell, D.; Kirwan, M. J., Eds. Taylor & Francis: **2003**.

(5) Maxwell, J., *Plastics in the Automotive Industry*. Elsevier Science: **1994**.

(6) Jenkins, M., *Biomedical Polymers*. Elsevier Science: **2007**.

(7) Leng, J.; Du, S., *Shape-Memory Polymers and Multifunctional Composites*. CRC Press: **2010**.

(8) Lang, S. B.; Muensit, S., Review of some lesser-known applications of piezoelectric and pyroelectric polymers. *Appl. Phys. A* **2006,** *85* (2), 125-134. doi:10.1007/s00339-006-3688-8

(9) Bernardo, C. A.; Simoes, C. L.; Pinto, L. M. C., Environmental and economic life cycle analysis of plastic waste management options. A review. *Aip. Conf. Proc.* **2016,** *1779*. doi:10.1063/1.4965581

(10) Jambeck, J. R.; Geyer, R.; Wilcox, C.; Siegler, T. R.; Perryman, M.; Andrady, A.; Narayan, R.; Law, K. L., Plastic waste inputs from land into the ocean. *Science* **2015,** *347* (6223), 768-771. doi:10.1126/science.1260352

(11) US Environmental Protection Agency (Gulf of Mexico Program) and Woods Hole Oceanographic Institution. *Marine Debris: Talking Trash & Taking Action* **2014**. (accessed **08/2019**).

(12) Eriksen, M.; Lebreton, L. C.; Carson, H. S.; Thiel, M.; Moore, C. J.; Borerro, J. C.; Galgani, F.; Ryan, P. G.; Reisser, J., Plastic Pollution in the World's Oceans: More than 5 Trillion Plastic Pieces Weighing over 250,000 Tons Afloat at Sea. *Plos One* **2014,** *9* (12), e111913. doi:10.1371/journal.pone.0111913

(13) Andrady, A. L., *Plastics and Environmental Sustainability*. Wiley: **2015**.

(14) Cressey, D., Bottles, bags, ropes and toothbrushes: the struggle to track ocean plastics. *Nature* **2016,** *536* (7616), 263-265. doi:10.1038/536263a

(15) Mintenig, S. M.; Int-Veen, I.; Löder, M. G. J.; Primpke, S.; Gerdts, G., Identification of microplastic in effluents of waste water treatment plants using focal plane array-based micro-Fourier-transform infrared imaging. *Water Res.* **2017,** *108*, 365-372. doi:10.1016/j.watres.2016.11.015

(16) Schmidt, C.; Krauth, T.; Wagner, S., Export of Plastic Debris by Rivers into the Sea. *Environ. Sci. Technol.* **2017,** *51* (21), 12246-12253. doi:10.1021/acs.est.7b02368

(17) Barnes, D. K. A.; Galgani, F.; Thompson, R. C.; Barlaz, M., Accumulation and fragmentation of plastic debris in global environments. *Philos. Trans. R. Soc. Lond. B. Biol. Sci.* **2009,** *364* (1526), 1985-1998. doi:10.1098/rstb.2008.0205

(18) Azwa, Z. N.; Yousif, B. F.; Manalo, A. C.; Karunasena, W., A review on the degradability of polymeric composites based on natural fibres. *Mater. Design* **2013,** *47*, 424-442. doi:10.1016/j.matdes.2012.11.025

(19) Göpferich, A., Mechanisms of polymer degradation and erosion. *Biomaterials* **1996,** *17* (2), 103-114. doi:10.1016/0142-9612(96)85755-3

(20) Lenz, R. W., Biodegradable polymers. In *Biopolymers I*, **1993**.

(21) Castilla-Cortázar, I.; Más-Estellés, J.; Meseguer-Dueñas, J. M.; Escobar Ivirico, J. L.; Marí, B.; Vidaurre, A., Hydrolytic and enzymatic degradation of a poly(ε-caprolactone) network. *Polym. Degrad. Stabil.* **2012,** *97* (8), 1241-1248. doi:10.1016/j.polymdegradstab.2012.05.038

(22) Banerjee, A.; Chatterjee, K.; Madras, G., Enzymatic degradation of polymers: a brief review. *Mater. Sci. Technol.* **2014,** *30* (5), 567-573. doi:10.1179/1743284713Y.0000000503

(23) Bellenger, V.; Ganem, M.; Mortaigne, B.; Verdu, J., Lifetime prediction in the hydrolytic ageing of polyesters. *Polym. Degrad. Stabil.* **1995,** *49* (1), 91-97. doi:10.1016/0141-3910(95)00049-R

(24) Delplace, V.; Nicolas, J., Degradable vinyl polymers for biomedical applications. *Nat. Chem.* **2015,** *7*, 771-784. doi:10.1038/nchem.2343

(25) Wiles, D. M.; Scott, G., Polyolefins with controlled environmental degradability. *Polym. Degrad. Stabil.* **2006,** *91* (7), 1581-1592. doi:10.1016/j.polymdegradstab.2005.09.010

(26) Ojeda, T.; Freitas, A.; Birck, K.; Dalmolin, E.; Jacques, R.; Bento, F.; Camargo, F., Degradability of linear polyolefins under natural weathering. *Polym. Degrad. Stabil.* **2011,** *96* (4), 703-707. doi:10.1016/j.polymdegradstab.2010.12.004

(27) Mersiowsky, I., Long-term fate of PVC products and their additives in landfills. *Prog. Polym. Sci.* **2002,** *27* (10), 2227-2277. doi:10.1016/S0079-6700(02)00037-0

(28) Brannigan, R. P.; Dove, A. P., Synthesis, properties and biomedical applications of hydrolytically degradable materials based on aliphatic polyesters and polycarbonates. *Biomater. Sci.* **2017,** *5* (1), 9-21. doi:10.1039/C6BM00584E

(29) Mohanty, A. K.; Misra, M.; Hinrichsen, G., Biofibres, biodegradable polymers and biocomposites: An overview. *Macromol. Mater. Eng.* **2000,** *276-277* (1), 1-24. doi:10.1002/(sici)1439-2054(20000301)276:1<1::Aid-mame1>3.0.Co;2-w

(30) Katz, J. S.; Burdick, J. A., Synthetic Biomaterials. In *Tissue Engineering: Principles and Practices*, Fisher, J. P.; Mikos, A. G.; Bronzino, J. D.; Peterson, D. R., Eds. CRC Press: **2017**.

(31) Davison, N. L.; Barrère-de Groot, F.; Grijpma, D. W., Chapter 6 - Degradation of Biomaterials. In *Tissue Engineering (Second Edition)*, Blitterswijk, C. A. V.; De Boer, J., Eds. Academic Press: Oxford, **2014**.

(32) Tamada, J. A.; Langer, R., Erosion kinetics of hydrolytically degradable polymers. *Proc. Natl. Acad. Sci.* **1993,** *90* (2), 552-556. doi:10.1073/pnas.90.2.552

(33) von Burkersroda, F.; Schedl, L.; Gopferich, A., Why degradable polymers undergo surface erosion or bulk erosion. *Biomaterials* **2002,** *23* (21), 4221-4231. doi:10.1016/S0142-9612(02)00170-9

(34) Andriano, K. P.; Tabata, Y.; Ikada, Y.; Heller, J., In vitro and in vivo comparison of bulk and surface hydrolysis in absorbable polymer scaffolds for tissue engineering. *J. Biomed. Mater. Res.* **1999,** *48* (5), 602-612. doi:10.1002/(sici)1097-4636(1999)48:5<602::Aid-jbm3>3.0.Co;2-6

(35) Heller, J.; Barr, J.; Ng, S. Y.; Abdellauoi, K. S.; Gurny, R., Poly(ortho esters): synthesis, characterization, properties and uses. *Adv. Drug. Deliv. Rev.* **2002,** *54* (7), 1015-1039. doi:10.1016/S0169-409X(02)00055-8

(36) Heller, J.; Barr, J., Poly(ortho esters) - From Concept to Reality. *Biomacromolecules* **2004,** *5* (5), 1625–1632. doi:S1525-7797(04)00049-2

(37) Heller, J.; Fritzinger, B. K.; Ng, S. Y.; Pennale, D. W. H., In vitro and in vivo release of levonorgestrel from poly(ortho esters): II. Crosslinked polymers. *J. Control. Release* **1985,** *1* (3), 233-238. doi:10.1016/0168-3659(85)90022-7

(38) Choi, N. S.; Heller, J. Drug delivery devices manufactured from poly(orthoesters) and poly(orthocarbonates). 4093709 A, 1978-6-6, 1978.

(39) Heller, J., Development of poly(ortho esters): a historical overview. *Biomaterials* **1990,** *11* (9), 659-665. doi:10.1016/0142-9612(90)90024-K

(40) Heller, J.; Penhale, D. W. H.; Helwing, R. F.; Fritzinger, B. K., Release of norethindrone from poly(ortho esters). *Polym. Eng. Sci.* **1981,** *21* (11), 727-731. doi:10.1002/pen.760211117

(41) Ng, S. Y.; Shen, H. R.; Lopez, E.; Zherebin, Y.; Barr, J.; Schacht, E.; Heller, J., Development of a poly(ortho ester) prototype with a latent acid in the polymer backbone for 5-fluorouracil delivery. *J. Control. Release* **2000,** *65* (3), 367-374. doi:10.1016/S0168-3659(99)00218-7

(42) Merkli, A.; Heller, J.; Tabatabay, C.; Gurny, R., Semi-solid hydrophobic bioerodible poly (ortho ester) for potential application in glaucoma filtering surgery. *J. Control. Release* **1994,** *29* (1), 105-112. doi:10.1016/0168-3659(94)90126-0

(43) Wang, C.; Ge, Q.; Ting, D.; Nguyen, D.; Shen, H.-R.; Chen, J.; Eisen, H. N.; Heller, J.; Langer, R.; Putnam, D., Molecularly engineered poly(ortho ester) microspheres for enhanced delivery of DNA vaccines. *Nat. Mat.* **2004,** *3* (3), 190-196. doi:10.1038/nmat1075

(44) Heller, J., Ocular delivery using poly(ortho esters). *Adv. Drug Deliver. Rev.* **2005,** *57* (14), 2053-2062. doi:10.1016/j.addr.2005.09.007

(45) Engelberg, I.; Kohn, J., Physico-mechanical properties of degradable polymers used in medical applications: A comparative study. *Biomaterials* **1991,** *12* (3), 292-304. doi:10.1016/0142-9612(91)90037-B

(46) Pogány, S. A.; Deeken, R. A.; Zentner, G. M., Gas chromatographic assay for 3,9-diethylidene-2,4,8,10 tetraoxaspiro[5.5]undecane. *J. Chromatogr. A* **1990,** *508*, 179-186. doi:10.1016/S0021-9673(00)91250-0

(47) Zhang, J.; Cui, J.; Deng, Y.; Jiang, Z.; Saltzman, W. M., Multifunctional Poly(amine-co-ester-co-ortho ester) for Efficient and Safe Gene Delivery. *ACS Biomater. Sci. Eng.* **2016,** *2* (11), 2080-2089. doi:10.1021/acsbiomaterials.6b00502

(48) Toncheva, V.; Schacht, E.; Ng, S. Y.; Barr, J.; Heller, J., Use of Block Copolymers of Poly(Ortho Esters) and Poly (Ethylene Glycol) Micellar Carriers as

Potential Tumour Targeting Systems. *J. Drug. Target.* **2003,** *11* (6), 345-353. doi:10.1080/10611860310001633839

(49) Schacht, E.; Toncheva, V.; Vandertaelen, K.; Heller, J., Polyacetal and poly(ortho ester)–poly(ethylene glycol) graft copolymer thermogels: Preparation, hydrolysis and FITC-BSA release studies. *J. Control. Release* **2006,** *116* (2), 219-225. doi:10.1016/j.jconrel.2006.07.026

(50) Paesen, B.; Baekelandt, T.; Heller, J.; Martins, J. C.; Schacht, E. H., Synthesis and complete NMR characterization of methacrylateendcapped poly(ortho-esters). *E-Polymers* **2007**. doi:10.1515/epoly.2007.7.1.1727

(51) Luo, S.; Tao, Y.; Tang, R.; Wang, R.; Ji, W.; Wang, C.; Zhao, Y., Amphiphilic block copolymers bearing six-membered ortho ester ring in side chains as potential drug carriers: synthesis, characterization, and in vivo toxicity evaluation. *J. Biomater. Sci. Polym. Ed.* **2014,** *25* (10), 965-984. doi:10.1080/09205063.2014.916095

(52) Tang, R.; Ji, W.; Panus, D.; Palumbo, R. N.; Wang, C., Block copolymer micelles with acid-labile ortho ester side-chains: Synthesis, characterization, and enhanced drug delivery to human glioma cells. *J. Control. Release* **2011,** *151* (1), 18-27. doi:10.1016/j.jconrel.2010.12.005

(53) Tang, R.; Palumbo, R. N.; Ji, W.; Wang, C., Poly(ortho ester amides): Acid-Labile Temperature-Responsive Copolymers for Potential Biomedical Applications. *Biomacromolecules* **2009,** *10* (4), 722-727. doi:10.1021/bm9000475

(54) Wei, B.; Tao, Y.; Wang, X.; Tang, R.; Wang, J.; Wang, R.; Qiu, L., Surface-Eroding Poly(ortho ester amides) for Highly Efficient Oral Chemotherapy. *ACS Appl. Mater. Inter.* **2015,** *7* (19), 10436-10445. 10.1021/acsami.5b01687

(55) Fu, S.; Yang, G.; Wang, J.; Wang, X.; Cheng, X.; Tang, R., Acid-degradable poly(ortho ester urethanes) copolymers for potential drug carriers: Preparation, characterization, in vitro and in vivo evaluation. *Polymer* **2017,** *114*, 1-14. doi:10.1016/j.polymer.2017.02.079

(56) Huang, Y.; Qin, J. J.; Wang, J.; Yan, G. Q.; Wang, X.; Tang, R. P., Dual-stimuli-sensitive poly(ortho ester disulfide urethanes)-based nanospheres with rapid intracellular drug release for enhanced chemotherapy. *Sci. China Chem.* **2018,** *61* (11), 1447-1459. doi:10.1007/s11426-018-9269-6

(57) Yang, G.; Fu, S.; Wang, X.; Wang, J.; Tang, R., pH-triggered poly(ethylene glycol) nanogels prepared through orthoester linkages as potential drug carriers. *Int. J. Polym. Mater. Po.* **2018,** *67* (18), 1059-1068. doi:10.1080/00914037.2017.1417288

(58) Cheng, X.; Qin, J.; Wang, X.; Zha, Q.; Yao, W.; Fu, S.; Tang, R., Acid-degradable lactobionic acid-modified soy protein nanogels crosslinked by ortho ester linkage for efficient antitumor in vivo. *Eur. J. Pharm. Biopharm.* **2018,** *128*, 247-258. doi:10.1016/j.ejpb.2018.05.011

(59) Bruyère, H.; Westwell, A. D.; Jones, A. T., Tuning the pH sensitivities of orthoester based compounds for drug delivery applications by simple chemical modification. *Bioorg. Med. Chem. Lett.* **2010,** *20* (7), 2200-2203. doi:10.1016/j.bmcl.2010.02.035

(60) Skrabal, A.; Ringer, O., Über die Hydrolysegeschwindigkeit des Orthoameisensäureäthyläthers. *Monatsh. Chem.* **1921,** *42* (1-2), 9-46. doi:10.1007/bf01829964

(61) Deslongchamps, P.; Chênevert, R.; Taillefer, R. J.; Moreau, C.; Saunders, J. K., The Hydrolysis of Cyclic Orthoesters. Stereoelectronic Control in the Cleavage of Hemiorthoester Tetrahedral Intermediates. *Can. J. Chem.* **1975,** *53* (11), 1601-1615. doi:10.1139/v75-226

(62) Deslongchamps, P.; Lessard, J.; Nadeau, Y., The products of hydrolysis of cyclic orthoesters as a function of pH and the theory of stereoelectronic control. *Can. J. Chem.* **1985,** *63* (9), 2485-2492. doi:10.1139/v85-412

(63) Basu, A.; Domb, A. J., Recent Advances in Polyanhydride Based Biomaterials. *Adv. Mat.* **2018,** *30* (41), 1706815. doi:10.1002/adma.201706815

(64) Anseth, K. S.; Shastri, V. R.; Langer, R., Photopolymerizable degradable polyanhydrides with osteocompatibility. *Nat. Biotechnol.* **1999,** *17* (2), 156-159. doi:10.1038/6152

(65) Determan, A. S.; Wilson, J. H.; Kipper, M. J.; Wannemuehler, M. J.; Narasimhan, B., Protein stability in the presence of polymer degradation products: Consequences for controlled release formulations. *Biomaterials* **2006,** *27* (17), 3312-3320. doi:10.1016/j.biomaterials.2006.01.054

(66) Cao, Y.; Uhrich, K. E., Salicylic Acid-Based Poly(anhydride-esters): Synthesis, Properties, and Applications. In *Green Polymer Chemistry: New Products, Processes, and Applications*, American Chemical Society: **2018**.

(67) Iñiguez-Franco, F.; Auras, R.; Ahmed, J.; Selke, S.; Rubino, M.; Dolan, K.; Soto-Valdez, H., Control of hydrolytic degradation of Poly(lactic acid) by incorporation of chain extender: From bulk to surface erosion. *Polym. Test.* **2018,** *67*, 190-196. doi:10.1016/j.polymertesting.2018.02.028

(68) da Silva, D.; Kaduri, M.; Poley, M.; Adir, O.; Krinsky, N.; Shainsky-Roitman, J.; Schroeder, A., Biocompatibility, biodegradation and excretion of polylactic acid (PLA) in medical implants and theranostic systems. *Chem. Eng. Trans.* **2018,** *340*, 9-14. doi:10.1016/j.cej.2018.01.010

(69) Li, X.; Qi, C.; Han, L.; Chu, C.; Bai, J.; Guo, C.; Xue, F.; Shen, B.; Chu, P. K., Influence of dynamic compressive loading on the in vitro degradation behavior of pure PLA and Mg/PLA composite. *Acta Biomater.* **2017,** *64*, 269-278. doi:10.1016/j.actbio.2017.08.004

(70) Vacaras, S.; Baciut, M.; Lucaciu, O.; Dinu, C.; Baciut, G.; Crisan, L.; Hedesiu, M.; Crisan, B.; Onisor, F.; Armencea, G.; Mitre, I.; Barbur, I.; Kretschmer, W.; Bran, S., Understanding the basis of medical use of poly-lactide-based resorbable polymers and composites – a review of the clinical and metabolic impact. *Drug Metab. Rev.* **2019**, 1-19. doi:10.1080/03602532.2019.1642911

(71) de Jong, S. J.; Arias, E. R.; Rijkers, D. T. S.; van Nostrum, C. F.; Kettenes-van den Bosch, J. J.; Hennink, W. E., New insights into the hydrolytic degradation of poly(lactic acid): participation of the alcohol terminus. *Polymer* **2001,** *42* (7), 2795-2802. doi:10.1016/S0032-3861(00)00646-7

(72) Kanno, T.; Sukegawa, S.; Furuki, Y.; Nariai, Y.; Sekine, J., Overview of innovative advances in bioresorbable plate systems for oral and maxillofacial surgery. *Jpn. Dent. Sci. Rev.* **2018,** *54* (3), 127-138. doi:10.1016/j.jdsr.2018.03.003

(73) Hamad, K.; Kaseem, M.; Yang, H. W.; Deri, F.; Ko, Y. G., Properties and medical applications of polylactic acid: A review. *Express Polym. Lett.* **2015,** *9* (5), 435-455. doi:10.3144/expresspolymlett.2015.42

(74) Farah, S.; Anderson, D. G.; Langer, R., Physical and mechanical properties of PLA, and their functions in widespread applications — A comprehensive

review. *Adv. Drug Deliver. Rev.* **2016,** *107*, 367-392. doi:10.1016/j.addr.2016.06.012

(75) Rupp, S.; Seil, R.; Schneider, A.; Kohn, D. M., Ligament graft initial fixation strength using biodegradable interference screws. *J. Biomed. Mater. Res.* **1999,** *48* (1), 70-74. doi:10.1002/(sici)1097-4636(1999)48:1<70::Aid-jbm12>3.0.Co;2-p

(76) Chacón, J. M.; Caminero, M. A.; García-Plaza, E.; Núñez, P. J., Additive manufacturing of PLA structures using fused deposition modelling: Effect of process parameters on mechanical properties and their optimal selection. *Mater. Design* **2017,** *124*, 143-157. doi:10.1016/j.matdes.2017.03.065

(77) Tanikella, N. G.; Wittbrodt, B.; Pearce, J. M., Tensile strength of commercial polymer materials for fused filament fabrication 3D printing. *Addit. Manuf.* **2017,** *15*, 40-47. doi:10.1016/j.addma.2017.03.005

(78) Singhvi, M. S.; Zinjarde, S. S.; Gokhale, D. V., Polylactic acid: synthesis and biomedical applications. *J. Appl. Microbiol.* **2019,** *tbd* (tbd), tbd. doi:10.1111/jam.14290

(79) Prakasam, M.; Locs, J.; Salma-Ancane, K.; Loca, D.; Largeteau, A.; Berzina-Cimdina, L., Biodegradable Materials and Metallic Implants-A Review. *J. Funct. Biomater.* **2017,** *8* (4), 44. doi:10.3390/jfb8040044

(80) Uhrich, K. E.; Cannizzaro, S. M.; Langer, R. S.; Shakesheff, K. M., Polymeric Systems for Controlled Drug Release. *Chem. Rev.* **1999,** *99* (11), 3181-3198. doi:10.1021/cr940351u

(81) Barrows, T. H., Degradable implant materials: A review of synthetic absorbable polymers and their applications. *Clin. Mater.* **1986,** *1* (4), 233-257. doi:10.1016/s0267-6605(86)80015-4

(82) Bîrcă, A.; Gherasim, O.; Grumezescu, V.; Grumezescu, A. M., Chapter 1 - Introduction in thermoplastic and thermosetting polymers. In *Materials for Biomedical Engineering*, Grumezescu, V.; Grumezescu, A. M., Eds. Elsevier: **2019**.

(83) Petzold, R.; Zeilhofer, H. F.; Kalender, W. A., Rapid prototyping technology in medicine—basics and applications. *Comput. Med. Imag. Grap.* **1999,** *23* (5), 277-284. doi:10.1016/S0895-6111(99)00025-7

(84) Ligon, S. C.; Liska, R.; Stampfl, J.; Gurr, M.; Mülhaupt, R., Polymers for 3D Printing and Customized Additive Manufacturing. *Chem. Rev.* **2017,** *117* (15), 10212-10290. doi:10.1021/acs.chemrev.7b00074

(85) Kruth, J. P.; Leu, M. C.; Nakagawa, T., Progress in Additive Manufacturing and Rapid Prototyping. *CIRP Ann.* **1998,** *47* (2), 525-540. doi:10.1016/S0007-8506(07)63240-5

(86) Conner, B. P.; Manogharan, G. P.; Martof, A. N.; Rodomsky, L. M.; Rodomsky, C. M.; Jordan, D. C.; Limperos, J. W., Making sense of 3-D printing: Creating a map of additive manufacturing products and services. *Addit. Manuf.* **2014,** *1-4*, 64-76. doi:10.1016/j.addma.2014.08.005

(87) Petrovic, V.; Haro Gonzalez, J. V.; Jordá Ferrando, O.; Delgado Gordillo, J.; Blasco Puchades, J. R.; Portolés Griñan, L., Additive layered manufacturing: sectors of industrial application shown through case studies. *Int. J. Prod. Res.* **2010**. doi:10.1080/00207540903479786

(88) Melchels, F. P. W.; Domingos, M. A. N.; Klein, T. J.; Malda, J.; Bartolo, P. J.; Hutmacher, D. W., Additive manufacturing of tissues and organs. *Prog. Polym. Sci.* **2012,** *37* (8), 1079–1104. 10.1016/j.progpolymsci.2011.11.007

(89) Lee, J.-Y.; An, J.; Chua, C. K., Fundamentals and applications of 3D printing for novel materials. *Appl. Mater. Today* **2017,** *7*, 120-133. doi:10.1016/j.apmt.2017.02.004

(90) Stansbury, J. W.; Idacavage, M. J., 3D printing with polymers: Challenges among expanding options and opportunities. *Dent. Mater.* **2016,** *32* (1), 54-64. doi:10.1016/j.dental.2015.09.018

(91) Watters, M. P.; Bernhardt, M. L., Curing parameters to improve the mechanical properties of stereolithographic printed specimens. *Rapid Prototyping J.* **2018,** *24* (1), 46-51. doi:10.1108/Rpj-11-2016-0180

(92) Melchels, F. P. W.; Feijen, J.; Grijpma, D. W., A review on stereolithography and its applications in biomedical engineering. *Biomaterials* **2010,** *31* (24), 6121-6130. doi:10.1016/j.biomaterials.2010.04.050

(93) Harris, M.; Potgieter, J.; Archer, R.; Arif, K. M., Effect of Material and Process Specific Factors on the Strength of Printed Parts in Fused Filament Fabrication: A Review of Recent Developments. *Materials (Basel)* **2019,** *12* (10). doi:10.3390/ma12101664

(94) de Leon, A. C.; Chen, Q.; Palaganas, N. B.; Palaganas, J. O.; Manapat, J.; Advincula, R. C., High performance polymer nanocomposites for additive

manufacturing applications. *React. Funct. Polym.* **2016,** *103*, 141-155. doi:10.1016/j.reactfunctpolym.2016.04.010

(95) Abrusci, C.; Pablos, J. L.; Marín, I.; Espí, E.; Corrales, T.; Catalina, F., Photodegradation and biodegradation by bacteria of mulching films based on ethylene-vinyl acetate copolymer: Effect of pro-oxidant additives. *J. Appl. Polym. Sci.* **2012,** *126* (5), 1664-1675. doi:10.1002/app.36989

(96) Scalenghe, R., Resource or waste? A perspective of plastics degradation in soil with a focus on end-of-life options. *Heliyon* **2018,** *4* (12), e00941. doi:10.1016/j.heliyon.2018.e00941

(97) Lackner, M., Bioplastics. In *Kirk-Othmer Encyclopedia of Chemical Technology*, **2015**.

(98) Wu, W. M.; Yang, J.; Criddle, C. S., Microplastics pollution and reduction strategies. *Front. Env. Sci. Eng.* **2017,** *11* (1). doi:10.1007/s11783-017-0897-7

(99) Tao, Y.; Wang, H.; Li, Z.; Li, P.; Shi, S. Q., Development and Application of Wood Flour-Filled Polylactic Acid Composite Filament for 3D Printing. *Materials* **2017,** *10* (4), 339. doi:10.3390/ma10040339

(100) Jones, R.; Haufe, P.; Sells, E.; Iravani, P.; Olliver, V.; Palmer, C.; Bowyer, A., RepRap – the replicating rapid prototyper. *Robotica* **2011,** *29* (1), 177-191. doi:10.1017/S026357471000069X

(101) Bártolo, P. J., *Stereolithography: Materials, Processes and Applications*. Springer, Boston, MA: Boston, MA, **2011**.

(102) Gong, H.; Beauchamp, M.; Perry, S.; Woolley, A. T.; Nordin, G. P., Optical approach to resin formulation for 3D printed microfluidics. *RSC Adv.* **2015,** *5* (129), 106621-106632. doi:10.1039/C5RA23855B

(103) Lebedevaite, M.; Ostrauskaite, J.; Skliutas, E.; Malinauskas, M., Photoinitiator Free Resins Composed of Plant-Derived Monomers for the Optical μ-3D Printing of Thermosets. *Polymers (Basel)* **2019,** *11* (1). doi:10.3390/polym11010116

(104) Miezinyte, G.; Ostrauskaite, J.; Rainosalo, E.; Skliutas, E.; Malinauskas, M., Photoresins based on acrylated epoxidized soybean oil and benzenedithiols for optical 3D printing. *Rapid Prototyping J.* **2019,** *25* (2), 378-387. doi:10.1108/rpj-04-2018-0101

(105) Ligon-Auer, S. C.; Schwentenwein, M.; Gorsche, C.; Stampfl, J.; Liska, R., Toughening of photo-curable polymer networks: a review. *Polym. Chem.* **2016,** *7* (2), 257-286. doi:10.1039/C5PY01631B

(106) Popal, M.; Volk, J.; Leyhausen, G.; Geurtsen, W., Cytotoxic and genotoxic potential of the type I photoinitiators BAPO and TPO on human oral keratinocytes and V79 fibroblasts. *Dent. Mater.* **2018,** *34* (12), 1783-1796. doi:10.1016/j.dental.2018.09.015

(107) Ikemura, K.; Endo, T., A review of the development of radical photopolymerization initiators used for designing light-curing dental adhesives and resin composites. *Dent. Mater. J.* **2010,** *29* (5), 1009140075. doi:10.4012/dmj.2009-137

(108) Skliutas, E.; Kasetaite, S.; Jonušauskas, L.; Ostrauskaite, J.; Malinauskas, M., Photosensitive naturally derived resins toward optical 3-D printing. *Opt. Eng.* **2018,** *57* (4), 1-9. doi:10.1117/1.OE.57.4.041412

(109) Decker, C.; Moussa, K., Kinetic study of the cationic photopolymerization of epoxy monomers. *J. Polym. Sci. A Polym. Chem.* **1990,** *28* (12), 3429-3443. doi:10.1002/pola.1990.080281220

(110) Esposito Corcione, C.; Greco, A.; Maffezzoli, A., Photopolymerization kinetics of an epoxy-based resin for stereolithography. *J. Appl. Polym. Sci.* **2004,** *92* (6), 3484-3491. doi:10.1002/app.20347

(111) Barker, I. A.; Ablett, M. P.; Gilbert, H. T. J.; Leigh, S. J.; Covington, J. A.; Hoyland, J. A.; Richardson, S. M.; Dove, A. P., A microstereolithography resin based on thiol-ene chemistry: towards biocompatible 3D extracellular constructs for tissue engineering. *Biomater. Sci.* **2014,** *2* (4), 472-475. doi:10.1039/C3BM60290G

(112) Carve, M.; Wlodkowic, D., 3D-Printed Chips: Compatibility of Additive Manufacturing Photopolymeric Substrata with Biological Applications. *Micromachines (Basel)* **2018,** *9* (2), 91. doi:10.3390/mi9020091

(113) Zarek, M.; Mansour, N.; Shapira, S.; Cohn, D., 4D Printing of Shape Memory-Based Personalized Endoluminal Medical Devices. *Macromol. Rapid Commun.* **2017,** *38* (2), 1600628. doi:10.1002/marc.201600628

(114) Yu, R.; Yang, X.; Zhang, Y.; Zhao, X.; Wu, X.; Zhao, T.; Zhao, Y.; Huang, W., Three-Dimensional Printing of Shape Memory Composites with Epoxy-Acrylate

Hybrid Photopolymer. *ACS Appl. Mater. Inter.* **2017,** *9* (2), 1820-1829. doi:10.1021/acsami.6b13531

(115) Kolb, H. C.; Finn, M. G.; Sharpless, B. K., Click Chemistry: Diverse Chemical Function from a Few Good Reactions. *Angew. Chem. Int. Ed.* **2001,** *40* (11), 2004-2021. doi:10.1002/1521-3773(20010601)40:11<2004::AID-ANIE2004>3.0.CO;2-5

(116) Barner-Kowollik, C.; Du Prez, F. E.; Espeel, P.; Hawker, C. J.; Junkers, T.; Schlaad, H.; Van Camp, W., "Clicking" Polymers or Just Efficient Linking: What Is the Difference? *Angew. Chem. Int. Ed.* **2011,** *50* (1), 60-62. doi:10.1002/anie.201003707

(117) Nuyken, O.; Pask, S. D., Ring-Opening Polymerization—An Introductory Review. *Polymers* **2013,** *5* (2), 361-403. doi:10.3390/polym5020361

(118) Jérôme, C.; Lecomte, P., Recent advances in the synthesis of aliphatic polyesters by ring-opening polymerization. *Adv. Drug Deliver. Rev.* **2008,** *60* (9), 1056-1076. doi:10.1016/j.addr.2008.02.008

(119) Qian, H.; Wohl, A. R.; Crow, J. T.; Macosko, C. W.; Hoye, T. R., A Strategy for Control of "Random" Copolymerization of Lactide and Glycolide: Application to Synthesis of PEG-b-PLGA Block Polymers Having Narrow Dispersity. *Macromolecules* **2011,** *44* (18), 7132-7140. doi:10.1021/ma201169z

(120) Dechy-Cabaret, O.; Martin-Vaca, B.; Bourissou, D., Controlled Ring-Opening Polymerization of Lactide and Glycolide. *Chem. Rev.* **2004,** *104* (12), 6147-6176. doi:10.1021/cr040002s

(121) Billiet, L.; Fournier, D.; Du Prez, F., Step-growth polymerization and 'click' chemistry: The oldest polymers rejuvenated. *Polymer* **2009,** *50* (16), 3877-3886. doi:10.1016/j.polymer.2009.06.034

(122) Flory, P. J., Fundamental Principles of Condensation Polymerization. *Chem. Rev.* **1946,** *39* (1), 137-197. doi:10.1021/cr60122a003

(123) Chiefari, J.; Chong, Y. K.; Ercole, F.; Krstina, J.; Jeffery, J.; Le, T. P. T.; Mayadunne, R. T. A.; Meijs, G. F.; Moad, C. L.; Moad, G.; Rizzardo, E.; Thang, S. H., Living Free-Radical Polymerization by Reversible Addition−Fragmentation Chain Transfer: The RAFT Process. *Macromolecules* **1998,** *31* (16), 5559-5562. doi:10.1021/ma9804951

(124) Tan, S.; Li, D.; Zhang, Y.; Niu, Z.; Zhang, Z., Base Catalyzed Thiol–Ene Click Chemistry toward Inner -CH=CF- Bonds for Controlled Functionalization of Poly(vinylidene fluoride). *Macromol. Chem. Phys.* **2018,** *219* (11), 1700632. doi:10.1002/macp.201700632

(125) Lowe, A. B., Thiol-ene "click" reactions and recent applications in polymer and materials synthesis: a first update. *Polym. Chem.* **2014,** *5* (17), 4820-4870. doi:10.1039/c4py00339j

(126) Worrell, B. T.; McBride, M. K.; Lyon, G. B.; Cox, L. M.; Wang, C.; Mavila, S.; Lim, C.-H.; Coley, H. M.; Musgrave, C. B.; Ding, Y.; Bowman, C. N., Bistable and photoswitchable states of matter. *Nat. Commun.* **2018,** *9* (1), 2804. doi:10.1038/s41467-018-05300-7

(127) Leonards, H.; Engelhardt, S.; Hoffmann, A.; Pongratz, L.; Schriever, S.; Bläsius, J.; Wehner, M. M.; Gillner, A., Advantages and drawbacks of Thiol-ene based resins for 3D-printing, *Proc. SPIE 9353*, Laser 3D Manufacturing II, **2015** *93530F*. doi:10.1117/12.2081169

(128) Sangermano, M.; Malucelli, G.; Delleani, G.; Priola, A., Bicyclo-orthoester as a low-shrinkage additive in cationic UV curing. *Polym. Int.* **2007,** *56* (10), 1224-1229. doi:10.1002/pi.2263

(129) Hoyle, C. E.; Lee, T. Y.; Roper, T., Thiol–enes: Chemistry of the past with promise for the future. *J. Polym. Sci. A Polym. Chem.* **2004,** *42* (21), 5301-5338. doi:10.1002/pola.20366

(130) Lalevée, J.; Fouassier, J. P., *Photopolymerisation Initiating Systems*. Royal Society of Chemistry: **2018**.

(131) Fairbanks, B. D.; Singh, S. P.; Bowman, C. N.; Anseth, K. S., Photodegradable, Photoadaptable Hydrogels via Radical-Mediated Disulfide Fragmentation Reaction. *Macromolecules* **2011,** *44* (8), 2444-2450. doi:10.1021/ma200202w

(132) Grim, J. C.; Marozas, I. A.; Anseth, K. S., Thiol-ene and photo-cleavage chemistry for controlled presentation of biomolecules in hydrogels. *J. Control. Release* **2015,** *219*, 95-106. doi:10.1016/j.jconrel.2015.08.040

(133) Kharkar, P. M.; Rehmann, M. S.; Skeens, K. M.; Maverakis, E.; Kloxin, A. M., Thiol-ene click hydrogels for therapeutic delivery. *ACS Biomater. Sci. Eng.* **2016,** *2* (2), 165-179. doi:10.1021/acsbiomaterials.5b00420

(134) Wang, J.; Wang, X.; Yan, G.; Fu, S.; Tang, R., pH-sensitive nanogels with ortho ester linkages prepared via thiol-ene click chemistry for efficient intracellular drug release. *J. Colloid Interface Sci.* **2017,** *508*, 282-290. doi:10.1016/j.jcis.2017.08.051

(135) Poetz, K. L.; Mohammed, H. S.; Shipp, D. A., Surface Eroding, Semicrystalline Polyanhydrides via Thiol–Ene "Click" Photopolymerization. *Biomacromolecules* **2015,** *16* (5), 1650-1659. doi:10.1021/acs.biomac.5b00280

(136) Shih, H.; Lin, C.-C., Cross-Linking and Degradation of Step-Growth Hydrogels Formed by Thiol–Ene Photoclick Chemistry. *Biomacromolecules* **2012,** *13* (7), 2003-2012. doi:10.1021/bm300752j

(137) Sarapas, J. M.; Tew, G. N., Poly(ether–thioethers) by Thiol–Ene Click and Their Oxidized Analogues as Lithium Polymer Electrolytes. *Macromolecules* **2016,** *49* (4), 1154-1162. doi:10.1021/acs.macromol.5b02513

(138) Chen, L.; Wu, Q.; Wei, G.; Liu, R.; Li, Z., Highly stable thiol–ene systems: from their structure–property relationship to DLP 3D printing. *J. Mater. Chem. C* **2018,** *6* (43), 11561-11568. doi:10.1039/C8TC03389G

(139) Morgan, C. R.; Magnotta, F.; Ketley, A. D., Thiol/ene photocurable polymers. *J. Polym. Sci. A Polym. Chem.* **1977,** *15* (3), 627-645. doi:10.1002/pol.1977.170150311

(140) Akindoyo, J. O.; Beg, M. D. H.; Ghazali, S.; Islam, M. R.; Jeyaratnam, N.; Yuvaraj, A. R., Polyurethane types, synthesis and applications – a review. *RSC Adv.* **2016,** *6* (115), 114453-114482. doi:10.1039/C6RA14525F

(141) Bayer, O., Das Di-Isocyanat-Polyadditionsverfahren (Polyurethane). *Angew. Chem.* **1947,** *59* (9), 257-272. doi:10.1002/ange.19470590901

(142) Silva, A. L.; Bordado, J. C., Recent Developments in Polyurethane Catalysis: Catalytic Mechanisms Review. *Catal. Rev.* **2004,** *46* (1), 31-51. doi:10.1081/CR-120027049

(143) Kausar, A., Polyurethane Composite Foams in High-Performance Applications: A Review. *Polymer Plast. Technol. Eng.* **2018,** *57* (4), 346-369. doi:10.1080/03602559.2017.1329433

(144) Sardon, H.; Pascual, A.; Mecerreyes, D.; Taton, D.; Cramail, H.; Hedrick, J. L., Synthesis of Polyurethanes Using Organocatalysis: A Perspective. *Macromolecules* **2015,** *48* (10), 3153-3165. doi:10.1021/acs.macromol.5b00384

(145) Alsarraf, J.; Ammar, Y. A.; Robert, F.; Cloutet, E.; Cramail, H.; Landais, Y., Cyclic Guanidines as Efficient Organocatalysts for the Synthesis of Polyurethanes. *Macromolecules* **2012,** *45* (5), 2249-2256. doi:10.1021/ma2026258

(146) Szycher, M., *Szycher's Handbook of Polyurethanes, First Edition*. Taylor & Francis: **1999**.

(147) Harrell, L. L., Segmented Polyurethans. Properties as a Funcation of Segment Size and Distribution. *Macromolecules* **1969,** *2* (6), 607-612. doi:10.1021/ma60012a008

(148) O'Sickey, M. J.; Lawrey, B. D.; Wilkes, G. L., Structure–property relationships of poly(urethane urea)s with ultra-low monol content poly(propylene glycol) soft segments. I. Influence of soft segment molecular weight and hard segment content. *J. Appl. Polym. Sci.* **2002,** *84* (2), 229-243. doi:10.1002/app.10168

(149) Flory, P. J., Thermodynamics of Crystallization in High Polymers. I. Crystallization Induced by Stretching. *J. Chem. Phys.* **1947,** *15* (6), 397-408. doi:10.1063/1.1746537

(150) Kalita, H., *Shape Memory Polymers: Theory and Application*. De Gruyter: **2018**.

(151) Pandya, M. V.; Deshpande, D. D.; Hundiwale, D. G., Effect of diisocyanate structure on viscoelastic, thermal, mechanical and electrical properties of cast polyurethanes. *J. Appl. Polym. Sci.* **1986,** *32* (5), 4959-4969. doi:10.1002/app.1986.070320518

(152) Lee, D.-K.; Tsai, H.-B., Properties of segmented polyurethanes derived from different diisocyanates. *J. Appl. Polym. Sci.* **2000,** *75* (1), 167-174. doi:10.1002/(sici)1097-4628(20000103)75:1<167::Aid-app19>3.0.Co;2-n

(153) Darby, T. D.; Johnson, H. J.; Northup, S. J., An evaluation of a polyurethane for use as a medical grade plastic. *Toxicol. Appl. Pharm.* **1978,** *46* (2), 449-453. doi:10.1016/0041-008X(78)90090-X

(154) Shintani, H.; Nakamura, A., Analysis of a Carcinogen, 4,4′-Methylenedianiline, from Thermosetting Polyurethane during Sterilization. *J. Anal. Toxicol.* **1989,** *13* (6), 354-357. doi:10.1093/jat/13.6.354

(155) Singhal, P.; Small, W.; Cosgriff-Hernandez, E.; Maitland, D. J.; Wilson, T. S., Low density biodegradable shape memory polyurethane foams for embolic

biomedical applications. *Acta Biomater.* **2014,** *10* (1), 67-76. doi:10.1016/j.actbio.2013.09.027

2

Synthesis of Rapidly Surface Eroding Polyorthoesters and Polyacetals Using Thiol-Ene Click Chemistry

2.1 Abstract

Polyorthoesters are generally considered to be highly biocompatible, surface eroding materials. However, sensitive intermediates and poor mechanical performance have largely prevented their wide-spread application to date. Herein, a simple and versatile method to synthesise orthoester- and acetal-based polymers is presented. Using 2-methylene-1,3-dioxe-5-pene as a stable bifunctional monomer, sequential highly selective 'click' reactions led initially to the formation of orthoesters (OE) in a Markovnikov alcohol addition or acetals (AT) via anti-Markovnikov thiol-ene addition. Subsequent photo-initiated thiol addition onto the remaining endocyclic and backbone alkene functionalities led to thioether (TE) formation to produce a novel class of poly(orthoester-thioether)s (POETEs) or poly(acetal-thioether)s (PATTEs) via step-growth polymerisation. While all obtained polymers were found to possess a weight-average molecular weight of above 10 kDa, the application of an OE monomer with additional double bond functionality led to a cross-linked polymer network, which displayed surface erosion behaviour.

2.2 Introduction

Control over the hydrolytic and biodegradation properties of polymeric materials has been a major focus in the biomedical field for decades. These studies range from early composite-materials that contain natural and naturally-derived polymers,[1-2] to biodegradable polyesters and polycarbonates,[3-5] and include the manufacturing of functional devices and materials.[6-7] A vast majority of degradable polymers such as polyesters, exemplified by polylactide and its copolymers, degrade *via* a bulk erosion mechanism, which restricts control over structural integrity and release time of incorporated drugs, as well as providing limited protection of the load against hydrolysis.[8] Preferentially, a controlled surface erosion in which the material degrades slowly from the surface inwards,[9] presents a more desirable mechanism by which to retain integrity throughout their lifetime,[10] as well as to deliver encapsulated molecules in a more controlled manner.[11-13] The underlying reason for surface erosion can commonly be found in the molecular structure of the polymer in which a generally hydrophobic structure is combined with hydrolysable linkages. Depending on the reactivity of

the hydrolysable bond and diffusion of water into the material, differences in both time and depth of the surface erosion can be observed.[14-15]

Despite the desirable nature of surface eroding materials, examples are largely limited to polycarbonates,[16] polyanhydrides,[17] polyacetals (PATs)[18-20] and polyorthoesters (POEs)[21-22] with polyanhydrides remaining the only biodegradable surface eroding material in FDA-approved systems.[23] While the reasons for the slow translation of these materials are multifaceted and complex, one of the major limitations to their wider study and uptake is no doubt a result of the complex syntheses and lack of customisability, as well as the low mechanical strength of devices made from these materials.[24]

Simple polyacetals such as polyoxymethylene (POM) have commonly been obtained from condensation reactions of aldehydes and diols, which can be as simple as formaldehyde in aqueous solution.[25] Similarly, by transesterification of cyclic orthoesters or trimethylorthoformate, a range of POEs have been reported.[26] While well known, these approaches provide a limited scope of possible polymer structures which in turn limit the materials properties that can be accessed from them. Moreover, such methods are inherently time and energy demanding as a constant distillation of condensate is required. However, customisability of the resulting chain polymers can be significantly enhanced *via* the use of alkenyl precursors and alcohol addition pathways.[27-28] Unfortunately, a lack of stability of the dimeric ketene acetal precursors, as well as complexities in alternative ring-opening approaches,[29-30] have limited industrial applications so far and only allowed for selected alcohol-containing precursors[28, 31] or copolymers[20, 32] to arise. While Ru-catalysed approaches such as the *in situ* double bond shift that Dove and co-workers reported,[31] or the ROMP methodology reported by Wurm and co-workers,[33] have allowed a wider range of POEs to be accessed through simple procedures, the development of milder, less expensive and non-toxic catalytic routes are required to further advance the field.

Considering the increasing importance of the highly efficient family of 'click' reactions,[34] thiol-ene coupling promises to provide a feasible and versatile route to unique POE- and PAT-based materials.[30, 35] Despite instances where this pathway did not strictly match 'click' specifications,[36] its application for the

synthesis of symmetric dendrimers, hybrid hydrogels and nanoparticles presents it as a useful and highly customisable addition reaction that provides opportunity to create and modify new polymers,[37-39] but also provides potential for application in nano-patterning,[40-41] thermo-responsive materials[42] and additive manufacturing.[43-44] Herein, reported is a simple route to poly(orthoester-thioester)s, POETEs, and poly(acetal-thioester)s, PATTEs *via* a stable orthoester or acetal intermediate that can be accessed on a multi-gram scale without the need for inert atmosphere. By utilizing the orthogonal reactivity of double-bonds in the 2-methylene-1,3-dioxe-5-pene cyclic ketene acetal (CKA), an orthoester or acetal bond can be formed before undertaking a radical thiol-ene addition reaction to form more complex products or polymers. Mild reaction conditions and the high orthogonality of double bond reactivity allow for a range of different orthoester and acetal compounds to be isolated in good yield. The formation of a surface-eroding polymer material further underlines how this technique could have wider applications in the biomedical materials field.

2.3 Results and Discussion

2.3.1 Synthesis of Small Molecules

Synthesis of the cyclic ketene acetal (CKA) 2-methylene-1,3-dioxe-5-pene (**2**) was undertaken as previously described by Plikk *et al.*[45] Briefly, 2-bromo-1,1-dimethoxyethane and butene-1,4-diolwere reacted *via* a transesterification condensation to form cyclic BrCKA (**1**), followed by dehydrohalogenation with potassium tert-butoxide. The resulting CKA is highly hydrophobic and stable to air and moisture indefinitely in bulk when stored below ambient temperature.

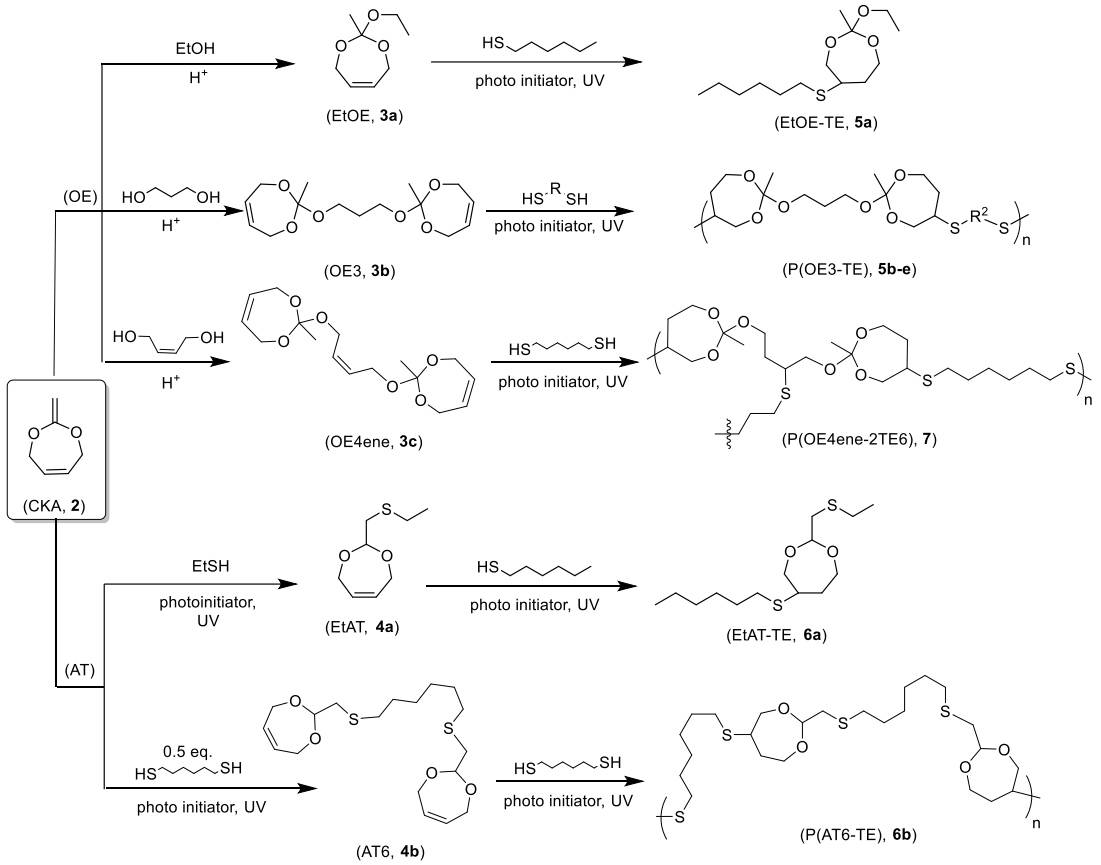

Scheme 2-1. Synthesis of a mono- and difunctional OEs and ATs, followed by thiol addition to form the respective TEs (small molecules, chain polymers and crosslinked networks). b: R = $HS(CH_2)_6SH$; c: R = $HS(CH_2CH_2O)_2CH_2CH_2SH$; d: R= $HS(CH_2)_3O(CO)CH_2CH_2(CO)O(CH_2)_3SH$; e: R = $HSCH_2CH(OH)CH(OH)CH_2SH$.

While CKAs such as **2** (Scheme 2-1) are susceptible to catalysed radical ring-opening polymerisation to form polyesters,[45] the exocyclic double bond in the ketene acetal functional group can also be subjected to a highly efficient acid-catalysed addition of nucleophiles such as alcohols.[46] The quantitative and rapid nature of the reaction compares favourably to several 'click' reactions.[34] Our initial studies focused on probing the efficiency of this reaction by addition of ethanol and ethanethiol to **2** as exemplary a primary alcohol and thiol to form the orthoester and acetal products **3a** and **4a**. These additions demonstrate the selective addition to Markovnikov and anti-Markovnikov products, respectively. Subsequently, the thiol-ene addition of hexanethiol to the endocyclic double-bond was performed to yield the respective thioethers **5a** and **6a**.

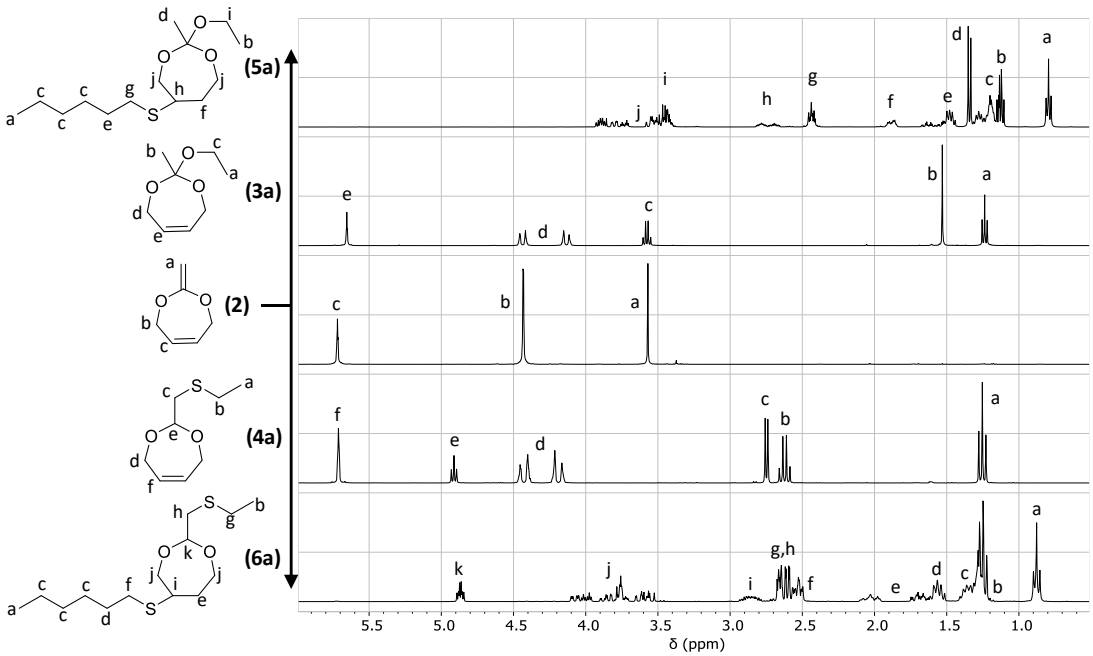

Figure 2-1. ^{1}H NMR spectra of small molecule CKA (**2**), OE (**3a**), AT (**4a**) and respective OE-TE (**5a**) and AT-TE (**6a**) ($CDCl_3$, 400 MHz, 298 K).

Comparison of the initial OE (**3a**) and AT (**4a**) products with the CKA (**2**) by ^{1}H NMR spectroscopy (Figure 2-1) revealed a significant splitting in the signals corresponding to the allylic protons between δ = 4.1-4.5 ppm. This is likely a result of the ring strain, which is amplified by the steric tension in the adjacent orthoester functionality compared to a less strained acetal functionality, ultimately leading to a difference in chemical shift of δ = 0.21 ppm in the OE spectrum, whereas a difference of only δ = 0.13 ppm is observed in the AT spectrum. Furthermore, a distinct coupling of the geminal protons into doublets with coupling constants of around J = 16 Hz occurs. In contrast, the vinylic protons show only a minor difference in chemical shift between the CKA and the products. Again however, a slightly larger difference in observed for the OE analogue, likely attributed to the higher ring strain. Both the splitting and coupling are also present in the final TE products (**5a** and **6a**), which in addition to the stereoisomer formation impedes the identification and assignment of signals significantly. Nevertheless, a batch assignment of signals to the respective protons was supported by two-dimensional NMR spectra and revealed a broad splitting and complex coupling pattern of the former allylic protons over up to 0.6 ppm between δ = 4.1 and 3.4 ppm. As a direct consequence of the differences in ring strain and electron density shifts in the stereoisomeric product, most

signals close to the ring appear doubled, with the most significant distinction found in the tertiary proton geminal to the newly formed thioether bond at around δ = 2.7 ppm. A shift difference of around 0.1 ppm permits the calculation of a relative quantity of the OE-TE (**5a**) diastereoisomers *via* integration of these signals, which reveals nearly equal proportion and hence suggests that there is no significant preference of the formation of either isomer. In contrast, the smaller corresponding shift difference between AT-TE isomers (**6a**) does not provide sufficient distinction.

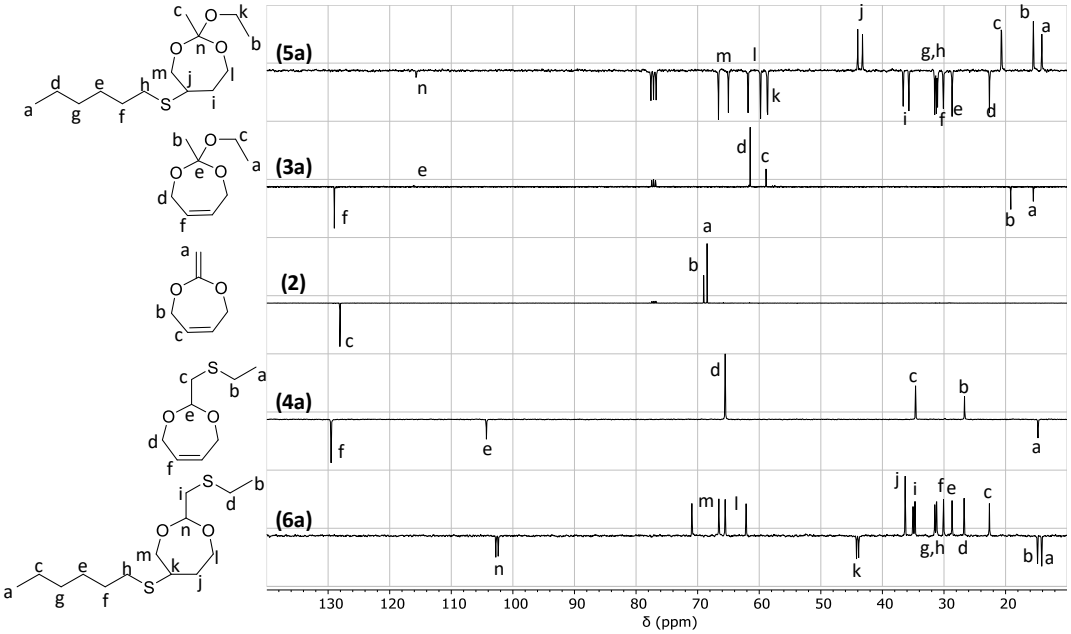

Figure 2-2. ^{13}C NMR spectra of small molecule CKA (**2**), OE (**3a**), AT (**4a**) and respective OE-TE (**5a**) and AT-TE (**6a**) ($CDCl_3$, 300 MHz, 298 K).

The assignments were further confirmed *via* ^{13}C NMR spectroscopy (Figure 2-2), with no splitting in the simple OE and AT, but rather significant differentiation in the TE products as a consequence of diastereoisomer formation. Nevertheless, the above observations clearly support the characterisation of the mechanism as a 'click' reaction after Sharpless, as no significant amount of side products were discovered after complete distillation of crude product, after a short reaction time to full conversion.[34]

2.3.2 Chain Polymerisation

In order to access OE- and AT- containing polymers, a dimeric OE (**3b**) and AT (**4b**) were synthesised by the addition of propane-1,3-diol or hexane-1,6-dithiol

to **2**, respectively. Subsequent polyaddition of the endocyclic double bonds with hexane-1,6-dithiol under radical conditions led to polymer formation (Scheme 2-1). As in the small molecule reactions, stoichiometric conditions and only catalytic amounts of initiator led to full conversion within a few hours. Noticeably, even the formation of the AT (**4b**) was almost completely selective under these conditions and only yielded polymer when excess thiol was used.

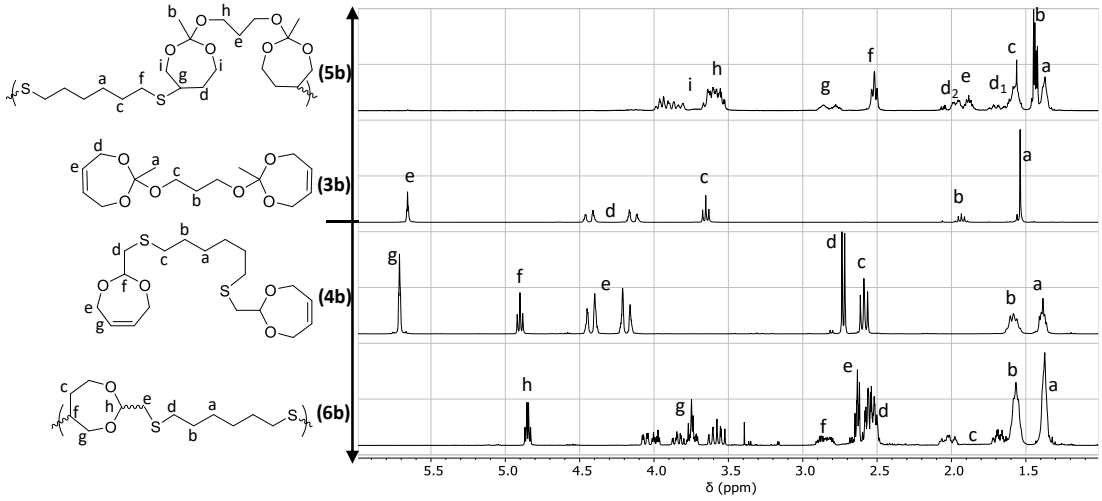

Figure 2-3. ^{1}H NMR spectra of bifunctional OE (**3a**) and AT (**4a**), and respective polymers OE-TE (**5a**) and AT-TE (**6a**) ($CDCl_3$, 400 MHz, 298 K).

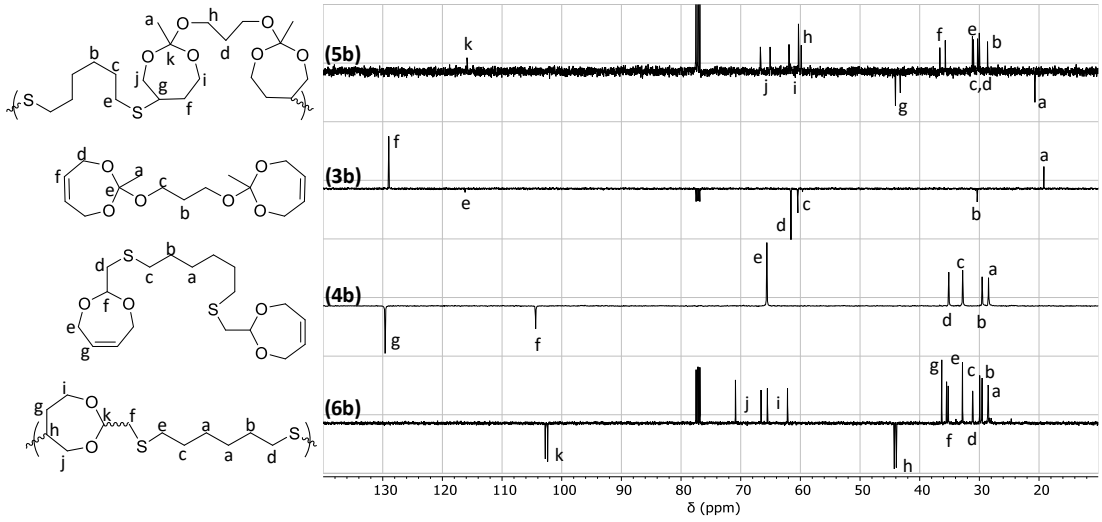

Figure 2-4. ^{13}C NMR spectra of bifunctional OE (**3a**) and AT (**4a**), and respective polymers OE-TE (**5a**) and AT-TE (**6a**) ($CDCl_3$, 300 MHz, 298 K).

Analysis of the resultant polymers by ^{1}H NMR spectroscopy revealed an analogous shift pattern for the dimers (**3b**, **4b**) and polymers (**5b**, **6b**, Figure 2-3) compared to those obtained for the small molecules (Figure 2-1). The significant difference in shift and distinct coupling pattern for the allylic protons was

maintained, as well as the even broader splitting in the formerly vinylic and allylic protons following thiol-ene coupling. Doubling of signals corresponding to stereoisomer formation can also be observed. Only negligible amounts of side products remain, specifically at δ = 2.8 ppm for the AT, which is probably caused by a small amount of endocyclic thiol-ene coupling products. Furthermore, under stoichiometric conditions the ^{1}H NMR spectra suggest full conversion into the respective polymers, as any signal for remaining endocyclic double bonds is below the detection threshold. Respective ^{13}C NMR spectra (Figure 2-4) confirm the absence of significant amounts of side products. A reoccurring issue however in ^{1}H NMR spectra is a resonance just above δ = 2.0 ppm. This is attributed to the presence of degradation products as a consequence of contact with acidic substances or substrates, such as untreated glass surfaces and chloroform, and increases over time. The most likely structures causing this resonance are acetic acid and derived esters, which is in accordance with proposed degradation mechanisms of the methylated orthoesters.[27] In order to further demonstrate the versatility of the polymerisation mechanism, a variety of other dithiol linkers were also chosen and employed in polymer formation (Scheme 2-1).

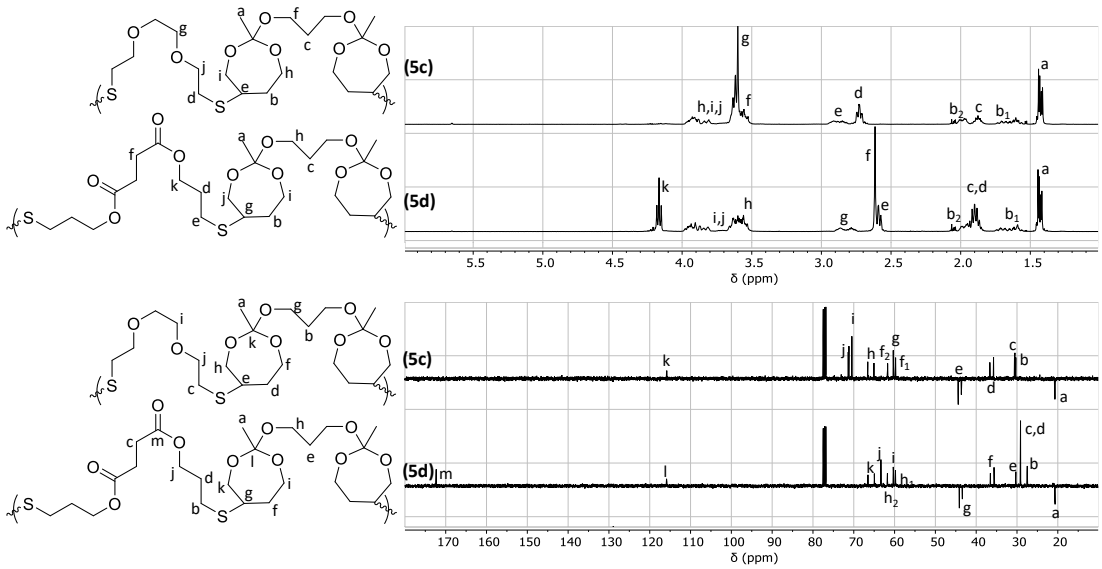

Figure 2-5. ^{1}H (top) and ^{13}C (bottom) NMR spectra of OE-TE polymer chains from thiolated ethylene glycol and succinate linkers (**5c** and **5d**) ($CDCl_3$, 300 MHz, 298 K).

^{1}H and ^{13}C NMR spectra (Figure 2-5) showed a signal pattern of both thiolated ethylene glycol (**5c**) and succinate (**5d**) linkers in accordance with the simple alkane analogue (**5b**), consisting of a complex splitting attributed to the

diastereomers. During sample preparation it was noted that prolonged exposure to air led to an increase in viscosity for these samples presumably by oxidative crosslinking, which resulted in solubility issues but barely affected the obtained NMR spectra. Unfortunately, the reaction with dithiothreitol did not lead to significant conversion either way and was disregarded for this analysis.

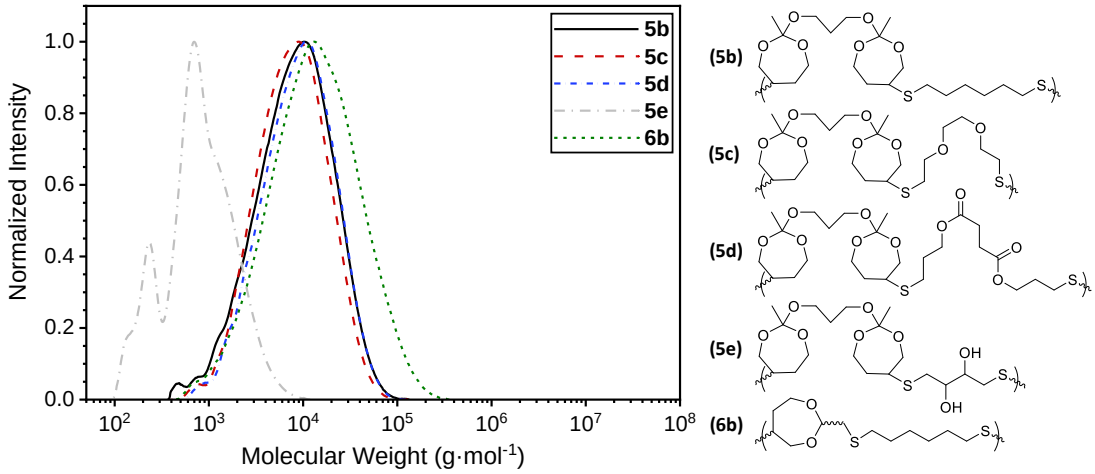

Figure 2-6. Size Exclusion Chromatograms of different POETE and PATTE polymers and oligomers (thiol end-capped, molecular weight determined in THF with 2 vol% NEt_3 against polystyrene standards).

	M_n (kg·mol^{-1})	M_w (kg·mol^{-1})	$Đ_M$
5b	4.4	11.6	2.6
5c	4.6	10.5	2.3
5d	5.4	12.2	2.3
5e	0.5	1.2	2.5
6b	5.9	22.4	3.8

Table 2-1. Calculated molecular weights and dispersities of different POETE and PATTE polymers and oligomers according to Figure 2-6.

After reduction and capping of the thiol end-groups *in situ* with tributyl phosphine and iodoacetamide to obtain representative polymer samples, size exclusion chromatography (SEC) (Figure 2-6 and Table 2-1) analysis was performed to determine the molecular weight. While from the polymerisation attempt with dithiothreitol as sterically restrictive linker (**5e**) only oligomers were obtained, all other POETE and PATTE formulations (**5b**, **5c**, **5d**, **6b**) resulted in polymers with number-averaged molecular weight (M_n) of around 5 kDa, weight-averaged molecular weight (M_w) above 10 kDa and dispersities ($Đ_M$) of between 2 and 4. While $Đ_M \approx 2$ would ideally be expected for a step growth

polymerisation, higher values indicate the existence of a secondary reaction such as oxidation or general impurity, whereas the latter should be minimal according to small molecule analyses. Using the Carothers equation for non-stochiometric conditions[47] despite employing equimolar amounts of reactants and assuming complete conversion to maximum attainable $Đ_M$, an actual monomer ratio of $r \approx 0.9$ is calculated, which indicates the deactivation of around 10% of thiol units.

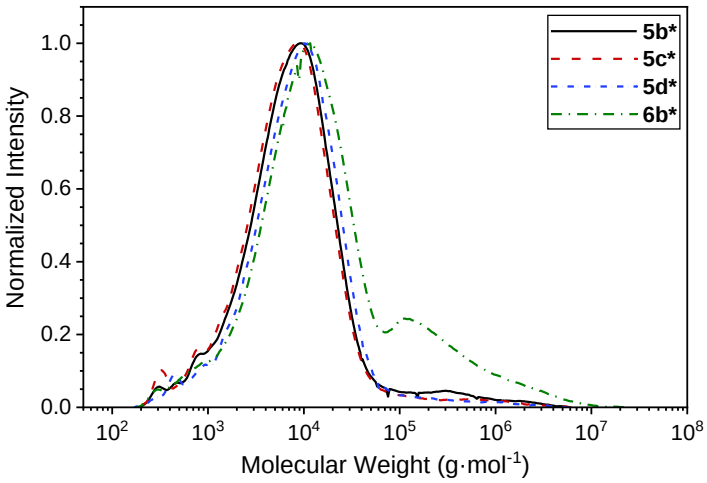

Figure 2-7. Size Exclusion Chromatograms of different crude POETE and PATTE polymers and oligomers (molecular weight determined in THF with 2 vol% NEt_3 against polystyrene standards).

Notably, a significant fraction of higher molecular weight polymer chains was found in size exclusion chromatograms if the reduction and capping of thiol-end groups was not performed (Figure 2-7), with the highest amount found in the compounds based on simple aliphatic dithiols. This indicates a tendency for further chain growth or crosslink *via* disulfide formation, which can be maximised by heat treatment on air (120 °C), resulting in clear, brittle and insoluble materials.

The above analyses prove that most of the 'click' criteria for polymerisations are fulfilled,[36] *i.e.* maximum conversion of equimolar ratio of monomers in bulk is achieved without the formation of significant amounts of side products within minutes and requires purification *via* precipitation at most. However, this reaction requires significantly longer reaction time or a stronger light source for larger batches and stops at relatively low molecular weights under competition with oxidation, which somewhat diminishes the 'click' classification. Hence, a controlled way to increase the molecular weight needs to be investigated.

2.3.3 Polymeric Network Formation

A crosslinked network polymer was synthesised to demonstrate the possibility to manufacture durable materials according to the presented mechanism. By selecting a simple unsaturated diol linker for use in the CKA alcohol addition (Scheme 2-1), a triple unsaturated OE monomer (**3c**) was synthesised and subsequently reacted under equimolar conditions relative to the thiol and ene groups to yield a strong polymeric network material (**7**).

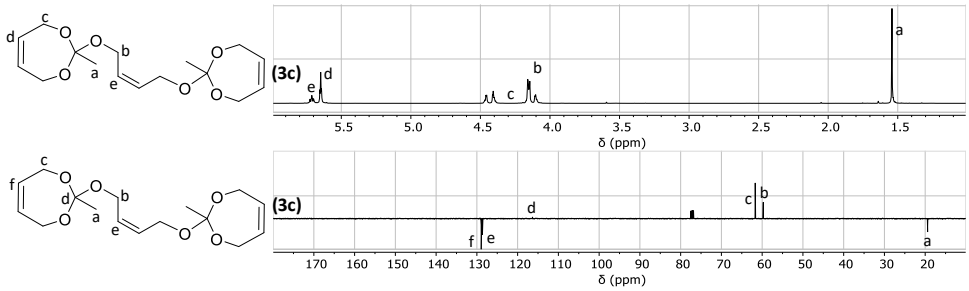

Figure 2-8. ^{1}H (top) and ^{13}C NMR (bottom) spectra of the trifunctional OE monomer (**3c**) ($CDCl_3$, 300 MHz, 298 K).

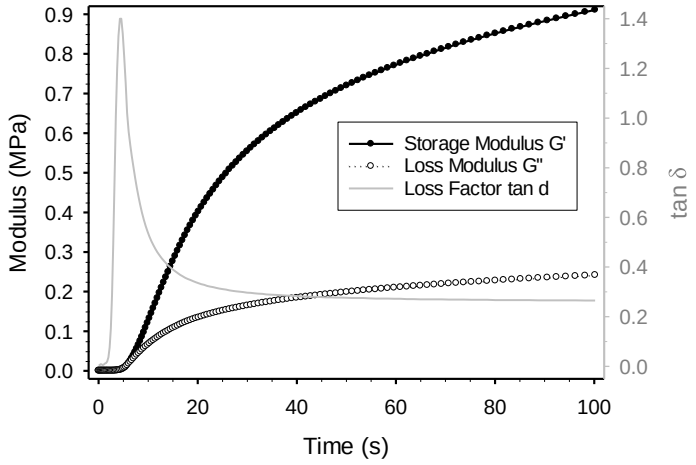

Figure 2-9. Progression of oscillatory storage and loss modulus during the polymerisation of P(OE4ene-2TE6) (**7**) (frequency 10 Hz, amplitude 1%, gap width 0.2 mm).

After the monomer was confirmed to be pure and in accordance with previous OEs *via* ^{1}H and ^{13}C NMR spectroscopy (Figure 2-8), the progress of the crosslinking reaction with hexane-1,6-dithiol and a radical photoinitiator under UV light and shear stress was monitored *via* oscillatory rheometry (Figure 2-9). A large increase in both loss and storage moduli can be observed just 5 s after switching on the light source, however more detailed information of the onset can be visualised by calculating the loss factor, tan δ as a ratio of both moduli. Notably, the reaction initiates 2 s after switching on the light source, and the peak in loss factor tan δ at 4 s indicates gelation at this point. Both moduli continue to

increase strongly until about 20 s after start of the reaction, at which point the increase in properties slows, but still proceeds. After 100 s the loss modulus starts to plateau at around 0.25 MPa, whereas the storage modulus continues to steadily increase above 0.9 MPa. This represents an increase in stiffness compared to that measured for previous POE-LAs that demonstrated a storage modulus of around 0.5 MPa at approximately 10 Hz.[48] However, even after 10 min the increase in storage modulus still continued, which points to limitations of the employed rheometer light source to the reaction. Instead, a procedure using a stronger photo-curing box with broader emission spectrum led to reproducibly strong materials within minutes, potentially aided by increase in temperature of the material and hence mobility of remaining reactant groups.

The final cured material was characterised using TGA and DSC and compared with the chain polymers in order to understand the thermal limitations of the materials (Figure 2-10 and Figure 2-11).

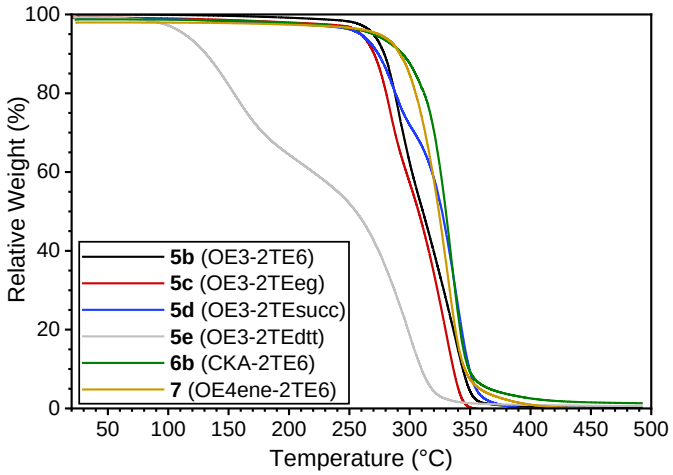

Figure 2-10. TGA thermograms of all polymeric compounds (**5b-7**) (10 K·min^{-1}).

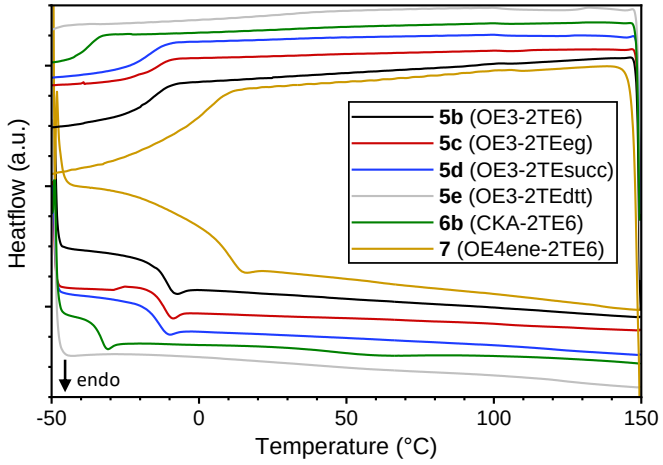

Figure 2-11. DSC thermograms of all polymeric compounds (**5b-7**) (10 K·min^{-1}, 3rd cycle).

Except for the barely reacted compound (**5e**, SEC), no significant mass loss was observed under nitrogen flow up to 250 °C, which indicates near complete conversion of the monomers, followed by the onset of thermal degradation. No unexpected thermal events were recorded with the exception of a glass transition between T_g = 3.4 °C and 10.2 °C during the heating and cooling cycle, respectively, which far surpassed analogue events in the chain polymers below -10 °C.

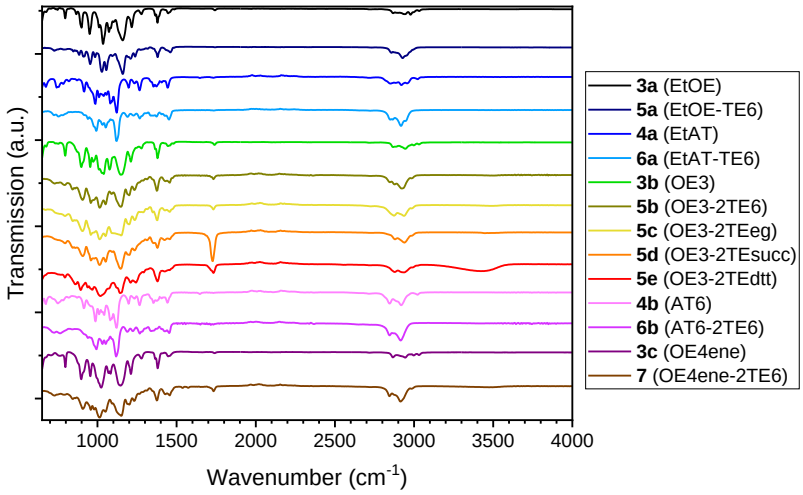

Figure 2-12. FT-IR spectra of all new compounds (**3a**-**7**, neat).

IR spectroscopic analysis (Figure 2-12) of all components revealed a remarkable similarity between all monomeric OE compounds (**3a**-**c**), with a characteristic obvious common signal at around $\tilde{\nu}$ = 800 cm^{-1}, which can most likely be attributed to the endocyclic double bond. A similar peak is observed in the AT species (**4a, 4b**) at around $\tilde{\nu}$ = 750 cm^{-1}, whereby the shift to lower wavenumber could be a result of lower ring-strain and charge density in the acetal. Additional reoccurring peaks for the OE moiety can be found just below $\tilde{\nu}$ = 1400 cm^{-1} and at $\tilde{\nu}$ = 1150 cm^{-1}, with the analogous AT vibration at $\tilde{\nu}$ = 1100 cm^{-1}. Generally however, only few significant peaks can be identified as a consequence of the rather diverse monomer structures. Nevertheless, a common residual peak at $\tilde{\nu}$ = 1750 cm^{-1} indicates the presence of carbonyl-containing impurities, such as the presumed acids and esters.

2.3.4 POETE Surface Erosion

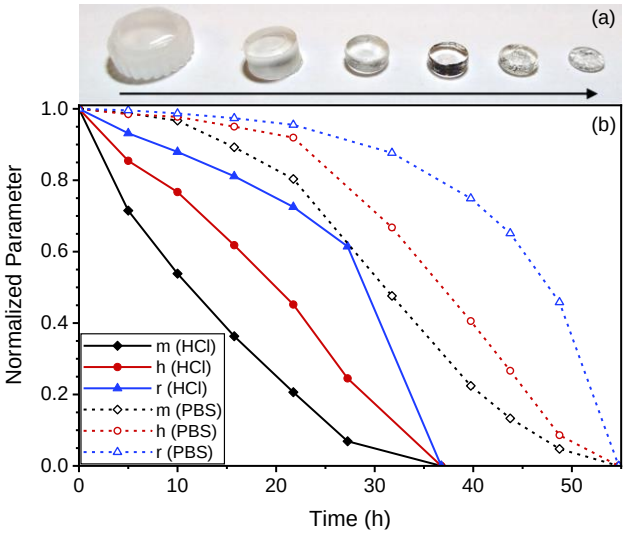

Figure 2-13. (a) Visual appearance and (b) relative average mass (*m*) and dimensions (height (*h*) and radius (*r*)) of cylindrical P(OE4ene-2TE6) (**7**) samples during degradation over time in D-PBS and 0.1 M HCl at 25 °C (3 samples each).

After subjecting cylindrical samples to ambient air or aqueous media for days or hours, respectively, a viscous film had built up, which revealed a puck of similar proportions but smaller size when removed. Changes in apparent transparency and reflectiveness of the sample were observed (Figure 2-13a), which could be caused by a change in surface roughness from micrometre to millimetre scale. A more specific divergence was determined in a comparison of mass and dimensions (height and radius) between samples degraded in acidic and neutral media (Figure 2-13b). While almost instant and constant degradation occurred in acidic media (0.1 M HCl, pH = 1.0), a delay of several hours was observed under buffered neutral conditions (D-PBS buffer, pH = 7.4) until the onset of surface degradation. This can be explained by the observation of an initial swelling period in PBS solution, whereby water diffuses into the outer layer of the material and causes low levels of degradation, inducing autocatalysis through the resulting acidic degradation products. A linear trend in the degradation in both media, between 4 to 27 h and 23 to 44 h, respectively, further supports the hypothesis of a consistent surface erosion mechanism. It should be noted that degradation in air was found to be highly inconsistent over the extended time scale, probably as a consequence of fluctuations in humidity, with storage under inert atmosphere causing no visible erosion whatsoever.

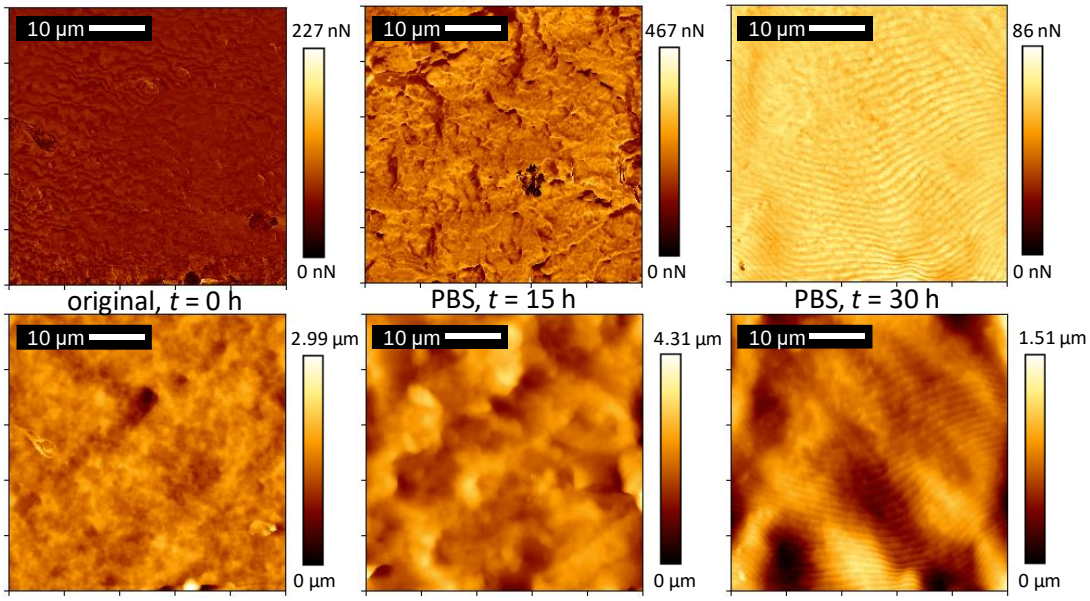

Figure 2-14. AFM images of P(OE4ene-2TE6) (**7**) samples degraded in D-PBS at three different time points. Top row: Adhesion images. Bottom row: Corresponding height images. Left to right: t = 0 h; t = 15 h (≈ 90 wt%); t = 30 h (≈ 50 wt%) (512 × 512 px, setpoint 25 nN, scale bar 10 µm).

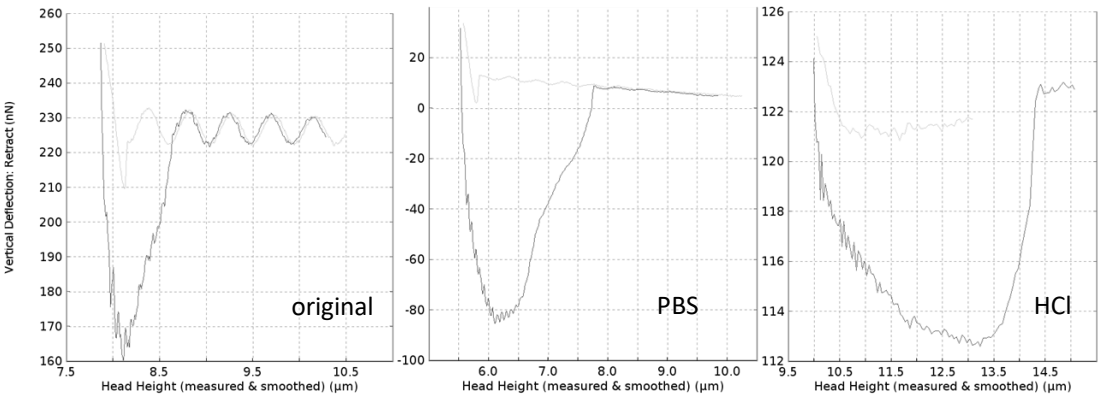

Figure 2-15. Exemplary AFM force curves on degraded samples of P(OE4ene-2TE6) (**7**) at roughly 50 wt%. From left to right: crude; D-PBS; 0.1 M HCl (25 nN, retraction maxed at 15 µm). Grey: approach; black: retract. Samples degraded on air did not return to baseline.

Visualisation of the surface erosion of the POETE network sample in PBS on a micro-scale was achieved *via* AFM analysis (Figure 2-14). Adhesion images reveal an increase in adhesive force after several hours, which indicates that swelling from water diffusion has occurred. Longer degradation times produced similar adhesion values and hence suggests no further increase in the depth of the layer of diffusion. An initial increase in height differences and subsequent smoothening of microstructures further supports the explanation of swelling, followed by consistent surface erosion. No pore formation was observed on a micro-scale, however a line pattern emerged with distances of around one micrometre, which can originate from either swelling or tension within the

material caused by strain during curing. It has to be noted however that imaging of acid and air-degraded samples *via* AFM failed as a consequence of excessive adhesive forces (Figure 2-15). The existence of free acids and additional ester groups as well as general viscous oligomeric degradation products in swollen material can cause stronger adhesion onto the AFM tip, whereas PBS solution neutralises superficial acids and forms less adhesive salt layers.

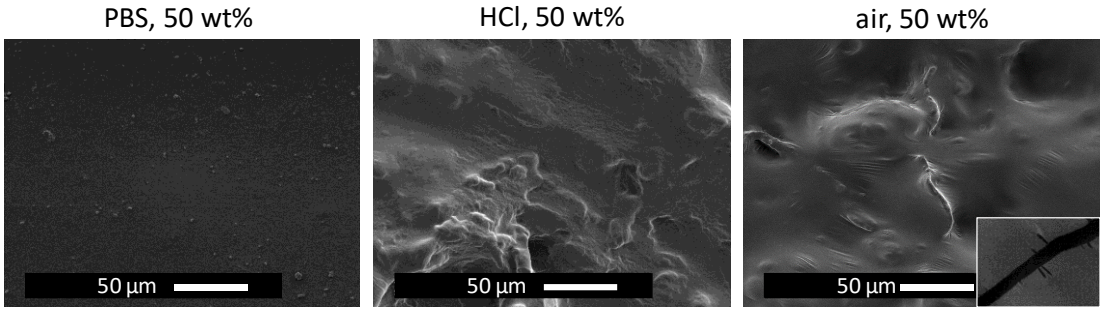

Figure 2-16. SEM images of P(OE4ene-2TE6) (**7**) samples degraded in neutral and acidic media, and in atmospheric conditions at roughly 50 wt%. From left to right: 0.1 M HCl; D-PBS; air (on average 70% humidity). Insert on the right shows an image of a crack in a different region taken at the same parameters (500× magnification, 5.00 kV, scale bar 50 µm).

In order to understand the surface structure of the network material in relation to the degradation medium SEM images were taken at a point of roughly 50 wt% total degradation (Figure 2-16). Interestingly, the microscopic sample structure of the acid-eroded sample appeared completely smooth apart from small superficial debris, which indicates a degradation rate faster than diffusion into the material can occur. In contrast, PBS and ambient moisture resulted in a rougher surface structure, which could arise if degradation and diffusion rate are roughly equal. The air-degraded sample in particular shows signs of swelling with smooth surfaces and microscopic wrinkles, as well as significant cracks at different areas in the material. This could be explained by the diffusion of water vapor deep into the material before the onset of degradation, in contrast to the diffusion from the liquid phase in the other two samples. Logically, this indicates a water vapor diffusion rate higher than the rate of degradation.

2.3.5 POETE Degradation Products

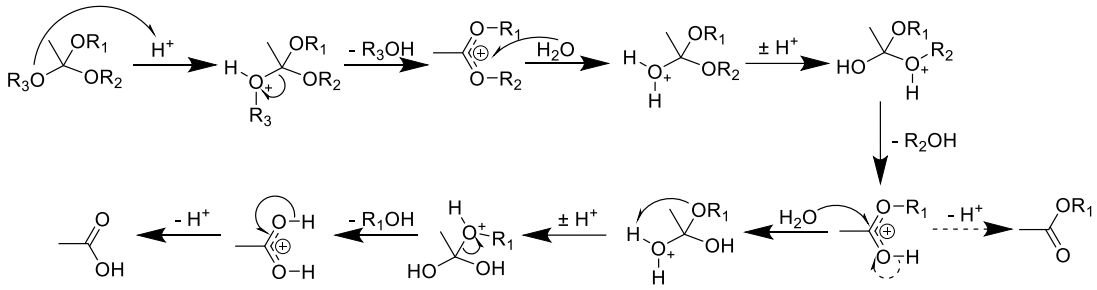

Scheme 2-2. Proposed hydrolytic degradation mechanism of OEs under acid catalysis in detail.

As discussed previously in this chapter and in literature,[27] the hydrolytic degradation of OEs is expected to yield alcoholic, acidic and ester compounds (Scheme 2-2). Depending on concentration, it is then feasible that further transesterification reactions occur. TE, on the other hand, is known to easily be oxidised to sulfoxides and sulfones upon exposure to air, as well as potentially be alkylated to form sulfonium salt species. Even though the oxygen diffusion through the viscous layer of degradation product could be considered minimal, that still leaves a broad spectrum of possible degradation products of the POETE system.

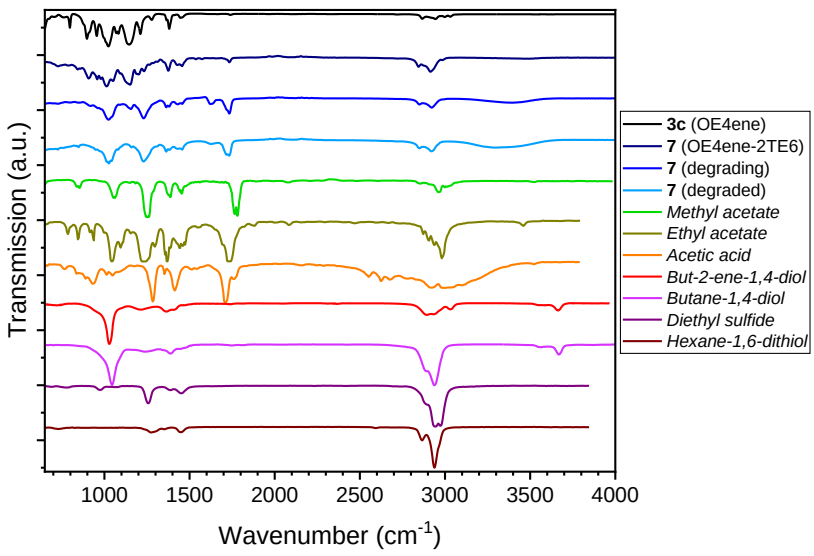

Figure 2-17. FT-IR spectra of P(OE4ene-2TE6) (**7**) during and after degradation on air (neat) in comparison with potential degradation product species. Spectra of reference substances (in italics) obtained from the NIST (National Institute of Standards and Technology) database.

In an attempt to identify the degradation products of P(OE4ene-2TE6) (**7**), analysis *via* IR spectroscopy (Figure 2-17) of the liquid residue after degradation in air was performed. The presence of predominantly acetic esters, acids and

alcohols is supported in the fingerprint region by a broad signal between $\tilde{\nu}$ = 1000 and 1100 cm^{-1}, which could arise as a combination of peaks exhibited by respective diols and acetates, as well as a broad signal between $\tilde{\nu}$ = 1200 and 1300 cm^{-1}, which is characteristic for acetic acetate and its derivatives. Vibrations corresponding to acetate species and the degradation products between $\tilde{\nu}$ = 1700 and 1800 cm^{-1} further indicate the presence of alkyl-acetates and are present in neither the OE nor the POETE.

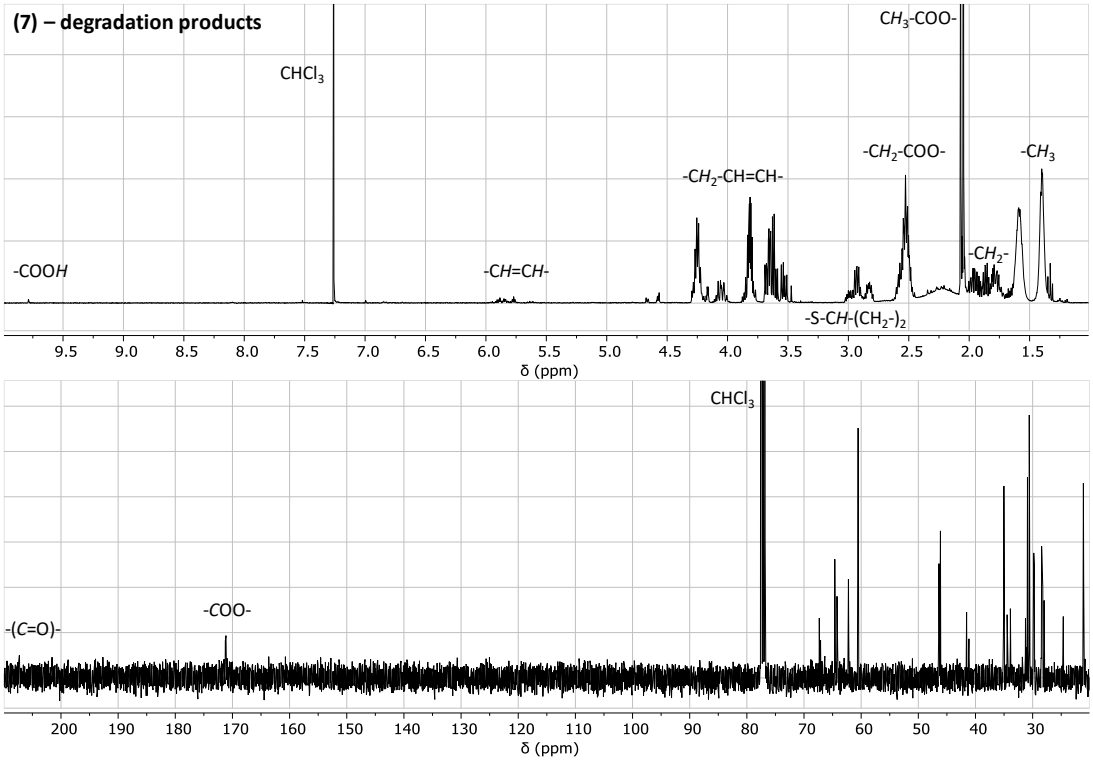

Figure 2-18. ^{1}H (top) and ^{13}C (bottom) NMR spectra of degradation products of the P(OE4ene-2TE6) (**7**) on air ($CDCl_3$, 400 MHz, 298 K).

Complementary ^{1}H NMR spectroscopy (Figure 2-18) on the same viscous degradation mixture underlined the presence of ester and acid compounds by signals around δ = 2.5 ppm and δ = 9.8 ppm, respectively. Two distinct species of presumably acetic acid and acetate can be deduced from two sharp singlets at δ = 2.1 ppm, which is in accordance with the proposed degradation mechanism (Scheme 2-2). Interestingly, the presence of both saturated and unsaturated hydrocarbons is indicated by peaks in the regions between δ = 1.5 and 2.0 ppm, as well as between δ = 3.5 and 6.0 ppm. Alkene groups could either stem from incomplete conversion during the polymerisation step or are formed by Retro-Michael addition. Unfortunately, the ^{13}C NMR spectrum does not enable the

identification of specific compounds, but rather indicates a multitude of species including esters and potentially carbonyl-containing moieties with the appearance of signals at δ = 172.0 and 207.0 ppm, respectively.

2.3.6 Thio-Orthoester (TOE) Formation and Degradation

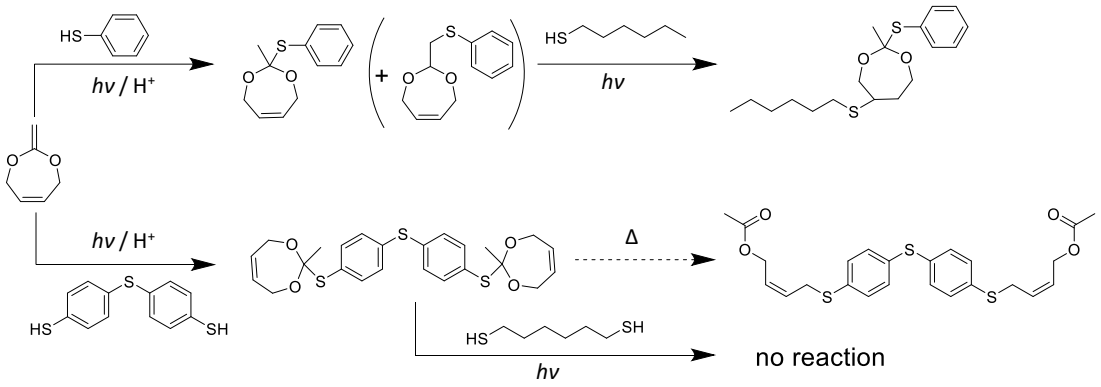

Scheme 2-3. Synthesis of a mono- and difunctional TOE compound (**8a**, **8b**) from highly activated thiols, followed by thiol addition to TOE-TE (**9a**) and thermolytic ring-opening (**8bX**).

During the synthesis of ATs an affinity of more nucleophilic aromatic thiols to form TOEs instead was discovered (Scheme 2-3). Thiophenol was reacted with CKA (**2**) analogous to the OE synthesis under acid-catalysis to yield the TOE (**8a**) with less than 0.1 eq. of the respective AT. This observation was true even when radical photoinitiation was employed, with only a slightly larger fraction of acetal product yielded. Nevertheless, this indicates that the product can be influenced by the choice of either a nucleophilic or a radical reaction pathway, and further points at a competing steric hindrance within the thermodynamically favoured TOE. Even though separation of the AT and OE isomers should be relatively simple from a chemical and physical perspective, a number of failed purification attempts resulting in comparable isomer ratios could suggest a state of equilibrium potentially caused by alkylation of the TOE sulfur with the adjacent methyl functionality. Similarly, a surprising instability of the dimeric TOE was discovered during distillation attempts. Elevated temperatures of just 80 °C led to the complete conversion to a different product, without any indication of further degradation or separation by mass-loss.

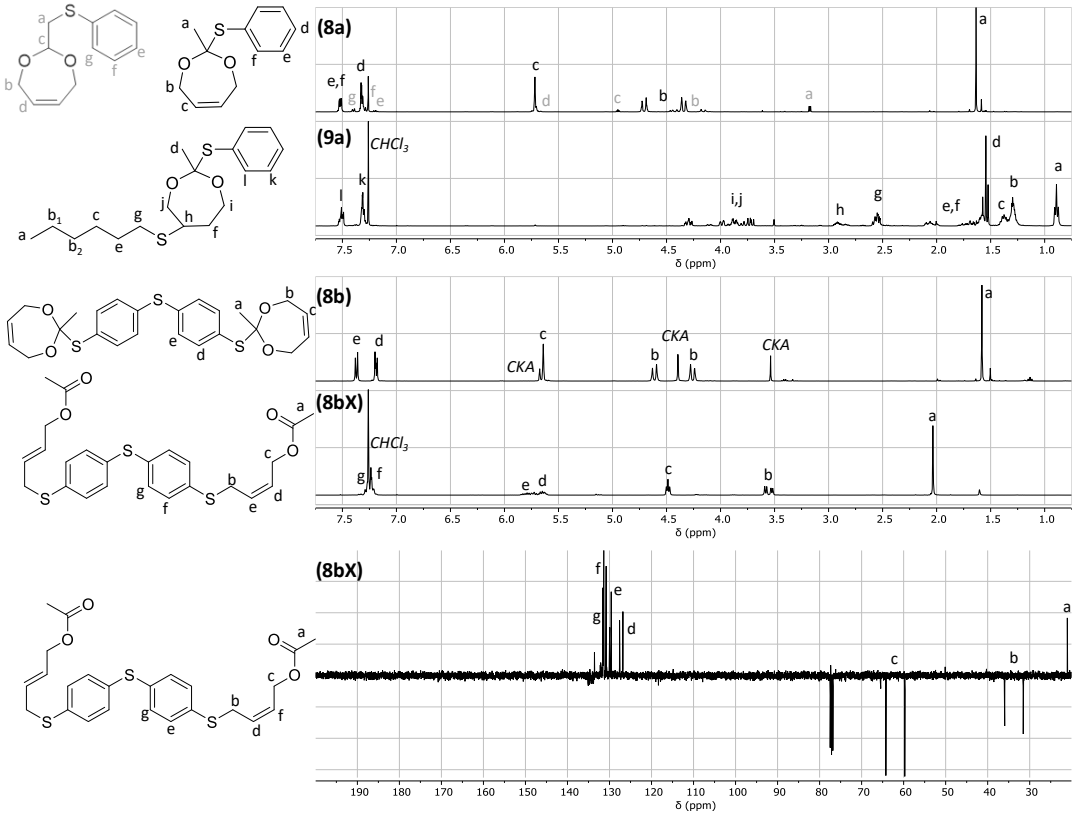

Figure 2-19. ^{1}H (top four) and ^{13}C (bottom) NMR spectra of TOE products (degradation products of the P(OE4ene-2TE6) (**7**) on air ($CDCl_3$, 400 MHz, 298 K).

This product was preliminarily identified *via* ^{1}H and ^{13}C NMR (Figure 2-19) as the ring-opened thioether with terminal acetate functionalities. A strong splitting pattern of the allylic methylene groups in the ^{13}C NMR around δ = 34 and 62 ppm, respectively, indicates that the original *cis*-conformation within the diol was only partially maintained. By formation of an intermediary intramolecular sulfonium ion, an allylic nucleophilic attack followed by circular electron density transfer (Scheme 2-4) could explain a statistical distribution in the conformation.

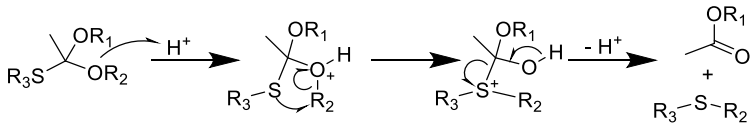

Scheme 2-4. Proposed ring-opening mechanism of TOEs under acid catalysis.

Despite these inconsistencies in the TOE synthesis, the subsequent thiol-ene Michael addition was investigated in order to determine the value of such materials. While the small molecule formation (**9a**) was efficiently accomplished, the polymerisation of the TOE dimer (**8b**) was entirely unsuccessful. Excess of initiator, radiation and reaction time did not lead to any significant conversion,

which could indicate that the activated dithiol-linker acts as a radical inhibitor and is hence unsuitable for this route. Moreover, small-scale polymerisation attempts with a TOE on 1,4-benzene-dithiol were equally unsuccessful, which suggests that aromatic thiols are generally unfavourable for this radical mechanism. Hence, as a consequence of the lack of other economically viable activated dithiols and rather unpleasant odours of the products, this route was not further investigated at this point.

2.4 Conclusion and Outlook

In conclusion, this chapter offers a new, facile and controlled route to sequentially synthesise acetals and orthoesters and use thiol crosslinkers to obtain OE-TEs and AT-TEs, respectively, from a stable cyclic ketene acetal. Additionally, TOE species can be obtained. The concept is proven on small molecules with reported reactions possessing 'click' character, producing neither significant amounts of side products nor requiring excessive reaction conditions or purification procedures. Generally, all involved compounds are stable under neutral and dry conditions, however high sensitivity to acidic media can be observed, which results in a necessity to avoid untreated glass surfaces. Versatility of the general synthesis method was further exemplified by formation of a variety of chain polymers from dithiols with a weight-average molecular weight of over 10 $kg \cdot mol^{-1}$ as potential degradable blocks in copolymers. In a final demonstration, the synthesis of a strong network polymer was demonstrated by crosslinking of an unsaturated OE. Surface erosion behaviour was observed and monitored *via* degradation studies and microscopic imaging of the network material, which confirmed smoothening of microscopic surface features and the absence of pore and crack formation in aqueous media. Degradation products consist of alcohol, ester and acid species in accordance with established degradation mechanisms and are hence promising to be biocompatible. The plasticity and transparency of both the polymer chains and the network promises implementation as biomedical polymeric materials or contents thereof. Applications for these materials can be envisioned in temporally and structurally controlled release, as well as in support structures with predetermined erosion behaviour.

2.5 Experimental Section

2.5.1 Materials

Acetone (Fisher), Aliquat 336 (Sigma-Aldrich), basic aluminium oxide (Sigma-Aldrich), 2-bromo-1,1-dimethoxyethane (Acros Organics), cis-2-butene-1,4-diol (Sigma-Aldrich), diethyl ether (Sigma-Aldrich), 3,6-dioxa-1,8-octane-dithiol (Sigma-Aldrich), ethanol (Sigma-Aldrich), ethanethiol (Sigma-Aldrich), hexane-1,6-dithiol (Sigma-Aldrich), hydrochloric acid (Fisher), iodoacetamide (Sigma-Aldrich), Irgacure 819 (IGM Resins Ltd.), potassium carbonate (anhydrous, Sigma-Aldrich), potassium *tert*-butoxide (Sigma-Aldrich), 1,3-propanediol (Sigma-Aldrich), terephthalic acid (Sigma-Aldrich), tetrahydrofuran (Sigma-Aldrich), tributylphosphine (Sigma-Aldrich), triethylamine (Sigma-Aldrich), preparation for Dulbecco's PBS (Sigma-Aldrich) and p-toluenesulfonic acid (Sigma) were used as received from the supplier. $CDCl_3$ (Sigma-Aldrich) was stored over anhydrous potassium carbonate and plug filtered through basic aluminium oxide immediately before use. Furthermore, all glassware used for handling and storage of OE containing compounds was silanised by treating the inner surface with Sigmacote (Sigma-Aldrich) for five minutes, followed by rinsing with water, acetone, diethyl ether and subsequent drying under compressed air for one hour.

2.5.2 Methods

A Formlabs Form Cure or an NK Optik Otoflash was used for curing of polymers. Nuclear Magnetic Resonance (NMR) spectra were acquired using a Bruker Avance III 400 MHz, processed by MestReNova software using the residual solvent peak as reference ($CDCl_3$, ^1H: δ = 7.26 ppm, ^{13}C: δ = 77.16 ppm). Mass spectra were obtained *via* a Bruker maXis plus. Elemental analysis was conducted on a CE Instruments EA1110 Elemental Analyzer. Size Exclusion Chromatograms were recorded on an Agilent Infinity II with RI detection on an Agilent PLgel MIXED-C, 7.5 × 300 mm, 5 µm column in THF with 2% NEt_3 and 0.01% BHT at a flow rate of 1 mL·min^{-1} at 50 °C compared to EasiVial Polystyrene Standard. Agilent GPC/SEC software V.A.02.01 (2015) was used for data analysis. An Agilent Cary 630 FTIR Spectrometer with Agilent Resolutions Pro software V.5.0 was used for IR spectroscopy. DSC and TGA thermograms were collected on

a Mettler-Toledo STARe DSC3+ system and a TA Instruments TGA Q500, respectively. Oscillatory rheometry was performed on an Anton Parr MCR-302 with PP25 plates, Omnicure S1500 UV source and RheoCompass™ V1.20.496 software at a frequency of 10 Hz, amplitude of 1% and gap width of 0.2 mm. AFM images were recorded on a JPK Nanowizard 4 in QI mode using Nanosensors PPP-NCHAuD tips and Nanowizard Control Software V.6.1.117. SEM images were obtained on a Philips XL30 ESEM-FEG Environmental SEM using Phoenix Software V.3.3 on gold-coated samples.

2.5.3 Synthesis of Bis(3-mercaptopropyl) succinate

Bis(3-mercaptopropyl) succinate was synthesised according to established procedure within the group. Briefly, 3-mercaptopropanol (7.30 g, 0.079 mol) and succinic acid (4.40 g, 0.037 mol) are dissolved in 120 mL of a 1:1 mixture of benzene and toluene with a catalytic amount of sulfuric acid. After stirring at 120 °C overnight and collection of the distilled water, the solution was left to cool to room temperature, followed by vacuum transfer of the solvent to yield crude product. The oil was re-dissolved in chloroform, extracted with sat. $NaHCO_3$ solution (2 × 200 mL) and dried over $MgSO_4$. Purification on a silica gel column (3:2 hexane/EtOAc) and subsequent distillation (0.2 mbar, 220°C) yielded clear colourless oil (7.8 g, 79% yield). R_f (3:2 Hex/EtOAc) = 0.4, ^{1}H NMR (400 MHz; 298 K; $CDCl_3$; ppm): δ 4.21 (t, $^3J_{HH}$ = 6.2 Hz, 4H), 2.62 (s, 4H), 2.58 (q, $^3J_{HH}$ = 6.6 Hz, 4H), 1.40 (t, $^3J_{HH}$ = 8.1 Hz, 2H); ^{13}C NMR (400 MHz; 298 K; $CDCl_3$; ppm): δ 172.31, 62.94, 32.92, 29.22, 21.20; MS (ESI-QTOF +ve): $(M + Na)^+$ *m/z* calculated for $C_{10}H_{18}O_4S_2Na^+$: 289.1, found: 289.0; Anal. Calcd for $C_{10}H_{18}O_4S_2$: C 45.09; H 6.81 %. Found: C 59.70; H 4.41 %.

2.5.4 Synthesis of 2-(bromomethyl)-1,3-dioxe-5-pene (BrCKA, 1)

The procedure follows a method described by Plikk *et al.*[45] Cis-2-butene-1,4-diol (33.30 g, 378 mmol) and 2-bromo-1,1-dimethoxyethane (63.89 g, 378 mmol) were weighed into a 100 mL round bottom flask, followed by p-toluenesulfonic acid (0.10 g, 0.1 wt%). A stirrer bar, Vigreux condenser and distillation bridge was added and the mixture incrementally heated to 130 °C under stirring, until no more methanol was distilled over. After cooling to room temperature and

gradually reducing the pressure, a residual methanol fraction was discarded and subsequently the pure product distilled at 38-42 °C and 0.05 mbar (62.1 g, 85%). Characterised as reported previously.[45] ^{1}H NMR (400 MHz; 298 K; $CDCl_3$; ppm): δ 5.70 (t, $^{3}J_{HH}$ = 1.5 Hz, 2H), 4.97 (t, $^{3}J_{HH}$ = 5.4 Hz, 1H), 4.44 (dm, $^{3}J_{HH}$ = 14.7 Hz, 2H), 4.20 (dm, $^{3}J_{HH}$ = 14.7 Hz, 2H), 3.39 (d, $^{3}J_{HH}$ = 5.4 Hz, 2H); ^{13}C NMR (400 MHz; 298 K; $CDCl_3$; ppm): δ 128.81, 106.92, 63.25, 24.99.

2.5.5 Synthesis of 2-methylene-1,3-dioxe-5-pene (CKA, 2).

Similarly to Plikk *et al.*'s method,[45] BrCKA **(1)** (40.00 g, 207 mmol) and Aliquat 336 (1.62 g, 4 mmol) were weighed into a 500 mL RBF, dissolved in 350 mL THF and cooled under stirring to 0 °C. Potassium *tert*-butoxide (46.50 g, 414 mmol) was added in small portions within one hour and the orange to yellow suspension left to stir for another two hours at 0 °C. THF was removed *in vacuo* (20 mbar, 18 °C) and the residual slurry dissolved in 200 mL diethyl ether and 200 mL distilled water, followed by separation of the layers and extraction of the aqueous phase with a further 100 mL diethyl ether. The combined organic layers were washed with 0.01M potassium carbonate solution (300 mL) for three times. The organic layer was concentrated *in vacuo* at 18 °C, followed by vacuum transfer of the residual oil at room temperature and 0.05 mbar to yield crude product. Repeat of the washing procedure, followed by drying over potassium carbonate and concentration at 30 °C and 20 mbar yielded pure product (12.50 g, 55%). ^{1}H NMR (400 MHz; 298 K; $CDCl_3$; ppm): δ 5.72 (t, $^{3}J_{HH}$ = 1.7 Hz, 2H), 4.43 (d, $^{3}J_{HH}$ = 1.7 Hz, 4H), 3.57 (s, 2H); ^{13}C NMR (400 MHz; 298 K; $CDCl_3$; ppm): δ 164.11, 127.83, 68.77, 68.21.

2.5.6 General procedure of the orthoester (OE) synthesis (3).

CKA **(2)** and diol were weighed into a silanised vial in a molar ratio of 1.05 to 0.5. Terephthalic acid (1 mol eq.) was added and the mixture stirred overnight. The crude product was dissolved in diethyl ether and washed four times with equivalent volumes of 0.01M potassium carbonate solution, followed by separation and drying of the organic layer over potassium carbonate. Plug filtration through minimal amounts of basic alumina and evaporation yielded pure OE product of fruity odour **(3)**. Additional distillation *in vacuo* in a silanised

setup before use was performed to remove any degradation products (around ^{1}H NMR δ 2.00 ppm).

2.5.7 Synthesis of 2-ethoxy-2-methyl-1,3-dioxe-5-pene (EtOE, 3a).

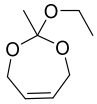

The reaction of CKA **(2)** (2.00 g, 17.84 mmol), ethanol (0.82 g, 8.92 mmol) and terephthalic acid (0.30 g, 0.18 mmol) yielded clear colourless oil (2.20 g, 78%; distillation at 0.05 mbar, 60 °C). ^{1}H NMR (400 MHz; 298 K; $CDCl_3$; ppm): δ 5.65 (t, $^3J_{HH}$ = 1.7 Hz, 2H, -C*H*CH$_2$CO$_3$-), 4.44 (dm, $^2J_{HH}$ = -16.4 Hz, 2H, -CHC*H*$_2$CO$_3$-), 4.13 (dm, $^2J_{HH}$ = -16.4 Hz, 2H, -CHC*H*$_2$CO$_3$-), 3.58 (q, $^3J_{HH}$ = 7.0 Hz, 2H, CH$_3$C*H*$_2$CO$_3$-), 1.53 (s, 3H, C*H*$_3$CO$_3$-), 1.24 (t, $^3J_{HH}$ = 7.0 Hz, 3H, C*H*$_3$CH$_2$CO$_3$-); ^{13}C NMR (400 MHz; 298 K; $CDCl_3$; ppm): δ 128.99 (-*C*HCH$_2$CO$_3$-), 116.08 (-*C*O$_3$-), 61.47 (-CH*C*H$_2$CO$_3$-), 58.89 (CH$_3$*C*H$_2$CO$_3$-), 19.15 (*C*H$_3$CO$_3$-), 15.49 (*C*H$_3$CH$_2$CO$_3$-); MS (ESI-QTOF +ve): (M + Na)$^+$ *m/z* calculated for $C_8H_{14}O_3Na^+$: 181.0835, found: 181.0836; Anal. Calcd for $C_8H_{14}O_3$: C 60.7; H 8.9%. Found: C 60.2; H 8.9; IR (neat; 298 K; cm^{-1}): 2980-2870 (-C-H), 1380 (-CH$_2$-), 1160-1040 (C-O), 900 (-CH$_2$-CH$_2$-), 800 (C=C), 640 (=C-H).

2.5.8 Synthesis of 1,3-bis(2-methyl-2-oxyl-1,3-dioxe-5-pene)-propane (OE3, 3b).

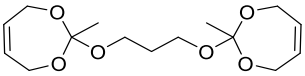

CKA **(2)** (4.00 g, 35.68 mmol), 1,3-propanediol (1.36 g, 17.84 mmol) and terephthalic acid (0.60 g, 0.36 mmol) were reacted to yield clear colourless oil (4.48 g, 84%; distillation at 0.02 mbar, 150 °C). ^{1}H NMR (400 MHz; 298 K; $CDCl_3$; ppm): δ 5.66 (t, $^3J_{HH}$ = 1.7 Hz, 4H, -C*H*CH$_2$CO$_3$-), 4.43 (dm, 4H, $^2J_{HH}$ = -15.5 Hz, -CHC*H*$_2$CO$_3$-), 4.15 (dm, 4H, $^2J_{HH}$ = -15.5 Hz, -CHC*H*$_2$CO$_3$-), 3.65 (t, 4H, $^3J_{HH}$ = 6.3 Hz, -OC*H*$_2$CH$_2$-), 1.93 (qi, 2H, $^3J_{HH}$ = 6.3 Hz, -OCH$_2$C*H*$_2$-), 1.54 (s, 6H, -CO$_3$C*H*$_3$); ^{13}C NMR (400 MHz; 298 K; $CDCl_3$; ppm): δ 128.99 (-*C*HCH$_2$CO$_3$-), 116.20 (-*C*O$_3$CH$_3$), 61.57 (-CH*C*H$_2$CO$_3$-), 60.42 (-CO$_3$*C*H$_2$CH$_2$-), 30.37 (-CO$_3$CH$_2$*C*H$_2$-), 19.18 (-CO$_3$*C*H$_3$); MS (ESI-QTOF +ve): (M + Na)$^+$ *m/z* calculated for $C_{15}H_{24}O_6Na^+$: 323.1465, found: 323.1468; Anal. Calcd for $C_{15}H_{24}O_6$: C 60.0; H 8.05%. Found: C

59.9; H 8.0; IR (neat; 298 K; cm^{-1}): 2950-2860 (-C-H), 1380 ($-CH_2-$), 1160-1040 (C-O), 900 ($-CH_2-CH_2-$), 800 (C=C), 640 (=C-H).

2.5.9 Synthesis of cis-1,3-bis(2-methyl-2-oxyl-1,3-dioxe-5-pene)-but-2-ene (OE4ene, 3c).

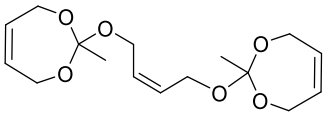

The reaction of CKA **(2)** (2.00 g, 17.84 mmol), cis-2-butene-1,4-diol (0.78 g, 8.92 mmol) and terephthalic acid (0.30 g, 0.18 mmol) yielded white crystals (2.25 g, 81%; recrystallisation from diethyl ether). Mp. ≈ 25 °C; ^{1}H NMR (400 MHz; 298 K; $CDCl_3$; ppm): δ 5.71 (tm, $^3J_{HH}$ = 3.6 Hz, 2H, -C*H*CH_2CO_3- *(linker)*), 5.56 (t, $^3J_{HH}$ = 1.7 Hz, 4H, -C*H*CH_2CO_3-), 4.43 (dm, 4H, $^2J_{HH}$ = -14.2 Hz, -CHC*H*$_2CO_3$-), 4.15 (d, 4H, $^3J_{HH}$ = 3.6 Hz, -CHC*H*$_2CO_3$- *(linker)*), 4.13 (dm, 4H, $^2J_{HH}$ = -14.2 Hz, -CHC*H*$_2CO_3$-), 1.54 (s, 6H, $-CO_3CH_3$); ^{13}C NMR (400 MHz; 298 K; $CDCl_3$; ppm): δ 128.94 (-*C*HCH_2CO_3-), 128.64 (-*C*HCH_2CO_3- *(linker)*), 116.35 (-*C*O_3CH_3), 61.70 (-CH*C*H_2CO_3-), 59.72 (-CH*C*H_2CO_3- *(linker)*), 30.37 ($-CO_3CH_2CH_2-$), 19.40 ($-CO_3CH_3$); MS (ESI-QTOF +ve): $(M + Na)^+$ *m/z* calculated for $C_{16}H_{24}O_6Na^+$: 335.1465, found: 335.1468; Anal. Calcd for $C_{16}H_{24}O_6$: C 61.5; H 7.7%. Found: C 61.5; H 7.8; IR (neat; 298 K; cm^{-1}): 2940-2870 (-C-H), 1380 ($-CH_2-$), 1160-1020 (C-O), 900 ($-CH_2-CH_2-$), 800 (C=C), 640 (=C-H).

2.5.10 General procedure of the acetal (AT) synthesis (4).

CKA **(2)** and thiol were weighed into a silanised vial under a nitrogen blanket in a molar ratio of 1.05 to 0.5. Irgacure 819 (0.3 wt%) was added and the mixture stirred until clear, followed by irradiation with UV light for 5 h at 60°C in a Formlabs Form Cure. Vacuum distillation yielded the pure AT product.

2.5.11 Synthesis of 2-((ethylthio)methyl)-1,3-dioxe-5-pene EtAT, 4a).

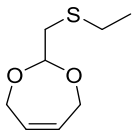

CKA **(2)** (2.10 g, 18.73 mmol), ethanethiol (1.10 g, 8.92 mmol) and Irgacure 819 (0.01 g) were reacted to yield clear colourless oil (3.02 g, 97%; distillation at

0.02 mbar, 60 °C). ^{1}H NMR (400 MHz; 298 K; $CDCl_3$; ppm): δ 5.71 (t, $^{3}J_{HH}$ = 1.8 Hz, 2H, -C*H*CH_2CHO_2-), 4.91 (t, 1H, $^{3}J_{HH}$ = 5.5 Hz, -C*H*O_2CH_2S-), 4.42 (dm, 2H, $^{2}J_{HH}$ = -15.2 Hz, -CHC*H*$_2CHO_2$-), 4.19 (dm, 2H, $^{2}J_{HH}$ = -15.2 Hz, -CHC*H*$_2CHO_2$-), 2.75 (d, 2H, $^{3}J_{HH}$ = 5.5 Hz, -CHO_2C*H*$_2$S-), 2.62 (d, 2H, $^{3}J_{HH}$ = 7.4 Hz, -SC*H*$_2CH_3$), 1.25 (s, 3H, $^{3}J_{HH}$ = 7.4 Hz, -SCH_2C*H*$_3$); ^{13}C NMR (400 MHz; 298 K; $CDCl_3$; ppm): δ 129.58 (-*C*HCH_2CHO_2-), 104.35 (-*C*HO_2CH_2S-), 65.59 (-CH*C*H_2CHO_2-), 34.66 (-CHO_2*C*H_2S-), 26.73 (-S*C*H_2CH_3), 14.81 (-SCH_2*C*H_3); MS (ESI-QTOF +ve): M^+ *m/z* calculated for $C_8H_{14}O_2S^+$: 174.0715, found: 174.0716; Anal. Calcd for $C_8H_{14}O_2S$: C 55.1; H 8.1; S 18.4%. Found: C 55.55; H 8.1; S 18.0; IR (neat; 298 K; cm^{-1}): 2950-2850 (-C-H), 1440-1350 (-CH_2-), 1120-980 (C-O), 910 (=C-H), 740 (=C-H).

2.5.12 Synthesis of 1,6-bis(2-methylthioyl-1,3-dioxe-5-pene)-hexane (AT6, 4b).

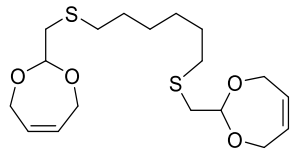

The reaction of CKA **(2)** (2.10 g, 18.73 mmol), 1,6-hexanedithiol (1.34 g, 8.92 mmol) and Irgacure 819 (0.01 g) yielded clear colourless oil (3.21 g, 96%; distillation at 0.02 mbar, 150 °C). ^{1}H NMR (400 MHz; 298 K; $CDCl_3$; ppm): δ 5.71 (t, $^{3}J_{HH}$ = 1.8 Hz, 4H, -C*H*CH_2CHO_2-), 4.90 (t, 2H, $^{3}J_{HH}$ = 5.5 Hz, -C*H*O_2CH_2S-), 4.42 (dm, 4H, $^{2}J_{HH}$ = -15.5 Hz, -CHC*H*$_2CHO_2$-), 4.19 (dm, 4H, $^{2}J_{HH}$ = -15.5 Hz, -CHC*H*$_2CHO_2$-), 2.73 (d, 4H, $^{3}J_{HH}$ = 5.5 Hz, -CHO_2C*H*$_2$S-), 2.59 (d, 4H, $^{3}J_{HH}$ = 7.5 Hz, -SC*H*$_2CH_2CH_2$-), 1.59 (m, 4H, -SCH_2C*H*$_2CH_2$-), 1.39 (m, 4H, -SCH_2CH_2C*H*$_2$-); ^{13}C NMR (400 MHz; 298 K; $CDCl_3$; ppm): δ 129.60 (-*C*HCH_2CHO_2-), 104.38 (-*C*HO_2CH_2S-), 65.62 (-CH*C*H_2CHO_2-), 35.13 (-CHO_2*C*H_2S-), 32.80 (-S*C*$H_2CH_2CH_2$-), 29.54 (-SCH_2*C*H_2CH_2-), 28.47 (-SCH_2CH_2*C*H_2-); MS (ESI-QTOF +ve): $(M + Na)^+$ *m/z* calculated for $C_{18}H_{30}O_4S_2Na^+$: 397.1478, found: 397.1307; Anal. Calcd for $C_{18}H_{30}O_4S_2$: C 57.7; H 8.1; S 17.1%. Found: C 57.7; H 8.9; S 16.9; IR (neat; 298 K; cm^{-1}): 2920-2850 (-C-H), 1440-1350 (-CH_2-), 1120-990 (C-O), 910 (=C-H), 750 (-CH_2-).

2.5.13 General procedure of the thiol-ene synthesis to form small molecule and chain thio-ethers (TE) (5, 6).

The respective OE or AT **(3, 4)** and thiol were weighed into a silanised vial under a nitrogen blanket in a molar ratio of 1.0 to 0.5. Irgacure 819 (0.3 wt% for small molecules, 1.0 wt% for polymers) was added and the mixture stirred under ambient light for one day until colourless. After vigorous stirring, the viscous preparations were subjected to 24 h of UV light at 60°C in a Formlabs Form Cure. Small molecules were finally distilled *in vacuo* to yield pure product, whereas polymeric products were generally used as is for further analysis.

2.5.14 Synthesis of 2-ethoxy-5-(hexylthio)-2-methyl-1,3-dioxepane (EtOE-TE, 5a).

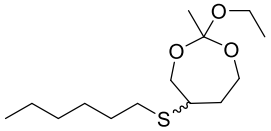

The reaction of EtOE **(3a)** (2.00 g, 12.64 mmol), 1-hexanethiol (1.49 g, 12.64 mmol) and Irgacure 819 (0.01 g) yielded clear oily product (3.30 g, 94%; distillation at 0.02 mbar, 150 °C). ^{1}H NMR (400 MHz; 298 K; $CDCl_3$; ppm): δ 3.96-3.42 (m, 4H), 3.48/3.46 (q, $^{3}J_{HH}$ = 7.1 Hz, 2H), 2.80/2.72 (m, 1H), 2.46 (m, 2H), 1.95-1.55 (m, 2H), 1.55-1.45 (m, 3H), 1.37/1.35 (s, 3H), 1.34-1.18 (m, 3H), 1.16/1.14 (t, $^{3}J_{HH}$ = 7.1 Hz, 3H), 0.82 (s, 3H); ^{13}C NMR (400 MHz; 298 K; $CDCl_3$; ppm): δ 115.72/115.64, 66.60/64.99, 61.81/59.77, 58.70/58.62, 43.98/43.21, 36.61/35.69, 31.51/31.48, 31.23/31.04, 30.15/30.09, 28.71/28.68, 22.63, 20.71/20.64, 15.49, 14.13; MS (ESI-QTOF +ve): $(M + Na)^+$ *m/z* calculated for $C_{14}H_{28}NO_3SNa^+$: 299.1651, found: 299.1657; Anal. Calcd for $C_{14}H_{28}O_3S$: C 60.8; H 10.2; S 11.6%. Found: C 60.8; H 10.3; S 11.5; IR (neat; 298 K; cm^{-1}): 2930-2860 (-C-H), 1380 ($-CH_2-$), 1160-1030 (C-O).

2.5.15 Synthesis of 2-((ethylthio)methyl)-5-(hexylthio)-1,3-dioxepane (EtAT-TE, 6a).

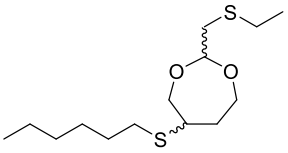

EtAT **(4a)** (2.00 g, 11.48 mmol), 1-hexanethiol (1.36 g, 11.48 mmol) and Irgacure 819 (0.01 g) were reacted to yield clear oily product (3.22 g, 95%; distillation at 0.02 mbar, 150 °C). ^{1}H NMR (400 MHz; 298 K; $CDCl_3$; ppm): δ 4.90-4.84 (m, 1H), 4.12-3.51 (m, 4H), 2.94-2.78 (m, 1H), 2.69-2.58 (m, 2H), 2.11-1.95 (m, 1H), 2.58-2.48 (m, 2H), 2.11-1.95 (m, 1H), 1.76-1.62 (m, 1H), 1.61-1.50 (m, 2H), 1.42-1.23 (m, 6H), 1.26 (qm, $^{3}J_{HH}$ = 7.2 Hz, 2H), 0.88 (tm, $^{3}J_{HH}$ = 7.2 Hz, 3H); ^{13}C NMR (400 MHz; 298 K; $CDCl_3$; ppm): δ 102.74/102.36, 70.91/66.53, 65.53/62.11, 44.18/43.84, 36.29, 35.01/34.68, 31.54/31.50, 31.24/31.18, 30.09/30.06, 28.69, 26.73, 22.63, 14.81, 14.13.; MS (ESI-QTOF +ve): $(M + K)^+$ *m/z* calculated for $C_{14}H_{28}O_2S_2K^+$: 331.1168, found: 331.1170; Anal. Calcd for $C_{14}H_{28}O_2S_2$: C 57.5; H 9.65; S 21.9%. Found: C 59.3; H 9.2; S 21.5; IR (neat; 298 K; cm^{-1}): 2920-2850 (-C-H), 1450-1340 ($-CH_2-$), 1120-990 (C-O), 740 ($-CH_2-$).

2.5.16 Synthesis of poly{[1,3-bis(2-methyl-2-oxyl-5-yl-1,3-dioxepane)-O-propane]-alt-(1,6-thioyl-hexane)} (OE3-2TE6, 5b).

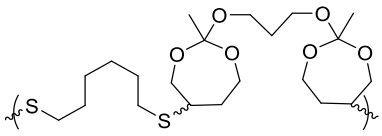

The reaction of OE3 **(3b)** (1.00 g, 3.33 mmol), 1,6-hexanedithiol (0.50 g, 3.33 mmol) and Irgacure 819 (0.015 g) yielded clear viscous product. ^{1}H NMR (400 MHz; 298 K; $CDCl_3$; ppm): δ 4.02-3.77 (m, 4H), 3.69-3.50 (m, 8H), 2.91-2.73 (m, 2H), 2.56-2.47 (m, 4H), 2.02-1.93 (m, 2H), 1.93-1.82 (m, 2H), 1.78-1.50 (m, 6H), 1.45-1.41 (ms, 6H), 1.41-1.34 (m, 4H); ^{13}C NMR (400 MHz; 298 K; $CDCl_3$; ppm): δ 115.88, 66.71/65.07, 61.91/60.32, 60.26/59.86, 44.06/43.27, 36.63/35.72, 31.16/31.00, 30.30, 30.03/30.00, 28.63, 20.69; IR (neat; 298 K; cm^{-1}): 2920-2850 (-C-H), 1370 ($-CH_2-$), 1150-1020 (C-O), 900 ($-CH_2-CH_2-$); GPC (THF): M_n = 4400 g·mol^{-1} ($Đ_M$ = 2.6).

2.5.17 Synthesis of poly{[1,3-bis(2-methyl-2-oxyl-5-yl-1,3-dioxepane)-O-propane]-alt-(3,6-dioxa-1,8-dithioyl-octane)} (OE3-2TEeg, 5c).

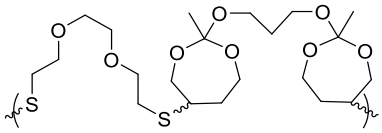

OE3 **(3b)** (1.00 g, 3.33 mmol) was reacted with 3,6-dioxa-1,8-octane-dithiol (0.61 g, 3.33 mmol) and Irgacure 819 (0.016 g) to yield clear viscous product. ^{1}H NMR (400 MHz; 298 K; CDCl3; ppm): δ 4.16 (t, $^{3}J_{HH}$ = 6.3 Hz, 4H), 3.99-3.79 (m, 4H), 3.67-3.50 (m, 8H), 2.91-2.74 (m, 2H), 2.63 (s, 4H), 2.61-2.53 (m, 4H), 2.02-1.93 (m, 2H), 1.93-1.83 (m, 6H), 1.75-1.57 (m, 2H), 1.48-1.37 (ms, 6H); ^{13}C NMR (400 MHz; 298 K; $CDCl_3$; ppm): δ 115.87/115.78, 71.36/71.18, 70.47, 66.58/65.05, 61.70/59.76, 60.32/60.28, 44.40/43.64, 36.65/35.75, 30.62/30.51, 30.29, 20.72; IR (neat; 298 K; cm^{-1}): 2940-2870 (-C-H), 1380 (-CH_2-), 1150-960 (C-O), 900 (-CH_2-CH_2-); GPC (THF): M_n = 4600 g·mol^{-1} ($Đ_M$ = 2.3).

2.5.18 Synthesis of poly{[1,3-bis(2-methyl-2-oxyl-5-yl-1,3-dioxepane)-O-propane]-alt-[bis(3-thioylpropyl) succinate]} (OE3-2TEsucc, 5d).

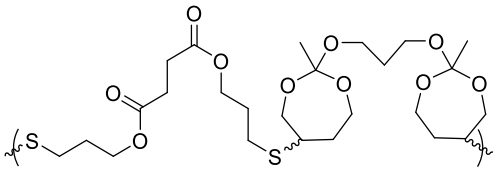

OE3 **(3b)** (1.00 g, 3.33 mmol), bis(3-mercaptopropyl) succinate (8.87 g, 3.33 mmol) and Irgacure 819 (0.019 g) were combined in the reaction to yielded clear viscous product. ^{1}H NMR (400 MHz; 298 K; CDCl3; ppm): δ 4.00-3.75 (m, 4H), 3.75-3.60 (m, 8H), 3.60-3.59 (s, 4H), 3.59-3.48 (m, 4H), 2.97-2.80 (m, 2H), 2.79-2.65 (m, 4H), 2.03-1.93 (m, 2H), 1.93-1.80 (m, 2H), 1.74-1.55 (m, 2H), 1.46-1.39 (ms, 6H); ^{13}C NMR (400 MHz; 298 K; $CDCl_3$; ppm): δ 172.33, 115.88, 66.52/64.96, 63.39/63.35, 61.75/59.79, 60.32/60.26, 44.12/43.39, 36.52/35.63, 30.29, 29.19, 29.13, 27.59/27.48, 20.66; IR (neat; 298 K; cm^{-1}): 2940-2880 (-C-H), 1730 (C=O); 1380 (-CH_2-), 1150-960 (C-O), 900 (-CH_2-CH_2-); GPC (THF): M_n = 5400 g·mol^{-1} ($Đ_M$ = 2.3).

2.5.19 Synthesis of poly{[1,3-bis(2-methyl-2-oxyl-5-yl-1,3-dioxepane)-O-propane]-alt-(dithioylthreitol)} (OE3-2TEdtt, 5e).

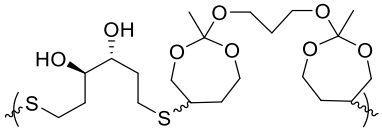

The reaction of OE3 **(3b)** (1.00 g, 3.33 mmol), dithiothreitol (0.51 g, 3.33 mmol) and Irgacure 819 (0.015 g) yielded an oily liquid. ^{1}H NMR spectroscopy and SEC chromatography suggest only low conversion. GPC (THF): M_n = 500 g·mol^{-1} ($Đ_M$ = 2.5).

2.5.20 Synthesis of poly{[1,6-bis(2-methylthioyl-5-yl-1,3-dioxepane)-S-hexane]-alt-(1,6-thioyl-hexane)} (AT6-2TE6, 6b).

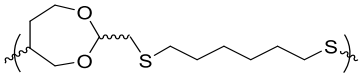

The reaction of AT6 **(4b)** (1.00 g, 3.20 mmol), 1,6-hexanedithiol (0.40 g, 2.67 mmol) and Irgacure 819 (0.014 g) yielded clear viscous product. ^{1}H NMR (400 MHz; 298 K; $CDCl_3$; ppm): δ 4.91-4.78 (2t, 1H), 4.13-3.95 (m, 1H), 3.91-3.70 (m, 2H), 3.66-3.50 (m, 1H), 2.93-2.76 (m, 1H), 2.67-2.60 (m, 2H), 2.60-2.47 (m, 4H), 2.10-1.95 (m, 1H), 1.73-1.63 (m, 1H), 1.63-1.48 (ms, 4H), 1.44-1.33 (ms, 4H); ^{13}C NMR (400 MHz; 298 K; $CDCl_3$; ppm): δ 102.36/102.36, 70.88/66.59, 65.52/62.15, 44.26/43.92, 36.30, 35.49/35.22, 32.83/32.81, 31.15/31.13, 31.09/29.94, 29.56/29.54, 29.53/28.49; IR (neat; 298 K; cm^{-1}): 2910-2850 (-C-H), 1450-1340 (-CH_2-), 1120-990 (C-O), 750 (-CH_2-); GPC (THF): M_n = 5900 g·mol^{-1} ($Đ_M$ = 3.8).

2.5.21 Reduction and end-capping of polymer chains.

Disulfide linkages were reduced to thiol groups and protected from oxidation following an adapted procedure in the style of commercially available ReadyPrep™ Reduction-Alkylation Kits. The sample was completely dissolved in THF with triethylamine (2%). Under a nitrogen blanket tributylphosphine (200 mol eq.) was added and the sealed vial shaken vigorously (300 rpm) for 4 h, followed by addition of a solution of iodoacetamide (300 mol eq.) in THF and further shaking for 4 h. Water (2 vol eq.) was added and the suspension

centrifuged to form a clear organic phase. Separation, washing with water and drying in the SEC solvent over potassium carbonate yielded the final chain polymer product.

2.5.22 Synthesis of net-poly{[1,3-bis(2-methyl-2-oxyl-5-yl-1,3-dioxepane)-2-yl-O-butane]-co-(1,6-thioyl-hexane)} (OE4ene-2TE6, 7).

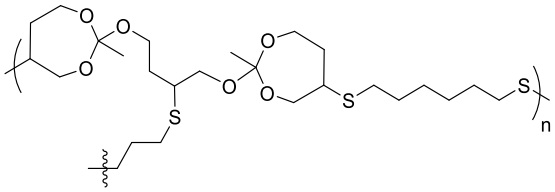

A mixture of OE4ene **(3c)** (2.00 g, 6.40 mmol), 1,6-hexanedithiol (1.44 g, 9.6 mmol) and Irgacure 819 (0.034 g, 1 wt%) was stirred in a silanised brown vial under a nitrogen blanket until the solution cleared. 0.3 mL of the solution was then each deposited into a PP mould (2 mL vial cap with lowered rim) to form a smooth top surface. Subsequent curing in an Otoflash G171 flash box for five times 1000 flashes with intermittent cooling, followed by extraction from the moulds and a further five times 1000 flashes, yielded the polymer material in clear cylindrical shapes. T_g = 10.2 °C (DSC, 10 K·min^{-1}, heat); IR (neat; 298 K; cm^{-1}): 2910-2840 (-C-H), 1370 (-CH_2-), 1150-1000 (C-O), 900 (-CH_2-CH_2-).

2.6 References

(1) Devi, K. S.; Vasudevan, P., Absorbable Surgical Sutures. *J. Macromol. Sci. Polymer Rev.* **1985,** *25* (3), 315-324. doi:10.1080/07366578508081959

(2) Barrows, T. H., Degradable implant materials: A review of synthetic absorbable polymers and their applications. *Clin. Mater.* **1986,** *1* (4), 233-257. doi:10.1016/s0267-6605(86)80015-4

(3) Amass, W.; Amass, A.; Tighe, B., A review of biodegradable polymers: uses, current developments in the synthesis and characterization of biodegradable polyesters, blends of biodegradable polymers and recent advances in biodegradation studies. *Polym. Int.* **1998,** *47* (2), 89-144. doi:10.1002/(SICI)1097-0126(1998100)47:2<89::AID-PI86>3.0.CO;2-F

(4) Okada, M., Chemical syntheses of biodegradable polymers. *Prog. Polym. Sci.* **2002,** *27* (1), 87-133. doi:10.1016/S0079-6700(01)00039-9

(5) Brannigan, R. P.; Dove, A. P., Synthesis, properties and biomedical applications of hydrolytically degradable materials based on aliphatic polyesters and polycarbonates. *Biomater. Sci.* **2017,** *5* (1), 9-21. doi:10.1039/C6BM00584E

(6) Middleton, J. C.; Tipton, A. J., Synthetic biodegradable polymers as orthopedic devices. *Biomaterials* **2000,** *21* (23), 2335-2346. doi:10.1016/S0142-9612(00)00101-0

(7) Manavitehrani, I.; Fathi, A.; Badr, H.; Daly, S.; Negahi Shirazi, A.; Dehghani, F., Biomedical Applications of Biodegradable Polyesters. *Polymers* **2016,** *8* (1), 20.

(8) Kamaly, N.; Yameen, B.; Wu, J.; Farokhzad, O. C., Degradable Controlled-Release Polymers and Polymeric Nanoparticles: Mechanisms of Controlling Drug Release. *Chem. Rev.* **2016,** *116* (4), 2602-2663. doi:10.1021/acs.chemrev.5b00346

(9) Burkoth, A. K.; Burdick, J.; Anseth, K. S., Surface and bulk modifications to photocrosslinked polyanhydrides to control degradation behavior. *J. Biomed. Mater. Res. A* **2000,** *51* (3), 352-359. doi:10.1002/1097-4636(20000905)51:3<352::Aid-jbm8>3.0.Co;2-c

(10) Tesfamariam, B., Bioresorbable vascular scaffolds: Biodegradation, drug delivery and vascular remodeling. *Pharmacol. Res.* **2016,** *107*, 163-171. doi:10.1016/j.phrs.2016.03.020

(11) Poetz, K. L.; Mohammed, H. S.; Shipp, D. A., Surface Eroding, Semicrystalline Polyanhydrides via Thiol–Ene "Click" Photopolymerization. *Biomacromolecules* **2015,** *16* (5), 1650-1659. doi:10.1021/acs.biomac.5b00280

(12) Rosen, H. B.; Chang, J.; Wnek, G. E.; Linhardt, R. J.; Langer, R., Bioerodible polyanhydrides for controlled drug delivery. *Biomaterials* **1983,** *4* (2), 131-133. doi:10.1016/0142-9612(83)90054-6

(13) Muggli, D. S.; Burkoth, A. K.; Anseth, K. S., Crosslinked polyanhydrides for use in orthopedic applications: Degradation behavior and mechanics. *J. Biomed. Mater. Res.* **1999,** *46* (2), 271-278. doi:10.1002/(SICI)1097-4636(199908)46:2<271::AID-JBM17>3.0.CO;2-X

(14) von Burkersroda, F.; Schedl, L.; Gopferich, A., Why degradable polymers undergo surface erosion or bulk erosion. *Biomaterials* **2002,** *23* (21), 4221-4231. doi:10.1016/S0142-9612(02)00170-9

(15) Iñiguez-Franco, F.; Auras, R.; Ahmed, J.; Selke, S.; Rubino, M.; Dolan, K.; Soto-Valdez, H., Control of hydrolytic degradation of Poly(lactic acid) by incorporation of chain extender: From bulk to surface erosion. *Polym. Test.* **2018,** *67*, 190-196. doi:10.1016/j.polymertesting.2018.02.028

(16) Artham, T.; Doble, M., Biodegradation of Aliphatic and Aromatic Polycarbonates. *Macromol. Biosci.* **2008,** *8* (1), 14-24. doi:10.1002/mabi.200700106

(17) Kumar, N.; Langer, R. S.; Domb, A. J., Polyanhydrides: an overview. *Adv. Drug Deliver. Rev.* **2002,** *54* (7), 889-910. doi:10.1016/S0169-409X(02)00050-9

(18) Bachelder, E. M.; Beaudette, T. T.; Broaders, K. E.; Dashe, J.; Fréchet, J. M. J., Acetal-Derivatized Dextran: An Acid-Responsive Biodegradable Material for Therapeutic Applications. *J. Am. Chem. Soc.* **2008,** *130* (32), 10494-10495. doi:10.1021/ja803947s

(19) Belloncle, B.; Bunel, C.; Menu-Bouaouiche, L.; Lesouhaitier, O.; Burel, F., Study of the Degradation of Poly(ethyl glyoxylate): Biodegradation, Toxicity and Ecotoxicity Assays. *J. Polym. Environ.* **2012,** *20* (3), 726-731. doi:10.1007/s10924-012-0429-2

(20) Paramonov, S. E.; Bachelder, E. M.; Beaudette, T. T.; Standley, S. M.; Lee, C. C.; Dashe, J.; Fréchet, J. M. J., Fully Acid-Degradable Biocompatible Polyacetal Microparticles for Drug Delivery. *Bioconjug. Chem.* **2008,** *19* (4), 911-919. doi:10.1021/bc7004472

(21) Merkli, A.; Heller, J.; Tabatabay, C.; Gurny, R., Synthesis and characterization of a new biodegradable semi-solid poly(ortho ester) for drug delivery systems. *J. Biomater. Sci. Polym. Ed.* **1993,** *4* (5), 505-516. doi:10.1163/156856293X00168

(22) Heller, J.; Barr, J., Poly(ortho esters) - From Concept to Reality. *Biomacromolecules* **2004,** *5* (5), 1625–1632. doi:S1525-7797(04)00049-2

(23) Katti, D. S.; Lakshmi, S.; Langer, R.; Laurencin, C. T., Toxicity, biodegradation and elimination of polyanhydrides. *Adv. Drug Deliver. Rev.* **2002,** *54* (7), 933-961. doi:10.1016/S0169-409X(02)00052-2

(24) Ulery, B. D.; Nair, L. S.; Laurencin, C. T., Biomedical applications of biodegradable polymers. *J. Polym. Sci. B. Polym. Phys.* **2011,** *49* (12), 832-864. doi:10.1002/polb.22259

(25) Cherdron, H.; Burg, K.; Kloos, F.; Reske, E.; Sextro, G., Technical developments in polyoxymethylene from an industrial point of view. *Macromol. Symp.* **1988,** *13-14* (1), 289-300. doi:10.1002/masy.19880130121

(26) Heller, J., Development of poly(ortho esters): a historical overview. *Biomaterials* **1990,** *11* (9), 659-665. doi:10.1016/0142-9612(90)90024-K

(27) Heller, J.; Barr, J.; Ng, S. Y.; Abdellauoi, K. S.; Gurny, R., Poly(ortho esters): synthesis, characterization, properties and uses. *Adv. Drug. Deliv. Rev.* **2002,** *54* (7), 1015-1039. doi:10.1016/S0169-409X(02)00055-8

(28) Tamotsu, H.; Koji, I.; Akihiro, U.; Toshiyuki, K., Synthesis of polyacetals with various main-chain structures by the self-polyaddition of vinyl ethers with a hydroxyl function. *J. Polym. Sci. A Polym. Chem.* **2002,** *40* (22), 4053-4064. doi:10.1002/pola.10490

(29) Baśko, M.; Kubisa, P., Synthesis of Double Hydrophilic Graft Copolymers with a Polyacetal Backbone. *Macromolecules* **2002,** *35* (24), 8948-8953. doi:10.1021/ma0207475

(30) Endo, T.; Sanda, F., A novel approach for the chemical 'recycling' of polymeric materials equilibrium polymerization system of spiro orthoesters. *React. Funct. Polym.* **1997,** *33* (2), 241-245. doi:10.1016/S1381-5148(97)00046-1

(31) Tschan, M. J.-L.; Ieong, N. S.; Todd, R.; Everson, J.; Dove, A. P., Unlocking the Potential of Poly(Ortho Ester)s: A General Catalytic Approach to the Synthesis of Surface-Erodible Materials. *Angew. Chem.* **2017,** *129* (52), 16891-16895. doi:10.1002/ange.201709934

(32) Fu, S.; Yang, G.; Wang, J.; Wang, X.; Cheng, X.; Tang, R., Acid-degradable poly(ortho ester urethanes) copolymers for potential drug carriers: Preparation, characterization, in vitro and in vivo evaluation. *Polymer* **2017,** *114*, 1-14. doi:10.1016/j.polymer.2017.02.079

(33) Haider, T.; Shyshov, O.; Suraeva, O.; Lieberwirth, I.; von Delius, M.; Wurm, F. R., Long-Chain Polyorthoesters as Degradable Polyethylene Mimics. *Macromolecules* **2019,** *52* (6), 2411-2420. doi:10.1021/acs.macromol.9b00180

(34) Kolb, H. C.; Finn, M. G.; Sharpless, B. K., Click Chemistry: Diverse Chemical Function from a Few Good Reactions. *Angew. Chem. Int. Ed.* **2001,** *40* (11), 2004-

2021. doi:10.1002/1521-3773(20010601)40:11<2004::AID-ANIE2004>3.0.CO;2-5

(35) Amato, D. N.; Amato, D. V.; Mavrodi, O. V.; Martin, W. B.; Swilley, S. N.; Parsons, K. H.; Mavrodi, D. V.; Patton, D. L., Pro-Antimicrobial Networks via Degradable Acetals (PANDAs) Using Thiol–Ene Photopolymerization. *ACS Macro Lett.* **2017,** *6* (2), 171-175. doi:10.1021/acsmacrolett.7b00009

(36) Barner-Kowollik, C.; Du Prez, F. E.; Espeel, P.; Hawker, C. J.; Junkers, T.; Schlaad, H.; Van Camp, W., "Clicking" Polymers or Just Efficient Linking: What Is the Difference? *Angew. Chem. Int. Ed.* **2011,** *50* (1), 60-62. doi:10.1002/anie.201003707

(37) Dondoni, A., The Emergence of Thiol–Ene Coupling as a Click Process for Materials and Bioorganic Chemistry. *Angew. Chem. Int. Ed.* **2008,** *47* (47), 8995-8997. doi:10.1002/anie.200802516

(38) Roth, P. J.; Boyer, C.; Lowe, A. B.; Davis, T. P., RAFT Polymerization and Thiol Chemistry: A Complementary Pairing for Implementing Modern Macromolecular Design. *Macromol. Rapid Commun.* **2011,** *32* (15), 1123-1143. doi:10.1002/marc.201100127

(39) Machado, T. O.; Sayer, C.; Araujo, P. H. H., Thiol-ene polymerisation: A promising technique to obtain novel biomaterials. *Eur. Polym. J.* **2017,** *86*, 200-215. doi:10.1016/j.eurpolymj.2016.02.025

(40) Hoyle, C. E.; Bowman, C. N., Thiol–Ene Click Chemistry. *Angew. Chem. Int. Ed.* **2010,** *49* (9), 1540-1573. doi:10.1002/anie.200903924

(41) Kade, M. J.; Burke, D. J.; Hawker, C. J., The power of thiol-ene chemistry. *J. Polym. Sci. A Polym. Chem.* **2010,** *48* (4), 743-750. doi:10.1002/pola.23824

(42) Lowe, A. B., Thiol-ene "click" reactions and recent applications in polymer and materials synthesis: a first update. *Polym. Chem.* **2014,** *5* (17), 4820-4870. doi:10.1039/c4py00339j

(43) Qin, X.-H.; Ovsianikov, A.; Stampfl, J.; Liska, R., Additive manufacturing of photosensitive hydrogels for tissue engineering applications. *BioNanoMaterials* **2014,** *15* (3-4), 49-70. doi:10.1515/bnm-2014-0008

(44) Leonards, H.; Engelhardt, S.; Hoffmann, A.; Pongratz, L.; Schriever, S.; Bläsius, J.; Wehner, M. M.; Gillner, A., Advantages and drawbacks of Thiol-ene

based resins for 3D-printing, *Proc. SPIE 9353*, Laser 3D Manufacturing II, **2015** *93530F*. doi:10.1117/12.2081169

(45) Plikk, P.; Tyson, T.; Finne-Wistrand, A.; Albertsson, A. C., Mapping the characteristics of the radical ring-opening polymerization of a cyclic ketene acetal towards the creation of a functionalized polyester. *J. Polym. Sci. A Polym. Chem.* **2009,** *47* (18), 4587-4601. doi:10.1002/pola.23511

(46) McElvain, S. M., The Ketene Acetals. *Chem. Rev.* **1949,** *45* (3), 453-492. doi:10.1021/cr60142a003

(47) Nomura, N.; Tsurugi, K.; RajanBabu, T. V.; Kondo, T., Homogeneous Two-Component Polycondensation without Strict Stoichiometric Balance via the Tsuji–Trost Reaction: Remote Control of Two Reaction Sites by Catalysis. *J. Am. Chem. Soc.* **2004,** *126* (17), 5354-5355. doi:10.1021/ja0492743

(48) Schwach-Abdellaoui, K.; Heller, J.; Gurny, R., Synthesis and characterization of self-catalyzed poly(ortho-esters) based on decanediol and decanediol-lactate. *J. Biomater. Sci. Polym. Ed.* **1999,** *10* (3), 375-389. doi:10.1163/156856299x00432

3

Customised Fading Scaffolds: Strong Polyorthoester Networks *via* Thiol-Ene Crosslinking for Cytocompatible Surface-Eroding Materials in 3D Printing

3.1 Abstract

Polyorthoesters are a well-documented class of biocompatible and rapidly surface-erodible materials, however issues with mechanical weakness and complex synthesis have significantly limited their application. In this work, a series of tough poly(orthoester-thioether) (POETE) materials suitable for 3D printing is presented. Specifically, the thiol-ene reaction is employed to form polymer networks based on a variety of bifunctional OE precursors containing different functional linker composition. The chemical linker structure determines the mobility of segments, while the number of reactive centres and functionalities correlates to the crosslinking density within the polymer structure, which in turn leads to customisable thermal and mechanical properties of the resulting materials. Similarly, post-processing conditions and architecture are crucial to the degradability of the specimens, which can be exploited for programmed bulk-release applications. Finally, the suitability of POETE materials for stereolithography applications is demonstrated on a commercial 3D printer, whereby the subsequent degradation can be controlled to obtain macro-porous stent models and structures incorporating mobile components. Analogue to acid-releasing PLA materials, degradation products of processed POETE materials show cytocompatibility below a certain concentration or acidity threshold. This research thus highlights the simplicity, versatility and applicability of POETE networks as new biocompatible surface-eroding materials for consideration in biomedicine and engineering.

3.2 Introduction

Additive manufacturing (AM) has been an essential scalable industrial technique for decades,[1] and finds application in engineering[2], architecture[3] and medicine[4-5]. In a typical approach for rapid prototyping, this process comprises of the 3D printing of a computer-aided design (CAD), followed by post treatment such as post-curing under heat or UV radiation and functionalisation.[6] Specific methods such as stereolithography (SLA) achieve superior structures with enhanced complexity and accuracy, as well as a decreased number of production steps compared to ordinary moulding techniques.[7] In fact, not only can SLA be used to produce masters in indirect manufacturing,[8] but it is also established as

the leading technique in guides for surgical orthopedics.[9] Strong but flexible 3D printed prostheses and tissue scaffolds are of particular concern for direct application in biomedicine, providing an accelerated option to manufacture customised support structures on site, rather than relying on external services. In order to expand the limited library of suitable resources, biodegradable materials for AM have been the focus of extensive research in recent years.[4-5, 10] In particular, novel biomaterials such as hydrogels,[11] as well as copolymers containing polyesters,[12-14] polycarbonates,[15] poly(ethylene glycols),[16-17] poly(propylene fumarate)[18] and polyanhydrides[19] have been proven to be promising materials.

In addition to a customisable manufacturing process, biomedical applications rely on specifically tailored material and degradation properties.[20] Of special interest are strong surface-erodible materials, which provide stability and a controlled degradation over time without the need for removal *via* invasive surgery, for example as scaffolds or drug delivery vehicles.[21] Hydrolytic degradation behaviour can be estimated based on the relation between reactivity of polymeric bonds, diffusion through the matrix and dimensions of a sample.[22] The most common classes of surface-erodible materials used in biomedical research include polyanhydrides,[23-24] polyacetals[25] and polyorthoesters (POEs),[26] aside from special compositions containing polycarbonates[27] and specific long-chain acids[28-30]. Unfortunately, such materials lack the ability to be manufactured quickly and efficiently with tailored features for a specific application.

Attempts to synthesise both photopolymerisable and surface-erodible biomaterials have thus far led to the development of polyanhydride-copolymers; however, these often raise issues regarding high local acidity on the surfaces by insoluble degradation products, sensitivity to oxygen and moisture during the manufacturing process, or limitation of mechanical diversity.[31] Surface degradable POEs as first discovered by Heller *et al.*[32] degrade mainly into alcohols and water soluble, small molecule acids[33] and have already been studied for potential biomedical applications.[34-35] However, complications during synthesis and inferior mechanical properties prevented their application to date.[36] Even recent poly(orthoester amide) and -urethane polymers require

harsh polymerisation conditions and exhibit no significant mechanical strength.[37-38] Herein, the suitability of novel poly(orthoester-thioether)s (POETEs) based on stable orthoester (OE) monomers and facile highly efficient thiol-ene "click" coupling reactions[39-40] for AM applications is explored. The comprehensive manufacturing process allows for a customisable linker composition and network structure, and thus the molecular architecture, which results in adequate mechanical and degradation properties, giving access to a diverse new library of materials.

3.3 Results and Discussion

3.3.1 Synthesis Strategy

All synthesised materials are based on a cyclic ketene acetal (Scheme 3-1, compound **1**, CKA), which was obtained according to the procedure by Plikk *et al*.[41] *via* ring formation from bromoacetaldehyde dimethyl acetal, followed by dehydrohalogenation.

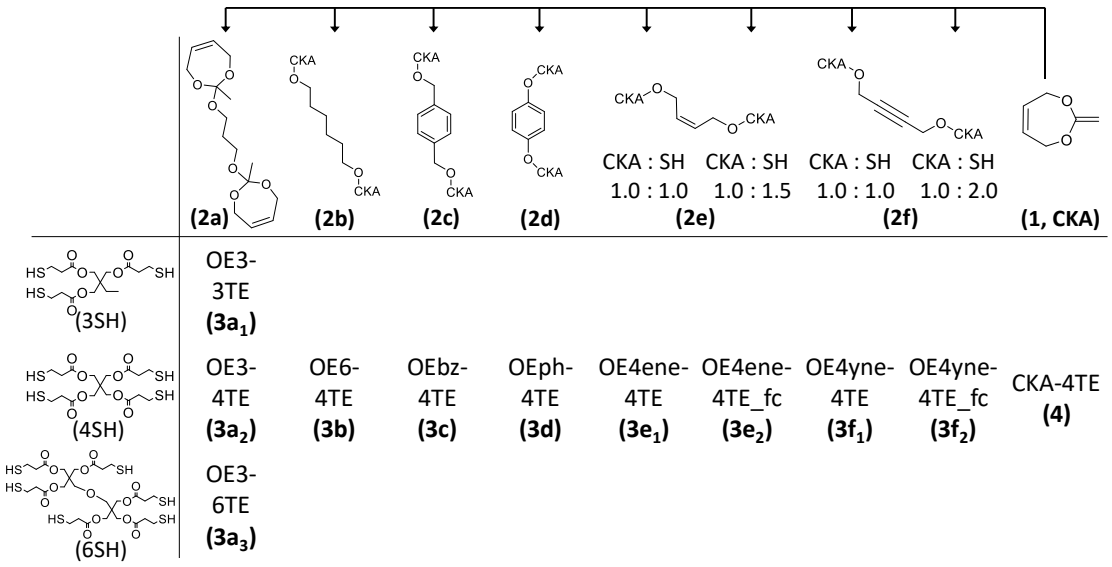

Scheme 3-1. Synthesis of different OE monomers (**2a-f**) from a cyclic ketene acetal (**1**) and composition of all POETE (**3a-f**) and PATTE (**4**) networks.

Subsequently, orthoester precursors (OEs, **2a-f**) were synthesised *via* addition reaction to different bifunctional alcohols. The resulting OEs contained linkers with aliphatic chains of different lengths (**2a, 2b**), aromatic compounds (**2c, 2d**) and unreacted unsaturated bonds (**2e**, **2f**) in order to comprehensively investigate the influence of the linker structure on the chemical and physical properties of the resulting polymer materials. As the final step, photoinitiated

thiol-ene 'click' reaction led to the formation of POETE networks (**3a-f**), which were compared to the simple poly(acetal-thioether) (PATTE) network (**4**) formed from the CKA (**1**). The crosslinking density of the resulting networks was controlled by the number of thiol (SH) functionalities on the crosslinker (**3a$_1$-3a$_3$**) and the unsaturated bonds present in the OE precursors (**3e$_2$**, **3f$_2$**) that acted as additional anchor points.

3.3.2 OE Synthesis and Characterisation

Before the manufacturing of the materials, the identity and purity of all synthesised OE monomers had to be confirmed *via* ^{1}H NMR, ^{13}C NMR, IR and Raman spectroscopy.

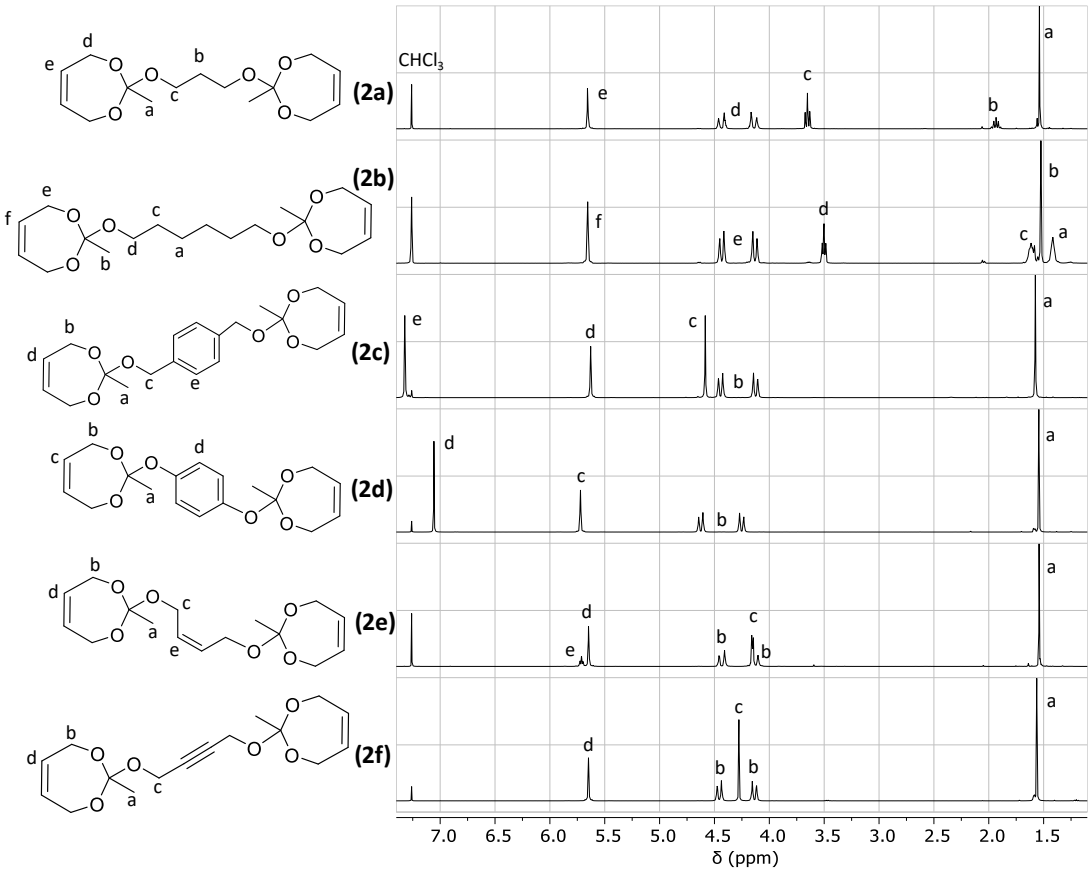

Figure 3-1. ^{1}H NMR spectra and structural assignment of all employed OE monomers (**2a-2f)** (CDCl3, 298 K, 300 MHz).

^{1}H NMR spectra of all prepared OE compounds (Figure 3-1) revealed no obvious impurities besides the occasional signal at δ = 2.00 ppm from acetic acid or ester degradation products, as discussed in the previous chapter. While the methyl and cyclic alkene functionalities appeared within a narrow range each for

all OEs around δ = 1.55 and 5.60 ppm, respectively, the cyclic methylene group in the hydroquinoic OE (**2d**) was shifted significantly downfield to δ = 4.25 and 4.62 ppm from around δ = 4.15 and 4.45 ppm, respectively. This indicates that the diamagnetic ring current of the aromatic group has a deshielding influence on the latter as a result of the close proximity.

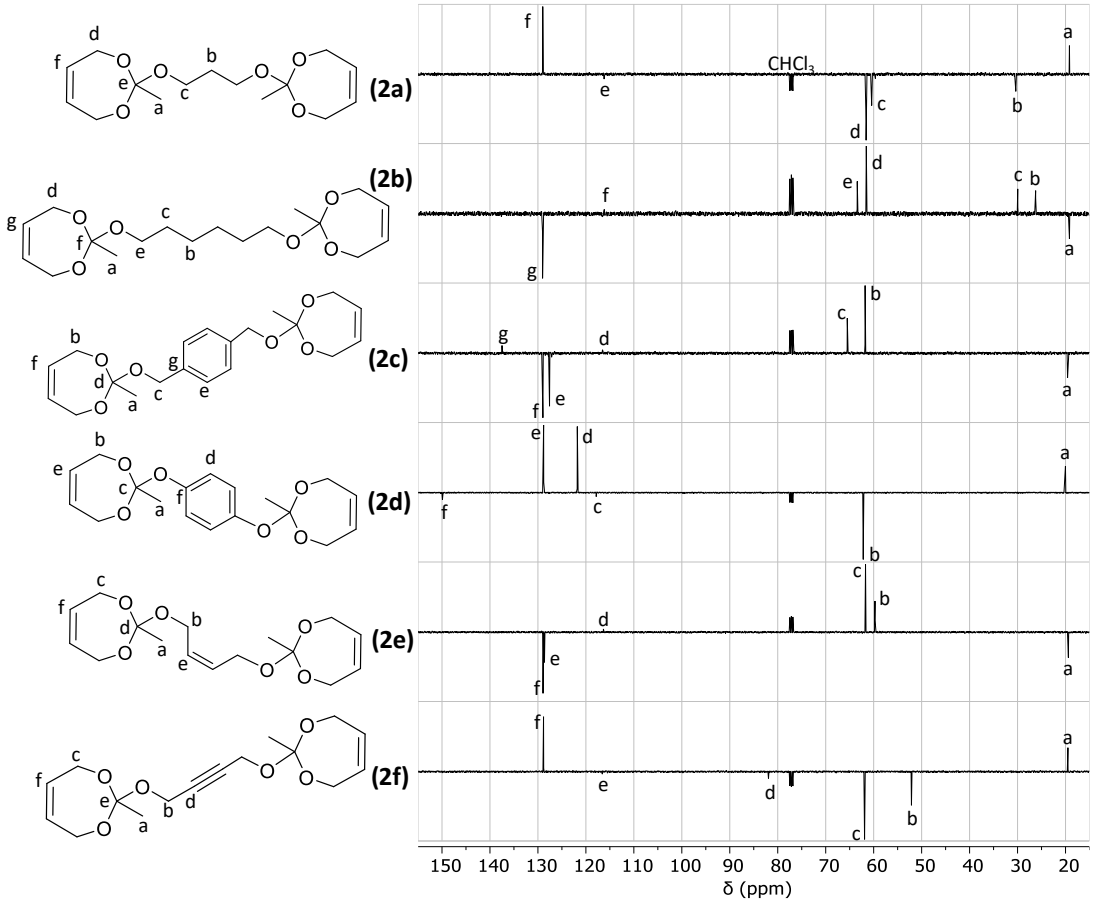

Figure 3-2. ^{13}C NMR spectra and structural assignment of all employed OE monomers (**2a-2f)** (CDCl3, 298 K, 300 MHz).

Interestingly, complementary ^{13}C NMR spectra (Figure 3-2) revealed a far less significant shift difference of the cyclic methylene carbons by only δ = 3.00 ppm. No further impurities are easily discernible, which further demonstrates the ease of the synthesis and purity of products.

For completion and to serve as reference for the following network formation, IR and Raman spectra of the OE monomers were recorded.

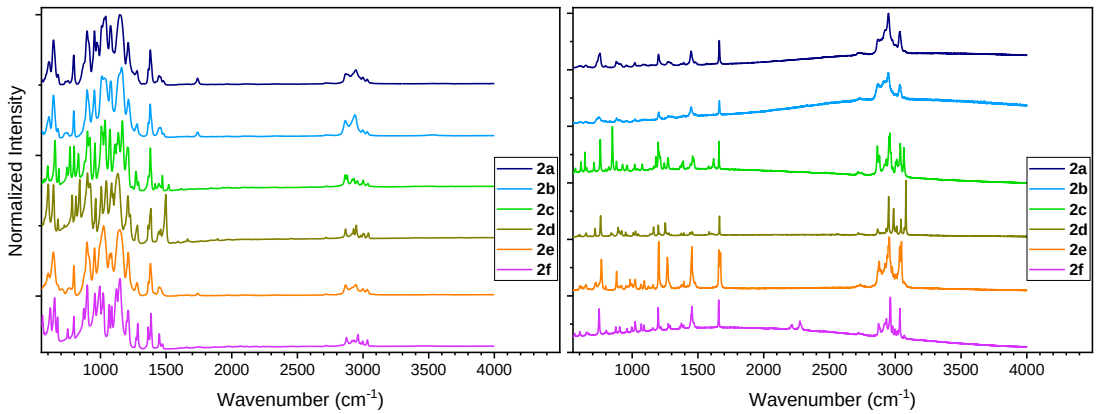

Figure 3-3. IR (left) and Raman (right, 633 nm excitation) absorption spectra of all employed OE monomers (**2a-2f**) (neat, room temperature).

While IR spectra of the OE samples (Figure 3-3) provided a unique fingerprint region for all monomer species, assignment to specific vibrations was complicated by the dense population. In contrast, several significant functionalities yielded distinct signals in the Raman spectra, such as the alkene and orthoester functionality around $\tilde{\nu}$ = 1660 and 750 cm^{-1}, respectively. As the cyclic alkene functionality will be consumed for the POETE synthesis, the disappearance of this signal can indicate the progress of the reaction.

3.3.3 Photo-Curing and Thermal Post-Curing of Virgin Materials

While most of the formulations were liquid at room temperature, the mixtures containing aromatic and unsaturated compounds (**2c**, **2d**, **2f**) needed to be prepared at elevated temperatures (around 50 °C and 120 °C, respectively) to keep the solutions homogenous during handling. Intense UV irradiation and a solid photoinitiator Irgacure 819 were then used to couple the precursors and form solid virgin materials. These showed extremely rapid surface wetting in contact with air and acidic surfaces, such as silicates, after several hours (Figure 3-4), which made them difficult to handle and was likely attributed to incomplete conversion and residual moisture.

Figure 3-4. Photographs of **3a**$_2$ virgin material samples (without post-curing) left on an untreated glass surface on air as is (day 0), after 2 days and after 4 days.

Consequently, a thermal post-curing strategy (*i.e.* 120 °C under vacuum) was followed in order to keep even alternative reactants in the liquid state and potentially improve crosslinking, as well as dry OE3-4TE (**3a$_2$**) samples. While a significant loss in surface wetting and increase in strength to the touch was noted, this step barely induced any significant change in the relative peak intensities of the materials as determined by IR and Raman spectroscopy.

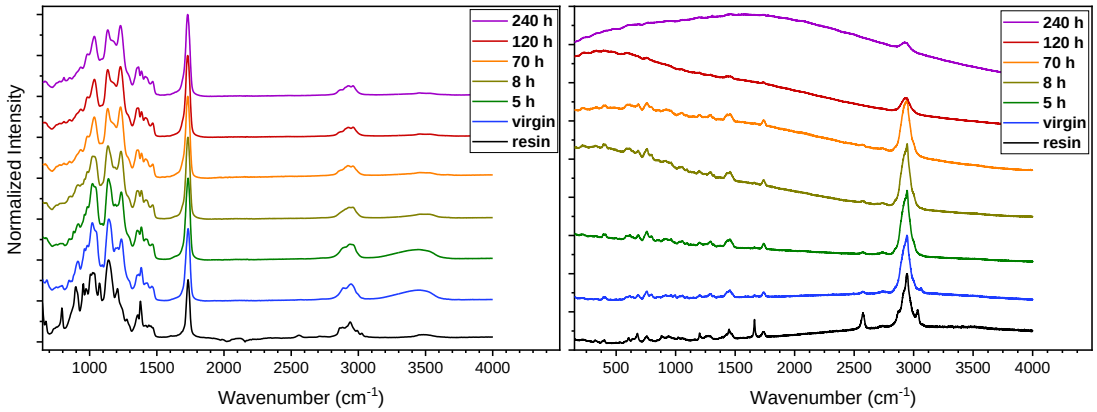

Figure 3-5. IR and Raman absorption spectra of **3a$_2$** formulations and materials after different times of thermal post-curing *in vacuo*. Left: IR (neat, room temperature), right: Raman (neat, room temperature, 633 nm excitation).

IR spectra (Figure 3-5) show small peaks around $\tilde{\nu}$ = 900 and 2900 cm^{-1} attributed to unreacted alkene bonds, which are shrinking over time until indistinct after 5 h of post-curing. A broad signal around $\tilde{\nu}$ = 3500 cm^{-1} further indicates the presence of water with O-H stretch vibration or potentially thiol, but also disappears after several hours. The Raman spectrum better visualises unsaturated and thiol vibrations because of increased resonance, however signals at $\tilde{\nu}$ = 1650 and 2550 cm^{-1}, respectively, are almost completely indistinguishable after 5 h. This indicates that very high conversion was reached after UV irradiation, which confirms the "click" character of the thiol-ene coupling step.[42]

In order to establish a more reliable measure for further optimisation, thermo-mechanical analysis was performed.

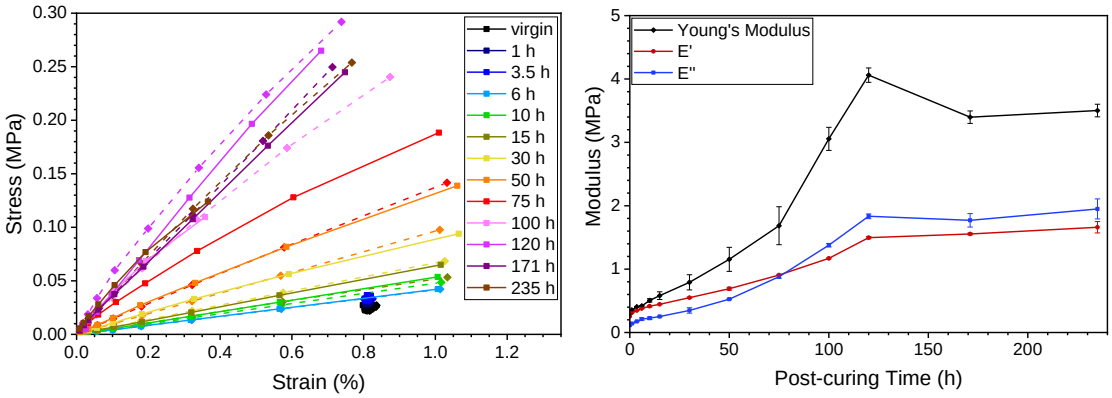

Figure 3-6. DMTA strain-stress curves (left) and corresponding temporal progression (right) of **3a$_2$** materials after different times of thermal post-curing *in vacuo* obtained from dynamic mechanical thermal analysis (37 °C, frequency 1 Hz, amplitude 1 to 100 µm, step size increased exponentially).

It should be noted that DMTA data (Figure 3-6) from virgin material, 1 h and 3.5 h post-curing was obtained at one constant amplitude over several cycles as surface wetting led to slipping of the sample otherwise. Nevertheless, an optimal curing time of 120 h was determined, as after such amount of time, a plateau in Loss and Storage Moduli, as well as a maximum in Young's Modulus, respectively, was reached. The drop in Young's Modulus at high curing temperature could be caused by oxidation after prolonged exposure to heat and intermittently to air.

3.3.4 Spectral Analyses of POETE and PATTE after Thermal Post-Curing

In order to further investigate the influence of the oxidative post-curing method, the following material studies were performed dually on two sets of post-cured materials with and without exposure to air (Figure 3-7).

Figure 3-7. Photographs of assorted samples of all materials (**3a$_1$-4**) after post-curing for 120 h at 120 °C *in vacuo* (left) and on air (right). Order of sample groups: **3a$_1$, 3a$_2$, 3b, 3c, 3d; 3a$_3$, 3e$_1$, 3e$_2$, 3f$_1$, 3f$_2$, 4** (each downwards).

Interestingly, the presence of oxygen during the thermal post-curing step had a significant effect on the samples, which resulted in obviously different levels of

discolouration. To establish if the difference in procedure directly oxidises carbon or sulfide atoms in the structure, XPS analysis can be utilised.

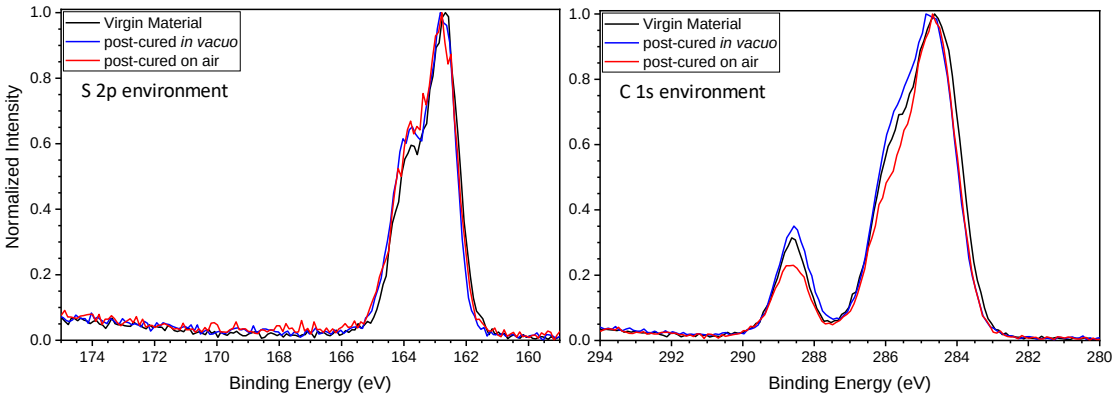

Figure 3-8. X-ray Photoelectron Spectra (XPS) of **3a**$_2$ samples before (virgin) and after post-curing for 120 h at 120 °C *in vacuo* and on air. Left: S 2p environment from 175 to 159 eV, right: C 1s environment from 294 to 280 eV.

Unfortunately, XPS analysis (Figure 3-8) revealed only minor differences in surface structure, which may be caused by the low penetration depth of the technique of typically only several Å, as well as immediate oxidation of exposed surfaces. While a difference between virgin and post-cured material is characterised by a difference in peak intensity around 164 and 283 eV, exposure to air during post-curing resulted in significant differences around 286 and 289 eV. Further quantification of such differences can be facilitated by fitting of the XPS curves and an assignment of species according to established databases.

Table 3-1. Assignments and fitted numerical composition of molecular environments and XPS binding energy of **3a**$_2$ samples before (virgin) and after post-curing for 120 h at 120 °C *in vacuo* and on air.

Binding Energy (eV)	Assignment	Fraction (%) (Virgin Mat.)	Fraction (%) *(In Vacuo)*	Fraction (%) (On Air)
162.7 - 162.8	-S-C-	89.35	94.04	85.59
163.4 - 163.8	-S-S-/-S-H	10.65	3.2	12.08
164.3 - 164.8	-SOR-/-S-H	-	2.77	1.07
167.7	-SO_2-	-	-	1.26
283.9	-C=C-	4.13	0	0
284.6	-C-C-/-CH-/-C-S-	53.93	52.6	61.27
285.8 - 258.9	-C-O-	28.56	32.29	26.24
287.5 – 287.6	-(C=O)-	0.96	0.91	0.64
288.5 – 288.6	-O-(C=O)-	8.27	10.14	8.6
288.8 – 288.9	-CO_3-	4.14	4.06	3.25

As expected, the fitting of the XPS curves (Table 3-1) revealed that S-C bond possessed highest intensity and further increased after post-curing *in vacuo*,

whereas a drop in this region in the air-exposed sample suggests the cleavage of a fraction of the virgin material bonds in favour of several oxidised species. Unfortunately, the sulfur 2p region was too populated and weak to properly distinguish these peaks and the overlying S-H peak. Instead, the carbon 1s region offered more distinct peaks, with an obvious drop in unsaturated carbon species at 283.9 eV in the post-cured materials. Interestingly, a drop in the oxidised species of the air-exposed sample was observed in favour of the 284.6 eV non-oxide species. This could indicate that instead of oxidizing, homolytically cleaved S-C bonds recombine to S-S and C-C bonds, which would be in agreement with the observation in the sulfur species. Oxidised species increased in the *in vacuo* cured sample, which could indicate the extraction of volatile components and carbon dioxide out of the network, as well as the formation of other ester species.

In order to increase penetration depth and both characterise and confirm the structural differences between the POETE and PATTE materials (**3a$_1$-4**), IR and Raman spectra were recorded.

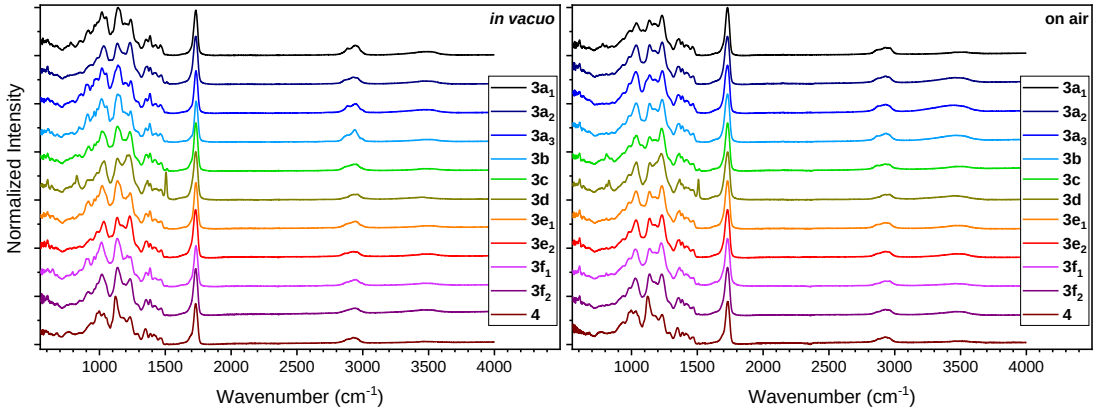

Figure 3-9. IR absorption spectra of all materials (**3a$_1$-4**) after post-curing for 120 h at 120 °C *in vacuo* (left) and on air (right) (neat, room temperature).

Similar to the observations from the OE monomers, IR spectra obtained from all POETE and PATTE materials (Figure 3-9) revealed barely any distinct signals depending on the OE linker but mostly facilitates identification by relative peak heights in the fingerprint region. The notable exception was again the material based on the hydroquinoic OE (**3d**), which exhibited strong vibrational signals at $\tilde{\nu}$ = 1550 and 850 cm^{-1}.

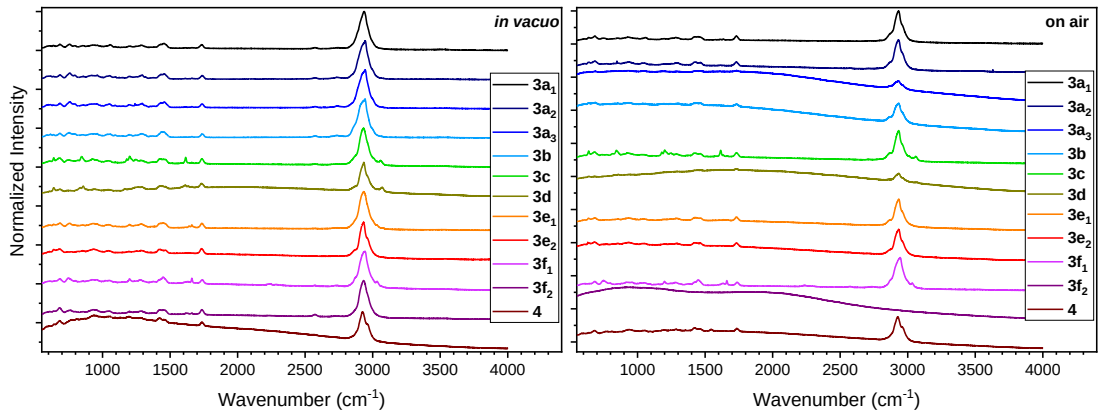

Figure 3-10. Raman absorption spectra of all materials (**3a$_1$-4**) after post-curing for 120 h at 120 °C *in vacuo* (left) and on air (right) (neat, room temperature, 633 nm excitation).

While the Raman spectra of the OE monomers revealed a number of clear vibrational signals, the same study for the POETE and PATTE materials did not resolve any clearly discernible signals except the aliphatic vibrations around $\tilde{\nu}$ = 2900 cm^{-1} (Figure 3-10). Most likely hindered by the dense network structure, a small reoccurring vibrational signal at $\tilde{\nu}$ = 1740 cm^{-1} could however be identified and attributed to the carbonyl functionalities within the thiol crosslinker.

3.3.5 Thermal Analyses of POETE and PATTE after Thermal Post-Curing

Complementary to the spectral observations, TGA, DMTA and DSC analyses were performed to characterise the more application-relevant difference in bulk material properties.

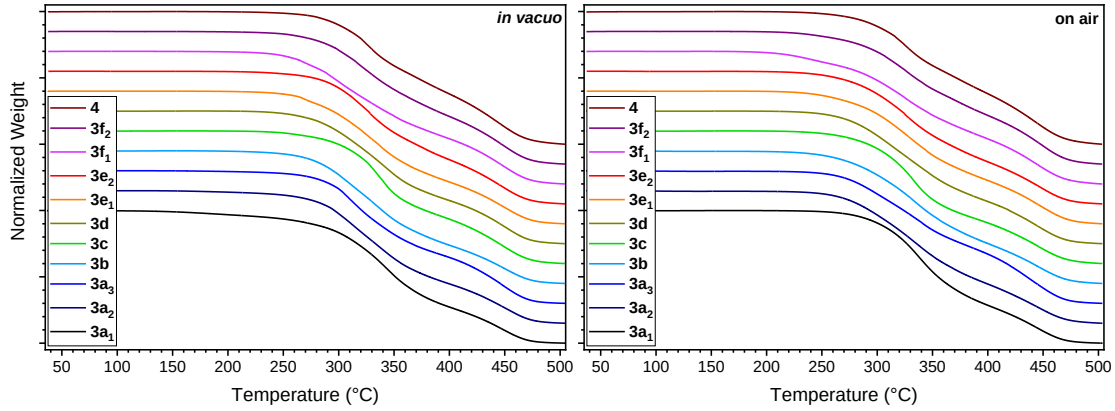

Figure 3-11. TGA thermograms of samples of all materials (**3a$_1$-4**) after post-curing for 120 h at 120 °C *in vacuo* (left) and on air (right) (10 K·min^{-1}).

TGA analyses (Figure 3-11) revealed a common degradation temperature of 250 °C for all materials irrespective of the post-curing method. As a noteworthy

exception, the material obtained from the acetylenic OE compound with lower crosslinking density (**3f$_1$**) showed an earlier decomposition onset at around 200 °C. This could be explained by incomplete conversion or partial decomposition during post-curing and hence evaporation. While some *in vacuo* treated aliphatic networks (**3a$_1$**, **3a$_2$**) also show earlier decomposition onset, this is likely a consequence of the higher sensitivity to moisture and hence partial degradation.

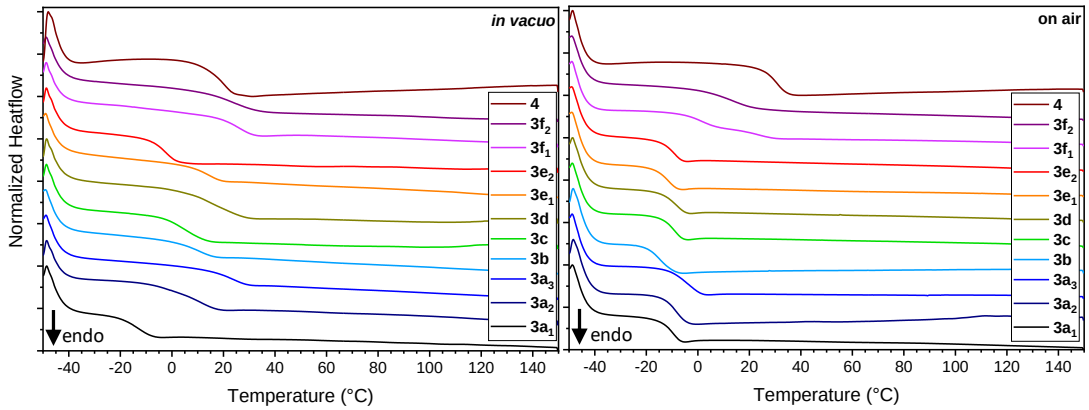

Figure 3-12. DSC thermograms of samples of all materials (**3a$_1$-4**) after post-curing for 120 h at 120 °C *in vacuo* (left) and on air (right) (heating, 3rd cycle, 10 K·min^{-1}).

Differences in the glass transition temperature (T_g) were visualised using DSC thermograms (Figure 3-12) and ranged between materials from -10 up to 40 °C. A clear trend to increase the T_g according to crosslinking density is observed in the OE3 polymers (**3a$_{1-3}$**). Similarly, the stiffer OEph linker (**3d**) and acetylenic compound OEyne (**3f**) both showed a glass transition at higher temperatures in vacuum-cured materials. In contrast, T_gs of POETE networks based on aliphatic (**3a$_1$-3b**) and aromatic OEs (**3c**, **3d**), which were exposed to air, were found in a narrow range of -10 to -5 °C. This suggests that a common secondary curing reaction based on oxidation occurred to result in a similar material structure.

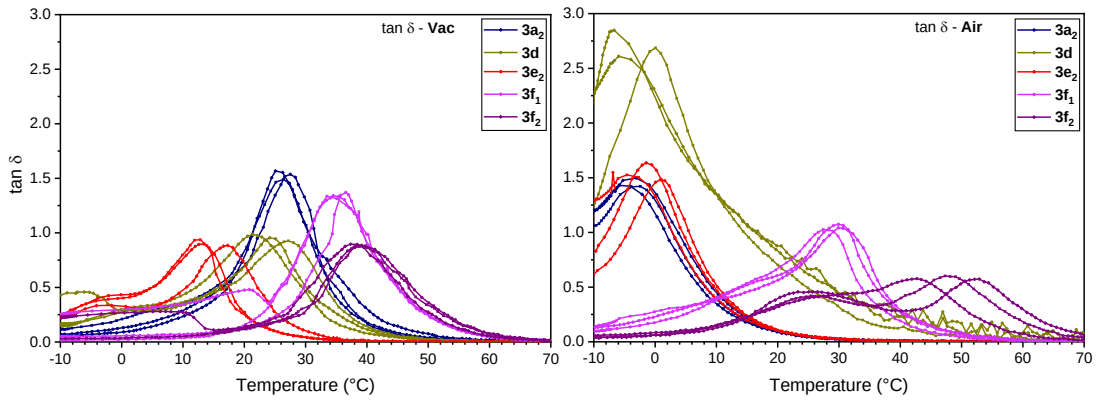

Figure 3-13. DMTA thermograms of samples of selected materials (**3a**$_2$, **3d**, **3e**$_2$, **3f**$_1$, **3f**$_2$) after post-curing for 120 h at 120 °C *in vacuo* (left) and on air (right) (frequency 1 Hz, amplitude 5 µm, 2 K·min^{-1}).

DMTA thermograms (Figure 3-13) supported the findings from DSC analyses, with a spread-out population of T_gs for the vacuum-cured materials and two narrower distributions of T_gs for air-exposed POETE network materials. For better comparison, the average T_gs of both methods were calculated and compared.

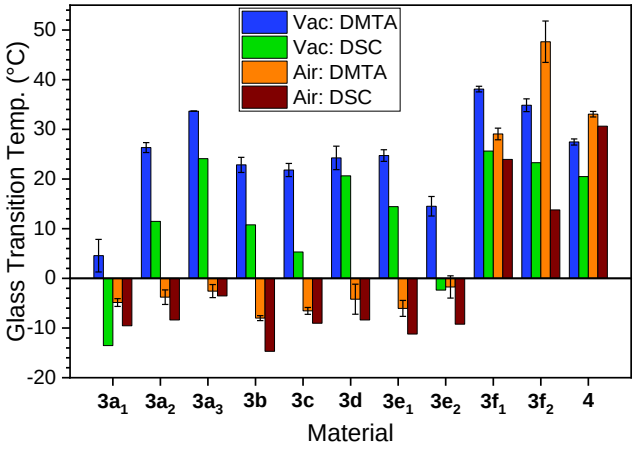

Figure 3-14. Comparison of glass transition temperatures obtained from DMTA and DSC temperature sweeps of all network materials (**3a**$_1$**-4**) after post-curing under vacuum and on air (DMTA: frequency 1 Hz, amplitude 5 µm, 2 K·min^{-1}; DSC: 10 K·min^{-1}).

An obvious difference in T_gs was revealed in direct comparison between values obtained from DSC (inflection point) and DMTA (maximum) analyses (Figure 3-14). It should be noted that this difference could arise from the difference in material thickness, heating rate and structural factors; accordingly, only values of the same techniques should be compared. Significant discrepancies of up to 35 °C were illustrated for both aliphatic and aromatic compositions, whereas highly unsaturated bond containing networks and PATTE (**4**) were less or even positively affected by exposure to oxygen.

3.3.6 Mechanical Analyses of POETE and PATTE after Thermal Post-Curing

As a consequence of the wide range of T_gs, all further mechanical analyses were conducted at 37 °C to improve reproducibility and simulate physiological conditions. As the most straight-forward test for bulk-mechanical behaviour, tensile testing on 10 samples each was performed.

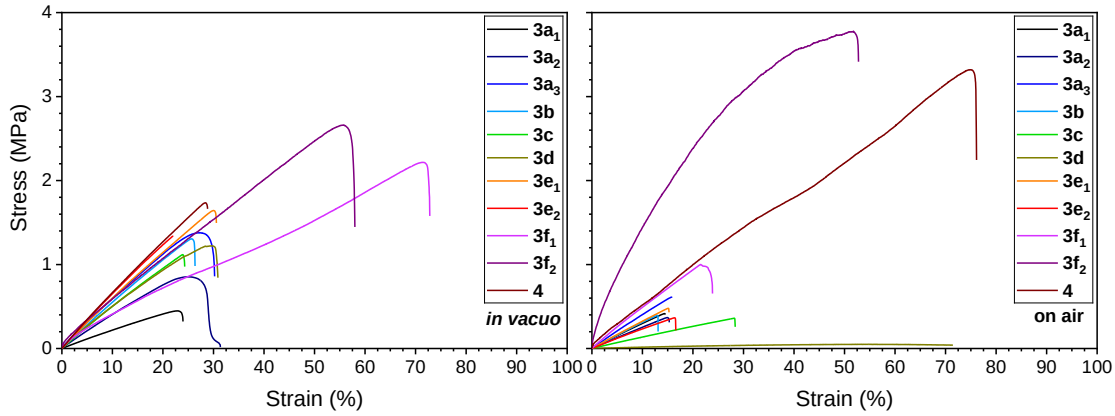

Figure 3-15. Representative tensile strain-stress curves of all network materials (**3a₁-4**) after post-curing under vacuum (left) and on air (right) (4 mm·min^{-1}, 37 °C).

Table 3-2. Peak strain, stress and elastic modulus values including standard deviation of all materials (**3a₁-4**) obtained from tensile testing at 37 °C after post-curing for 120 h at 120 °C *in vacuo* (left) and on air (right) (4 mm·min^{-1}, 37 °C).

	In Vacuo			On Air		
	Strain @ Peak (%)	Stress @ Peak (MPa)	Elastic Modulus (MPa)	Strain @ Peak (%)	Stress @ Peak (MPa)	Elastic Modulus (MPa)
$3a_1$	22.6 ± 0.9	0.44 ± 0.03	2.22 ± 0.12	16.8 ± 5.1	0.47 ± 0.14	2.99 ± 0.42
$3a_2$	24.7 ± 5.1	1.31 ± 0.25	6.64 ± 0.32	15.4 ± 1.0	0.61 ± 0.04	4.14 ± 0.46
$3a_3$	24.2 ± 1.9	0.84 ± 0.08	4.08 ± 0.13	15.4 ± 1.6	0.38 ± 0.08	2.61 ± 0.52
3b	26.1 ± 4.5	1.26 ± 0.20	5.43 ± 0.23	12.7 ± 2.4	0.37 ± 0.06	3.08 ± 0.30
3c	24.4 ± 4.1	1.14 ± 0.14	5.23 ± 0.40	24.1 ± 4.8	0.34 ± 0.14	1.59 ± 0.66
3d	31.1 ± 5.1	1.27 ± 0.20	5.27 ± 0.31	40.9 ± 16.7	0.06 ± 0.06	0.18 ± 0.11
$3e_1$	21.9 ± 1.7	1.34 ± 0.09	6.72 ± 0.08	17.0 ± 3.5	0.38 ± 0.06	2.48 ± 0.71
$3e_2$	29.7 ± 2.8	1.59 ± 0.17	6.04 ± 0.17	16.1 ± 3.6	0.50 ± 0.12	3.28 ± 0.63
$3f_1$	71.4 ± 4.2	2.19 ± 0.17	4.61 ± 0.90	21.9 ± 1.7	1.02 ± 0.07	5.24 ± 0.16
$3f_2$	54.9 ± 5.8	2.62 ± 0.19	7.95 ± 2.11	54.3 ± 11.3	3.60 ± 1.57	14.30 ± 5.50
4	28.6 ± 0.2	1.77 ± 0.37	7.00 ± 0.03	72.4 ± 11.1	3.21 ± 0.48	6.37 ± 0.87

As a general trend, the vacuum-treated materials (**3a-e**) showed a moderate ultimate strain of up to 30% with a high peak stress in a range between 0.5 and 1 MPa during tensile testing (Figure 3-15 and Table 3-2), which is plausible for crosslinked networks. In contrast, a decrease in ultimate strain by almost half was observed for most samples when subjected to air instead, combined with a general weakening of the elastic modulus as characterised by a decrease in slope.

Interestingly, while both materials based on the acetylenic OE (**3f**) possessed superior ultimate tensile strength and elasticity after post-curing *in vacuo* with 2.2 MPa at 71% and 2.6 MPa at 55%, respectively, the performance of the less crosslinked POETE (**3f$_1$**) drops close to the general POETE average after exposure to air. However, the highly crosslinked species further improved to 3.6 MPa at 54%, and the PATTE (**4**) reached 3.2 MPa at 72%. A possible explanation for this lies in the oxidative degradation of the less crosslinked material, whereas the dense POETE (3**f$_2$**) and less sensitive and more tightly structured PATTE (**4**) benefit from oxidative crosslinking. Thereby, the densest network (**3f$_2$**) followed a non-linear strain-stress curve, which could be an artefact from exceeding the limitations of the used tensile testing setup or clamping force.

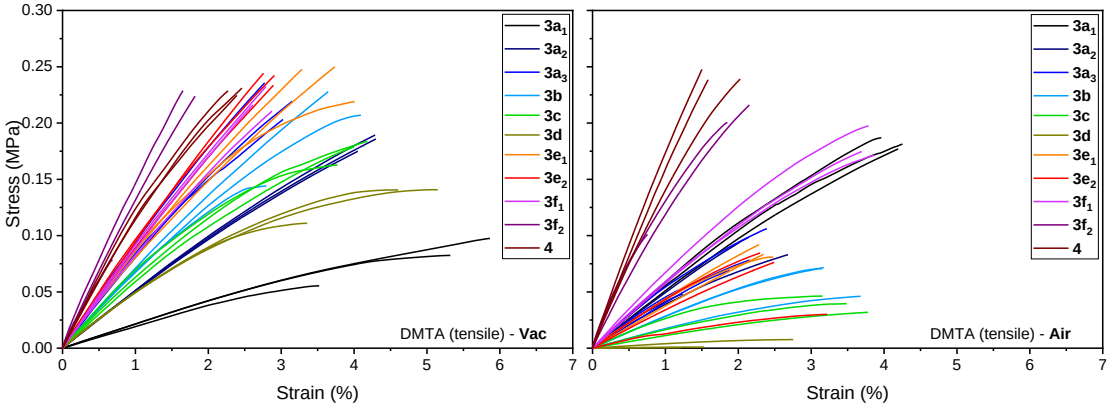

Figure 3-16. Strain-stress curves of all materials (**3a$_1$-4**) obtained from DMTA at 37 °C after post-curing for 120 h at 120 °C *in vacuo* (left) and on air (right) (0.1 to 4 N, 0.2 N·min^{-1}).

Analogous tensile strain-stress curves were recorded *via* DMTA (Figure 3-16) in order to further characterise the onsets and hence true Young's moduli. The slopes roughly correspond to those found in the tensile testing studies, with the lowest density crosslinked material (**3a$_1$**) consistently achieving lower elastic moduli than the other materials in both post-curing procedures. Also corresponding to the observations in tensile testing, PATTE (**4**) and the densest crosslinked POETE (**3f$_2$**) achieved the steepest slopes after treatment on air.

While these simple strain-stress investigations permit an adequate impression on how the material will react towards occasional mechanical stimuli, DMTA in oscillatory mode mimics the fluctuating mechanical stress in biological systems.

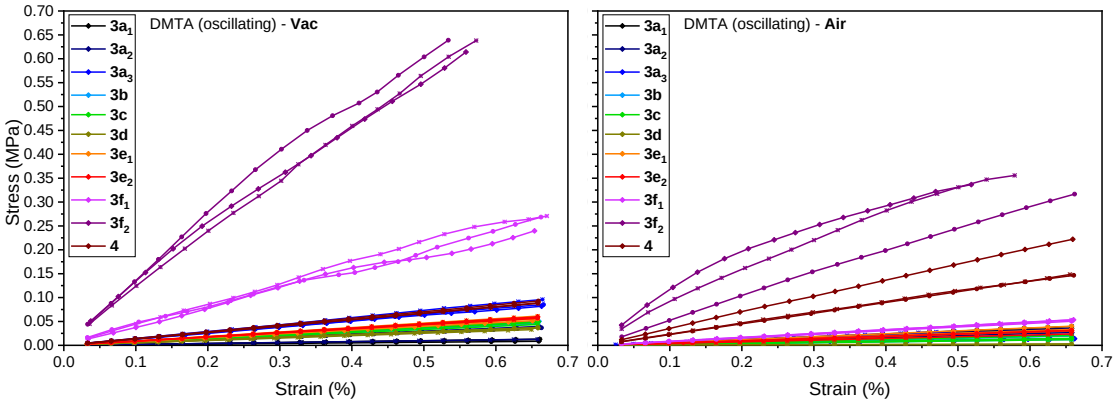

Figure 3-17. Strain-stress curves of all materials (**3a₁-4**) obtained from DMTA in oscillatory mode at 37 °C after post-curing for 120 h at 120 °C *in vacuo* (left) and on air (right) (frequency 1 Hz, amplitude 5 to 100 µm, step size 5 µm).

Stress-strain curves obtained from DMTA under oscillation with step-wise increasing strain (Figure 3-17) revealed an intermediary mechanical behaviour between ultimate tensile testing and DMTA stress-strain curves. The slope and hence elastic modulus of most curves presented within a narrow band, and the lowest crosslinked POETE (**3a₁**) achieved the lowest strength. Interestingly, the difference in slope of the two best-performing materials for each processing method compared to the rest is highly significant. The highest crosslinked POETE (**3f₂**) as the overall strongest material reached a 10-fold higher modulus than the average other POETE material after post-curing *in vacuo*. Even after treatment with exposure to air this material is still strongest, however only half as strong as after the alternative treatment. This mechanical superiority corresponds to the observations from tensile testing in terms of highest ultimate strain and stress, however the trend of Young's moduli is more akin to the DMTA strain-stress observations. Similarly, the network with the most rigid acetylenic OE linker (**3f₁**) stood out in both tensile testing and oscillatory strain-stress curves. In contrast, the curves of the samples exposed to air generally appear less reproducible, which could be explained by an inconsistent secondary oxidative curing mechanism. This could also explain why the acetylenic POETE (**3f₁**) possessed reduced strength after post-curing in air, with the triple-bond susceptible to oxidation or recombination with cleaved thiol functionalities, whereas the tight PATTE network (**4**) benefits from oxidative crosslinks.

In order to facilitate and summarise the previous results, a direct comparison between Young's moduli was conducted.

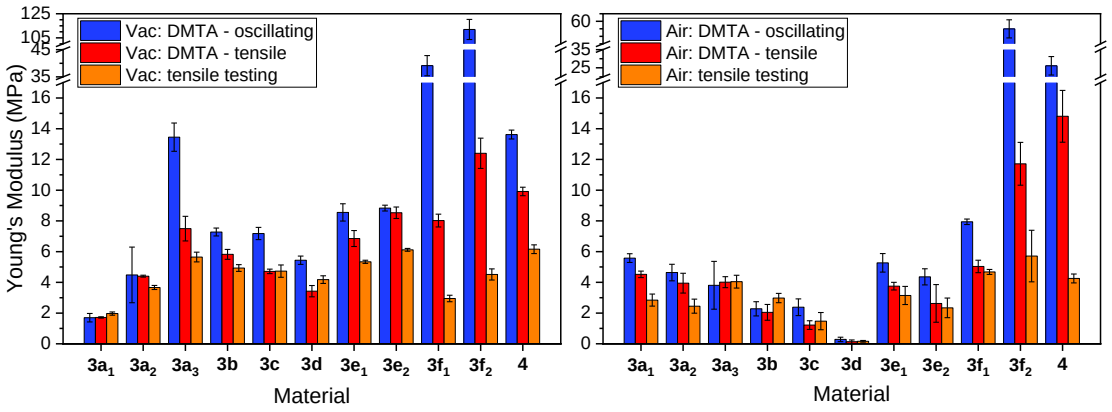

Figure 3-18. Comparison of Young's modulus obtained from DMTA measurements in tensile and oscillatory mode as well as from tensile testing curves of networks (**3a₁**-**4**) after post-curing under vacuum (left) and on air (right) (DMTA oscillatory: frequency 1 Hz, amplitude 5 to 100 µm, step size 5 µm; DMTA tensile: 0.1 to 4 N, 0.2 N·min^{-1}; tensile testing: 4 mm·min^{-1}; all measurements at 37 °C).

By visualizing Young's moduli obtained from tensile testing and analogous calculations from oscillatory and tensile DMTA (Figure 3-18), the superior mechanical performance of the vacuum-treated materials is clearly established, which suggests a secondary curing mechanism under oxygen exposure, potentially by oxidation of remaining functionalities such as thioethers or orthoesters to form ester, ether or peroxide linkages. It should be noted that the POETE with the highest crosslinking density (**3f₂**) and PATTE (**4**) exhibited unusually high mechanical strength and lower susceptibility to oxidation, likely because the susceptible orthoester and linker functionalities are less accessible or not existent. Interestingly, the OEph-4TE (**3d**) based on hydroquinone was most affected by the contact with oxygen and turned into a gel, which could be attributed to the high charge density and tension in the OE facilitating oxidation. As a final measure of material strength, loss and storage moduli were recorded at a constant temperature and oscillation with a constant maximum amplitude.

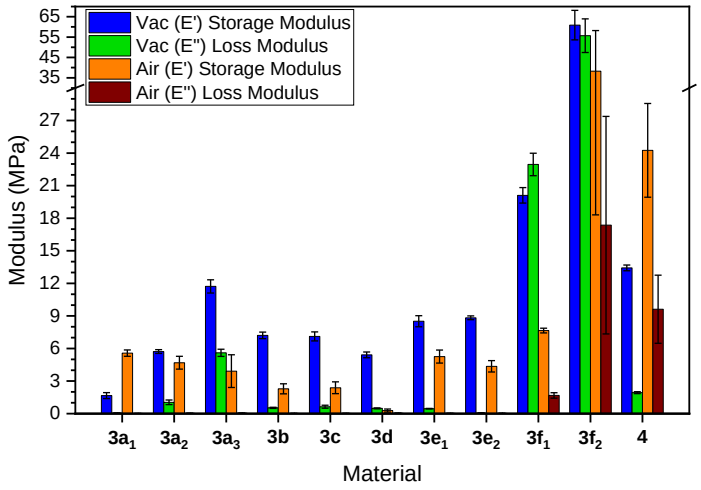

Figure 3-19. Loss and storage modulus of all materials (**3a₁-4**) obtained from DMTA at 37 °C and constant amplitude after post-curing for 120 h at 120 °C *in vacuo* and on air (frequency 1 Hz, amplitude 20 µm (approximately 0.13 % strain), 10 min equilibration time).

Comparison of the dynamic storage and loss moduli of the materials (**3a₁-4**) under the same conditions (Figure 3-19) provides insight into the predominance of either elastic or viscous behaviour, respectively. As 37 °C exceeds the glass transition temperature of most POETE materials, barely any resistance is recorded and the materials behave mostly elastic with high storage and low loss moduli. In contrast, the high T_g of the acetylenic POETE (**3f₁** and **3f₂**) result in a glassier material with high viscosity and resistance to any deformation after curing *in vacuo*. Depending on the application, this stiffness might be desirable.

Generally, exposure to air led to inconsistencies and a higher deviation from the average as indicated by the error bars, because oxidation is introduced as a secondary factor. This was particularly obvious in strong materials (such as **3f₂**), which were prone to show micro-ruptures and non-linear stress-strain curves. Therefore, considering the influence of linkers and crosslinkers on the material performance and the previous observations, the vacuum-treated samples should be used as main reference for POETE materials.

According to Young's moduli (Figure 3-18) and ultimate tensile stresses (Table 3-2), the effect of crosslinking density (**3a₁-3a₃**) significantly outperformed that of the linker structure (**3b-d**). This could be explained by the low impact of only three additional methylene groups on chain flexibility, whereas bulky aromatic groups interfere with the network and at the same time are too restricted for stacking to occur. Similarly, the incorporation of alkene

groups (**3e**) did not significantly alter the material properties, probably because the linker is too small to contribute significant stiffness to the network and even gains flexibility upon further crosslinking. The alkyne-linked materials (**3f**), however, exhibited the highest mechanical performance of all POETEs, which could be attributed to both the stiffest linker structure, as well as the highest crosslinking density and generally the highest glass transition temperature. In fact, such features render segments sterically hindered, thus locking the structure in place, which even outperformed the PATTE network (**4**) in several experiments.

3.3.7 Degradation and Release Studies of POETEs and PATTE Materials

With this comprehensive analysis of the thermo-mechanical properties concluded, further analysis was conducted to characterise the degradation properties the POETE and PATTE materials.

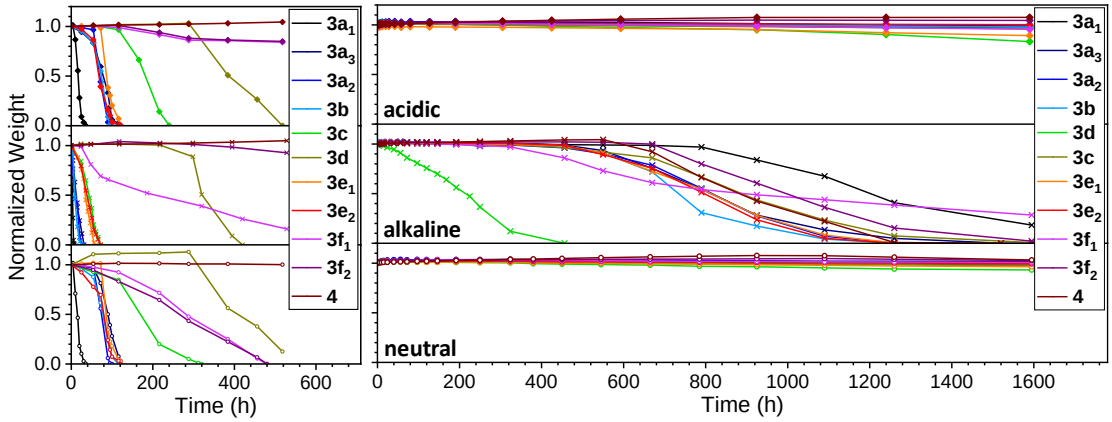

Figure 3-20. Average relative weight progress over time of POETE and PATTE network (**3a**-**4**) samples after post-curing under vacuum (left) and on air (right) in aqueous media at 37 °C. Top: 0.1 M HCl (pH = 1.0), centre: 0.1 M NaOH (pH = 13.0), bottom: D-PBS solution (pH = 7.4).

In order to investigate the effect of functional groups and crosslinking density on the degradability of the networks, the weight loss of cylindrical samples over time was monitored in 0.1 M HCl (pH = 1.0), 0.1 M NaOH (pH = 13.0) and Dulbeco-PBS solution (pH = 7.4) (Figure 3-20). While the air-exposed POETE samples (**3a-f**) generally showed slow to no degradation in acidic and neutral media, a slow degradation in basic medium was observed for all samples, including the PATTE (**4**). Hence, the secondary post-curing reaction led likely to the formation of a protective layer of secondary material, which either outnumbered or transformed the OE functionalities, such as in a

transesterification. Either those new functionalities or the TE bonds are then susceptible to alkaline hydrolysis, especially in the gel-like OEph-4TE (**3d**).

In contrast, the *in vacuo* treated samples started to degrade within hours until fully degraded up to three weeks later. Surprisingly, the samples in basic solution showed the highest degradation rates, with all aliphatic-containing samples (**3a**-**c, 3e**) fully degraded after up to 4 days. This increased degradation rate could be ascribed to the higher segment mobility of the samples, which would enable higher water diffusion and is most obvious in the almost instantly degrading OE3-3TE (**3a**$_1$) with the lowest crosslinking density. In both acidic and neutral media, a delayed onset of around one day is observed, *i.e.* hydrolysis starts only after a certain diffusion period. Similar to the observed higher mechanical strength and glass transition temperature, acetylenic POETE species (**3f**$_1$, **3f**$_2$) showed improved stability in all media, especially under acidic conditions, most likely as a result of the dominating sterical hindrance and hydrophobicity. This performance is only topped by PATTE (**4**), which remains stable under all conditions as a consequence of the lack of OE groups. OEph-4TE (**3d**) should again be noted as a special case with potential counteraction of highly hydrophobic but strain-inducing linker structure. In this case, OEph-4TE (**3d**) exhibits an even more delayed onset, followed by rapid degradation and constant coloured release of presumably hydroquinone.

While this study demonstrated the broad scope of the materials, a more application-focused approach was conducted on rapidly eroding virgin material.

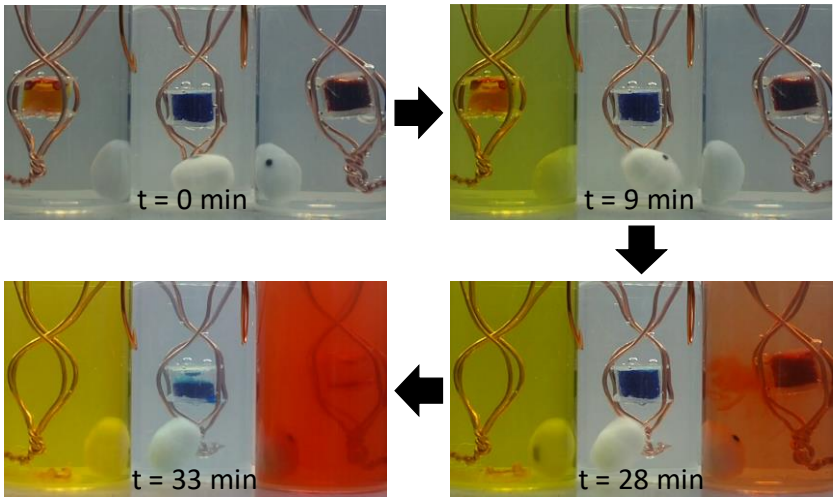

Figure 3-21. Video frames documenting the dye release from filled cylinders of OE3-4TE (**3a**$_2$) virgin material in 1 M HCl at 22 °C. In order of increasing wall thickness: yellow, red, blue.

A simple potential application of the more susceptible virgin material was demonstrated *via* erosion studies (Figure 3-21), mimicking programmed delivery or protective coatings of varying thickness. Acidic medium (1 M HCl, pH = 0) was chosen for most rapid and clear degradation, as the high concentration of degradation products caused turbidity in alkaline or neutral solution. No discolouration was observed until bulk release after several minutes, which underlines the nonporous nature of the network with erosion only occurring on the very surface of the material.

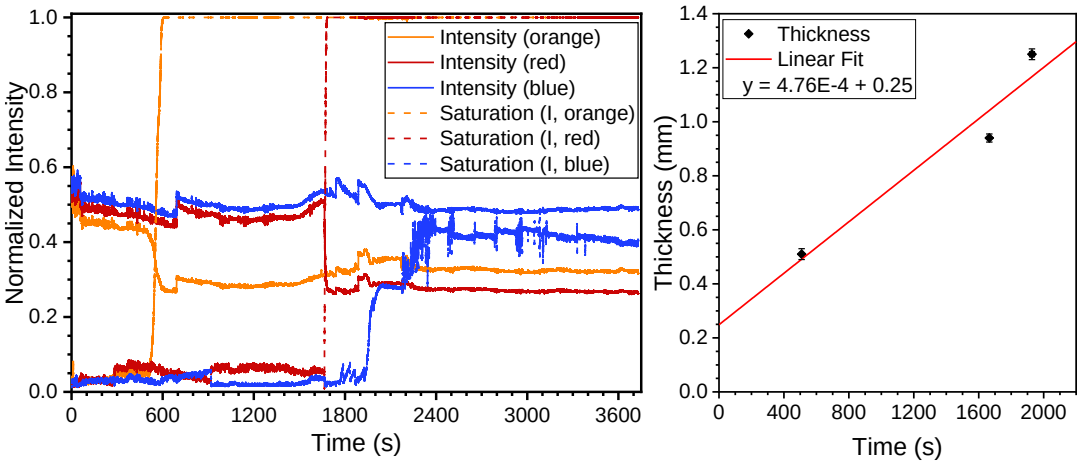

Figure 3-22. Intensity and saturation versus time (HSI system, left) and complementary thickness versus release time (right) diagram documenting the dye release from filled cylinders of OE3-4TE (**3a**$_2$) virgin material in 1 M HCl at 22 °C. Time points obtained from onset of saturation value change.

Layer thickness and release time as determined by video colour analysis (Figure 3-22) were found to be in a roughly linear relationship. The intercept of 0.25 mm

can be seen as both a minimum layer thickness and a reasonable indication of the critical dimension calculated by Burkersroda *et al.*[22], who determined a just slightly higher value of 0.6 mm for linear polyorthoesters as opposed to the here investigated network.

3.3.8 3D Printing and Cytocompatibility of a Selected POETE

As a final step, the suitability of the materials for 3D printing and biomedical applications was explored using OE3-4TE (**3a**$_2$), for consistency and chemical simplicity, as the model material and stereolithography as printing technique.

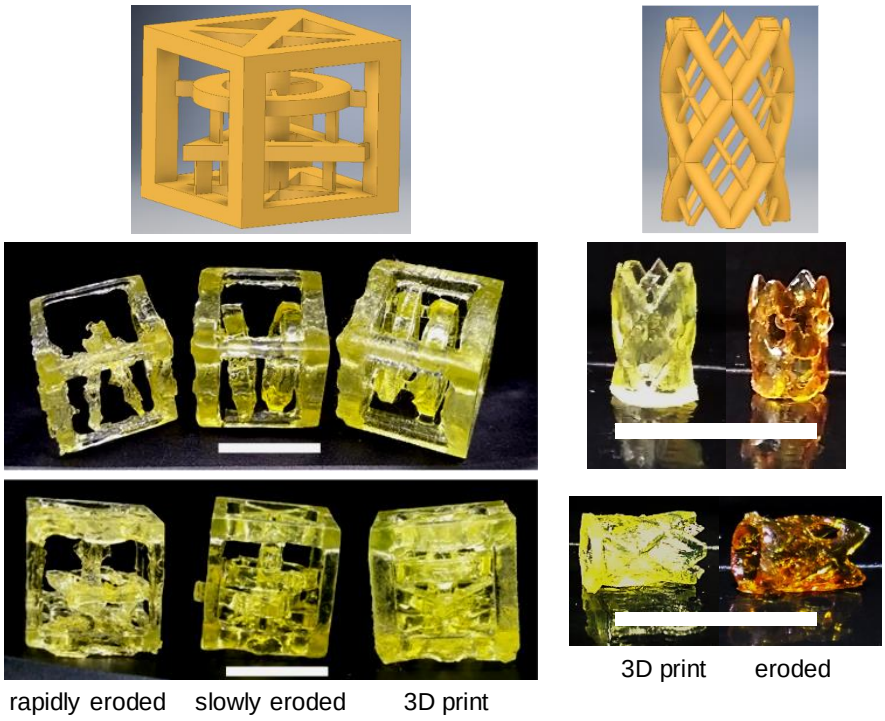

Figure 3-23. 3D CAD models (top) and photographs (bottom) of a cuboid construct (right to left: after post-curing; after activation in conc. HCl, slow erosion in water, rinsing, mechanical manipulation and post-curing; after rapid erosion in conc. HCl, rinsing and post-curing) and stent (left: after post-curing, right: after erosion and post-curing with residues). Scale bar: 1 cm.

After optimisation of the resolution and layer thickness, the final 3D printing formulation was prepared containing propylene carbonate (33 wt%), the photoinitiator (Irgacure 819, 0.5 wt%) and paprika extract as the photoinhibitor (0.5 wt%). Two different models were designed and printed in order to demonstrate the versatility of the material and its unique degradation behaviour (Figure 3-23). Both structures were post-cured under vacuum at 120 °C for 120 h and subsequently subjected to concentrated acidic medium (37% HCl) for several minutes to accelerate surface erosion and remove the secondary

passivating oxidised layers, followed by rinsing with water. This resulted in subsequent continuous slow surface erosion, whereas faster erosion was achieved by leaving samples to degrade in concentrated HCl for roughly 30 min. After erosion, the final shape could be consolidated by drying *in vacuo* at 120 °C for several hours. The printed cuboid construct incorporated two components on thin supporting beams, which were released as trapped mobile parts after surface erosion. Expectedly, the rapidity of the erosion process determined the regularity of the appearance; hence, a better-defined model was obtained from slow erosion. In contrast, a stent model consisting of strands of two different diameters resulted in an initial model without pores as a consequence of surface tension in the resin. After rapid surface erosion however, a porous scaffold was obtained. In this case, consolidation of the structure was conducted with a layer of degradation products still present, as the model appeared too fragile, which resulted in stronger discolouration from an apparently formed passivating layer, analogous to the reported observations following post-curing in air. These experiments clearly demonstrate the applicability of POETE materials in stereolithography.

However, for any biomedical application, it is essential to also investigate the biocompatibility of the material. Because of the fast degradation of the system in aqueous solutions at 37 °C and its auto-fluorescence, seeding cells on the surface of a specimen was complicated, and thus the determination of its cytotoxicity by a 2D cell experiment on the scaffold was hindered.

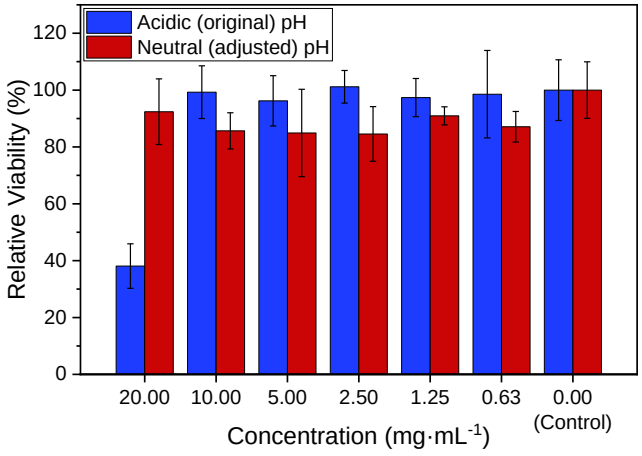

Figure 3-24. Metabolic activity of NOR-10 cells exposed for 48 h to cell culture media with increasing concentration of sample without pH adjustment (blue) and after increasing the pH by adding NaOH (red). Cell viability in % relative to control.

Hence, the cytocompatibility of the system was assessed by determining the relative viability of NOR-10 cells after being exposed to cell culture media that contained different concentrations of the 3D printed material (from 0.63 to 20 mg·mL^{-1}, Figure 3-24). For that purpose, samples of the 3D printed models were taken after activation, rinsed and left to degrade in cell medium. Then, NOR-10 cells were exposed to those cell media. After 48 h of incubation, the cell viability at a concentration of 20 mg/mL (38%) was significantly lower in comparison to lower concentrations. Accordingly, the cell viability was recovered (99%) after diluting the cell media (10 mg·mL^{-1}) and remained higher than 96% for the rest of conditions tested. *A priori*, the decrease in cell viability can be attributed to the acidic pH caused by the POETE degradation products, with a plausible release of acetic acid and diol compounds. Indeed, when the pH of the cell culture solutions was increased by adding 1 M NaOH, the cell viability was determined to be higher than 84% regardless of the sample concentration and comparable to the control (*i.e.* original cell culture medium).

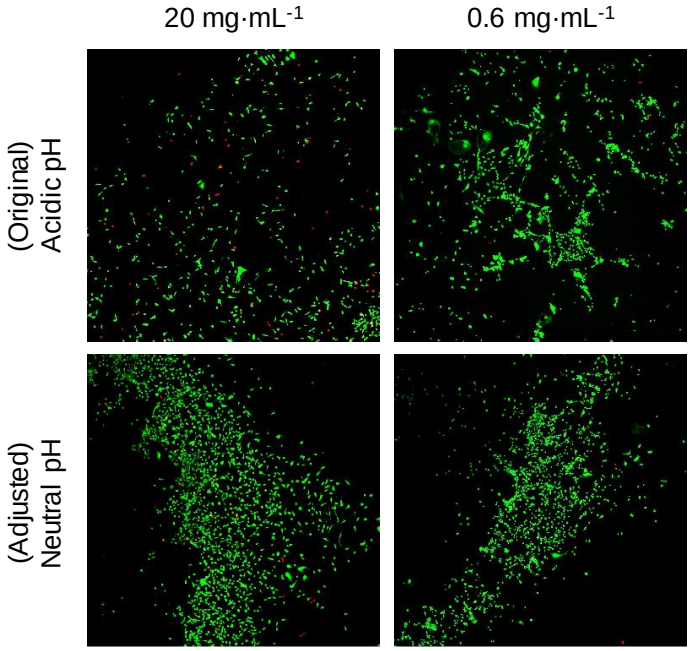

Figure 3-25. Representative live/dead images of cells after being exposed to cell culture media containing 20 mg·mL^{-1} (left column) and 0.6 mg·mL^{-1} (right column) of sample with (top) and without (bottom) pH adjustment. Image size 3.5 × 3.5 mm.

Additional live-dead fluorescent staining supported these results (Figure 3-25). Whereas living (green) cells dominated in media with low concentration of OE3-4TE (**3a**$_2$) and all concentration of neutralised media, dead cells (red) are

clearly discernible in the medium containing highly concentrated and non-neutralised sample. Consequently, future studies of design and application of POETE devices *in vivo* have to take in account the resulting environmental acidity as a function of surface area and degradation rate. It is worth noting that commonly used PLA-based implants also share this issue. Therefore, future works can focus on tuning the composition of the 3D printed scaffolds to include pH-adjusting compounds to be released during degradation, thus maintaining a neutral pH harmless to cells and tissue.

3.4 Conclusion and Outlook

In conclusion, this chapter demonstrates the manufacturing of surface-erodible POETE and PATTE networks and offers comprehensive material characterisation by thermo-mechanical analyses under physiological conditions. A broad spectrum of thermo-mechanical properties including parameters such as T_gs, Storage, Loss and Young's moduli, as well as ultimate tensile stress and strain was revealed. A dependence of these properties on the linker structure and crosslinking density was revealed while all POETE materials outperformed those previously reported for POEs and other orthoester-containing homopolymers. Similarly, degradation rates in aqueous media varied from complete surface erosion within hours for virgin materials, over days to several months for most POETEs in aqueous media, to no mass loss at all over months in acidic and neutral media for air-exposed POETEs and a PATTE. Furthermore, delayed bulk-release of dyes as test for drug delivery or coating applications was demonstrated on a representative material. It was also successfully established that POETEs can be 3D printed, and that the subsequent surface erosion of the resulting devices can be exploited for controlled fading of support and sub-structures. Biocompatibility investigations were complicated as a consequence of the rapid surface erosion; however, the degradation products were proved to be nontoxic for cells, either with pH regulation or below a certain concentration. In this, POETEs resemble currently used biomedical materials. Overall, POETE networks show great potential for future applications based on the combination of customisable mechanical properties, surface-erosion and their suitability for 3D printing techniques.

3.5 Experimental Section

3.5.1 Materials

Acetone (Fisher), Aliquat 336 (Sigma-Aldrich), basic aluminium oxide (Sigma-Aldrich), 1,4-benzenedimethanol (Alfa Aesar), 2-bromo-1,1-dimethoxyethane (Acros Organics), 2-butyne-diol (Sigma-Aldrich), cis-2-butene-1,4-diol (Sigma-Aldrich), diethyl ether (Sigma-Aldrich), dipentaerythritol hexa(3-mercaptopropionate) (**6SH**) (Bruno Bock Chemische Fabrik GMBH & Co.KG), 1,6-hexanediol (Sigma-Aldrich), hydrochloric acid (37%, Fisher Scientific), hydroquinone (Sigma-Aldrich), Irgacure 819 (IGM Resins Ltd.), pentaerythritol tetrakis(3-mercaptopropionate) (**4SH**) (Sigma-Aldrich), phosphate buffered saline preparation (Sigma-Aldrich), potassium carbonate (anhydrous, Sigma-Aldrich), potassium *tert*-butoxide (Sigma-Aldrich), 1,3-propanediol (Sigma-Aldrich), propylene carbonate (Alfa Aesar), terephthalic acid (Sigma-Aldrich), tetrahydrofuran (Sigma-Aldrich), p-toluenesulfonic acid (Sigma), trimethylolpropane tris(3-mercaptopropionate) (**3SH**) (Sigma-Aldrich) and sodium hydroxide (Sigma-Aldrich) were used as received from the supplier. Paprika extract (Durabrite, Kalsec) and food colourings (Tesco Stores Ltd.) were also used as are. $CDCl_3$ (Sigma-Aldrich) was stored over anhydrous potassium carbonate and plug filtered through basic aluminium oxide immediately before use. All glassware used for handling and storage of OE containing compounds and liquid resins was silanised by treating the inner surface with Sigmacote (Sigma-Aldrich) for five minutes, followed by rinsing with water, acetone, diethyl ether and subsequent drying under compressed air for one minute.

3.5.2 Methods

DSC and TGA thermograms were collected on a Mettler-Toledo STARe DSC/TGA 3+ system with STARe Excellence Thermal Analysis Software V2.22. DMTA studies were performed using a Mettler-Toledo Mettler Toledo DMA1 STAR-e device with the same software and, for oscillatory measurements, a common constant distance resulting in a maximum force of around 5 N for the strongest samples in the glassy state (CKA-4TE). Tensile testing was performed on a Testometric M350-5CT with environmental setup, 5 kgF load cell and

adjustable manual grips at a rate of 4 mm·min^{-1} with an offset of 0.1 N while operated and analysed *via* Win TestAnalysis (v.5.0.34) software. Nuclear Magnetic Resonance (NMR) spectra were acquired using a Bruker Avance III 300 or 400 MHz, processed by MestReNova software using the residual solvent peak as reference ($CDCl_3$, ^1H: δ = 7.26 ppm, ^{13}C: δ = 77.16 ppm). Mass spectra were obtained *via* a Bruker maXis plus. Elemental analysis was conducted on a CE Instruments EA1110 Elemental Analyser. An Agilent Cary 630 FTIR Spectrometer with Agilent Resolutions Pro software V.5.0 was used for IR spectroscopy. Raman spectroscopy was performed on a Renishaw inVia Reflex Raman Microscope using a 633 nm HeNe excitation laser and 20× objective. Oscillatory rheometry was performed on an Anton Parr MCR-302 with PP25 plates, Omnicure S1500 UV source and RheoCompass™ V1.20.496 software at a frequency of 10 Hz, amplitude of 1% and gap width of 0.2 mm.

Thickness-dependent cylinder erosion and release studies. Hollow cylindrical OE3-4TE samples were produced according to the synthesis described below. After measuring the lowest thickness and confirming the samples were free of rips and bubbles, Araldite 2-part epoxy glue was mixed and added to one full edge, followed by pressing this side onto a silanised circular glass slide. After drying for 1 h, undiluted food colouring (blue, red and yellow - Tesco Stores Ltd.) was added into the well until the formed meniscus was approximately 2 mm away from the top rim. This edge was subsequently covered in a slightly more viscous epoxy-glue formulation and closed off with a silanised circular glass slide, while making sure not to leave any gap or weak spot. After drying for 1 h the samples were clipped into a self-made sample holder of copper wire, which was then fixated onto a 50 mL plastic tub. The tub was then filled with 40 mL of 1 M HCl and the time measurement started. A video was recorded at 59.94 fps and subsequently evaluated frame-by-frame *via* MATLAB to calculate the development of HSI-values over time for each sample solution. The onset of the change in Saturation (HSI) was used as time point for the release diagram.

Cytotoxicity of degradation products. To verify that OE3-4TE shows non-cytotoxicity, cell viability tests on NOR-10 cells (ATCC® CCL-197™, mouse

skeletal muscle fibroblasts) were undertaken. To that end, 100 mg of 3D printed and with concentrated acid treated OE3-4TE were immersed in 5 mL of cell culture media (DMEM-high glucose; 20% FBS; 1% pen/strep) at 37 °C for several days until complete dissolution (i.e. 20 $mg \cdot mL^{-1}$). Then, the cell media was recovered and filtered before being used. Because of the acidic nature of the degradation products, the pH of the cell media decreased and it displayed a light orange colour. NOR-10 cells were cultured in 175 cm^2 tissue culture flasks using DMEM-high glucose (D6429-Sigma Aldrich), as advised by the supplier, with addition of 20% FBS and 1% pen/strep, at 37 °C, 5% CO_2. Cells were seeded on 24 well plates (5000 $cells \cdot cm^{-2}$) for viability assays. Cells were left to adhere and proliferate on the wells for 48 h, then incubated with the cell media containing the sample at six different concentrations, ranging from 20 $mg \cdot mL^{-1}$ to 0.63 $mg \cdot mL^{-1}$. To evaluate the effect of the pH drop, cells were exposed also to cell media containing the sample but with neutral pH (increased by adding 10 µL of NaOH 1 M). Then, cell viability was measured after 48 h of incubation using PrestoBlue® Cell Viability Reagent (InvitrogenTM). Experiments were performed in triplicate, and the results are reported as relative viability in comparison to the control (cell culture media without dissolved sample). Cell viability was also assessed using Live/Dead™ Viability/Cytotoxicity Kit (Invitrogen™), which includes calcein AM for live cells ($\lambda_{Ex.}$ = 495 nm, $\lambda_{Em.}$ = 515 nm) and ethidium homodimer for dead cells ($\lambda_{Ex.}$ = 528 nm, $\lambda_{Em.}$ = 617 nm). The staining solution was prepared by dissolving calcein AM (0.5 $\mu L \cdot mL^{-1}$) and ethidium homodimer (2 $\mu L \cdot mL^{-1}$) in PBS and incubated with the samples for 30 minutes. Samples were imaged using an Olympus Confocal Laser Scanning Microscope (Fluoview FV3000) at 4X magnification and excited using the 488 and 561 nm lasers. Images were processed using CellSens (Olympus) and ImageJ software (1.52i).

XPS studies. The x-ray photoelectron spectroscopy (XPS) data were collected using an Omicron Multiprobe instrument at the University of Warwick Photoemission Facility. The samples investigated in this study were mounted on Omicron sample plates using conductive carbon tape and loaded in to the fast-entry chamber. Once a pressure of less than $1 \cdot 10^{-7}$ mbar had been achieved (approx. 1 hour), the samples were transferred to a 12-stage storage carousel,

located between the preparation and main analysis chambers, for storage at pressures of less than $2 \cdot 10^{-10}$ mbar. XPS measurements were conducted in the main analysis chamber (base pressure $2 \cdot 10^{-11}$ mbar), with the sample being illuminated using an XM1000 monochromatic Al kα x-ray source (Omicron Nanotechnology). The measurements were conducted at room temperature and at a take-off angle of 90°. The photoelectrons were detected using a SPHERA electron analyser (Omicron Nanotechnology), with the core level spectra recorded using a pass energy of 10 eV (resolution approx. 0.47 eV). The data were analysed using the CasaXPS package, using Shirley backgrounds, mixed Gaussian-Lorentzian (Voigt) line shapes and asymmetry parameters where appropriate. Due to the insulating nature of the samples, the surfaces became positively charged during the experiment. To compensate for this, a low energy electron gun was used to negate surface charging effects and the spectra were energy-corrected using the main C-C/C-H component in the C 1s region at 284.6 eV.

3.5.3 Synthesis of 2-(Bromomethyl)-1,3-dioxe-5-pene (BrCKA).

The procedure follows a method described by Plikk *et al.*[41] Cis-2-butene-1,4-diol (33.30 g, 378 mmol) and 2-bromo-1,1-dimethoxyethane (63.89 g, 378 mmol) were weighed into a 100 mL round bottom flask, followed by p-toluenesulfonic acid (0.10 g, 0.1 wt%). A stirrer bar, Vigreux condenser and distillation bridge was added and the mixture incrementally heated to 130 °C under stirring, until no more methanol was distilled over. After cooling to room temperature and gradually reducing the pressure, a residual methanol fraction was discarded and subsequently the pure product distilled at 38-42 °C and 0.05 mbar (62.1 g, 85%). Characterised as reported previously.[41] ^{1}H NMR (400 MHz; 298 K; $CDCl_3$; ppm): δ 5.70 (t, $^{3}J_{HH}$ = 1.5 Hz, 2H), 4.97 (t, $^{3}J_{HH}$ = 5.4 Hz, 1H), 4.44 (dm, $^{3}J_{HH}$ = 14.7 Hz, 2H), 4.20 (dm, $^{3}J_{HH}$ = 14.7 Hz, 2H), 3.39 (d, $^{3}J_{HH}$ = 5.4 Hz, 2H); ^{13}C NMR (400 MHz; 298 K; $CDCl_3$; ppm): δ 128.81, 106.92, 63.25, 24.99.

3.5.4 Synthesis of 2-Methylene-1,3-dioxe-5-pene (CKA, 1).

Similarly to Plikk *et al.*'s method,[41] **BrCKA** (40.00 g, 207 mmol) and Aliquat 336 (1.62 g, 4 mmol) were weighed into a 500 mL RBF, dissolved in 350 mL THF and cooled under stirring to 0 °C. Potassium *tert*-butoxide (46.50 g, 414 mmol)

was added in small portions within one hour and the orange to yellow suspension left to stir for another two hours at 0 °C. THF was removed *in vacuo* (20 mbar, 18 °C) and the residual slurry dissolved in 200 mL diethyl ether and 200 mL distilled water, followed by separation of the layers and extraction of the aqueous phase with a further 100 mL diethyl ether. The combined organic layers were washed with 0.01 M potassium carbonate solution (300 mL) for three times. The organic layer was concentrated *in vacuo* at 18 °C, followed by vacuum transfer of the residual oil at room temperature and 0.05 mbar to yield crude product. Repeat of the washing procedure, followed by drying over potassium carbonate and concentration at 30 °C and 20 mbar yielded pure product (12.50 g, 55%). ^{1}H NMR (400 MHz; 298 K; $CDCl_3$; ppm): δ 5.72 (t, $^{3}J_{HH}$ = 1.7 Hz, 2H), 4.43 (d, $^{3}J_{HH}$ = 1.7 Hz, 4H), 3.57 (s, 2H); ^{13}C NMR (400 MHz; 298 K; $CDCl_3$; ppm): δ 164.11, 127.83, 68.77, 68.21.

3.5.5 General Procedure of the Orthoester (OE) Synthesis (2).

CKA **(1)** and diol were weighed into a silanised vial in a molar ratio of 1.05 to 0.5. Terephthalic acid (1 mol eq.) was added and the mixture stirred overnight. The crude product was dissolved in 5 vol. eq. diethyl ether and washed four times with equivalent volumes of 0.01 M potassium carbonate solution, followed by separation and drying of the organic layer over potassium carbonate. Plug filtration through minimal amounts of basic alumina and evaporation yielded pure OE product of fruity odour (**2**). Additional distillation *in vacuo* in a silanised setup before use was performed to remove any degradation products (around ^{1}H NMR δ = 2.00 ppm).

3.5.6 Synthesis of 1,3-Bis(2-methyl-2-oxyl-1,3-dioxe-5-pene)-propane (OE3, 2a).

CKA **(1)** (10.00 g, 89.18 mmol), 1,3-propanediol (3.40 g, 44.59 mmol) and terephthalic acid (0.15 g, 0.89 mmol) were reacted to yield clear colourless oil (11.20 g, 84%; distillation at 0.02 mbar, 150 °C). ^{1}H NMR (400 MHz; 298 K; $CDCl_3$; ppm): δ 5.66 (t, $^{3}J_{HH}$ = 1.7 Hz, 4H, -C*H*CH_2CO_3-), 4.43 (dm, 4H, $^{2}J_{HH}$ = -15.5 Hz, -CHC*H*$_2CO_3$-), 4.15 (dm, 4H, $^{2}J_{HH}$ = -15.5 Hz, -CHC*H*$_2CO_3$-), 3.65 (t, 4H, $^{3}J_{HH}$ = 6.3 Hz, -OC*H*$_2CH_2$-), 1.93 (qi, 2H, $^{3}J_{HH}$ = 6.3 Hz, -OCH$_2$C*H*$_2$-), 1.54 (s, 6H, -CO_3CH_3);

^{13}C NMR (400 MHz; 298 K; $CDCl_3$; ppm): δ 128.99 (-*C*HCH$_2$CO$_3$-), 116.20 (-*C*O$_3$CH$_3$), 61.57 (-CH*C*H$_2$CO$_3$-), 60.42 (-CO$_3$*C*H$_2$CH$_2$-), 30.37 (-CO$_3$CH$_2$*C*H$_2$-), 19.18 (-CO$_3$*C*H$_3$); MS (ESI-QTOF +ve): $(M + Na)^+$ *m/z* calculated for $C_{15}H_{24}O_6Na^+$: 323.1465, found: 323.1468; Anal. Calcd for $C_{15}H_{24}O_6$: C 60.0; H 8.05%. Found: C 59.9; H 8.0; IR (neat; 298 K; cm^{-1}): 2950-2860 (-C-H), 1380 (-CH$_2$-), 1160-1040 (C-O), 900 (-CH$_2$-CH$_2$-), 800 (C=C), 640 (=C-H); Raman (neat; 298 K; cm^{-1}): 3030 (=C-H), 2950-2870 (C-H), 1660 (C=C), 1450 (-CH$_2$-), 1200 (C-C), 750 (C-O).

3.5.7 Synthesis of 1,6-Bis(2-methyl-2-oxyl-1,3-dioxe-5-pene)-hexane (OE6, 2b).

CKA **(1)** (10.00 g, 89.18 mmol) was combined with 1,6-hexanediol (5.27 g, 44.59 mmol) and terephthalic acid (0.15 g, 0.89 mmol), reacted and clear oil was obtained (12.52 g, 82%). ^{1}H NMR (300 MHz; 298 K; $CDCl_3$; ppm): δ 5.66 (s, 4H, -OCH$_2$C$_2$*H*$_2$CH$_2$O-), 4.43 (d, 4H, $^2J_{H\text{-}H}$ = -14.1 Hz, -OC*H*$_2$C$_2$H$_2$C*H*$_2$O-), 4.15 (d, 4H, $^2J_{H\text{-}H}$ = -14.1 Hz, -OC*H*$_2$C$_2$H$_2$C*H*$_2$O-), 3.50 (t, 4H, $^3J_{H\text{-}H}$ = 6.6 Hz, -OC*H*$_2$CH$_2$CH$_2$-), 1.62 (tm, 4H, $^3J_{H\text{-}H}$ = 6.7 Hz, -OCH$_2$C*H*$_2$CH$_2$-), 1.52 (s, 6H, -C*H*$_3$) , 1.42 (q, 2H, $^3J_{H\text{-}H}$ = 3.8 Hz, -OCH$_2$CH$_2$C*H*$_2$-); ^{13}C NMR (300 MHz; 298 K; $CDCl_3$; ppm): δ 129.03 (-OCH$_2$*C*$_2$H$_2$CH$_2$O-), 116.17 (-O$_3$*C*CH$_3$), 63.42 (-O*C*H$_2$C$_2$H$_2$*C*H$_2$O-), 61.54 (-O*C*H$_2$CH$_2$CH$_2$-), 29.96 (-OCH$_2$*C*H$_2$CH$_2$-), 26.23 (-OCH$_2$CH$_2$*C*H$_2$-), 19.18 (-*C*H$_3$); MS (ESI-QTOF +ve): $(M + Na)^+$ *m/z* calculated for $C_{18}H_{30}O_6Na^+$: 365.1935, found: 365.1935; Anal. Calcd for $C_{18}H_{30}O_6$: C 63.1; H 8.8%. Found: C 62.9; H 8.9; IR (neat; 298 K; cm^{-1}): 2940-2860 (-C-H), 1380 (-CH$_2$-), 1210-1010 (C-O), 900 (-C-H), 800 (C=C), 640 (=C-H); Raman (neat; 298 K; cm^{-1}): 3040 (=C-H), 2950-2870 (C-H), 1660 (C=C), 1450 (-CH$_2$-), 1200 (C-C), 750 (C-O).

3.5.8 Synthesis of 1,4-Bis((2-methyl-1,3-dioxe-5-pene-2-yl)oxymethyl)-benzene (OEbz, 2c).

Acetone (10 mL) was added to CKA **(1)** (10.00 g, 89.18 mmol), 1,4-bis(hydroxymethyl)-benzene (6.16 g, 44.59 mmol) and terephthalic acid (0.15g, 0.89 mmol), and the mixture was reacted to yield white crystals. (11.69 g, 72%; recrystallisation from diethyl ether, drying *in vacuo* from melt). Mp. 95-98 °C; ^{1}H NMR (300 MHz; 298 K; $CDCl_3$; ppm): δ 7.32 (s, 4H, -C$_6$*H*$_4$-), 5.63 (s, 4H, -OCH$_2$C$_2$*H*$_2$CH$_2$O-), 4.58 (s, 4H, -OC*H*$_2$C$_6$H$_4$-), 4.44 (d, 4H, $^2J_{H\text{-}H}$ = -15.5

Hz, -OC*H*$_2$C$_2$H$_2$C*H*$_2$O-), 4.12 (d, 4H, $^2J_{H\text{-}H}$ = -15.5 Hz, -OC*H*$_2$C$_2$H$_2$C*H*$_2$O-), 1.58 (s, 6H, -C*H*$_3$); ^{13}C NMR (400 MHz; 298 K; $CDCl_3$; ppm): δ 137.49 (-OCH$_2$*C*C$_4$H$_4$*C*CH$_2$O-), 128.96 (-OCH$_2$C*C*$_4$H$_4$CCH$_2$O-), 127.58 (-O*C*H$_2$C$_2$H$_2$*C*H$_2$O-), 116.53 (-O$_3$*C*CH$_3$), 65.51 (-O*C*H$_2$C$_6$H$_4$-), 61.78 (-OCH$_2$*C*$_2$H$_2$CH$_2$O-), 19.58 (-*C*H$_3$); MS (ESI-QTOF +ve): $(M + Na)^+$ *m/z* calculated for $C_{20}H_{26}O_6Na^+$: 385.1622, found: 385.1622; Anal. Calcd for $C_{20}H_{26}O_6$: C 66.3; H 7.2%. Found: C 66.4; H 7.3; IR (neat; 298 K; cm^{-1}): 2960-2860 (-C-H), 1380 (-CH$_2$-), 1210-1010 (C-O), 920-900 (-C-H), 830-770 (C=C), 650 (=C-H); Raman (neat; 298 K; cm^{-1}): 3070-3040 (=C-H), 2960-2860 (C-H), 1660 (C=C), 1460 (-CH$_2$-), 1200-1180 (C-C), 760 (C-O).

3.5.9 Synthesis of 1,4-Bis((2-methyl-1,3-dioxe-5-pene-2-yl)oxy)-benzene (OEph, 2d).

Analogous to **(2c)**, dissolving CKA **(1)** (10.00 g, 89.18 mmol), benzene-1,4-diol (4.91 g, 44.59 mmol) and terephthalic acid (0.15 g, 0.89 mmol) in acetone (10 mL) and reacting yielded the product as white platelets (10.66, 71%; recrystallisation from diethyl ether). Mp. 105-108 °C; ^{1}H NMR (300 MHz; 298 K; $CDCl_3$; ppm): δ 7.06 (s, 4H, -C$_6$H$_4$-), 5.72 (s, 4H, -OCH$_2$C$_2$*H*$_2$CH$_2$O-), 4.62 (d, 4H, $^2J_{H\text{-}H}$ = -15.5 Hz, -OC*H*$_2$C$_2$H$_2$C*H*$_2$O-), 4.25 (d, 4H, $^2J_{H\text{-}H}$ = -15.5 Hz, -OC*H*$_2$C$_2$H$_2$C*H*$_2$O-), 1.54 (s, 6H, -C*H*$_3$); ^{13}C NMR (400 MHz; 298 K; $CDCl_3$; ppm): δ 149.91 (-O*C*C$_4$H$_4$*C*O-), 128.81 (-O*C*H$_2$C$_2$H$_2$*C*H$_2$O-), 121.79 (-OC*C*$_4$H$_4$CO-), 117.85 (-O$_3$*C*CH$_3$), 62.17 (-OCH$_2$*C*$_2$H$_2$CH$_2$O-), 20.02 (-*C*H$_3$); MS (ESI-QTOF +ve): $(M + Na)^+$ *m/z* calculated for $C_{18}H_{22}O_6Na^+$: 357.1309, found: 357.1304; Anal. Calcd for $C_{18}H_{22}O_6$: C 64.7; H 6.6%. Found: C 64.9; H 6.65; IR (neat; 298 K; cm^{-1}): 2950-2870 (-C-H), 1500 (C=C), 1380 (-CH$_2$-), 1210-1010 (C-O), 920-900 (-C-H), 840-780 (C=C), 640 (=C-H); Raman (neat; 298 K; cm^{-1}): 3080-3040 (=C-H), 2990-2950 (C-H), 1664 (C=C), 1250-1200 (C-C), 760 (C-O).

3.5.10 Synthesis of Cis-1,4-bis(2-methyl-2-oxyl-1,3-dioxe-5-pene)-but-2-ene (OE4ene, 2e).

The reaction of CKA **(1)** (10.00 g, 89.18 mmol), cis-2-butene-1,4-diol (3.93 g, 44.59 mmol) and terephthalic acid (0.15 g, 0.89 mmol) yielded white crystals (2.25 g, 81%; recrystallisation from diethyl ether). Mp. 24-26 °C; ^{1}H NMR (400 MHz; 298 K; $CDCl_3$; ppm): δ 5.71 (tm, $^3J_{HH}$ = 3.6 Hz, 2H, -C*H*CH$_2$CO$_3$- *(linker)*),

5.56 (t, $^{3}J_{HH}$ = 1.7 Hz, 4H, -C*H*CH$_2$CO$_3$-), 4.43 (dm, 4H, $^{2}J_{HH}$ = -14.2 Hz, -CHC*H*$_2$CO$_3$-), 4.15 (d, 4H, $^{3}J_{HH}$ = 3.6 Hz, -CHC*H*$_2$CO$_3$- *(linker)*), 4.13 (dm, 4H, $^{2}J_{HH}$ = -14.2 Hz, -CHC*H*$_2$CO$_3$-), 1.54 (s, 6H, -CO$_3$C*H*$_3$); ^{13}C NMR (400 MHz; 298 K; CDCl$_3$; ppm): *δ* 128.94 (-*C*HCH$_2$CO$_3$-), 128.64 (-*C*HCH$_2$CO$_3$- *(linker)*), 116.35 (-*C*O$_3$CH$_3$), 61.70 (-CH*C*H$_2$CO$_3$-), 59.72 (-CH*C*H$_2$CO$_3$- *(linker)*), 30.37 (-CO$_3$CH$_2$*C*H$_2$-), 19.40 (-CO$_3$*C*H$_3$); MS (ESI-QTOF +ve): (M + Na)$^+$ *m/z* calculated for $C_{16}H_{24}O_6Na^+$: 335.1465, found: 335.1468; Anal. Calcd for $C_{16}H_{24}O_6$: C 61.5; H 7.7%. Found: C 61.5; H 7.8; IR (neat; 298 K; cm^{-1}): 2950-2860 (-C-H), 1380 (-CH$_2$-), 1140-1020 (C-O), 900 (-C-H), 800 (C=C), 640 (=C-H); Raman (neat; 298 K; cm^{-1}): 3050-3030 (=C-H), 2950-2880 (C-H), 1670-1660 (C=C), 1450 (-CH$_2$-), 1200 (C-C), 770 (C-O).

3.5.11 Synthesis of 1,4-Bis((2-methyl-2-oxyl-1,3-dioxe-5-pene)-but-2-yne (OE4yne, 2f).

Reacting CKA **(1)** (10.00 g, 89.18 mmol), benzene-1,4-diol (3.84 g, 44.59 mmol) and terephthalic acid (0.15 g, 0.89 mmol) yielded the product as fine white crystals (13.73 g, 99%; recrystallisation from diethyl ether). Mp. 40-43 °C; ^{1}H NMR (300 MHz; 298 K; CDCl$_3$; ppm): *δ* 5.65 (s, 4H, -OCH$_2$C$_2$*H*$_2$CH$_2$O-), 4.46 (d, 4H, $^{2}J_{H\text{-}H}$ = -15.5 Hz, -OC*H*$_2$C$_2$H$_2$C*H*$_2$O-), 4.28 (s, 4H, -C*H*$_2$C$_2$C*H*$_2$-), 4.14 (d, 4H, $^{2}J_{H\text{-}H}$ = -15.5 Hz, -OC*H*$_2$C$_2$H$_2$C*H*$_2$O-), 1.56 (s, 6H, -C*H*$_3$) ; ^{13}C NMR (400 MHz; 298 K; CDCl$_3$; ppm): *δ* 128.83 (-O*C*H$_2$C$_2$H$_2$*C*H$_2$O-), 116.55 (-O$_3$*C*CH$_3$), 81.93 (-CH$_2$*C*$_2$CH$_2$-), 61.90 (-OCH$_2$*C*$_2$H$_2$CH$_2$O-), 52.12 (-*C*H$_2$C$_2$*C*H$_2$-), 19.50 (-*C*H$_3$); MS (ESI-QTOF +ve): (M + Na)$^+$ *m/z* calculated for $C_{16}H_{22}O_6Na^+$: 333.1309, found: 333.1317; Anal. Calcd for $C_{16}H_{22}O_6$: C 61.9; H 7.15%. Found: C 61.9; H 7.0; IR (neat; 298 K; cm^{-1}): 2960-2870 (-C-H), 1390-1360 (-CH$_2$-), 1150-990 (C-O), 900 (-C-H), 800 (C=C), 650 (=C-H); Raman (neat; 298 K; cm^{-1}): 3030 (=C-H), 2960-2870 (C-H), 1660 (C=C), 1450 (-CH$_2$-), 1200 (C-C), 750 (C-O).

3.5.12 General Procedure for the Preparation of P(OE-TE) Materials (3).

The melt of the respective OE monomer and thiol linker in a 1:1 ratio of thiol to cyclic alkene functionalities together with 1.0 wt% total of the initiator was stirred in a darkened silanised vial for 10 minutes until homogeneous. A stainless-steel mould with cut-out shapes for tensile testing samples and DMA

bars was one-sidedly covered with Sellotape and filled with the mixture. Alternatively, a clear plastic template made from a 5mL PP syringe with a parafilm-wrapped core or a 2 mL PP vial cap was used for hollow cylinders and degradation pucks, respectively. Photocuring was performed in an NK-Optik Otoflash G171 applying 8 times 500 flashes, followed by extraction of the materials from the mould and further curing for another 4 times with 500 flashes each, cooling the sample to room temperature in between each set for quasi-isothermal curing conditions. Post-curing was conducted at 120 °C either (a) *in vacuo* at ≤ $5 \cdot 10^{-2}$ mbar after purging with nitrogen or (b) on air using a hot plate or ventilated oven. The samples were stored in between experiments at -25 °C.

3.5.13 Preparation of OE3-3TE ($3a_1$).

A mixture of OE3 **(2a)** (1.00 g, 3.33 mmol), 3SH (0.89 g, 1.66 mmol) and Irgacure 819 (0.02 g, 1 wt%) were prepared in a silanised glass vial and reacted to form clear colourless polymer. IR (neat; 298 K; cm^{-1}): 2950-2880 (-C-H), 1730 (C=O), 1460-1360 (-CH_2-), 1240-1140 (C-O), 1050-1020 (C-O), 910 (-C-H); Raman (neat; 298 K; cm^{-1}): 2940 (C-H), 1730 (C=O), 1460-1430 (-CH_2-), 1060 (C-O-C), 750 (C-O).

3.5.14 Preparation of OE3-4TE ($3a_2$).

OE3 **(2a)** (1.00 g, 3.33 mmol), 4SH (0.81 g, 1.66 mmol) and Irgacure 819 (0.02 g, 1 wt%) were mixed in a silanised glass vial and polymerised into a clear colourless material. IR (neat; 298 K; cm^{-1}): 2950-2880 (-C-H), 1730 (C=O), 1470-1360 (-CH_2-), 1240-1140 (C-O), 1030 (C-O); Raman (neat; 298 K; cm^{-1}): 2940 (C-H), 1740 (C=O), 1460-1430 (-CH_2-), 750 (C-O).

3.5.15 Preparation of OE3-6TE ($3a_3$).

OE3 **(2a)** (1.00 g, 3.33 mmol), 6SH (0.87 g, 1.66 mmol) and Irgacure 819 (0.02 g, 1 wt%) were combined for the mixture and brought to reaction to form clear colourless polymer. IR (neat; 298 K; cm^{-1}): 2950-2880 (-C-H), 1730 (C=O), 1460-1350 (-CH_2-), 1240-1140 (C-O), 1050-1020 (C-O), 910 (-C-H); Raman (neat; 298 K; cm^{-1}): 2940 (C-H), 1740 (C=O), 1460-1430 (-CH_2-), 750 (C-O).

3.5.16 Preparation of OE6-4TE (3b).

A mixture of OE6 **(2b)** (1.00 g, 2.92 mmol), 4SH (0.71 g, 1.46 mmol) and Irgacure 819 (0.02 g, 1 wt%) was prepared for the material, a clear colourless polymer. IR (neat; 298 K; cm^{-1}): 2940-2870 (-C-H), 1730 (C=O), 1460-1350 ($-CH_2-$), 1240-1140 (C-O), 1050-1010 (C-O), 910 (-C-H); Raman (neat; 298 K; cm^{-1}): 2940 (C-H), 1740 (C=O), 1450-1430 ($-CH_2-$), 750 (C-O).

3.5.17 Preparation of OEbz-4TE (3c).

The clear colourless material was made of OEbz **(2c)** (1.00 g, 2.76 mmol), 4SH (0.671 g, 1.38 mmol) and Irgacure 819 (0.02 g, 1 wt%) at 120 °C. IR (neat; 298 K; cm^{-1}): 2950-2870 (-C-H), 1730 (C=O), 1510 (-HC=CH-), 1470-1350 ($-CH_2-$), 1230-1130 (C-O), 1010 (C-O), 920 (-C-H), 810 (=C-H); Raman (neat; 298 K; cm^{-1}): 3060 (=C-H), 2930 (C-H), 1740 (C=O), 1620 (C=C), 1460-1420 ($-CH_2-$), 1200 (C-O), 840 (=C-H).

3.5.18 Preparation of OEph-4TE (3d).

The photoreaction of OEph **(2d)** (1.00 g, 2.99 mmol), 4SH (0.73 g, 1.50 mmol) and Irgacure 819 (0.02 g, 1 wt%) was conducted at 120 °C and yielded the clear brown material. IR (neat; 298 K; cm^{-1}): 2960-2910 (-C-H), 1730 (C=O), 1510 (-HC=CH-), 1470-1360 ($-CH_2-$), 1230-1130 (C-O), 1030 (C-O), 830 (=C-H); Raman (neat; 298 K; cm^{-1}): 3070 (=C-H), 2940 (C-H), 1740 (C=O), 1620 (C=C), 1460-1420 ($-CH_2-$), 830-860 (=C-H).

3.5.19 Preparation of OE4ene-4TE ($3e_1$).

The mixture was prepared of OE4ene **(2e)** (1.00 g, 3.20 mmol), 4SH (0.78 g, 1.60 mmol) and Irgacure 819 (0.02 g, 1 wt%) and clear colourless polymer was obtained. IR (neat; 298 K; cm^{-1}): 2950-2880 (-C-H), 1730 (C=O), 1470-1350 ($-CH_2-$), 1230-1130 (C-O), 1020 (C-O), 910 (-C-H); Raman (neat; 298 K; cm^{-1}): 2930 (C-H), 1740 (C=O), 1450-1420 ($-CH_2-$).

3.5.20 Preparation of OE4ene-4TE, Full Conversion ($3e_2$).

Clear colourless material was formed by the reaction of OE4ene **(2e)** (1.00 g, 3.20 mmol), 4SH (1.17 g, 2.40 mmol) and Irgacure 819 (0.02 g, 1 wt%). IR (neat;

298 K; cm^{-1}): 2950-2880 (-C-H), 1730 (C=O), 1470-1350 (-CH_2-), 1230-1130 (C-O), 1030 (C-O); Raman (neat; 298 K; cm^{-1}): 2930 (C-H), 1740 (C=O), 1660 (C=O), 1450-1420 (-CH_2-), 750 (C-O).

3.5.21 Preparation of OE4yne-4TE ($3f_1$).

At 50 °C, OE4yne **(2f)** (1.00 g, 3.22 mmol), 4SH (0.79 g, 1.61 mmol) and Irgacure 819 (0.02 g, 1 wt%) were reacted to yield clear colourless polymer. IR (neat; 298 K; cm^{-1}): 2950-2880 (-C-H), 1730 (C=O), 1460-1350 (-CH_2-), 1240-1130 (C-O), 1020 (C-O), 910-900 (-C-H); Raman (neat; 298 K; cm^{-1}): 2940 (C-H), 1740 (C=O), 1660 (C=O), 1450-1420 (-CH_2-), 750 (C-O).

3.5.22 Preparation of OE4yne-4TE, Full Conversion ($3f_2$).

A mixture of OE4yne **(2f)** (1.00 g, 3.22 mmol), 4SH (1.58 g, 3.22 mmol) and 0.03 g (1 wt%) Irgacure 819 was prepared at 50 °C and clear colourless polymer was obtained. IR (neat; 298 K; cm^{-1}): 2950-2930 (-C-H), 1730 (C=O), 1470-1350 (-CH_2-), 1230-1140 (C-O), 1020 (C-O), 920 (-C-H); Raman (neat; 298 K; cm^{-1}): 2930 (C-H), 2570 (-SH:HS-), 1740 (C=O), 1460-1420 (-CH_2-).

3.5.23 Preparation of CKA-4TE (4).

A mixture of CKA **(1)** (1.00 g, 8.92 mmol), 4SH (2.18 g, 4.46 mmol) and 0.03 g (1 wt%) Irgacure 819 was prepared at 50 °C and clear colourless polymer was obtained. IR (neat; 298 K; cm^{-1}): 2940-2880 (-C-H), 1730 (C=O), 1470-1350 (-CH_2-), 1230-1120 (C-O), 1030-1000 (C-O); Raman (neat; 298 K; cm^{-1}): 2930-2920 (C-H), 1740 (C=O), 1460-1420 (-CH_2-).

3.5.24 Preparation and Printing of the 3D Printing Resin.

OE3 **(2a)** (10.00 g, 33.29 mmol), 4SH (8.13 g, 16.65 mmol), propylene carbonate (9.07 g, 50 wt%) and equal masses of Irgacure 819 and Durabrite Paprika Extract (0.09 g, 0.5 wt% each) were weighed into a brown silanised bottle under exclusion of ambient lighting. The mixture was stirred in the dark at room temperature until homogeneous and clear, which occasionally required short exposure to ambient lighting. The resin was stored in the dark at 25 °C until use. For stereolithography, a printing tray was filled with about 25 mL of resin

and locked into place, which was usable for approximately 5 hours of printing until insufficient photoinitiated curing occurred. After that, no solid material was formed as a consequence of hydrolysis and separation from hygroscopic effects, except *via* post-curing. Alternatively, approximately 3 mL of resin could be used at a time on the build plate and rearranged after every 5 to 10 printing steps, while topping up the batch regularly and completely replacing after around 5 hours. The pre-set "slow" printing setup was selected with a modified step size of 100 (stents) or 200 µm (cuboid) as well as intensity of 350% and irradiation time of 14 s. 3 base layers at 24 s each and 4 buffer layers were set up and the model offset from the base plate adjusted so that it was printed transition-free. The prints were further cured for 2 h in an NK-Optik G136/6 and a further 4 × 500 flashes in an NK-Optik Otoflash G171, before being post-cured in the oven. Finally, the timed erosion was achieved by placing the samples in concentrated (37%) HCl for 15-30 minutes (to initiate degradation of the passivating layer), followed by rinsing in distilled water and peeling-off of solidified residual layers to reveal the self-wetting surface-eroding stable material.

3.6 References

(1) Kruth, J.-P.; Leu., M. C.; Nakagawa, T., Progress in Additive Manufacturing and Rapid Prototyping - ScienceDirect. *CIRP Ann.-Manuf. Techn.* **1989,** *47* (2), 525-540. doi:10.1016/S0007-8506(07)63240-5

(2) Gibson, I.; Rosen, D.; Stucker, B., *Additive Manufacturing Technologies*. Springer New York: **2015**.

(3) Lim, S.; Buswell, R. A.; Le, T. T.; Austin, S. A.; Gibb, A. G. F.; Thorpe, T., Developments in construction-scale additive manufacturing processes. *Autom. Constr.* **2012,** *21*, 262–268. 10.1016/j.autcon.2011.06.010

(4) Rengier, F.; Mehndiratta, A.; von Tengg-Kobligk, H.; Zechmann, C. M.; Unterhinninghofen, R.; Kauczor, H. U.; Giesel, F. L., 3D printing based on imaging data: review of medical applications. *Int. J. Comput. Assist. Radiol. Surg.* **2010,** *5* (4), 335-341. 10.1007/s11548-010-0476-x

(5) Melchels, F. P. W.; Domingos, M. A. N.; Klein, T. J.; Malda, J.; Bartolo, P. J.; Hutmacher, D. W., Additive manufacturing of tissues and organs. *Prog. Polym. Sci.* **2012,** *37* (8), 1079–1104. 10.1016/j.progpolymsci.2011.11.007

(6) Wendel, B.; Rietzel, D.; Kühnlein, F.; Feulner, R.; Hülder, G.; Schmachtenberg, E., Additive Processing of Polymers. *Macromol. Mater. Eng.* **2008,** *293* (10), 799-809. doi:10.1002/mame.200800121

(7) Petrovic, V.; Vicente Haro Gonzalez, J.; Jordá Ferrando, O.; Delgado Gordillo, J.; Ramón Blasco Puchades, J.; Portolés Griñan, L., Additive layered manufacturing: sectors of industrial application shown through case studies. *Int. J. Prod. Res.* **2010,** *49* (4), 1061-1079. doi:10.1080/00207540903479786

(8) Gebhardt, A., *Understanding Additive Manufacturing*. Carl Hanser Verlag GmbH & Co. KG: Munich, Germany, **2011**.

(9) Popescu, D.; Laptoiu, D., Rapid prototyping for patient-specific surgical orthopaedics guides: A systematic literature review. *Proc. Inst. Mech. Eng. H* **2016,** *230* (6), 495-515. doi:10.1177/0954411916636919

(10) Mota, C.; Puppi, D.; Chiellini, F.; Chiellini, E., Additive manufacturing techniques for the production of tissue engineering constructs. *J. Tissue Eng. Regen. Med.* **2015,** *9* (3), 174-190. doi:10.1002/term.1635

(11) Jungst, T.; Smolan, W.; Schacht, K.; Scheibel, T.; Groll, J., Strategies and Molecular Design Criteria for 3D Printable Hydrogels. *Chem. Rev.* **2016,** *116* (3), 1496-1539. 10.1021/acs.chemrev.5b00303

(12) Hutmacher, D. W.; Schantz, J. T.; Lam, C. X.; Tan, K. C.; Lim, T. C., State of the art and future directions of scaffold-based bone engineering from a biomaterials perspective. *J. Tissue Eng. Regen. Med.* **2007,** *1* (4), 245-260. 10.1002/term.24

(13) Probst, F. A.; Hutmacher, D. W.; Muller, D. F.; Machens, H. G.; Schantz, J. T., [Calvarial reconstruction by customized bioactive implant]. *Handchir. Mikrochir. Plast. Chir.* **2010,** *42* (6), 369-373. 10.1055/s-0030-1248310

(14) Youssef, A.; Hollister, S. J.; Dalton, P. D., Additive manufacturing of polymer melts for implantable medical devices and scaffolds - IOPscience. *Biofabrication* **2017,** *9* (1), 1-29. doi:10.1088/1758-5090/aa5766

(15) Barker, I. A.; Ablett, M. P.; Gilbert, H. T. J.; Leigh, S. J.; Covington, J. A.; Hoyland, J. A.; Richardson, S. M.; Dove, A. P., A microstereolithography resin based on thiol-ene chemistry: towards biocompatible 3D extracellular constructs for tissue engineering. *Biomater. Sci.* **2014,** *2* (4), 472-475. doi:10.1039/C3BM60290G

(16) Arcaute, K.; Mann, B. K.; Wicker, R. B., Stereolithography of Three-Dimensional Bioactive Poly(Ethylene Glycol) Constructs with Encapsulated Cells | SpringerLink. *Ann. Biomed. Eng.* **2006,** *34* (9), 1429-1441. 10.1007/s10439-006-9156-y

(17) Leigh, S. J.; Gilbert, H. T. J.; Barker, I. A.; Becker, J. M.; Richardson, S. M.; Hoyland, J. A.; Covington, J. A.; Dove, A. P., Fabrication of 3-Dimensional Cellular Constructs via Microstereolithography Using a Simple, Three-Component, Poly(Ethylene Glycol) Acrylate-Based System. *Biomacromolecules* **2012,** *14* (1), 186-192. 10.1021/bm3015736

(18) Cooke, M. N.; Fisher, J. P.; Dean, D.; Rimnac, C.; Mikos, A. G., Use of stereolithography to manufacture critical-sized 3D biodegradable scaffolds for bone ingrowth. *J. Biomed. Mater. Res. B* **2002,** *64B* (2), 65-69. 10.1002/jbm.b.10485

(19) Griffin, J.; Delgado-Rivera, R.; Meiners, S.; Uhrich, K. E., Salicylic acid-derived poly(anhydride-ester) electrospun fibers designed for regenerating the peripheral nervous system. *J. Biomed. Mater. Res. A* **2011,** *97A* (3), 230-242. 10.1002/jbm.a.33049

(20) Ulery, B. D.; Nair, L. S.; Laurencin, C. T., Biomedical applications of biodegradable polymers. *J. Polym. Sci. B. Polym. Phys.* **2011,** *49* (12), 832-864. doi:10.1002/polb.22259

(21) Shoichet, M. S., Polymer Scaffolds for Biomaterials Applications. *Macromolecules* **2010,** *43* (2), 581-591. 10.1021/ma901530r

(22) von Burkersroda, F.; Schedl, L.; Gopferich, A., Why degradable polymers undergo surface erosion or bulk erosion. *Biomaterials* **2002,** *23* (21), 4221-4231. doi:10.1016/S0142-9612(02)00170-9

(23) Burkoth, A. K.; Burdick, J.; Anseth, K. S., Surface and bulk modifications to photocrosslinked polyanhydrides to control degradation behavior. *J. Biomed. Mater. Res. A* **2000,** *51* (3), 352-359. doi:10.1002/1097-4636(20000905)51:3<352::Aid-jbm8>3.0.Co;2-c

(24) Kumar, N.; Langer, R. S.; Dom, A. J., Polyanhydrides: an overview. *Adv. Drug Deliv. Rev.* **2002,** *54* (7), 889–910. doi:10.1016/S0169-409X(02)00050-9

(25) Falco, E. E.; Patel, M.; Fisher, J. P., Recent Developments in Cyclic Acetal Biomaterials for Tissue Engineering Applications | SpringerLink. *Pharm. Res.* **2008,** *25* (10), 2348-2356. 10.1007/s11095-008-9620-5

(26) Andriano, K. P.; Tabata, Y.; Ikada, Y.; Heller, J., In vitro and in vivo comparison of bulk and surface hydrolysis in absorbable polymer scaffolds for tissue engineering. *J. Biomed. Mater. Res.* **1999,** *48* (5), 602-612. doi:10.1002/(SICI)1097-4636(1999)48:5<602::AID-JBM3>3.0.CO;2-6

(27) Sommerfeld, S. D.; Zhang, Z.; Costache, M. C.; Vega, S. L.; Kohn, J., Enzymatic Surface Erosion of High Tensile Strength Polycarbonates Based on Natural Phenols. *Biomacromolecules* **2014,** *15* (3), 830-836. doi:10.1021/bm4016539

(28) Langer, R., Biomaterials and biomedical engineering. *Chem. Eng. Sci.* **1995,** *50* (24), 4109-4121. doi:10.1016/0009-2509(95)00226-X

(29) Lee, J. W.; Gardella, J. A., Jr., Surface perspectives in the biomedical applications of poly(alpha-hydroxy acid)s and their associated copolymers. *Anal. Bioanal. Chem.* **2002,** *373* (7), 526-537. 10.1007/s00216-002-1339-2

(30) Zou, T.; Cheng, S.-X.; Zhang, X.-Z.; Zhuo, R.-X., Novel cholic acid functionalized star oligo/poly(DL-lactide)s for biomedical applications. *J. Biomed. Mater. Res. B* **2007,** *82B* (2), 400-407. doi:10.1002/jbm.b.30745

(31) Poetz, K. L.; Mohammed, H. S.; Shipp, D. A., Surface Eroding, Semicrystalline Polyanhydrides via Thiol–Ene “Click” Photopolymerization. *Biomacromolecules* **2015,** *16* (5), 1650-1659. doi:10.1021/acs.biomac.5b00280

(32) Choi, N. S.; Heller, J. Drug delivery devices manufactured from poly(orthoesters) and poly(orthocarbonates). 4093709 A, 1978-6-6, 1978.

(33) Heller, J., Development of poly(ortho esters): a historical overview. *Biomaterials* **1990,** *11* (9), 659-665. doi:10.1016/0142-9612(90)90024-K

(34) Heller, J.; Barr, J.; Ng, S. Y.; Abdellauoi, K. S.; Gurny, R., Poly(ortho esters): synthesis, characterization, properties and uses. *Adv. Drug. Deliv. Rev.* **2002,** *54* (7), 1015-1039. doi:10.1016/S0169-409X(02)00055-8

(35) Dutta, D. Biodegradable stent of a polyorthoester polymer or a polyanhydride polymer. 6527801, 2003.

(36) Haider, T.; Shyshov, O.; Suraeva, O.; Lieberwirth, I.; von Delius, M.; Wurm, F. R., Long-Chain Polyorthoesters as Degradable Polyethylene Mimics. *Macromolecules* **2019,** *52* (6), 2411-2420. doi:10.1021/acs.macromol.9b00180

(37) Wei, B.; Tao, Y.; Wang, X.; Tang, R.; Wang, J.; Wang, R.; Qiu, L., Surface-Eroding Poly(ortho ester amides) for Highly Efficient Oral Chemotherapy. *ACS Appl. Mater. Inter.* **2015,** *7* (19), 10436-10445. 10.1021/acsami.5b01687

(38) Fu, S.; Yang, G.; Wang, J.; Wang, X.; Cheng, X.; Tang, R., Acid-degradable poly(ortho ester urethanes) copolymers for potential drug carriers: Preparation, characterization, in vitro and in vivo evaluation. *Polymer* **2017,** *114*, 1-14. doi:10.1016/j.polymer.2017.02.079

(39) Kolb, H. C.; Finn, M. G.; Sharpless, B. K., Click Chemistry: Diverse Chemical Function from a Few Good Reactions. *Angew. Chem. Int. Ed.* **2001,** *40* (11), 2004-2021. doi:10.1002/1521-3773(20010601)40:11<2004::AID-ANIE2004>3.0.CO;2-5

(40) Kolb, H. C.; Finn, M. G.; Sharpless, B. K., Click-Chemie: diverse chemische Funktionalität mit einer Handvoll guter Reaktionen. *Angew. Chem.* **2001,** *113* (11), 2056-2075. 10.1002/1521-3757(20010601)113:11<2056::AID-ANGE2056>3.0.CO;2-W

(41) Plikk, P.; Tyson, T.; Finne-Wistrand, A.; Albertsson, A. C., Mapping the characteristics of the radical ring-opening polymerization of a cyclic ketene acetal towards the creation of a functionalized polyester. *J. Polym. Sci. A Polym. Chem.* **2009,** *47* (18), 4587-4601. doi:10.1002/pola.23511

(42) Barner-Kowollik, C.; Du Prez, F. E.; Espeel, P.; Hawker, C. J.; Junkers, T.; Schlaad, H.; Van Camp, W., "Clicking" Polymers or Just Efficient Linking: What Is the Difference? *Angew. Chem. Int. Ed.* **2011,** *50* (1), 60-62. doi:10.1002/anie.201003707

4

Synthesis of Poly(Orthoester-Thioether-Thiourethane-Urethanes) (POETE-Us) from Oligomeric Thiol-Terminated POETEs as Degradable Elastomers

4.1 Abstract

Polyurethanes represent an important class of durable and biocompatible elastomers; however, they generally show low degradability in mild biological environments. This work focusses on the synthesis and manufacturing of recyclable and hydrolytically degradable polyurethanes based on orthoester functionalities. To that end, the previously established poly(orthoester thioethers) (POETEs; Chapter 2), which were synthesised with a molecular weight of *ca.* 2 kDa, were employed as soft segments, whereas a selection of biocompatible aliphatic diisocyanates were chosen as hard segments. Their combination afforded a wide a variety of polymeric materials. Unfortunately, several difficulties were observed in some formulations, such as inhomogeneous and inconsistent material properties, the limitation to mostly either glassy or weak elastic behaviour, as well as the unfavourable degradation following a bulk erosion mechanism. Despite these challenges, diverse and easily processable PU materials were obtained, with some exhibiting typical phase separation on a micrometre scale. Furthermore, the presented methodology produced materials with more diverse properties by simply adjusting the experimental conditions during synthesis, manufacturing and post-processing. Initial tests yielded strong elastomeric POETE-Us for which promising applications in the biotechnological field can be envisioned.

4.2 Introduction

Polyurethanes (PUs) are not only known for their durability and versatility in various formulations for home applications,[1] but also constitute an important class of elastomers.[2] In order to achieve this elasticity, the chemical composition and synthetic procedure is chosen so that separate hard and soft segments are formed.[3] The stiffness of the hard segments originates in the strong intermolecular hydrogen bonds formed between the urethane functionalities, which also determines the mechanical strength and thermal properties of the materials.[3-6] In a typical procedure, diisocyanates are coupled with a low molecular weight diol as chain extender to form the PU, which can release diamines upon degradation.[7] As aromatic amines are generally toxic,[7-8] biological considerations favour the use of aliphatic diisocyanates, which in turn limit the

mechanical properties of the resulting polymers. In contrast, the soft segments usually consist of oligomeric or polymeric diol components, which can be tailored to achieve the desired properties.[6, 9] While the use of short macrodiols is associated with the production of tougher materials in general, long macrodiols of up to 5 kDa are employed preferably for the development of elastomers. Furthermore, the structure of the macrodiol determines the hydrolytic and enzymatic degradation properties of the final polymer, which was proven in a variety of studies using PLA, PEG and PCL components.[10-14]

The material properties of PU are generally determined by the content of hard segments (%HS), which can be calculated using Flory's Equation.[6, 15-16] While the excessive content of hard segments results in brittle materials, a predominantly soft composition produces gel-like materials or polymers with low glass transition temperatures.[17-21] Within those boundaries, however, variations in the post-processing conditions, like temperature and duration of melt processing and annealing, for example, can separate the glassy segments or induce crystallisation and, specifically, influence crystallite size and distribution.[22-26] This structure-property relationship has been understood for more than half a century and has been exploited to optimise polyurethane-based materials for applications in everyday life.

Within the last decade, replacing the diol compounds with dithiol species has been explored more widely with the aim of creating more versatile functional and biocompatible poly(thiourethane urethane)s (PTUUs). Such approaches have led to the development of self-healing composite materials with thiol-containing reservoirs,[27] tough PTUU networks,[28] as well as diverse elastic PTUUs by Kultys and co-workers.[9, 29-30] Specifically, maximum elongation values between 60 and 800% at ultimate tensile strengths between 33 and 6 MPa, respectively, were achieved,[29] with optimised material even reaching 49 MPa ultimate strength.[30] Indeed, the production of materials with elastic moduli ranging from 16.6 to 409.0 MPa, with hard segment melting temperatures between 45 and 174 °C,[29] further demonstrates the mechanical versatility of such chemistry. Interestingly, Eglin *et al.* employed PCL and a dithiol as chain extender to obtain surface erodible PTUUs,[31] which is a behaviour usually limited to gel-like materials, such as polyorthoesters or biomedically problematic polyanhydrides. In fact, Tang and

coworkers[32-33] previously demonstrated that the incorporation of orthoester (OE) segments into polyurethane polymers can be used to manufacture surface erodible nanoparticles with a temporally and dimensionally uniform degradation profile, which can be exploited in a biomedical context. However, the air and moisture sensitive synthesis of these orthoester components, as well as the weak mechanical properties of the resulting materials, still limit their scope and application. These complications are in fact the limiting factors of most homopolymeric polyorthoesters (POE) materials to date.[34-36]

So far, the production of customised strong surface erodible poly(orthoester-thioether) (POETE) network materials (Chapter 3), as well as thiol-terminated POETE chain polymers (Chapter 2) have been reported on. Based entirely on click reactions, these approaches provided access to macrodithiols with the latent capability of facilitating surface erosion, while also ensuring biocompatibility. Herein, a simple route to obtain degradable poly(orthoester-thioester-urethane)s (POETE-Us) *via* POETE macrodithiols is described, which was employed to produce and reprocess polymeric material on a multi-gram scale. Despite several complications, this methodology was easily modified, and optimisations are suggested to yield POETE-Us as a versatile class of polymers for potential applications in biomedicine.

4.3 Results and Discussion

4.3.1 Synthesis and Characterisation of POETE Macrodithiols

POETE oligomers as macrodithiols were synthesised as previously reported by simple UV irradiation of a mixture of the dimeric OE3 (***3***) with hexane-1,6-dithiol and trace amounts of photoinitiator (Chapter 2); however, an excess of dithiol was employed in order to access thiol terminated polymers of the desired chain length of *ca.* 2 kDa (Scheme 4-1).

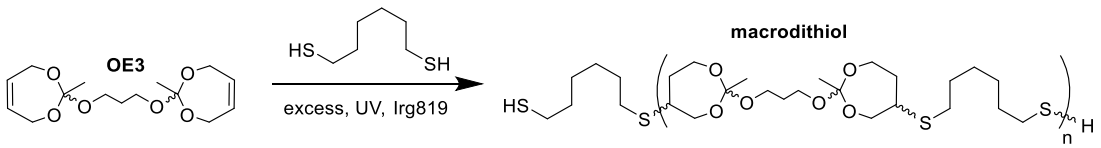

Scheme 4-1. Synthesis of the macrodithiol from a dimeric OE species and excess dithiol.

Indeed, an unexpectedly high excess of 1.4:1 was required to yield oligomers close to the target value, which indicates that oxidative disulfide formation competed with the chain formation. While this has been observed during POETE chain polymer formation before (Chapter 2), heating conditions during the synthesis, as well as the solvent and methodology used during chromatographic analysis, significantly affected the obtained size exclusion chromatograms (SECs) of oligomeric POETEs (Figure 4-1).

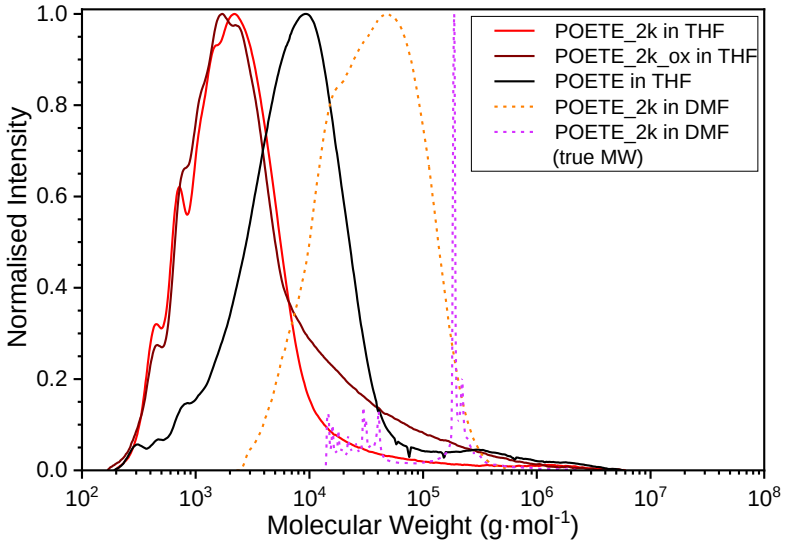

Figure 4-1. Size Exclusion Chromatograms of the OE3-2TE6 POETE oligomer (POETE_2k) in comparison with a POETE polymer (molecular weight determined in THF with 2 vol% NEt_3 or DMF with 2 vol% NH_4BF_4 against polystyrene standards).

Table 4-1. Calculated molecular weights and dispersities of the POETE oligomers according to Figure 4-1.

	M_n (kg·mol^{-1})	M_p (kg·mol^{-1})	M_w (kg·mol^{-1})	$Đ_M$
POETE_2k in THF	1.4	2.2	43.4	31.1
POETE_2k_ox in THF	1.5	1.7	35.8	23.7
POETE in THF	4.4	11.6	11.6	2.6
POETE_2k in DMF	54.2	-	169.6	3.1
POETE_2k in DMF (true MW)	22.3	-	53.6	2.4

The size exclusion chromatograms of the POETE macrodithiol revealed a stepwise distribution towards lower molecular weight (*MW*), which is approximately in accordance with the *MW* of the OE3 (***3***) subunit (450 g·mol^{-1}). Hence, the target *MW* of 2 kDa constitutes only a tetramer; however, a narrow distribution cannot be expected as a consequence of the step-growth mechanism and was indeed not observed (Table 4-1). Furthermore, a high molecular weight shoulder was present whenever the reaction mixture was allowed to heat above

room temperature, which can be attributed to disulfide formation *via* oxidation (POETE_2k_ox). While the longer POETE chain polymers were generally more soluble in THF, the POETE oligomer was also analysed in DMF as carrier solvent. Interestingly, in DMF, the distribution shifted significantly to higher molecular weights, which could be caused by assembly, aggregation, crosslinking or increased disulfide formation. Whereas absolute size exclusion chromatography (ASEC) by combination with dynamic light scattering (DLS) was used to determine the 'true *MW*' in DMF, the result suggested a narrow *MW* distribution around 22 kDa, which is in stark contrast to all other results. This illustrates that the method is unable to accurately detect polymers of *MWs* below 10 kDa and hence selectively characterised species with high *MW*. As the exact nature of these species is unclear and high *MWs* are undesirable in such precursors for elastomeric PUs, the macrodithiol obtained under mild conditions was used for further investigation. In order to calculate more accurately the average *MW* of the compound for manufacturing purposes without the inconsistencies of the SECs, complementary ^{1}H NMR spectroscopic analyses were performed.

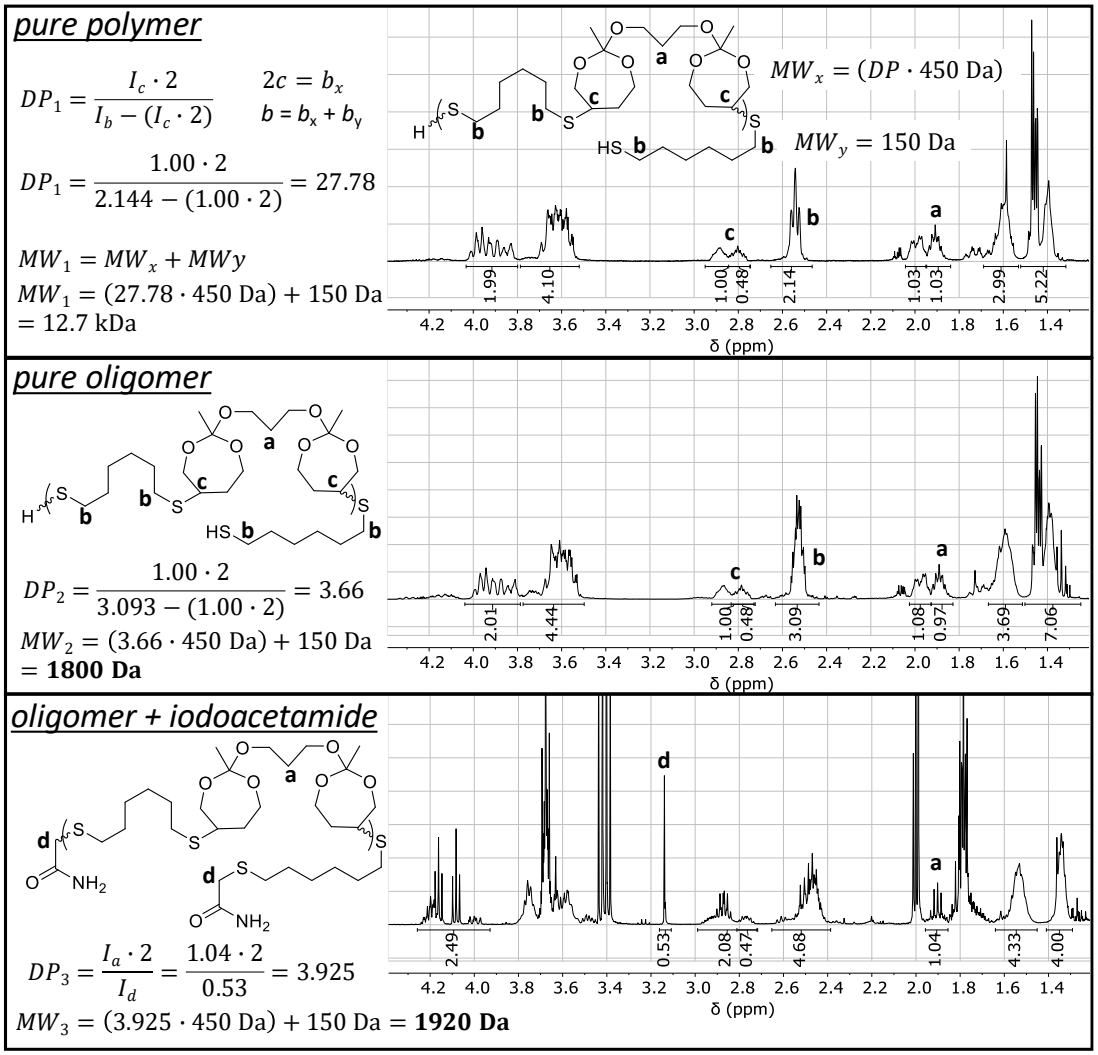

Figure 4-2. ^{1}H NMR spectra of POETE polymer, macrodithiol and iodoacetamide derivative with calculation of the respective molecular weight ($CDCl_3$, 300 MHz, 298 K).

The ^{1}H NMR spectra of the macrodithiol proved difficult to assign and quantify as a consequence of overlapping signals (Figure 4-2). Nevertheless, the distinctive double-population cyclic thioether signal from the two diastereomers at around δ = 2.7-2.9 ppm (c) and the propyl linker methylene at δ = 1.9 ppm (b) appeared separated enough to represent the degree of polymerisation or, more descriptively, the number of repeat units (*DP*, MW_x). Based on the spectra of the pure polymer and oligomer, the hexyl thioether signal around δ = 2.5-2.6 ppm represents both the repeat unit and terminal hexane dithiol functionality. Hence, compensating for the amount of proton signals (double) and dividing the integral values of the reference signal (c) by the combined signal (b) minus the reference signal yields the average amount of repeat units (*DP*). *MWs* were then calculated and found to be close to the peak molecular weights (M_p) as obtained by SEC, with

12.7 kDa and 1.8 kDa compared to 11.6 kDa and 2.2 kDa for the polymeric and oligomeric POETE, respectively.

Because of the relatively small value of the single hexane dithiol end group, however, a significant error needs to be considered in these calculations. Hence, the quantitative reaction of the free thiol end groups with iodoacetamide was investigated as an alternative approach, which resulted in a sharp singlet signal at δ = 3.15 ppm that represents only the terminal functionalities. Overall, this method, which indicated a calculated average *MW* of 1.92 kDa, was considered as the most accurate and used for the subsequent calculation of the POETE-U composition.

4.3.2 Synthesis and Manufacturing of POETE-U Materials

The content of hard segments (%HS) in any PU can be calculated applying an equation derived by Flory (Equation 4.1), where the *MW* of each component and the mol ratio of diisocyanate to macrodithiol (R) are factored in. [6, 15-16] In order to cover a range of properties, POETE-U materials displaying %HS values equal to 30, 40, and 50% were targeted in two sets using different aliphatic diisocyanates (Scheme 4-2).

$$\%\mathrm{HS} = \frac{100(R-1)(M_{diol}+M_{diiso})}{(M_{poly}+R(M_{diiso})+(R-1)(M_{diol}))} \qquad \text{Equation 4.1}$$

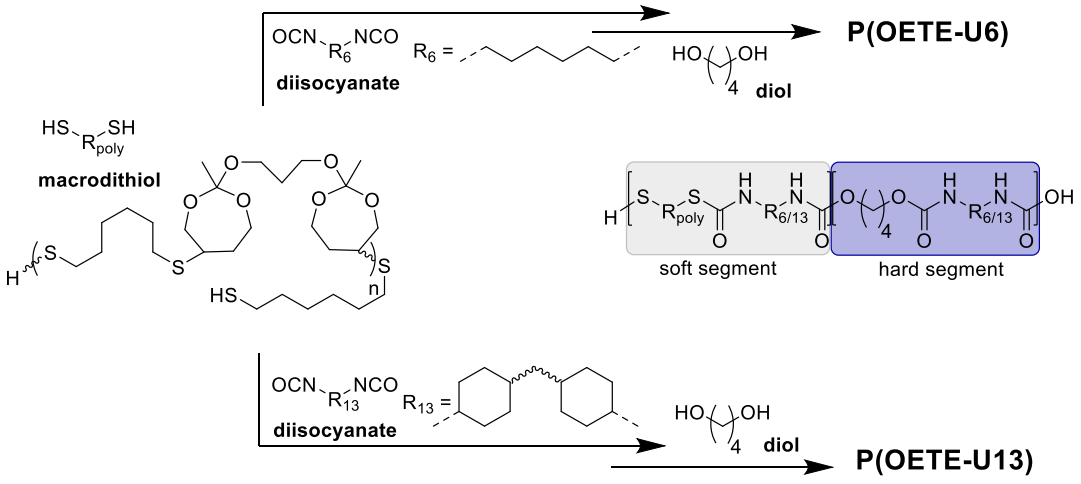

Scheme 4-2. Stepwise synthesis of two sets of POETE-Us with different diisocyanates.

The synthesis of POETE-Us was performed in a stepwise fashion: the diisocyanate and catalyst were added to the macrodithiol under nitrogen flow, followed by reaction overnight (15 h) at 100 °C and the addition of the respective amount of chain extender to the viscous heated mixture. Unfortunately, superficial solidification occurred almost immediately after addition of the diol, which impeded proper mixing. Nevertheless, continued reaction and external stirring yielded clear glassy polymers, which were pressed for further homogenisation and sample preparation.

It should be noted that the bicyclic diisocyanate (H_{12}MDI, POETE-U13) consists of three diastereomers in *cis-cis*, *cis-trans* and *trans-trans* (*t-t*) configuration. Despite being present at the lowest content in the crude mixture, the latter is the most crystalline and most promising for PU applications, as well as relatively easy to obtain in higher purity by following a simple sequential fractional crystallisation strategy.[37-38] At temperatures around 4 °C, a solid fraction of increased *t-t* isomer is formed, which is separated and left to partially melt at room temperature. After further separation and repetition of this process at 40 °C, a crystalline high *t-t* isomer containing fraction was obtained. The combined liquid residues were used as a low *t-t* fraction. GC-MS confirmed the expected trend of *t-t* isomer content: 55% for the high *t-t* fraction, 19% for the crude, and 16.5% for the low *t-t* configuration (Table 4-2).

Table 4-2. Isomer content in three different formulations of H_{12}MDI according to integration of GC-MS signals (THF, 100 to 260 °C over 30 min).

	cis-cis	*cis-trans*	*trans-trans*
crude	31.0%	50.3%	18.7%
high t-t	16.5%	28.6%	54.9%
low t-t	31.8%	51.7%	16.5%

Because of the glassy consistency of the higher %HS samples at room temperature, heating was required during sample manufacturing. Hence, clear films were obtained after heat pressing the materials at 150 °C, which is a typical temperature for PU materials and was confirmed by preliminary melting experiments. Then, using a dye cutter, samples for DSC/TGA, DMTA and tensile testing were prepared.

4.3.3 Thermal Analyses of POETE-U Materials

In order to assess and confirm suitable annealing and pressing temperatures for crystallite growth, TGA and DSC experiments were performed.

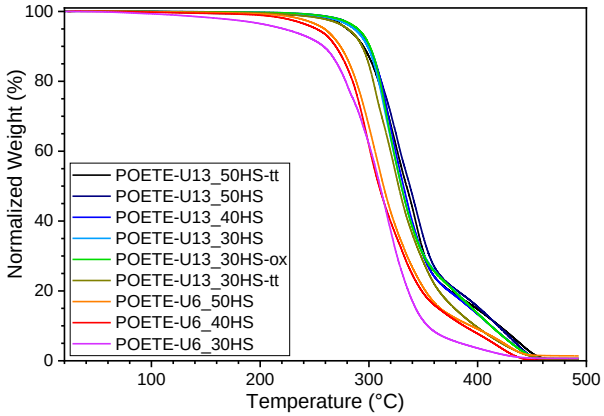

Figure 4-3. TGA thermograms of all POETE-U materials (POETE-U6, POETE-U13) at various hard segment contents, diastereomer composition and synthesis conditions (10 K·min^{-1}).

According to TGA thermograms, a range of different POETE-U6 and POETE-U13 materials displayed a common decomposition onset around 250 °C (Figure 4-3), with some POETE-U6 shedding mass at slightly lower temperatures, which was ascribed to the inhomogeneous mixture and incomplete reaction.

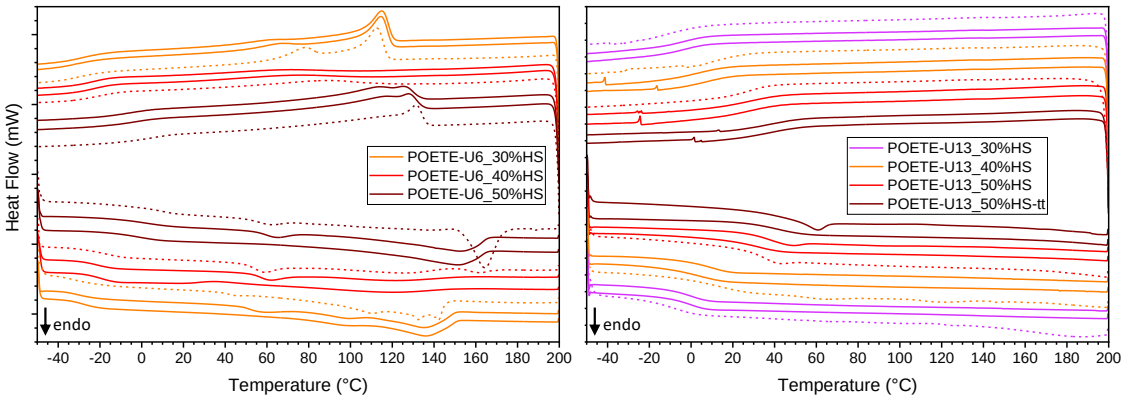

Figure 4-4. DSC thermograms of POETE-U6 (left) and POETE-U13 (right) at hard segment contents of 30, 40 and 50%HS, each after annealing at 40 °C for 5 days (10 K·min^{-1}).
Continuous lines (outwards): 1st cycle; 3rd cycle. Dashed line: re-pressed sample, 1st cycle.

Indeed, DSC analysis further confirmed the inhomogeneity hypothesis. POETE-U6 materials showed a relatively low glass transition temperature (T_g) between -30 and 10 °C at 30 to 50%HS (Figure 4-4), respectively, while a minor signal around 60 °C indicates a secondary melting point or glass transition. The primary melting temperature (T_m), between 140 and 150 °C, confirmed 150 °C as a suitable pressing temperature. While the 30 and 40%HS samples showed no

obvious changes after re-pressing, the re-pressed 50%HS sample exhibited a slight increase in T_g and T_m, which could be a consequence of incomplete mixing during the reaction and first pressing procedure. In contrast, the POETE-U13 materials with a %HS content of 30 and 50% exhibited a wider range of T_g (*i.e.* between -10 and 40 °C) and a significant decrease in T_g when the material was re-pressed, which indicates either thermal or constant gradual degradation, with the latter more likely as samples tended to liquify after storage for several weeks. Furthermore, no obvious T_m could be distinguished despite the material melting at elevated temperature, which suggests that the hard segment content is either too low or not crystalline enough. In fact, a small sample of POETEU13 with 50%HS prepared from high *t*-*t* isomer diisocyanate revealed a slight overshoot after the glass transition temperature, which could constitute a T_m just after the T_g at around 60 °C. This thermal event would coincide with the T_g of the POETE-U6 and confirm a structural involvement of the butanediol linker or, even though less likely, the POETE macrodithiol.

Overall, these materials appeared either too glassy or soft and, consequently, were unsuitable for elastomer applications; hence, a series of 30%HS materials was investigated in regard to the crystalline content.

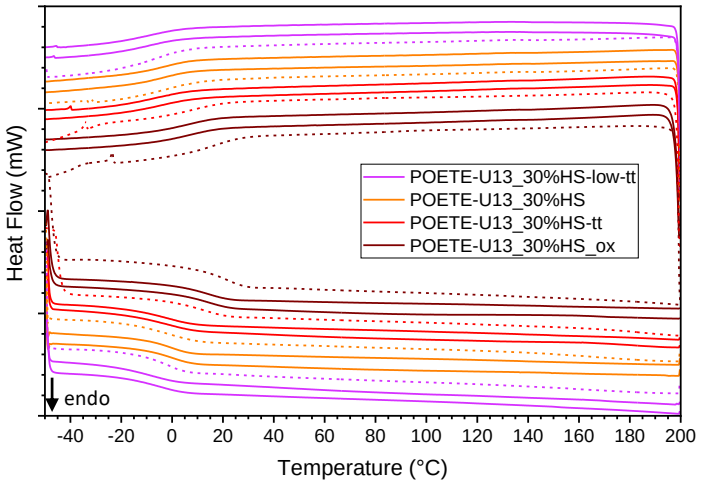

Figure 4-5. DSC thermograms of POETE-U13 at a hard segment content of 30%HS with different diastereomer content and after thermal post-curing at 120 °C for 5 days (ox), each after annealing at 40 °C for 5 days (10 K·min^{-1}).
Continuous lines (outwards): 1st cycle; 3rd cycle. Dashed line: re-pressed sample, 1st cycle.

Analogous to the comparison of %HS of POETE-U13, the crystalline content of all materials was too low to identify any meaningful T_m peak in the DSC thermogram (Figure 4-5). As expected, T_g were narrowly distributed between 0 and 10 °C for

varying crystallinity, with a thermally post-cured material displaying higher T_g as a consequence of the higher conversion or additional crosslinking. Curiously, in contrast to the crude and low *t-t* materials, the high *t-t* isomer containing and crosslinked material showed an increase in T_g after re-pressing. This could be ascribed to either the limited water diffusion and hence hydrolysis through the stronger material or to the presence of residual crystallites and, consequently, more efficient annealing.

4.3.4 Microscopic Structural Analysis of POETE-U Materials

In order to understand the microstructure of the manufactured materials, AFM imaging on thin pressed films was conducted.

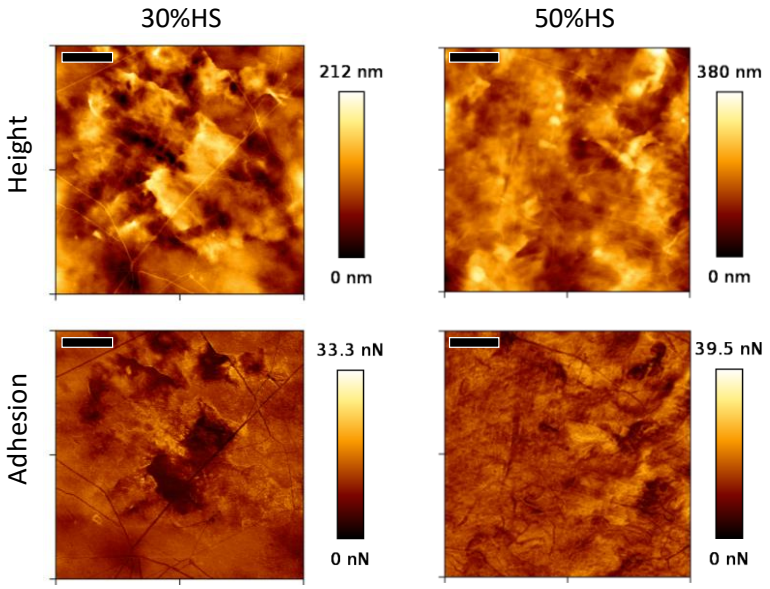

Figure 4-6. AFM images of POETE-U6 samples with different hard segment content. Top row: Height images. Bottom row: Corresponding adhesion images. Left: 30%HS, right: 50%HS (512 × 512 px, setpoint 25 nN, 40 °C, scale bar 2 µm).

Neither height nor adhesion images of the low and high %HS POETE-U6 materials revealed any obvious separation into different phases (Figure 4-6). Adhesion images suggested that some separation of the soft segments occurred in the 30%HS sample, which indicates that an even lower %HS content might be required for elastic materials to be formed. Alternatively, the sequential synthesis procedure might have led to more macroscopic separation phenomena and hence a one-pot approach might be more favourable. It is further worth noting that the AFM images showed several fibre-like structures that, rather than

being part of the material, were stemmed from the pressing process and highly static behaviour of both the material itself and the protective Teflon sheets, which attracted dust and textile fibres. While this was also the case for POETE-U13 materials, it was anticipated that their higher crystallinity would reveal a more interesting microstructure.

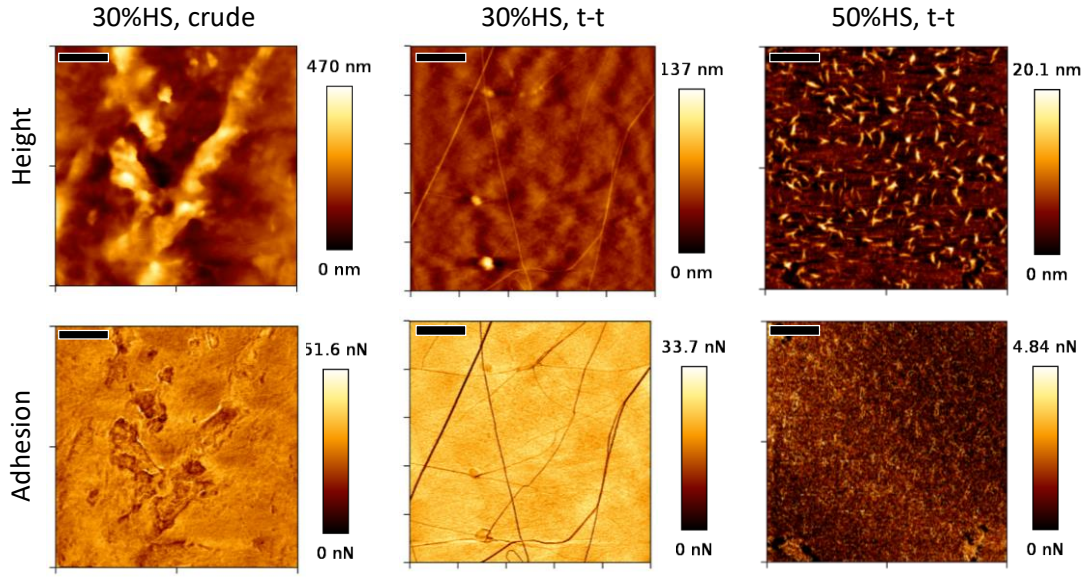

Figure 4-7. AFM images of POETE-U13 samples with different hard segment content and higher crystalline stereoisomer composition.
Top row: Height images. Bottom row: Corresponding adhesion images. Left to right: 30%HS crude, 30%HS *t-t*, 50%HS *t-t* (512 × 512 px, setpoint 25 nN, room temperature, scale bar 2 µm).

Indeed, although fibrous structures were still visible in the AFM images of the POETE-U13 samples, a more differential substructure was noted (Figure 4-7). The 30%HS material based on crude diisocyanate showed areas of high adhesion similar to the POETE-U6 material; however, at a higher *t-t* content these areas disappeared and revealed a more homogeneous material. Small bulky inhomogeneities were present, which indicated phase separation or crystallites. In contrast, a distinctive crystallite structure was observed in the 50%HS material based on high *t-t* isomer content. With a diameter of approximately 0.5 mm, the size of the crystallites required a more detailed imaging and micro-mechanical investigation.

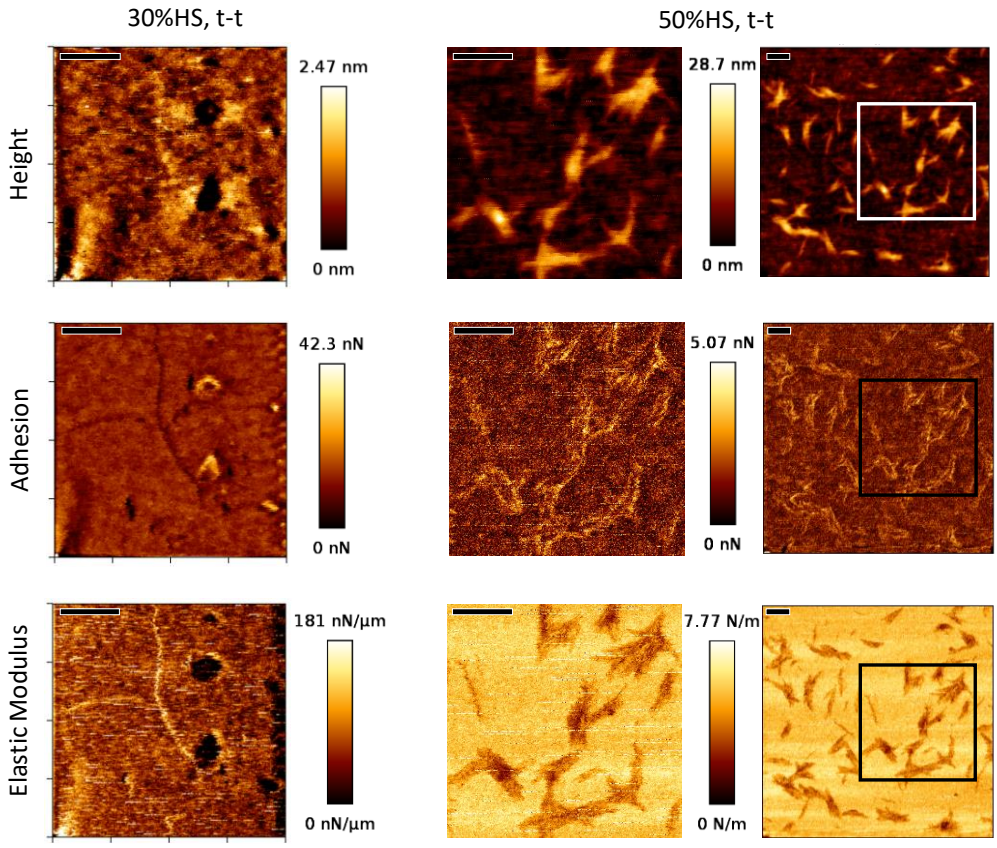

Figure 4-8. AFM images of crystallites in POETE-U13 samples with different hard segment content at high trans-trans stereoisomer composition.
Top row: Height images. Middle row: Adhesion images, Bottom row: Elastic Modulus.
Left: 30%HS, right: 50%HS (256 × 256 px, setpoint 25 nN, room temperature, scale bar 0.5 µm).

More detailed AFM images of POETE-U13 with high *t-t* content revealed that crystallites in the 50%HS material appeared on top of the film, whereas the potential analogous structures of similar size in the 30%HS material appeared submerged but much further spread out. Similarly, these crystalline regions exhibited slightly higher adhesive force on the outline and a significantly lower compression modulus than the surrounding material. While the higher adhesion can simply be explained by interaction with the AFM tip from an x-y direction as a height artefact, the lower elastic modulus could arise from some mobility of the superficial crystallites away from the z movement. From a chemical perspective, further contribution to the higher adhesion of crystallites could be found in the increased presence of hydrogen bonding between urethane-rich crystallites and the silicon AFM tip.

4.3.5 Thermo-Mechanical Analyses of POETE-U Materials

Although the previous microscopic and thermal investigations provided insight into the microstructure of the material, the application-relevant bulk mechanical properties of the POETE-Us are more accurately investigated by dynamic mechanical thermal analysis (DMTA).

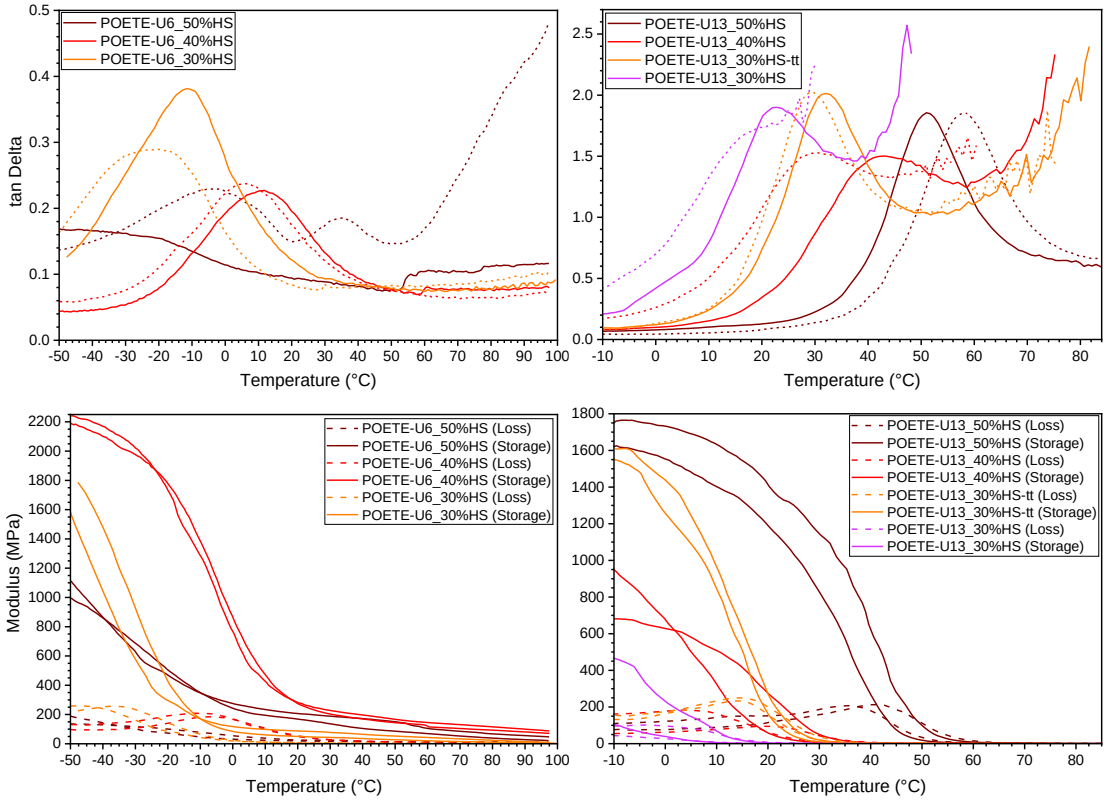

Figure 4-9. DMTA thermograms of POETE-U6 (left) and POETE-U13 (right) at hard segment contents of 30, 40 and 50%HS and with high crystalline content, each after annealing at 40 °C for 5 days (heating, 2 K·min^{-1}).
Top: tan δ (dashed: re-pressed). Bottom: Loss (dashed) and storage (continuous) modulus.

DMTA thermograms of POETE-U6 and POETE-U13 materials in tensile mode were recorded in order to confirm the determined T_g and record mechanical moduli (Figure 4-9). The T_g, as indicated by the maximum in tan δ values, were consistently slightly elevated compared to the DSC results, which is a logical consequence of the difference between static and dynamic methods. As a general trend, materials with higher %HS showed higher T_g values, albeit several inconsistencies were observed. Specifically, the initial sample of POETE-U6 showed no distinctive T_g, whereas the re-pressed sample does, which further confirms the hypothesis that the reaction did not proceed as intended. Furthermore, almost all T_g decrease in the re-pressed samples for both POETE-

U6 and POETE-U13, which indicates issues in sample preparation and partial degradation. Correspondingly, the thermograms of the POETE-U13 samples show a significant reduction in T_m onset, at which point the recording had to be stopped. A separate inconsistency was found in the recorded storage moduli, which did not follow the individual %HS trend, possibly because of sample preparation issues.

In order to investigate the mechanical material limits for potential applications, the mechanical characterisation of POETE-U6 and POETE-U13 samples was further complemented by performing uniaxial tensile testing.

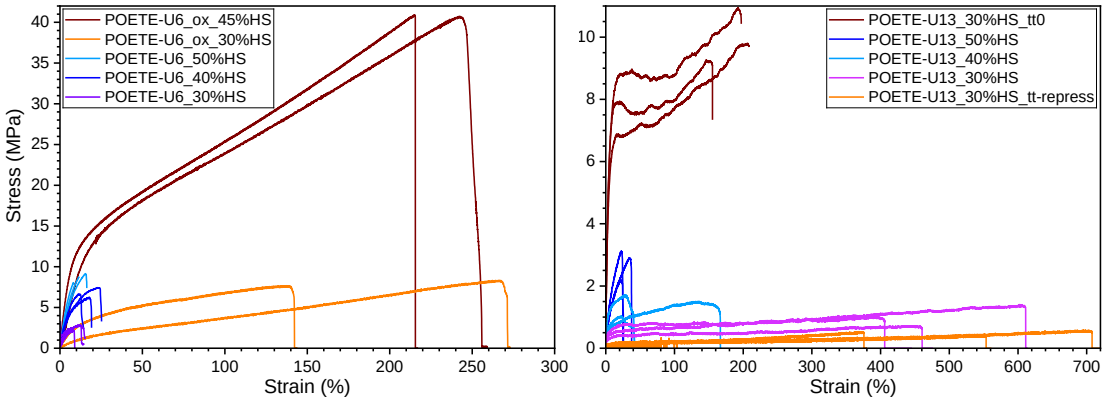

Figure 4-10. Strain-stress diagrams obtained from tensile testing of POETE-U6 (left) and POETE-U13 (right) samples at different hard segment ratios, synthesis procedures and crystalline content (room temperature, 4 mm·min^{-1}).

As indicated by the previous results, tensile strain-stress curves of the simple sequential POETE-U6 materials at 30, 40 and 50%HS confirmed their weak mechanical performance with maximum elongations of around 20% and ultimate stress values of up to 8 MPa. While the steepness of the curves and hence the Young's Moduli followed the trend in %HS, clearly no elastic properties were observed. Interestingly, preliminary samples synthesised in a one-pot approach from less carefully prepared partially oxidised POETE exhibited vastly superior elastomeric properties. Ultimate strains of over 250% and ultimate stress values of over 40 MPa demonstrated promising adjustments to the material synthesis. In contrast, the POETE-U13 materials exhibited generally lower ultimate stress values of up to 3 MPa, with the 30%HS samples showing remarkable elasticity of up to 600% elongation.

In order to combine both elasticity and higher mechanical strength through crystalline content instead of glassiness, the 30%HS high *t-t* material was

investigated and found to display superior mechanical strength up to 10 MPa with ultimate elongation of 200% and a Young's Modulus close to the POETE-U6 materials. Interestingly, after re-pressing these samples and the same 5-day annealing procedure, a complete drop in mechanical strength in favour of elongation up to 700% was observed. The previously discussed potential causes, such as thermal or hydrolytic degradation, disruption of crystallisation, and other processing complications, could also apply in this case. Nevertheless, the possibility to achieve competitive material properties has clearly been evidenced.

4.3.6 Degradation Studies on POETE-U Materials

As a final consideration for application and suitability of POETE-Us, their degradation behaviour was characterised in a preliminary study (Figure 4-11). It should be noted that all material samples used in thermo-mechanical studies started to soften after weeks of testing, with the low %HS materials already liquefied at room temperature. Unfortunately, the produced POETE-Us exhibited low reproducibility with significant changes in material properties between reprocessing steps and batches, and only a small amount of 'original' material from the first pressing remained. In order to limit the influence of hydrolysis or thermolysis over time, that material was used in this investigation.

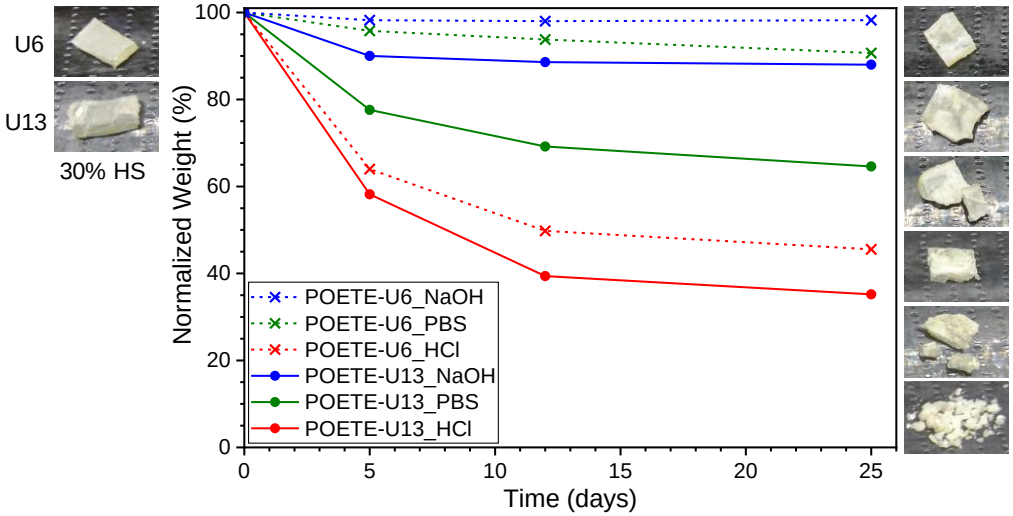

Figure 4-11. Visual appearance (left: before, right: after 5 d, following order of the curves) and relative average mass progress of POETE-U6 (dashed) and POETE-U13 (continuous) samples during degradation over time in 1 M NaOH, D-PBS and 1 M HCl at 25 °C.

Specifically, a single representative sample of POETE-U6 and POETE-U13 at 30%HS was divided into three samples of 0.4 g each, which were subjected to neutral (pH = 7), acidic (pH = 0) and alkaline (pH = 14) aqueous media, respectively. Under these accelerated hydrolytic degradation conditions, mass loss proceeded quickest in acidic and slowest in alkaline media, as expected from the previously reported POETE network materials (Chapter 3). The significantly faster degradation of POETE-U13 in neutral media compared to POETE-U6 could be caused by the longer diisocyanate linker unit and hence increased sensitivity to diffusion and hydrolysis, which would further explain the constant degradation and lowering of T_g. Moreover, in contrast to POETE networks, both POETE-Us exhibited a bulk erosion behaviour, with the samples disintegrating entirely after just 5 days in acidic media. Interestingly, the final weight roughly coincides with the expected content of hard segments, thus indicating that only the soft segments degraded. Because of the stability of the urethane-linkages at this time scale hard PU segments should indeed remain intact; however, the resulting particle size should depend on the segment length, aggregate stability and homogeneity. This observation further supports the hypothesis that the sequential synthesis route produced macroscopically inhomogeneous materials, and that the suggested optimisations (*i.e.* one-pot synthesis and higher *t-t* content) provide promising improvements to these POETE-U materials. Specifically, a one-pot synthesis offers more homogeneous distribution of the POETE functionalities and hence the potential for surface erosion.

4.4 Conclusion and Outlook

In summary, this chapter describes a facile and controlled route to synthesise POETE-Us while offering insight into potential optimisations for targeted material properties. Our approach was demonstrated by comparing linear and cyclic diisocyanates. Click reactions and a time-efficient polymerisation method yielded final reprocessable POETE-Us materials, which possessed a wide range of mechanical properties; however, obvious inconsistencies occurred. For instance, the synthesis of the underlying POETE oligomers and the determination of their molecular weight was hindered by oxidation or agglomeration events. Moreover, POETE-Us materials exhibited heterogeneous appearance, rapid

disintegration *via* bulk erosion in acidic media, and a gradual lowering of the melt and glass transition temperatures below room temperature after several reprocessing steps and long-term storage. The latter was ascribed to degradation (either hydrolysis or thermolysis), which was presumably facilitated further by water diffusion throughout the material. Furthermore, strong elastomers were difficult to achieve and required either a high crystalline hard segment content (*i.e*. strong semi-crystalline structure) or manufacturing in a one-pot bulk synthesis. Microscopic analysis *via* AFM confirmed the lack of phase separation unless a crystalline diisocyanate was employed. Overall, the final optimised preparation conditions produced materials with improved mechanical properties, especially regarding elasticity - elongation values of up to 200% at 10 to 40 MPa. Unfortunately, all materials were insoluble in any organic solvent and could hence only be processed *via* heat pressing, which limits industrial application. However, the use of biocompatible POETE components, as well as the promising mechanical properties obtained, verify the potential of POETE-U materials to be employed in various biomedical applications.

4.5 Experimental Section

4.5.1 Materials

Acetone (Sigma-Aldrich), Aliquat 336 (Sigma-Aldrich), basic aluminium oxide (Sigma-Aldrich), 2-bromo-1,1-dimethoxyethane (Acros Organics), butane-1,4-diol (Sigma-Aldrich), cis-2-butene-1,4-diol (Sigma-Aldrich), dibutyltin dilaurate (DBTDL, Sigma-Aldrich), diethyl ether (Sigma-Aldrich), hexane-1,6-diisocyanate (HDI, Sigma-Aldrich), hydrochloric acid (Fisher), iodoacetamide (Sigma-Aldrich), Irgacure 819 (IGM Resins Ltd.), carbonate (anhydrous, Sigma-Aldrich), potassium *tert*-butoxide (Sigma-Aldrich), 1,3-propanediol (Sigma-Aldrich), sodium hydroxide (Fisher), terephthalic acid (Sigma-Aldrich), tetrahydrofuran (Sigma-Aldrich), triethylamine (Sigma-Aldrich), preparation for Dulbecco's PBS (Sigma-Aldrich) and p-toluenesulfonic acid (Sigma) were used as received (unless otherwise stated). 4,4'-methylene dicyclohexyl diisocyanatepotassium (H_{12}MDI, mixture of isomers, Sigma-Aldrich) was used crude and enriched in trans-trans isomer by leaving 100 mL of the crude material under a nitrogen blanket at 4 °C for 2 weeks, separation from liquid material, leaving to separate

at room temperature for 2 weeks, and separating again from liquid material. The discarded fractions were combined as a slightly enriched cis-cis isomer mixture. $CDCl_3$ (Sigma-Aldrich) was stored over anhydrous potassium carbonate and plug filtered through basic aluminium oxide immediately before use. Furthermore, all glassware used for handling, analysis and storage of OE containing compounds was silanised by treating the inner surface with Sigmacote (Sigma-Aldrich) for five minutes, followed by rinsing with water, acetone, diethyl ether and subsequent drying under compressed air for 5 minutes.

4.5.2 Methods

A Formlabs Form Cure or a UVP UVL-230W was used for curing of POETE oligomers. Nuclear Magnetic Resonance (NMR) spectra were acquired using a Bruker Avance III 400 MHz, processed by MestReNova software using the residual solvent peak as reference ($CDCl_3$, ^1H: δ = 7.26 ppm, ^{13}C: δ = 77.16 ppm). Mass spectra were obtained *via* a Bruker maXis plus. Elemental analysis was conducted on a CE Instruments EA1110 Elemental Analyzer. The isomer ratio of $H_{12}MDI$ was determined from solution in THF at 1 mg·mL^{-1} using a Shimadzu GC-2010 with ZB-5 (5% phenyl polysiloxane/95% dimethyl polysiloxane) 30m x 0.25mm (ID) x 0.25µm (film thickness) column with a method heating from 100 to 260 °C over 30 min and injector and FID temperatures of 180 and 270 °C, respectively, on GCMSsolution Verison 4.45 SP1 software. Size Exclusion Chromatograms were recorded on an Agilent Infinity II with RI detection on an Agilent PLgel MIXED-C, 7.5 × 300 mm, 5 µm column in THF with 2% NEt_3 and 0.01% BHT at a flow rate of 1 mL·min^{-1} at 50 °C compared to EasiVial Polystyrene Standard. An analogue setup with additional PDA and Wyatt Dawn Helios II with a COMET ultrasonic transducer was used to record Absolute Size Exclusion Chromatograms (ASEC) in DMF with 2% NH_4BF_4. Agilent GPC/SEC software V.A.02.01 (2015) and ASTRA V 7.1.3.15 (ASEC) was used for data analysis. An Agilent Cary 630 FTIR Spectrometer with Agilent Resolutions Pro software V.5.0 was used for IR spectroscopy. DSC and TGA thermograms were collected on a Mettler-Toledo STARe DSC3+ system and a TA Instruments TGA Q500, respectively. DMTA data was recorded on a Mettler-Toledo DMA1-STARe using STARe Excellence Thermal Analysis Software V2.22. Tensile testing was

performed on a Testometric M350-5CT using Win TestAnalysis (v.5.0.34). AFM images were recorded on a JPK Nanowizard 4 in QI mode using Nanosensors PPP-NCHAuD tips and Nanowizard Control Software V.6.1.117.

4.5.3 Synthesis of 2-(Bromomethyl)-1,3-dioxe-5-pene (BrCKA, 1)

The procedure follows a method described by Plikk *et al.*[39] Cis-2-butene-1,4-diol (33.30 g, 378 mmol) and 2-bromo-1,1-dimethoxyethane (63.89 g, 378 mmol) were weighed into a 100 mL round bottom flask, followed by p-toluenesulfonic acid (0.10 g, 0.1 wt%). A stirrer bar, Vigreux condenser and distillation bridge was added and the mixture incrementally heated to 130 °C under stirring, until no more methanol was distilled over. After cooling to room temperature and gradually reducing the pressure, a residual methanol fraction was discarded and subsequently the pure product distilled at 38-42 °C and 0.05 mbar (62.1 g, 85%). Characterised as reported previously.[39] ^{1}H NMR (400 MHz; 298 K; $CDCl_3$; ppm): δ 5.70 (t, $^{3}J_{HH}$ = 1.5 Hz, 2H), 4.97 (t, $^{3}J_{HH}$ = 5.4 Hz, 1H), 4.44 (dm, $^{3}J_{HH}$ = 14.7 Hz, 2H), 4.20 (dm, $^{3}J_{HH}$ = 14.7 Hz, 2H), 3.39 (d, $^{3}J_{HH}$ = 5.4 Hz, 2H); ^{13}C NMR (400 MHz; 298 K; $CDCl_3$; ppm): δ 128.81, 106.92, 63.25, 24.99.

4.5.4 Synthesis of 2-Methylene-1,3-dioxe-5-pene (CKA, 2).

Similarly to Plikk *et al.*'s method,[39] BrCKA **(1)** (40.00 g, 207 mmol) and Aliquat 336 (1.62 g, 4 mmol) were weighed into a 500 mL RBF, dissolved in 350 mL THF and cooled under stirring to 0 °C. Potassium *tert*-butoxide (46.50 g, 414 mmol) was added in small portions within one hour and the orange to yellow suspension left to stir for another two hours at 0 °C. THF was removed *in vacuo* (20 mbar, 18 °C) and the residual slurry dissolved in 200 mL diethyl ether and 200 mL distilled water, followed by separation of the layers and extraction of the aqueous phase with a further 100 mL diethyl ether. The combined organic layers were washed with 0.01 M potassium carbonate solution (300 mL) for three times. The organic layer was concentrated *in vacuo* at 18 °C, followed by vacuum transfer of the residual oil at room temperature and 0.05 mbar to yield crude product. Repeat of the washing procedure, followed by drying over potassium carbonate and concentration at 30 °C and 20 mbar yielded pure product (12.50 g, 55%). ^{1}H NMR (400 MHz; 298 K; $CDCl_3$; ppm): δ 5.72 (t, $^{3}J_{HH}$ = 1.7 Hz, 2H), 4.43 (d, $^{3}J_{HH}$

= 1.7 Hz, 4H), 3.57 (s, 2H); ^{13}C NMR (400 MHz; 298 K; $CDCl_3$; ppm): δ 164.11, 127.83, 68.77, 68.21.

4.5.5 Synthesis of 1,3-Bis(2-methyl-2-oxyl-1,3-dioxe-5-pene)-propane (OE3, 3).

CKA **(2)** (4.00 g, 35.68 mmol), 1,3-propanediol (1.36 g, 17.84 mmol) and terephthalic acid (0.60 g, 0.36 mmol) were weighed into a silanised bottle, put in an ice bath and reacted overnight. The crude product was dissolved in diethyl ether and washed four times with equivalent volumes of 0.01 M potassium carbonate solution, followed by separation and drying of the organic layer over potassium carbonate. Plug filtration through minimal amounts of basic alumina and evaporation yielded crude OE3 product. Additional distillation *in vacuo* before use was performed to remove any degradation products (around ^{1}H NMR δ 2.00 ppm) and to yield clear colourless oil of fruity odour (4.48 g, 84%; distillation at 0.02 mbar, 150 °C). ^{1}H NMR (400 MHz; 298 K; $CDCl_3$; ppm): δ 5.66 (t, $^3J_{HH}$ = 1.7 Hz, 4H, -C*H*CH_2CO_3-), 4.43 (dm, 4H, $^2J_{HH}$ = -15.5 Hz, -CHC*H*$_2CO_3$-), 4.15 (dm, 4H, $^2J_{HH}$ = -15.5 Hz, -CHC*H*$_2CO_3$-), 3.65 (t, 4H, $^3J_{HH}$ = 6.3 Hz, -OC*H*$_2CH_2$-), 1.93 (qi, 2H, $^3J_{HH}$ = 6.3 Hz, -OCH$_2$C*H*$_2$-), 1.54 (s, 6H, -CO_3C*H*$_3$); ^{13}C NMR (400 MHz; 298 K; $CDCl_3$; ppm): δ 128.99 (-*C*HCH_2CO_3-), 116.20 (-*C*O_3CH_3), 61.57 (-CH*C*H_2CO_3-), 60.42 (-CO_3*C*H_2CH_2-), 30.37 (-CO_3CH_2*C*H_2-), 19.18 (-CO_3*C*H_3); MS (ESI-QTOF +ve): $(M + Na)^+$ *m/z* calculated for $C_{15}H_{24}O_6Na^+$: 323.1465, found: 323.1468; Anal. Calcd for $C_{15}H_{24}O_6$: C 60.0; H 8.05%. Found: C 59.9; H 8.0; IR (neat; 298 K; cm^{-1}): 2950-2860 (-C-H), 1380 (-CH_2-), 1160-1040 (C-O), 900 (-CH_2-CH_2-), 800 (C=C), 640 (=C-H).

4.5.6 Synthesis of Poly{[1,3-bis(2-methyl-2-oxyl-5-yl-1,3-dioxepane)-O-propane]-alt-(1,6-thioyl-hexane)} (OE3-2TE6, poly, macrodithiol, 4).

The reaction of OE3 **(3)** (1.00 g, 3.33 mmol), 1,6-hexanedithiol (0.50 g, 3.33 mmol) and Irgacure 819 (0.015 g) in a silanised clear bottle under UV irradiation from a Formlabs Form Cure for 16 h yielded clear viscous product. For the thiol terminated oligomers of around 2 kDa, OE3 ***(3)*** (1.00 g, 3.33 mmol) and 1,6-hexanedithiol (0.70 g, 4.66 mmol) were reacted in a 1:1.4 ratio instead under a UVP UVL-230W for 16 h. ^{1}H NMR (400 MHz; 298 K; $CDCl_3$; ppm): δ 4.02-3.77 (m,

4H), 3.69-3.50 (m, 8H), 2.91-2.73 (m, 2H), 2.56-2.47 (m, 4H), 2.02-1.93 (m, 2H), 1.93-1.82 (m, 2H), 1.78-1.50 (m, 6H), 1.45-1.41 (ms, 6H), 1.41-1.34 (m, 4H); ^{13}C NMR (400 MHz; 298 K; $CDCl_3$; ppm): δ 115.88, 66.71/65.07, 61.91/60.32, 60.26/59.86, 44.06/43.27, 36.63/35.72, 31.16/31.00, 30.30, 30.03/30.00, 28.63, 20.69; IR (neat; 298 K; cm^{-1}): 2920-2850 (-C-H), 1370 (-CH_2-), 1150-1020 (C-O), 900 (-CH_2-CH_2-); GPC (THF, polymer): M_n = 4400 g·mol^{-1} ($Đ_M$ = 2.6).

4.5.7 Synthesis of POETE-Us

According to Flory's Equation (Equation 1),[6, 15-16] the calculated amount of OE3-2TE6 (poly, **4**, 2 kDa) was combined with dibutyltin dilaurate (DBTDL) and the respective diisocyanate in a silanised vial equipped with a rare-earth magnetic stirrer, purged under nitrogen flow and heated to 100 °C. After 4 hours reaction time, butanediol is quickly added to the viscous mixture and stirred at 100 °C overnight. In the alternative approach, all reagents were combined at room temperature under stirring, the vial flushed with nitrogen, closed and then heated at 100 °C overnight. The transparent colourless or yellowish material was subsequently removed from the glass vial either by heating to melt or breaking the glass and extracting the material. This crude heterogeneous polymer was then pressed in a steel template between Teflon sheets at 150 °C and up to 5 t to yield a more homogenous film of 1 mm thickness and cut into the desired shape with a dye cutter around the glass transition temperature to avoid cracks.

4.5.8 Synthesis of POETE-U6

OE3-2TE6 **(4)** (1.05 g, 0.55 mmol / 0.90 g, 0.47 mmol / 0.75 g, 0.39 mmol), HDI (0.39 mL, 2.44 mmol / 0.48 mL, 3.00 mmol / 0.57 mL, 3.55 mmol), butanediol (0.17 mL, 1.89 mmol / 0.22 mL, 2.53 mmol / 0.28 mL, 3.16 mmol) and DBTDL (7.23 µL, 0.12 mmol / 8.87 µL, 0.15 mmol / 10.51 µL, 0.18 mmol) were reacted to yield the clear colourless polymer material with a hard segment ratio of %HS = 30 / 40 / 50. T_g (DSC) = -10 – 20 °C, T_{pyro} (TGA) = 220 °C.

4.5.9 Synthesis of POETE-U13

OE3-2TE6 **(4)** (1.05 g, 0.55 mmol / 0.90 g, 0.47 mmol / 0.75 g, 0.39 mmol), H_{12}MDI (0.50 mL, 2.00 mmol / 0.60 mL, 2.40 mmol / 0.70 mL, 2.81 mmol),

butanediol (0.13 mL, 1.45 mmol / 0.17 mL, 1.94 mmol / 0.21 mL, 2.42 mmol) and DBTDL (5.92 µL, 0.10 mmol / 7.12 µL, 0.12 mmol / 8.32 µL, 0.14 mmol) were reacted to yield the clear colourless polymer material with a hard segment ratio of %HS = 30 / 40 / 50. T_g (DSC) = -5 – 50 °C, T_{pyro} (TGA) = 250 °C.

4.6 References

(1) Kausar, A., Polyurethane Composite Foams in High-Performance Applications: A Review. *Polymer Plast. Technol. Eng.* **2018,** *57* (4), 346-369. doi:10.1080/03602559.2017.1329433

(2) Harrell, L. L., Segmented Polyurethans. Properties as a Funcation of Segment Size and Distribution. *Macromolecules* **1969,** *2* (6), 607-612. doi:10.1021/ma60012a008

(3) Lee, D.-K.; Tsai, H.-B., Properties of segmented polyurethanes derived from different diisocyanates. *J. Appl. Polym. Sci.* **2000,** *75* (1), 167-174. doi:10.1002/(sici)1097-4628(20000103)75:1<167::Aid-app19>3.0.Co;2-n

(4) Kumagai, S.; Motokucho, S.; Yabuki, R.; Anzai, A.; Kameda, T.; Watanabe, A.; Nakatani, H.; Yoshioka, T., Effects of hard- and soft-segment composition on pyrolysis characteristics of MDI, BD, and PTMG-based polyurethane elastomers. *J. Anal. Appl. Pyrolysis* **2017,** *126*, 337-345. doi:10.1016/j.jaap.2017.05.012

(5) Pandya, M. V.; Deshpande, D. D.; Hundiwale, D. G., Effect of diisocyanate structure on viscoelastic, thermal, mechanical and electrical properties of cast polyurethanes. *J. Appl. Polym. Sci.* **1986,** *32* (5), 4959-4969. doi:10.1002/app.1986.070320518

(6) O'Sickey, M. J.; Lawrey, B. D.; Wilkes, G. L., Structure–property relationships of poly(urethane urea)s with ultra-low monol content poly(propylene glycol) soft segments. I. Influence of soft segment molecular weight and hard segment content. *J. Appl. Polym. Sci.* **2002,** *84* (2), 229-243. doi:10.1002/app.10168

(7) Darby, T. D.; Johnson, H. J.; Northup, S. J., An evaluation of a polyurethane for use as a medical grade plastic. *Toxicol. Appl. Pharm.* **1978,** *46* (2), 449-453. doi:10.1016/0041-008X(78)90090-X

(8) Shintani, H.; Nakamura, A., Analysis of a Carcinogen, 4,4′-Methylenedianiline, from Thermosetting Polyurethane during Sterilization. *J. Anal. Toxicol.* **1989,** *13* (6), 354-357. doi:10.1093/jat/13.6.354

(9) Rogulska, M.; Kultys, A.; Olszewska, E., New thermoplastic poly(thiourethane-urethane) elastomers based on hexane-1,6-diyl diisocyanate (HDI). *J. Therm. Anal. Calorim.* **2013,** *114* (2), 903-916. doi:10.1007/s10973-013-3007-5

(10) Ding, M.; Qian, Z.; Wang, J.; Li, J.; Tan, H.; Gu, Q.; Fu, Q., Effect of PEG content on the properties of biodegradable amphiphilic multiblock poly(ε-caprolactone urethane)s. *Polym. Chem.* **2011,** *2* (4), 885-891. doi:10.1039/C0PY00376J

(11) Cauich-Rodriguez, J. V.; Chan-Chan, L. H.; Hernandez-Sanchez, F.; Cervantes-Uc, J. M., Degradation of Polyurethanes for Cardiovascular Applications. In *Advances in Biomaterials Science and Biomedical Applications*, Pignatello, R., Ed. **2013**.

(12) Cherng, J. Y.; Hou, T. Y.; Shih, M. F.; Talsma, H.; Hennink, W. E., Polyurethane-based drug delivery systems. *Int. J. Pharm.* **2013,** *450* (1), 145-162. doi:10.1016/j.ijpharm.2013.04.063

(13) Singhal, P.; Small, W.; Cosgriff-Hernandez, E.; Maitland, D. J.; Wilson, T. S., Low density biodegradable shape memory polyurethane foams for embolic biomedical applications. *Acta Biomater.* **2014,** *10* (1), 67-76. doi:10.1016/j.actbio.2013.09.027

(14) Kucharczyk, P.; Pavelková, A.; Stloukal, P.; Sedlarík, V., Degradation behaviour of PLA-based polyesterurethanes under abiotic and biotic environments. *Polym. Degrad. Stabil.* **2016,** *129*, 222-230. doi:10.1016/j.polymdegradstab.2016.04.019

(15) Flory, P. J., Fundamental Principles of Condensation Polymerization. *Chem. Rev.* **1946,** *39* (1), 137-197. doi:10.1021/cr60122a003

(16) Flory, P. J., Thermodynamics of Crystallization in High Polymers. I. Crystallization Induced by Stretching. *J. Chem. Phys.* **1947,** *15* (6), 397-408. doi:10.1063/1.1746537

(17) Bengtson, B.; Feger, C.; MacKnight, W. J.; Schneider, N. S., Thermal and mechanical properties of solution polymerized segmented polyurethanes with butadiene soft segments. *Polymer* **1985,** *26* (6), 895-900. doi:10.1016/0032-3861(85)90134-X

(18) Speckhard, T. A.; Cooper, S. L., Ultimate Tensile Properties of Segmented Polyurethane Elastomers: Factors Leading to Reduced Properties for

Polyurethanes Based on Nonpolar Soft Segments. *Rubber Chem. Technol.* **1986,** *59* (3), 405-431. doi:10.5254/1.3538208

(19) Martin, D. J.; Meijs, G. F.; Gunatillake, P. A.; Yozghatlian, S. P.; Renwick, G. M., The influence of composition ratio on the morphology of biomedical polyurethanes. *J. Appl. Polym. Sci.* **1999,** *71* (6), 937-952. doi:10.1002/(sici)1097-4628(19990207)71:6<937::Aid-app9>3.0.Co;2-0

(20) Brunette, C. M.; Hsu, S. L.; Rossman, M.; MacKnight, W. J.; Schneider, N. S., Thermal and mechanical properties of linear segmented polyurethanes with butadiene soft segments. *Polym. Eng. Sci.* **1981,** *21* (11), 668-674. doi:10.1002/pen.760211108

(21) Willkomm, W. R.; Chen, Z. S.; Macosko, C. W.; Gobran, D. A.; Thomas, E. L., Properties and phase separation of reaction injection molded and solution polymerized polyureas as a function of hard block content. *Polym. Eng. Sci.* **1988,** *28* (14), 888-900. doi:10.1002/pen.760281403

(22) Li, Y.; Gao, T.; Liu, J.; Linliu, K.; Desper, C. R.; Chu, B., Multiphase structure of a segmented polyurethane: effects of temperature and annealing. *Macromolecules* **1992,** *25* (26), 7365-7372. doi:10.1021/ma00052a045

(23) Saiani, A.; Novak, A.; Rodier, L.; Eeckhaut, G.; Leenslag, J. W.; Higgins, J. S., Origin of Multiple Melting Endotherms in a High Hard Block Content Polyurethane: Effect of Annealing Temperature. *Macromolecules* **2007,** *40* (20), 7252-7262. doi:10.1021/ma070332p

(24) Hu, W.; Koberstein, J. T., The effect of thermal annealing on the thermal properties and molecular weight of a segmented polyurethane copolymer. *J. Polym. Sci. B. Polym. Phys.* **1994,** *32* (3), 437-446. doi:10.1002/polb.1994.090320304

(25) Leung, L. M.; Koberstein, J. T., DSC annealing study of microphase separation and multiple endothermic behavior in polyether-based polyurethane block copolymers. *Macromolecules* **1986,** *19* (3), 706-713. doi:10.1021/ma00157a038

(26) Yanagihara, Y.; Osaka, N.; Murayama, S.; Saito, H., Thermal annealing behavior and structure development of crystalline hard segment domain in a melt-quenched thermoplastic polyurethane. *Polymer* **2013,** *54* (8), 2183-2189. doi:10.1016/j.polymer.2013.02.005

(27) Szmechtyk, T.; Sienkiewicz, N.; Strzelec, K., Polythiourethane microcapsules as novel self-healing systems for epoxy coatings. *Polym. Bull.* **2018,** *75* (1), 149-165. doi:10.1007/s00289-017-2021-3

(28) Qin, X.-H.; Ovsianikov, A.; Stampfl, J.; Liska, R., Additive manufacturing of photosensitive hydrogels for tissue engineering applications. *BioNanoMaterials* **2014,** *15* (3-4), 49-70. doi:10.1515/bnm-2014-0008

(29) Kultys, A.; Rogulska, M.; Pikus, S., The synthesis and characterization of new thermoplastic poly(thiourethane-urethane)s. *J. Polym. Sci. A Polym. Chem.* **2008,** *46* (5), 1770-1782. 10.1002/pola.22520

(30) Kultys, A.; Puszka, A., Transparent poly(thiourethane-urethane)s based on dithiol chain extender. *J. Therm. Anal. Calorim.* **2014,** *117* (3), 1427-1439. doi:10.1007/s10973-014-3877-1

(31) Eglin, D.; Griffon, S.; Alini, M., Thiol-Containing Degradable Poly(thiourethane-urethane)s for Tissue Engineering. *J. Biomater. Sci. Polym. Ed.* **2010,** *21* (4), 477-491. doi:10.1163/156856209X424404

(32) Fu, S.; Yang, G.; Wang, J.; Wang, X.; Cheng, X.; Tang, R., Acid-degradable poly(ortho ester urethanes) copolymers for potential drug carriers: Preparation, characterization, in vitro and in vivo evaluation. *Polymer* **2017,** *114*, 1-14. doi:10.1016/j.polymer.2017.02.079

(33) Huang, Y.; Qin, J. J.; Wang, J.; Yan, G. Q.; Wang, X.; Tang, R. P., Dual-stimuli-sensitive poly(ortho ester disulfide urethanes)-based nanospheres with rapid intracellular drug release for enhanced chemotherapy. *Sci. China Chem.* **2018,** *61* (11), 1447-1459. doi:10.1007/s11426-018-9269-6

(34) Heller, J., Development of poly(ortho esters): a historical overview. *Biomaterials* **1990,** *11* (9), 659-665. doi:10.1016/0142-9612(90)90024-K

(35) Heller, J.; Barr, J., Poly(ortho esters) - From Concept to Reality. *Biomacromolecules* **2004,** *5* (5), 1625–1632. doi:S1525-7797(04)00049-2

(36) Heller, J.; Barr, J.; Ng, S. Y.; Abdellauoi, K. S.; Gurny, R., Poly(ortho esters): synthesis, characterization, properties and uses. *Adv. Drug. Deliv. Rev.* **2002,** *54* (7), 1015-1039. doi:10.1016/S0169-409X(02)00055-8

(37) Seneker, S. D.; Born, L.; Schmelzer, H. G.; Eisenbach, C. D.; Fischer, K., Diisocyanato dicyclohexylmethane: structure/property relationships of its

geometrical isomers in polyurethane elastomers. *Colloid Polym. Sci.* **1992,** *270* (6), 543-548. doi:10.1007/BF00658285

(38) Saralegi, A.; Etxeberria, A.; Fernández-d'Arlas, B.; Mondragon, I.; Eceiza, A.; Corcuera, M. A., Effect of H12MDI isomer composition on mechanical and physico-chemical properties of polyurethanes based on amorphous and semicrystalline soft segments. *Polym. Bull.* **2013,** *70* (8), 2193-2210. doi:10.1007/s00289-013-0930-3

(39) Plikk, P.; Tyson, T.; Finne-Wistrand, A.; Albertsson, A. C., Mapping the characteristics of the radical ring-opening polymerization of a cyclic ketene acetal towards the creation of a functionalized polyester. *J. Polym. Sci. A Polym. Chem.* **2009,** *47* (18), 4587-4601. doi:10.1002/pola.23511

5
Conclusions and Future Work

5.1 Conclusions

This thesis comprises a methodology for the synthesis of poly(orthoester thioether)s (POETEs) and a poly(acetal thioether) (PATTE) from stable orthoester (OE) monomers *via* thiol-ene Michael addition, the subsequent manufacturing based on photo polymerisation and polyurethane formation, as well as comprehensive thermo-mechanical, spectroscopic and microscopic investigation of the resulting materials and investigations into the cytocompatibility and degradation behaviour. Despite the rather complex synthesis of the common starting compound, an established cyclic ketene acetal (CKA) with two highly reactive centres, the stability of this compound and all subsequent stages to moisture and air permits all reactions to be conducted without any protective atmosphere, which is a major improvement compared to the POE synthesis to date.

Initially, a wide variety of OE monomers was obtained depending on the diol linker in a scale of up to several grams after simply stirring the reactants overnight with an acidic catalyst, followed by a washing procedure. In most cases, the OEs could be used right away, however pure OEs were easily obtained after distillation or recrystallisation. If however a thiol was reacted with the CKA, acetals (ATs) and thioorthoesters (TOEs) could be accessed. Unfortunately, complications such as thermal instability and radical inhibition prevented TOEs to form any polymers. OEs and ATs on the other hand reacted with thiols under radical initiation to complete conversion and with high purity within minutes to form the respective thioethers (TEs), which proved the 'click' character of this reaction. Similarly, a selection of bifunctional thiols was employed to form POETEs of around M_n = 10 kDa, whereby oxidative disulfide formation was discovered as a limiting factor. This limitation however had no discernible effect when an OE with unsaturated linker structure was employed, and a strong crosslinked POETE material was obtained after just minutes of photo curing. It was demonstrated that samples of this polymer degraded in a typical surface erosion profile in acidic aqueous media, whereas a delayed onset of degradation was observed in a neutral phosphate-buffered saline solution (PBS), which was attributed to a swelling and diffusion phase before the onset of hydrolysis. AFM and SEM analysis confirmed a smooth non-porous surface for the acidic and

slight swelling for the neutral degradation samples, respectively. In contrast, when samples were left to degrade in air with ambient moisture, crack formation, as well as excessive swelling and adhesion suggested degradation further into the material. IR and ^{1}H NMR spectroscopic analysis of the adhesive degradation products confirmed the presence of acids, esters and alcohols in accordance with established degradation mechanisms.

In a further approach, more versatile networks were obtained by crosslinking a range of OEs with different linker structure and additional functionalities with multi-functional thiols. Ultimate mechanical strengths of up to 3 MPa and elongations of up to 75%, as well as a range of elastic moduli from 2 to 8 MPa and glass transition temperatures between -10 and 40 °C were documented, which further underlined the versatility of this methodology. As expected, all but the PATTE material fully degraded in aqueous media over the course of 100 hours (for aliphatic POETEs) or 30 days (for aromatic, acetylenic and highly crosslinked POETEs). Surprisingly, degradation rates in alkaline medium exceeded those in both neutral and acidic media, which was attributed to the hydrolysis of the thioether or secondary ester functionalities instead. Similar to the POETE chain polymers however, oxidative conditions during thermal post-curing impacted the material strength of materials mostly negatively, whereas complete resistance to acidic or neutral media was gained. The fact that alkaline medium again achieved degradation over the course of two months further supported the hypothesis of alkaline hydrolysis of a secondary oxidised material. Nevertheless, potential applications for the POETE material were explored, such as controlled drug release or protective coating utilizing the direct relationship between wall thickness and degradation time for delayed release, or the 3D printing of functional objects like porous stents and constructs with moving parts after some surface erosion was allowed to proceed. Finally, cytocompatibility of the system was demonstrated by subjecting a cell line to diluted degradation products and registering complete viability in all dilutions except when acidity rose to intolerable levels at 20 $mg \cdot mL^{-1}$. Neutralisation of this medium restored viability. These results clearly established the qualification of POETEs for medical applications using 3D printing, however as all materials consisted of crosslinked networks, an alternative pathway to recyclable materials was desired.

Hence, the possibility to employ degradable POETE segments in polyurethane (PU) formulations to poly(orthoester thioether thiourethane urethane)s (POETE-Us) was explored. Severe reproducibility issues were encountered with the initial strategy of sequential addition of diisocyanate and chain extender to the POETE, especially as every instance of re-pressing led to decreased mechanical performance. Similarly, degradation proceeded *via* a bulk erosion mechanism, as the POETE soft segment phase hydrolysed and the material disintegrated into hard segment fragments, which was indicated by the remaining weight close to the hard segment ratio. However, optimisations were suggested, as both a one-pot reaction and employment of more crystalline diisocyanates produced semi-crystalline and strong elastomers.

5.2 Future Work

The methodology was demonstrated on several examples, however virtually endless possibilities for customised materials remain. To this regard, various biologically relevant diols and dithiols could be employed in the process to further improve biocompatibility. While the reaction with small multifunctional alcohols led to incomplete OE conversion in preliminary studies, this could be rectified by using more extensive alcohol linkers or potentially even 2D and 3D substrates for surface functionalisation, as illustrated by significant mass losses when working with untreated glass surfaces. Further customisations could be explored by utilizing free thiol groups after OE-TE formation, including as degradable linker in R-TE-OE-TE-R systems such as in thiol-yne elastomers, or as degradable scavengers for gold nanoparticles. More relevant from an economic perspective would further be the optimisation of the CKA synthesis, for example by adaptation into a flow process, and the recovery of degradation products, which should contain the diol and dithiol reactants for re-synthesis. Similarly, POETE chain polymerisation could be driven to higher MW by working completely oxygen-free in controlled atmosphere, using a reduction agent such as TBP to counteract oxidation, or switch to the base-catalysed Michael addition mechanism. The synthesis of A-B type thiol-ene monomers could further compliment such strategies, whereby preliminary approaches based on

affordable mercaptoethanol were unsuccessful and indicate that steric and financial aspects constitute significant obstacles.

From a material-focussed point of view, the POETE networks could further be improved by incorporating acid-neutralizing or acidic compounds into mixtures to either extend lifetime or accelerate the erosion rate of networks, respectively, as well as other additives for combined drug or particle release. After further investigation of the oxidation mechanism, the incorporation of antioxidants or in fact targeted modification for nanopatterning might be of interest. Limitations in the shelf-life of the 3D printing resin with premature hydrolysis and in fact hygroscopy and oxidation could further be overcome by creating a more stable and hydrophobic mixture, as well as more efficient composition of initiator and inhibitor. While the observed surface erosion rates of POETE networks proved to be too rapid for cell attachment and growth, this indicates the potential use of POETEs in temporary and consumable anti-fouling coatings or as self-lubricating tubing and scaffolds in biomedical applications. Moreover, initial complications with their auto-fluorescence could be transformed into an advantage with gradually increasing intensity of background fluorescence or self-indication of the presence of remaining POETE films.

Finally, several optimisation strategies for POETE-Us have already been proposed, such as the one-pot synthesis and incorporation of more crystalline diisocyanates, which should lead to the development of strong, surface erodible elastomers. Milder processing conditions should be tested to prevent or limit the decline of material properties during re-pressing, however further investigations into the exact mechanism behind this phenomenon might indicate the use of specific additives for the same purpose. In order to shift the degradation mechanism in favour of surface erosion, higher molecular weight soft segments should be employed in the one-pot method to provide more homogeneity and degradable matrix material. Subsequently, the degradation products should be analysed for particles on a nanometre and micrometre scale, as the documented disintegration raises concerns of stable fragments forming. In contrast, acylations using acid chlorides and OE functionalities could be used to access potentially surface-erodible dense PU-based networks.